Imperial College London

Natural Deep Eutectic Solvents (NADESs) for Lead Acid Battery Recycling

Yanying Wang

Submitted in partial fulfilment of the requirements for the degree of Doctor of Philosophy

Department of Materials

Imperial College London

April 2023

Statement of Originality

I declare that the work in this thesis herein was my own result, except where external contributions have been acknowledged and referenced appropriately.

Yanying Wang

April 2023

Copyright Declaration

The copyright of this thesis rests with the author. Unless otherwise indicated, its contents are licensed under a Creative Commons Attribution-NonCommercial 4.0 International Licence (CC BY-NC). Under this licence, you may copy and redistribute the material in any medium or format. You may also create and distribute modified versions of the work. This is on the condition that: you credit the author and do not use it, or any derivative works, for a commercial purpose. When reusing or sharing this work, ensure you make the licence terms clear to others by naming the licence and linking to the licence text. Where a work has been adapted, you should indicate that the work has been changed and describe those changes. Please seek permission from the copyright holder for uses of this work that are not included in this licence or permitted under UK Copyright Law.

Abstract

Lead acid batteries (LABs) are commonly used in automotives since their invention. LABs are also the most recycled batteries among all batteries. Currently, pyrometallurgy is the dominating recycling route of a LAB in industry. Pyrometallurgy is a process which converts metal compounds into metal at a temperature above 1000 ^{o}C. One of the main challenges in pyrometallurgy is thus the energy consumption. Another challenge is the risk of pollution of lead particulates to the environment during pyrometallurgy.

In this thesis, a solution-based recycling route was developed to minimize the environmental risk during LABs recycling. LAB waste components were recycled via a green solvent, Natural deep eutectic solvent (NADES), through a precipitation followed by calcination method.

Two types of NADESs were used, one is malic acid-based NADES, and the other is lactic acid-based NADES. The corresponding precipitates achieved by using these two NADESs were lead malate dihydrate and lead lactate, both of which were limited studied. Both precipitates were analysed and calcined at 550 ^{o}C to β-PbO.

The reaction behaviour of lead compounds from lead paste (LAB waste) in NADESs were also analysed. Results have shown that the reaction behaviour of lead compounds in NADESs were a dissolution followed by slow precipitation. This offers the possibility of the removal of impurities such as fibres or plastics in lead paste.

Acknowledgements

Time flies and it is now getting towards the end of my PhD. The PhD life was challenging but with lots of fun. The people I met at Imperial, friends and my family have offered me great support throughout my PhD journey and I want to express my gratitude to you all.

First of all, I want to express my sincere thanks to my supervisor, Prof. David Payne for offering me an opportunity to conduct the research and for his patient guidance during the whole PhD. I really enjoyed my PhD, as it was of lots of freedom and I have never felt being pushed, but David would never be absent if I need his support. Moreover, he also provides me with lots of creative ideas. This has widened my research perspectives and given me the chance to collaborate with both internal and external researchers.

In addition, I have met lots of helpful people in the department. I would like to say thank you to Mr Richard Sweeney for support in XRD. Richard has given me an opportunity for graduate teaching assistant in supporting XRD tutorial. I have learned in delivering my knowledge to undergraduates or junior people. Wish you all the best in your retirement and hopefully Arsenal can win the Premier League this season! Thanks to Dr. Andrew Cairns and Muzi Chen for teaching me XRD refinement. This helped me a lot in terms of data analysis.

And of course, I would like to thank Ola, Enrico, Eleonora, Gwilherm, Vincent, Syuhada, Will, Xiaoru and Paul from David's group. Thanks to Ola for giving guidance and advice on thesis structure. Thanks to Enrico for setting things up at the beginning of my PhD. Thanks to Eleonora and Xiaoru for chatting whenever I need. Thanks to Gwilherm for teaching me XPS. Special thanks to Adam for many things. Adam has taught me the knowledge of growing a single crystal, has brought me to the world of NMR and has proofread my thesis. Without Adam's help, the PhD work would be less effective. I would also thank all students I have supervised, Jac, Haolan, Dewen and Clara. You have made my PhD more enjoyable.

Also, I have met lots of good friends, Zhu (Alice) Meng, Juntao Li, Zhongyao Jiang, Jiaxin Pan, Muzi Chen, Weidong Xu and Gege (Chengyu) Ji at Imperial. We have spent lots of time on playing cards during happy weekend.

Finally, I want to express my dearest gratitude to my parents who provided the financial support for my PhD. I am very grateful for your kindness and support that you gave me. To my beloved husband, Li (Lukas) for accompany. It was of best luck in having you in my life.

Patent

Payne D., Hekselman O., **Wang Y.,** Ballantyne A. Recycling of Lead and Tin-based Materials. (2020).

Abbreviations

Abbreviation	Meaning
LAB	Lead Acid Battery
SLI	Starting Lighting Ignition
QSL	Queneau Schumann Lurgi
ISASMELT	Mount Isa Mines
KIVCET	Flash Cyclone Oxygen Electric
TBRC	Top Blown Rotary Converter
RSR	Revere Smelting Refining
Alk	Alkali
P	Phosphorous
AAS	Ammoniacal Ammonium Sufate
Placid	Plomo Acido
aq	aqueous
EDTA	Ethylenediaminetetraacetic Acid
MSA	Methane Sulfonic Acid
NTA	Nitrilotriacetic Acid
IDA	Iminodiacetic Acid
DTPA	Diethylenetriaminepenta Acetic Acid
IL	Ionic Liquid
RTIL	Room Temperature Ionic Liquid
DES	Deep Eutectic Solvent
ChCl	Choline Chloride
EG	Ethylene Glycol
ISSA	Incinerated Sewage Sludge Ash
NADES	Natural Deep Eutectic Solvent
ICP-OES	Inductively Coupled Plasma – Optical Emission Spectroscopy
XRD	X-ray Diffraction
ICDD	International Centre for Diffraction Data
PXRD	Powder X-ray Diffraction

SCXRD	Single Crystal X-ray Diffraction
SEM	Scanning Electron Microscopy
SE	Secondary Electrons
BSE	Backscattered Electrons
XPS	X-ray Photoelectron Spectroscopy
KE	Kinetic Energy
BE	Binding Energy
TGA	Thermal Gravimetric Analysis
DSC	Differential Scanning Calorimetry
FTIR	Fourier Transform Infrared Spectroscopy
NMR	Nuclear Magnetic Resonance
MA	D, L-Malic Acid
BA	β-alanine
DI	De-ionized water
SOS	Spin Orbit Splitting
LA	Lactic acid
Bet	Betaine
RT	Room Temperature
ATR	Attenuated Total Reflection

Table of Contents

Statement of Originality 1

Copyright Declaration 2

Abstract 3

Acknowledgements 4

Patent 6

Abbreviations 7

List of Tables 13

List of Figures 13

Chapter 1 Introduction 18

1.1 Impact of lead acid batteries (LABs) 18

1.2 Aims and Objectives 19

1.3 Thesis Outline 20

Chapter 2 Literature Review 22

2.1 Principles of lead acid batteries (LABs) 22

2.1.1 End of life of a LAB 24

2.2 Recycling of a LAB 26

2.2.1 Pyrometallurgy 27

2.2.2 Hydrometallurgy 39

2.2.3 Leaching followed by precipitation method – the Aurelius process 49

2.3 Solvent Development 51

2.3.1 Ionic liquids (ILs) 51

2.3.2 Deep Eutectic Solvents (DESs) 52

2.3.3 Applications of DESs 55

2.3.4 Lead Recycling in DESs 57

2.3.5 Natural deep eutectic solvents (NADESs) 59

2.4 Perspective of lead recycling with new solvents 60

Chapter 3 Experimental methods 63

3.1 Inductively Coupled Plasma – Optical Emission Spectroscopy (ICP-OES) 63

3.2 X-ray Diffraction (XRD) 64
3.2.1 Powder X-ray Diffraction (PXRD) 65
3.2.2 Refinement of PXRD 66
3.2.3 Single Crystal X-ray Diffraction (SCXRD) 67
3.3 Scanning Electron Microscopy (SEM) 68
3.4 X-ray Photoelectron Spectroscopy (XPS) 69
3.5 Thermal Gravimetric Analysis - Differential Scanning Calorimetry (TGA-DSC) 72
3.6 Fourier Transform Infrared Spectroscopy (FTIR) 72
3.7 Nuclear Magnetic Resonance (NMR) 74
Chapter 4 Synthesis, Characterisation and Decomposition of Lead Malate Dihydrate 77
4.1 Introduction 77
4.2 Experimental 78
4.2.1 Chemical Reagents 78
4.2.2 Synthesis of NADES and precipitates 78
4.2.3 Crystallisation and characterisation of a single crystal 79
4.2.4 Characterisation of precipitates 79
4.2.5 Calcination of precipitates and characterisation of calcined products 80
4.3 Results and Discussion 80
4.3.1 Structure identification of the precipitate 80
4.3.2 Characterisation of lead malate dihydrate 83
4.3.3 Chemical composition evolution upon thermal decomposition of lead malate dihydrate 89
4.3.4 XPS analysis of calcined products from lead malate dihydrate 93
4.3.5 Morphology analysis of calcined products from lead malate dihydrate 95
4.4 Conclusions 97
Chapter 5 Synthesis, Characterisation and Decomposition of Lead Lactate 99
5.1 Introduction 99
5.2 Experimental 99
5.2.1 Chemical Reagents 99
5.2.2 Synthesis of NADES and precipitates 100
5.2.3 Crystallisation and characterisation of a single crystal 101
5.2.4 Characterisation of precipitates 101
5.2.5 Calcination of precipitates and characterisation of calcined products 102

5.3 Results and Discussion 102
5.3.1 Analysis of single crystals 102
5.3.2 Identification of the precipitate 107
5.3.3 Analysis of calcined products 110
5.4 Limitations 117
5.4.1 Limitation in analysis of lead lactate 117
5.4.2 Limitation in precipitation followed by calcination methods 117
5.5 Conclusions 119
Chapter 6 Solubility behaviour of lead compounds in malic acid-based NADESs 120
6.1 Introduction 120
6.2 Experimental 121
6.2.1 Chemical Reagents 121
6.2.2 Synthesis of Natural deep eutectic solvents (NADESs) 121
6.2.3 Analysis of lead paste 122
6.2.4 Dissolution of lead compounds in NADESs 122
6.2.5 Dissolution and precipitation behaviour of lead compounds in MABA5 123
6.2.6 Analysis of MABA5 123
6.2.7 ^{1}H NMR 124
6.3 Results and Discussion 124
6.3.1 Characterisation of lead paste 124
6.3.2 Justification for the use of individual lead compounds 127
6.3.3 Characterisation of MABA5 127
6.3.4 Maximum lead concentration in solution of lead compounds ($2PbCO_3 \cdot Pb(OH)_2$, $PbCO_3$, PbO and PbO_2) 130
6.3.5 Dissolution and precipitation behaviour of lead compounds 139
6.3.6 Replacement of β-alanine by another amino acid – L-proline 142
6.4 Advantages, Limitation and Future work 143
6.4.1 Advantages 143
6.4.2 Limitations and future work 144
6.5 Conclusions 145
Chapter 7 Solubility behaviour of lead compounds in lactic acid-based NADESs 147
7.1 Introduction 147
7.2 Experimental 148

7.2.1 Synthesis of NADESs 148
7.2.2 Solubility of Lead compounds in NADESs 148
7.2.3 Precipitation behaviour analysis 149
7.2.4 Analysis of NADESs 149
7.3 Results and Discussion 150
7.3.1 Characterisation of NADES 150
7.3.2 Maximum lead concentration in solution versus loading of lead compounds (PbO and PbO_2) 155
7.3.3 Dissolution and precipitation behaviour of lead compounds 162
7.4 Advantages, Limitation and Future work 166
7.4.1 Advantages 166
7.4.2 Limitations 167
7.5 Conclusions 167
Chapter 8 Industrial application – Re-usability test of NADESs 169
8.1 Introduction 169
8.2 Experimental 170
8.2.1 EDX characterization of lead paste 170
8.2.2 Re-usability test of MABA5 170
8.2.3 Characterisation and calcination of precipitate 171
8.3 Results and Discussion 172
8.3.1 Characterisation of lead paste 172
8.3.2 Re-usability test of MABA5 173
8.3.3 Characterisation of precipitate 174
8.3.4 Calcination of the precipitate 175
8.4 Conclusions 177
Chapter 9 Conclusions 178
Appendix A 181
References 199

List of Tables

Table 2.1 Products formed with varying of reaction temperature and Na_2CO_3 concentration based on study from Y. Gong et al. [31] 30
Table 4.1 Chemical reagents.....78
Table 5.1 Summary of Chemical Reagents in Chapter 5.....100
Table 6.1 Maximum lead concentration comparison among various solvents. The concentrations of lead compounds are given in g Pb^{2+} /L solution, which are measured from the ICP. The solubility of Pb paste in MSA was given in g Pb paste/ L solution as stated in the literature. 133
Table 7.1 Change in water content of LABet5-10 after stirring at RT and 50 ^oC for 4 days. .158
Table 7.2 Volume change of LABet5-10 at RT and 50 ^oC. 158
Table 8.1 Weight percentage of all elements from the lead paste 2019. 172

List of Figures

Figure 2.1 Schematic composition of a LAB. Adapted from Reference.[10].....22
Figure 2.2 Schematic migration of electrons and H^+ in a LAB during discharging.....23
Figure 2.3 Schematic diagram of sulfation on negative electrodes. Adapted from Reference.[19] 26
Figure 2.4 Schematic diagram of a pyrometallurgy process. Adapted from Reference.[26].....28
Figure 2.5 Schematic diagram of a blast furnace. Redrawn based on Reference.[34] 31
Figure 2.6 Schematic diagram of a TBRC. Redrawn based on Reference.[37].....32
Figure 2.7 Schematic diagram of a ISASMELT smelting furnace. Redrawn based on Reference.[39] 33
Figure 2.8 Schematic diagram of a QSL furnace. Redrawn based on Reference.[44].....35
Figure 2.9 Schematic diagram of a KIVCET furnace. Redrawn based on Reference.[48].....36
Figure 2.10 Schematic phase diagram of melting temperature of two mixed components. Adapted from Reference.[91].....52
Figure 2.11 Melting point of a DES versus an ideal mixture. Adapted from Reference.[91].....52

Figure 2.12 Schematic diagram of a proposed recycling route of LAB waste with the use of a chloride free NADES. 62
Figure 3.1 Schematic diagram of PXRD. 65
Figure 3.2 Inelastic mean free path (IMFP) as a function of electron energy. Adapted from Reference.[141] 70
Figure 3.3 Vibrational modes of water molecules. 74
Figure 4.1 Asymmetric unit of lead malate dihydrate. 81
Figure 4.2 Extended version of lead malate dihydrate. 82
Figure 4.3 a) ^{1}H NMR (CD_3COOD) spectrum of lead malate dihydrate and b) corresponding protons of the ^{1}H NMR peaks. 84
Figure 4.4 FTIR of lead malate dihydrate. 85
Figure 4.5 Rietveld refinement for lead malate dihydrate including the experimental and calculated XRD patterns along with difference and Bragg positions. 86
Figure 4.6 SEM images of lead malate dihydrate at a low (a) and high (b) magnification. 87
Figure 4.7 XPS core levels of lead malate dihydrate precipitate a) Pb 4*f*, b) O 1s and c) C 1s. 88
Figure 4.8 TGA and DSC analysis of lead malate dihydrate under air flow. 89
Figure 4.9 FTIR of lead malate dihydrate calcined at 116 ^{o}C for 2 hours. 90
Figure 4.10 XRD pattern of lead malate dihydrate calcined at 116 ^{o}C for 2 hours. 91
Figure 4.11 XRD pattern of lead malate dihydrate calcined for 2 hours at (a) 116 ^{o}C, (b) 222 ^{o}C, (c) 335 ^{o}C, (d) 384 ^{o}C, (e) 414 ^{o}C and (f) 550 ^{o}C. 92
Figure 4.12 Weight percentage of $PbMa{\cdot}2H_2O$, $2PbO{\cdot}PbCO_3$, $2PbO{\cdot}PbCO_3$, α-PbO and β-PbO at room temperature as pristine precipitate and at different calcination temperatures. 93
Figure 4.13 Evolution of XPS core levels (a) Pb 4*f*, (b) C 1*s* and (c) O 1*s* upon decomposition of lead malate dihydrate from as-received precipitate to calcination from 116 ^{o}C to 550 ^{o}C. 94
Figure 4.14 SEM images of lead malate dihydrate calcined for 2 hours at (a) 116 ^{o}C, (b) 222 ^{o}C, (c) 335 ^{o}C, d) 384 ^{o}C, (e) 414 ^{o}C and (f) 550 ^{o}C. 96
Figure 5.1 Asymmetric unit of lead dilactate $Pb(C_3H_5O_3)_2$. 102
Figure 5.2 Crystal structure of $Pb(D,L\text{-}C_3H_5O_3)_2$. 103
Figure 5.3 Asymmetric unit of $Pb(D\text{-}C_3H_4O_3)$. 104
Figure 5.4 Asymmetric unit of $Pb(L\text{-}C_3H_4O_3)$. 105

Figure 5.5 Crystal structure of Pb(D- $C_3H_4O_3$). 106
Figure 5.6 Crystal structure of Pb(L- $C_3H_4O_3$). 106
Figure 5.7 XRD pattern of the precipitate. 107
Figure 5.8 FTIR of the precipitate, lead lactate. 108
Figure 5.9 XPS core levels of precipitated lead lactate a) Pb 4*f*, b) C 1*s* and c) O 1*s*. 109
Figure 5.10 SEM image of precipitate lead lactate. 110
Figure 5.11 XRD patterns of lead lactate from (a) as-synthesized precipitate and calcined products for 2 hours at (b) 100 °C, (c) 200 °C, (d) 300 °C, (e) 400 °C and (f) 550 °C. 111
Figure 5.12 Weight percentage of $Pb(LA)_x$, $2PbO{\cdot}PbCO_3$, $2PbO{\cdot}PbCO_3$, α-PbO and β-PbO at toom temperature as the as-synthesized precipitate and at different calcination temperatures. 112
Figure 5.13 FTIR spectra of lead lactate and its calcined products at 100 °C and 200 °C for 2 hours. 113
Figure 5.14 Evolution of XPS core levels (a) Pb 4*f*, (b) O 1*s* and (c) C 1*s* upon decomposition of lead lactate from as-synthesized precipitate to calcination from 100 °C to 550 °C. 114
Figure 5.15 SEM images of lead lactate from (a) as-synthesized precipitate to calcined products for 2 hours at (b) 100 °C, (c) 200 °C, (d) 300 °C, (e) 400 °C and (f) 550 °C. 116
Figure 5.16 SEM images of β-PbO obtained from (a) this work and (b) referenced work using lead citrate.[80] 117
Figure 6.1 XRD analysis of lead paste from a) Year 2017 and b) Year 2019. 125
Figure 6.2 Relative quantification of each phase present in two batches of lead paste. 125
Figure 6.3 XPS core levels of Pb paste from Year 2017 a) Pb 4*f*, b) O 1*s*, c) C 1*s*, d) Na 1*s* and e) Si 2*p*. 126
Figure 6.4 XPS core levels of Pb paste from Year 2019 a) Pb 4*f*, b) O 1*s*, c) C 1*s*, d) Na 1*s* and e) Si 2*p*. 126
Figure 6.5 ^1H NMR (D_2O) of a) malic acid, b) β-alanine and c) MABA5. 128
Figure 6.6 FTIR of malic acid, β-alanine and MABA5. 129
Figure 6.7 Lead concentration in solution and in precipitate with a variety of a) $2PbCO_3{\cdot}Pb(OH)_2$, b) $PbCO_3$ and c) PbO loading at RT and 50 °C after reaction for 4 days. 131
Figure 6.8 Lead concentration in solution and as solid with a variety of PbO_2 loading at RT and 50 °C after reaction for 4 days. 132

Figure 6.9 Appearance of solution from left to right: (i) pure MABA5, (ii) MABA5 + 10 g/L PbO_2 + 10 g/L Pb, (iii) MABA5 + 10 g/L PbO_2, (iv) MABA5 + 20 g/L PbO_2, (v) MABA5 + 50 g/L PbO_2, (vi) MABA5 + 100 g/L PbO_2. 137
Figure 6.10 Lead concentration in MABA5 with 200 g/L and 250 g/L $2PbCO_3{\cdot}Pb(OH)_2$ as a function of stirring time for reaction at room temperature. 140
Figure 6.11 Lead concentration in MABA5 with 250 g/L $2PbCO_3{\cdot}Pb(OH)_2$, $PbCO_3$ and PbO as a function of stirring time for reaction at room temperature. 141
Figure 6.12 Lead concentration in MABA5 with 250 g/L $2PbCO_3{\cdot}Pb(OH)_2$, $PbCO_3$ and PbO as a function of stirring time for reaction at 50 ^oC. 141
Figure 6.13 Lead concentration in solution and as precipitate of $2PbCO_3{\cdot}Pb(OH)_2$ in MABA5 and MALP5 after reaction at room temperature for 4 days. 143
Figure 7.1 Viscosity of LABet5-10 as an increase of temperature. 150
Figure 7.2 ^1H NMR (D_2O) of a) betaine and b) lactic acid solution. 151
Figure 7.3 ^1H NMR (D_2O) of LABet5. 152
Figure 7.4 FTIR of betaine, lactic acid solution, LABet5, LABet7.5 and LABet10. 154
Figure 7.5 Lead concentration in solution and in precipitate with a variety PbO loading at RT and 50 ^oC after reaction in a) LABet5, b) LABet7.5 and c) LABet10 for 4 days. 156
Figure 7.6 Lead concentration in solution and in solid with a variety PbO_2 loading at RT and 50 ^oC after reaction in a) LABet5 and b) LABet7.5 for 4 days. 160
Figure 7.7 Appearance of solution from left to right: (i) pure LABet5, (ii) LABet5 + 200 g/L PbO_2, (iii) LABet5 + 500 g/L PbO_2, (iv) LABet5 + 600 g/L PbO_2, (v) LABet5 + 700 g/L PbO_2, (vi) LABet5 + 800 g/L PbO_2, (vii) LABet5 + 900 g/L PbO_2, (viii)LABet5 + 1,000 g/L PbO_2 reacted at RT for 4 days. 161
Figure 7.8 Appearance of solution from left to right: (i) LABet7.5 + 500 g/L PbO_2, (ii) LABet7.5 + 600 g/L PbO_2, (iii) LABet7.5 + 700 g/L PbO_2, (iv) LABet7.5 + 800 g/L PbO_2, (v) LABet7.5 + 900 g/L PbO_2, (vi) LABet7.5 + 1,000 g/L PbO_2 reacted at RT for 4 days. 162
Figure 7.9 Lead concentration in LABet5-10 with 900 g/L PbO as a function of stirring time at RT. 163
Figure 7.10 Lead concentration in LABet5-10 with 900 g/L PbO as a function of stirring time at 50 ^oC. 164

Figure 7.11 Lead concentration in LABet5 with 900 g/L PbO_2 as a function of stirring time at RT and at 50 °C. 165
Figure 7.12 a) full pattern and b) focused range of XRD analysis of left-over solids from reaction between LABet5 + 900 g/L PbO_2 at 50 °C. 166
Figure 8.1 Process flow chart of re-usability test on MABA5 for lead paste recycling. 170
Figure 8.2 SEM image of lead paste 2019 provided by Envirowales Ltd. 172
Figure 8.3 EDX images of lead paste 2019 provided by Envirowales Ltd. 173
Figure 8.4 Lead concentration of MABA5 recycling lead paste under different conditions upon cycles 174
Figure 8.5 XRD pattern of precipitate. 175
Figure 8.6 XPS core levels a) Pb 4*f*, b) C 1*s* and c) O 1*s* of precipitate. 175
Figure 8.7 XRD pattern of calcined product. 176
Figure 8.8 XPS core levels a) Pb 4*f*, b) C 1*s* and c) O 1*s* of calcined product. 177

Chapter 1 Introduction

1.1 Impact of lead acid batteries (LABs)

LABs were invented by Gaston Planté in 1859. They have been used as starting lighting ignition (SLI) batteries in automobiles. An SLI battery is an open circuit battery operating at 12 V with thin electrodes plates so that it can produce a higher surge current while in use.[1] LABs have also been used as deep cycle batteries with thicker electrodes plates so that the batteries can be fully charged and discharged. These batteries are applied as uninterruptible power supplies (UPS) in submarines or as secondary storage batteries in electric vehicles.

As the number of vehicles on the road keeps growing, as does the market for LABs. The global LAB market had achieved a value of $39.7 billion in 2018 and is expected to achieve a value of $59.7 billion in 2026.[2] The production of LABs makes up 85% of the lead usage worldwide.[3] LABs have the highest recovery rate among all batteries, approximately 99% in the US and Europe, while other batteries such as zinc, nickel, cobalt and lithium batteries have a recycle rate of only 53-68 %.[4,5]

At the end-of-life, a LAB is collected from an automobile and the acid from the battery is drained out. Subsequently, plastic containers are removed and recycled via plastic recycling routes. The battery components are crushed into pieces forming “lead paste”. The lead paste is then recycled to metallic lead via pyrometallurgical or hydrometallurgical methods, which will be discussed in detail in the next chapter.

The most mature industrial LAB recycling technology is pyrometallurgy, which processes lead paste at temperatures higher than 1000 ^{o}C. During the process, in addition to the emission of CO_2 and SO_2, heavy metal ash consisting of Pb, Hg, and Cd can also be generated. CO_2 is the primary cause of global warming via the greenhouse effect, and SO_2 is known to cause acid rain, thus, inappropriate treatment of these gases has severe environmental implications.

Moreover, if the toxic heavy metal ash is emitted into the environment and inhaled by humans or indeed other organisms, it can cause serious health problems.

Lead pollution can cause irreversible damage to the human body, especially the nervous system. Lead blocks N-methyl-D-aspartate receptors in the brain, which control the neuroplasticity in response to extrinsic or intrinsic activities.[6] These receptors also affect the learning and memory abilities. The developing tissues of children are more susceptible to adverse effects than adults upon exposure of lead.[7] The standard blood lead levels for adults and children are set to 10 $\mu g/dL$ and 5 $\mu g/dL$, respectively, according to the Centres for Disease Control and Prevention in the USA. Children who are exposed to lead can suffer from health problems such as IQ deficits, behavioural problems, and learning diabilities.[8] Apart from affecting the nervous system, lead also acts as a secondary messenger and binds with calmodulin, leading to changes in protein conformation.[6] As a result, lead poisoning can also cause severe problems in renal and reproductive systems. Due to the irreversible toxicity of lead in humans, safe methods for recycling lead are vital.

An improved recycling method, hydrometallurgy, which uses an aqueous solvent to dissolve lead paste, has been developed to mitigate the pollution of hazardous gases and toxic particles. Then the lead is recovered from the solution via electro-deposition or electro-winning processes. Hydrometallurgy is a less polluting process than pyrometallurgy, however, these aqueous solutions are normally strong acids, which is a health hazard for workers. Accordingly, an alternative safer and more economic method needs to be developed to improve the current recycling system of LABs.

1.2 Aims and Objectives

Though current recycling methods including pyrometallurgy and hydrometallurgy have been used on an industrial scale for decades, both have their own drawbacks. Pyrometallurgy is generally cheaper but the generation of hazardous ash during the process is always a concern; hydrometallurgy is comparatively a safer method compared to pyrometallurgy as the lead is recovered in a non-volatile solution via an electro-chemical process, but the cost is higher

than pyrometallurgy and the use of strong acids is also a concern. The aim of this project is, therefore, to develop a greener and more economic method than incumbent technologies to enable cost-competitive LAB recycling while reducing the environmental impact of lead.

This method involves the use of a recently developed class of green solvents to dissolve components of lead paste: natural deep eutectic solvent (NADES). NADES will be discussed in detail in the next chapter. In this project, a precipitation-calcination method will be used to recover lead components ($PbCO_3$, PbO and PbO_2). This method will have two main approaches. First, to develop hydrophilic NADESs which can dissolve the lead components of lead paste and precipitate them to be later calcined to recover lead. Second, to develop hydrophilic NADESs which can dissolve the lead components of lead paste efficiently, to later precipitate them with the use of a precipitation agent and calcine to recover lead. In the second approach, ideally, the hydrophilic NADESs should be recycled, and so the potential of re-using NADESs will also be analyzed.

1.3 Thesis Outline

Chapter 2, the Literature Review, will start by introducing the working principle of a LAB, and move on to a discussion of the two main incumbent recycling technologies, pyrometallurgy and hydrometallurgy. The green solvents used in this thesis, NADESs, will also be discussed in detail from their chemistry to applications.

Chapter 3 introduces all the analysis techniques including the working principles of all equipment used throughout the research.

Chapter 4 presents the development of recycling of the main components ($PbCO_3$) of desulfurized lead paste through precipitation methods with the use of a malic acid/ β alanine/water-based NADES. The precipitate was analysed and confirmed to be lead malate dihydrate. It was then calcined to PbO and the calcined products were also analysed.

Chapter 5 develops the route of recycling PbO with the use of another NADES (lactic acid/betaine/water) based on the precipitation routes as in Chapter 4. The precipitate obtained from the solvent was analysed and confirmed to be lead lactate. It was calcined to PbO and the calcined products were analysed.

Chapter 6 investigates the maximum lead concentration of different lead components ($2PbCO_3 \cdot Pb(OH)_2$, $PbCO_3$, PbO and PbO_2) of lead paste in a malic acid/β-alanine/water-based NADES before precipitation occurred. The precipitation behaviour of the lead components in this solvent was also analysed.

Chapter 7 investigates the solubility of PbO and PbO_2 in a series of lactic acid/betaine/water based NADESs. Three NADESs with different water concentrations were used to analyse the effect of water concentration on the solubility of the lead compounds. The precipitation behaviour of PbO was analysed in three NADESs, and the precipitation behaviour of PbO_2 was analysed in the NADES with the lowest water concentration.

Chapter 8 uses a malic acid/β-alanine/water-based NADES to dissolve lead paste. Then a precipitation agent, oxalic acid dihydrate, was used to leach the lead from the solution out. Subsequently, the precipitates were calcined to PbO and the solvent was re-used to dissolve lead paste, assessing the re-usability of NADESs.

Finally, Chapter 9 summarizes the research carried out in this thesis, suggesting improvements to the processes, and future work.

Chapter 2 Literature Review

2.1 Principles of lead acid batteries (LABs)

The LAB was invented in 1859 by Gaston Planté.[9] A LAB consists of an electrolyte (dilute sulfuric acid), a negative electrode covered with metallic lead (Pb), and a positive electrode covered with lead dioxide (PbO_2). The overall charging and discharging processes can be expressed as shown in Equation 2.1. Schematic electrodes of a LAB are shown as in Figure 2.1.

$$PbO_2(\mathrm{s}) + Pb(s) + 2H_2SO_4(\mathrm{aq}) \leftrightarrow 2PbSO_4(\mathrm{s}) + 2H_2O(l) \qquad \textbf{Equation 2.1}$$

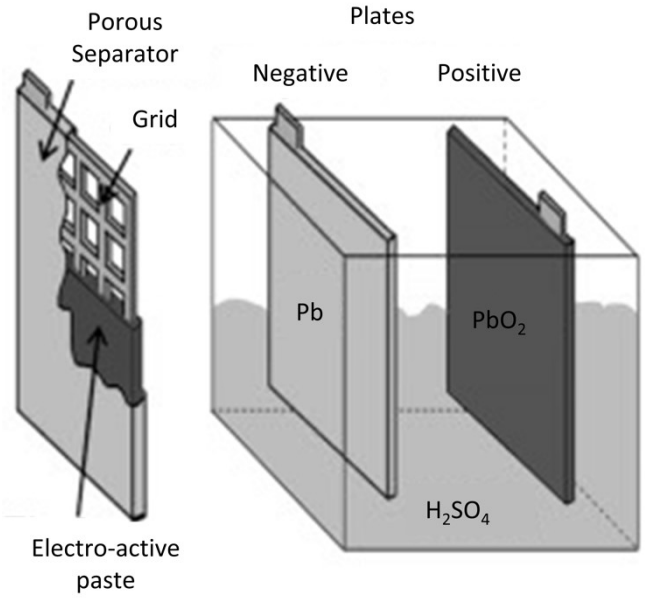

Figure 2.1 Schematic composition of a LAB. Adapted from Reference.[10]

During the discharging process, H^+ migrates towards the PbO_2 plate (positive electrode), while at the same time the electrode gains electrons and reacts with the PbO_2 plate to form lead oxide (PbO) and water. PbO reacts further with the electrolyte to form lead sulfate. Simultaneously, the SO_4^{2-} migrates towards the Pb plate (negative electrode), the electrode loses electrons and reacts with the Pb plate to form lead sulfate. The process is described as shown in Equation 2.2 and the electrons migration schematic in Figure 2.2. After discharging, both the electrodes convert completely to lead sulfate. The solubility of PbO and $PbSO_4$ in water are 0.017 g/L and 0.04 g/L, respectively.

$$positive\ electrode:\ PbO_2(s) + 2H^+(aq) + 2e^- \rightarrow\ PbO(s) + H_2O(l)$$
$$PbO(s) + H_2SO_4(aq) \rightarrow PbSO_4(s) +\ H_2O(l)$$
$$negative\ electrode: Pb(s) + SO_4^{2-}(aq) - 2e^- \rightarrow\ PbSO_4(s)$$

Equation 2.2

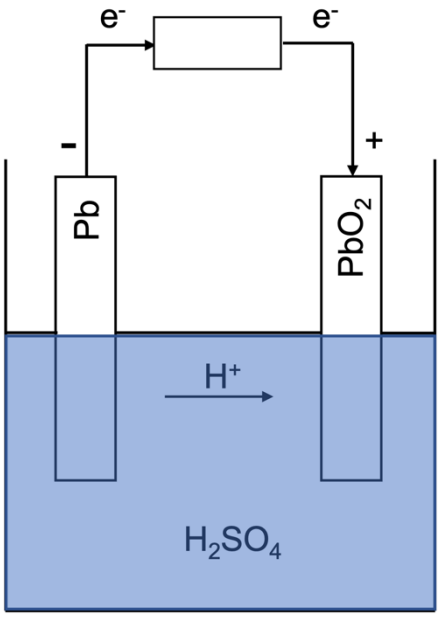

Figure 2.2 Schematic migration of electrons and H^+ in a LAB during discharging.

The overall charging process can be described as shown in Equation 2.3. During charging, the two electrodes are connected to an external power supply. The migration of the ions and electrons in the electrolyte is the reverse of the discharging process. Electrons migrates towards the negative electrode and reacts with the $PbSO_4$ to form Pb and SO_4^{2-}. At the same time, water migrates towards the positive electrode, which loses electrons and reacts with water $PbSO_4$ to form PbO_2 and H_2SO_4. After the charging process, the electrodes components convert from $PbSO_4$ back to Pb and PbO_2.

$$positive\ electrode: PbSO_4(s) + H_2O(l) - 2e^- \rightarrow\ PbO_2(s) + 4H^+(aq) + {SO_4}^{2-}(aq)$$
$$negative\ electrode: PbSO_4^{2-}(aq) + 2e^- \rightarrow Pb(s) +\ SO_4^{2-}(aq)$$

Equation 2.3

In an ideal battery, the discharging and charging processes can be repeated indefinitely. However, $PbSO_4$ cannot convert completely to PbO_2 and Pb in real applications.[11] This leads to the accumulation of $PbSO_4$ crystals on the surface of the electrodes or degradation of the electrode materials. As a result, the LAB will lose its capacity gradually until it fails to operate.

2.1.1 End of life of a LAB

2.1.1.1 Positive electrode failure

The positive electrode consists of two types of PbO_2: orthorhombic α-PbO_2 and tetragonal β-PbO_2.[11] α-PbO_2 has a larger crystal size but lower initial capacity than β-PbO_2. Electrodes with higher α-PbO_2 concentration have a lower capacity. The life cycle of the positive electrode depends on the active mass of the electrodes. As β-PbO_2 is smaller in crystal size, it is more likely to shed from the electrode during the re-charging process. As a result, it leads more easily to "softening" of the electrode.[11–13] Therefore, electrodes with a higher proportion of β-PbO_2 will have a lower life cycle and, thus, the performance of the positive electrode is related to the ratio of α-PbO_2 and β-PbO_2.[14]

In an ideal LAB, the ratio of α-PbO_2 and β-PbO_2 should remain constant during charging and re-charging processes through transformation between PbO_2 and $PbSO_4$. However, α-PbO_2 and β-PbO_2 have different stabilities. α-PbO_2 is formed preferentially in weak acid solutions (pH = 2 ~3), while β-PbO_2 is formed preferentially in strong acid solutions (pH <2).[13,15] Moreover, β-PbO_2 has a lower electrical potential than α-PbO_2.[13] This means that $PbSO_4$ transforms more easily to β-PbO_2 than to α-PbO_2. With increasing of life cycles, the ratio of α-PbO_2 to β-PbO_2 decreases gradually. Higher β-PbO_2 concentration shortens the life cycles of the electrode due to softening, and finally causes the failure of a LAB. Positive electrode "softening" is one of the most common failure modes of a LAB.

Another explanation for the "softening" phenomenon of the electrode is the "crystal-gel" theory proposed by D. Pavlov.[16] The "crystal-gel" system considers the positive electrode as two parts: gel and crystal. The crystal part consists α-PbO_2 and β-PbO_2 particle agglomerates, while the gel part consists of $PbO(OH)_2$. $PbO(OH)_2$ forms as a result of H_2O and the PbO_2 surface.[17] $PbO(OH)_2$ acts as a polymer chain in the gel zone which connects different crystal

zones enhancing electrons and ion mobility.[16] During repeated charging and discharging process, the ions from the electrolyte reacts with PbO_2 and generates more $PbO(OH)_2$, leading to a higher ratio of the gel zone to crystal zone.[11] The gel zone has a higher resistance than the crystal zone,[18] and as a result, the resistance of the gel zone increases and blocks the ion transportation causing failure of the LAB.

2.1.1.2 Negative Electrode failure

The failure of negative electrodes is mainly due to sulfation on the electrode. The sulfation process can be shown in Figure 2.3.[19] For a fresh LAB, during the discharging process, small $PbSO_4$ crystals are initially formed on the surface of the electrode. The dissolution of $PbSO_4$ in the electrolyte can be described in Equation 2.4. While some of the Pb^{2+} formed from the dissolution of $PbSO_4$ convert back to Pb during charging, some Pb^{2+} participate in the growth of $PbSO_4$. The concentration of small crystals and big crystals can be determined by the Ostwald-Freundlich equation as shown in Equation 2.5,[20] where $C_{Pb^{2+}}$ is the equilibrium Pb^{2+} concentration of Pb crystals with radius of r,$C_{big}{}^{\infty}$ is the equilibrium Pb^{2+} concentration of big crystals, V_m is the molar volume of $PbSO_4$ (equals to 47.96 $cm^3 \cdot mol^{-1}$), σ is the surface free energy, R is the gas constant, T is the temperature, r is the radius of $PbSO_4$ crystals.[20,21] Small crystals have higher solubility, and the smallest crystal determines the Pb^{2+} concentration in the electrolyte.[21] With the increase of radius of $PbSO_4$ crystals, the amount of the initial small crystals reduces. Consequently, the big $PbSO_4$ crystals isolates the electrode from the electrolyte and, hence, leading to electrode failure.

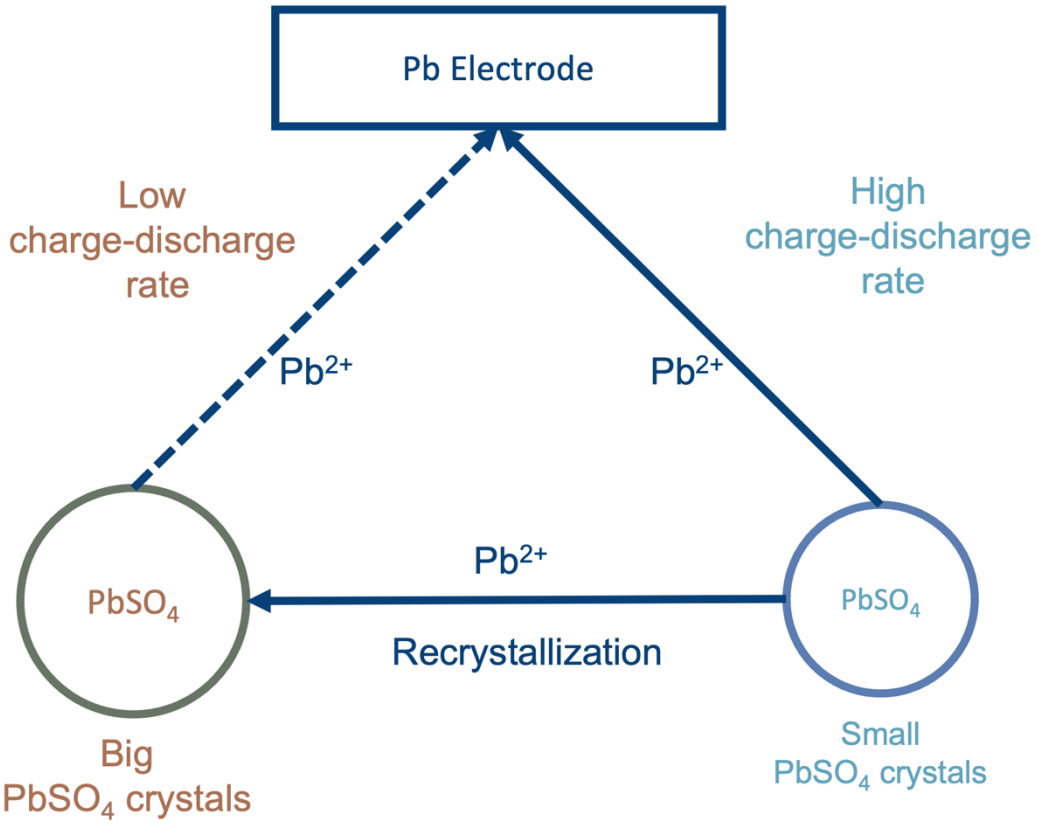

Figure 2.3 Schematic diagram of sulfation on negative electrodes. Adapted from Reference.[19]

$$PbSO_4(s) \rightarrow Pb^{2+}(aq) + {SO_4}^{2-}(aq) \qquad \textbf{Equation 2.4}$$

$$\ln\left(\frac{C_{Pb^{2+}}}{C_{big}{}^{\infty}}\right) = \frac{2V_m\sigma}{RT}\left(\frac{1}{\mathrm{r}}\right) \qquad \textbf{Equation 2.5}$$

2.2 Recycling of a LAB

Once the electrodes of a LAB fail to operate, post-treatment of a LAB is the main challenge. Recycling a used LAB is the optimum option as lead is a toxic but valuable heavy metal. The highest among all types of batteries, 99 % of LAB can be recycled.[22] A spent LAB consists of 11-30 wt% acid solution, 22-30.5 wt% plastics, 24-30 wt% of lead grid and 30-40 wt% of lead paste.[23] A spent LAB grid consists of 92 wt% to 95 wt% Pb and small amounts of PbO, PbO_2, $PbSO_4$ and Sb.[23] Spent lead paste consists of 60 wt% $PbSO_4$, 28 wt% PbO_2, 9 wt% PbO, and 3 wt% metallic Pb and impurities (Fe, Sb, Sn and Ba).[24,25] A LAB is firstly crushed into pieces

and the sulfuric acid is drained out. The casing materials of a LAB, which are normally polypropylene (PP) or acrylonitrile butadiene styrene (ABS), are separated from the lead components using a hydrodynamic separation method based on the density difference of different materials.[26] These are collected from the top of the separation tank, cleaned, and recycled. Lead grids and lead paste are much denser than plastics and are collected at the bottom of the separation tank. Recycling of Pb grid and Pb paste is the primary focus of a LAB recycling as these two LAB components are encompass the vast majority of the Pb from the battery. Pb grids have a relatively simple composition (high purity lead metal) so they can be recycled via low temperature smelting.[27] The recycling of lead paste is much more complicated. The current two common recycling routes for lead paste are pyrometallurgy and hydrometallurgy.

2.2.1 Pyrometallurgy

Pyrometallurgy is a high-temperature process which converts metal compounds into metallic form.[28] Pyrometallurgy for lead recycling consists of two main steps: smelting and refining. Smelting is a process, where lead compounds are decomposed into metallic lead with the application of heat and reducing agents. The metallic lead bullion obtained from the smelting process contains lots of impurities and a refining process is required to remove impurities to obtain pure metal or be processed to lead alloys. A schematic recycling process is shown in Figure 2.4.[26]

Prior to smelting, the lead concentrates are mixed with reducing agents and fluxes. Coke is a commonly used reducing agent, which reduces lead compounds into metallic form. Limestones, silica, or lime are commonly used flux materials, which lower the melting temperature of lead concentrates.

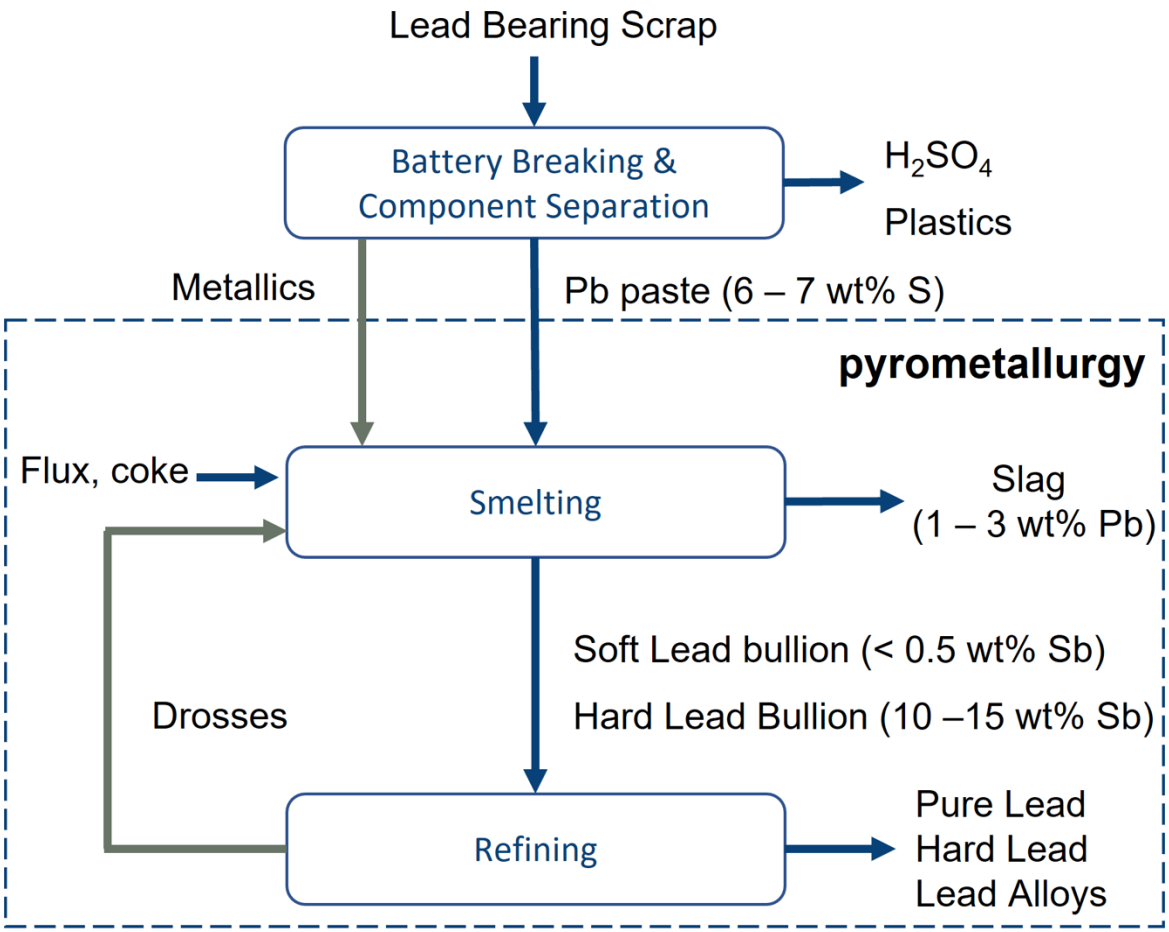

Figure 2.4 Schematic diagram of a pyrometallurgy process. Adapted from Reference.[26]

Smelting can be separated into two methods, direct smelting and indirect smelting. In indirect smelting routes, lead paste is de-sulfurized with de-sulfurizing agents such as soda ash. Then the desulfurized lead paste can then be smelted at a lower temperature to lead bullion. In direct smelting, sulfurized lead compounds are directly smelted and decomposed around 1000 ^{o}C to lead bullion.[27] Based on different types of smelters and furnaces, smelting can be categorized as Queneau-Schumann-Lurgi (QSL) process, Mount Isa Mines (ISASMELT) process, Flash Cyclone Oxygen Electric (KIVCET) process, Top Blown Rotary Converter (TBRC or Kaldo) process, blast furnace, or reverberatory furnace processes.[28]

2.2.1.1 Indirect smelting

In direct smelting, lead paste is desulfurized with aqueous solutions. Then the de-sulfurized paste is smelted in a furnace similarly in the direct smelting process discussed later but at a lower temperature.

2.2.1.1.1 Desulfurization

$PbSO_4$ from lead paste is desulfurized via a desulfurizing agent, which is normally Na_2CO_3 or NaOH solution.[29] The overall simplified reaction of $PbSO_4$ with desulfurizing agent can be shown in Equation 2.6.

$$PbSO_4(s) + Na_2CO_3(aq) \rightarrow PbCO_3(s) + Na_2SO_4\ (aq)$$

Equation 2.6

Although $PbCO_3$ is the ideal final product of the reaction, several by-products can be formed based on pH value and concentration of the Na_2CO_3 aqueous solution, reaction temperature, and $PbSO_4$ concentration.[30] Y. Gong et al. [31] analysed the final products from varying aqueous solution concentrations and reaction temperature and found that $PbCO_3 \cdot 2Pb(OH)_2$ (lead carbonate basic) and $NaOH \cdot 2PbCO_3$ (sodium hydroxide lead carbonate) were the main products at a reaction condition of 50 °C in 0.1 M Na_2CO_3(aq) solution. Additionally, $NaOH \cdot 2PbCO_3$ with trace $PbCO_3$ was formed when $PbSO_4$ was reacted in 0.1 M Na_2CO_3(aq) solution at 89 °C. The formation of these products can be described as shown in Equation 2.7 and Equation 2.8.[31]

$$3PbSO_4(s) + 2Na_2CO_3(aq) + 2H_2O(l) \rightarrow 2PbCO_3 \cdot Pb(OH)_2(s) + 2Na_2SO_4(aq) + 2H_2SO_4(aq)$$

Equation 2.7

$$2PbCO_3 \cdot Pb(OH)_2(s) + 2Na_2CO_3(aq) \rightarrow 3NaOH \cdot PbCO_3(s) + 2NaOH(aq)$$

Equation 2.8

The above study[31] also showed that $PbCO_3$ forms when the concentration of Na_2CO_3(aq) solution is above 0.7 M, and that $PbCO_3$ with trace $NaOH \cdot 2PbCO_3$ was formed in 3.0 M Na_2CO_3(aq) solution at 50 °C.

The lead products based on different reaction conditions are summarized in Table 2.1.

Table 2.1 Products formed with varying of reaction temperature and Na_2CO_3 concentration based on study from Y. Gong et al. [31]

Products summary	Reaction Temperature (°C)	Na_2CO_3(aq) concentration (M)
$PbCO_3 \cdot 2Pb(OH)_2$ Minor $NaOH \cdot 2PbCO_3$	50	0.1
$NaOH \cdot 2PbCO_3$ Trace $PbCO_3$	80	0.1
$PbCO_3$ Minor $NaOH \cdot 2PbCO_3$	50	3.0

2.2.1.2 Direct Smelting

2.2.1.2.1 Blast furnace process

The Varta process was developed by "Varta automotive batteries". The process smelts lead using a shaft or blast furnace. The feed mix including lead concentrates, limestone, coke, iron scrap and fluxes is fed into a vertical shaft furnace. The temperature inside the furnace increases with the depth of the furnace. Oxygen-enriched air is preheated to 400-500 °C and blasted into the furnace through tuyere near the bottom end of the furnace. A schematic diagram of a shaft furnace is shown in Figure 2.5. The operation temperature of the furnace is around 1200-1400 °C where lead concentrates are combusted.[32] The overall reaction in the shaft can be summarized in Equation 2.9.

$$Fe(s) + PbSO_4(s) + CO(g) \rightarrow FeS(s) + Pb(s) + 2CO_2(g) \qquad \textbf{Equation 2.9}$$

During the decomposition of lead concentrates, a molten slag is formed on top of the lead bullion. Slags and lead bullion are tapped out and collected through different holes. During the Varta process, slags only contain 1-3 wt% of metal content with an electricity consumption of the furnace of 160 kWh for every ton (equivalent to 157.5 kWh/tonne) of lead produced.[33] The lead bullion has 25 wt% of alloy impurities[32] and further refining processes are required

to purify it. Alternatively, several advanced processes such as the Kaldo or Mount Isa Mines (ISASMELT) process can be used to smelt lead.

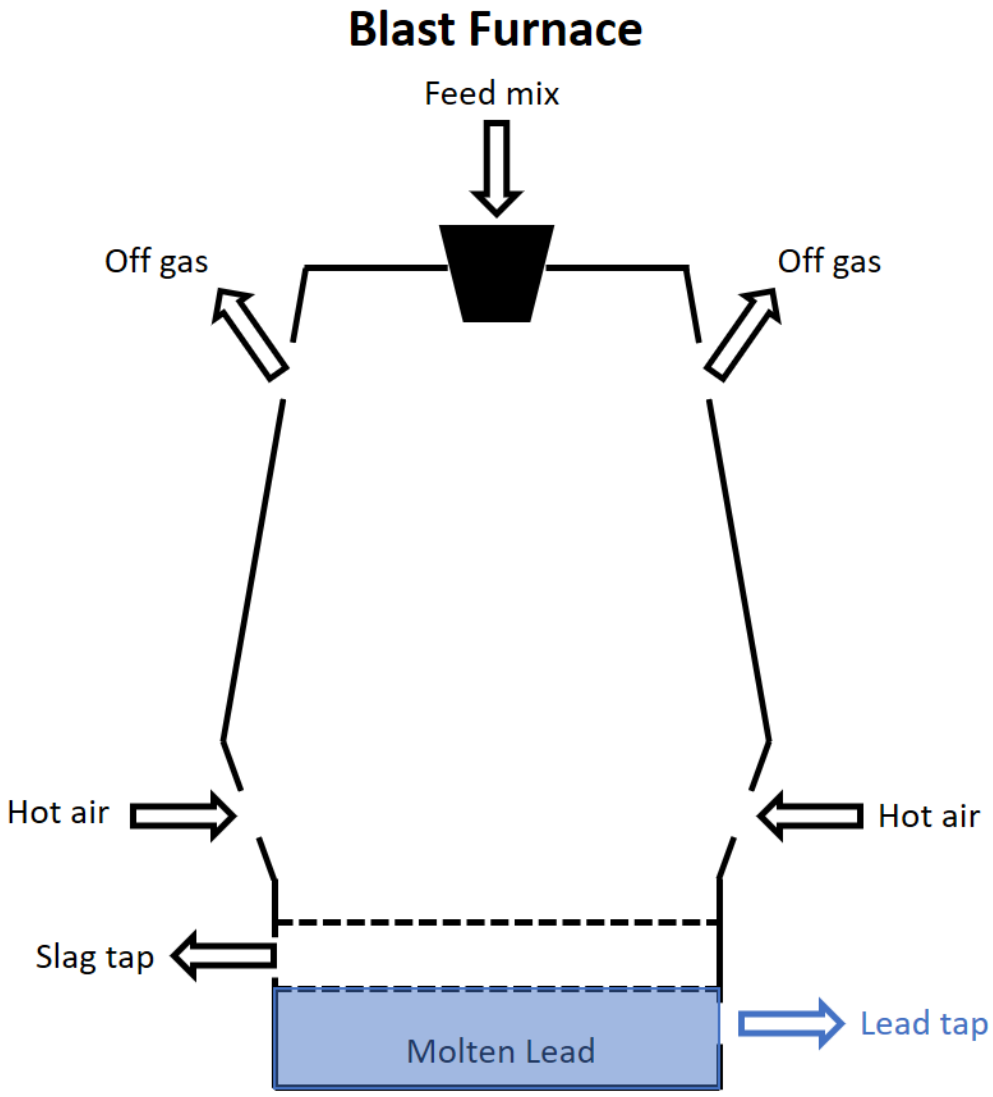

Figure 2.5 Schematic diagram of a blast furnace. Redrawn based on Reference.[34]

2.2.1.2.2 Kaldo Process

The Kaldo process was developed by Boliden AB in Rönnskär in 1976 based on the use of a top blown rotary converter as shown in Figure 2.6.[19] This process was initially used for copper smelting and applied to lead smelting in the early 1980s.

First, lead concentrates, soda, and lime are charged to the furnace. Then O_2 is fed through a lance to the furnace to react with the lead concentrates. The ratio of O_2 to lead concentrates

determines the reaction temperature, which varies based on the concentrate grades.[35] During the reaction, $PbSO_4$ is desulfurized to PbO. Coke is then charged to the furnace to reduce PbO to Pb. Lead slags, of which the Pb concentration is less than 1 wt% are tapped out.[36] The lead bullion remaining in the furnace is collected for refining.

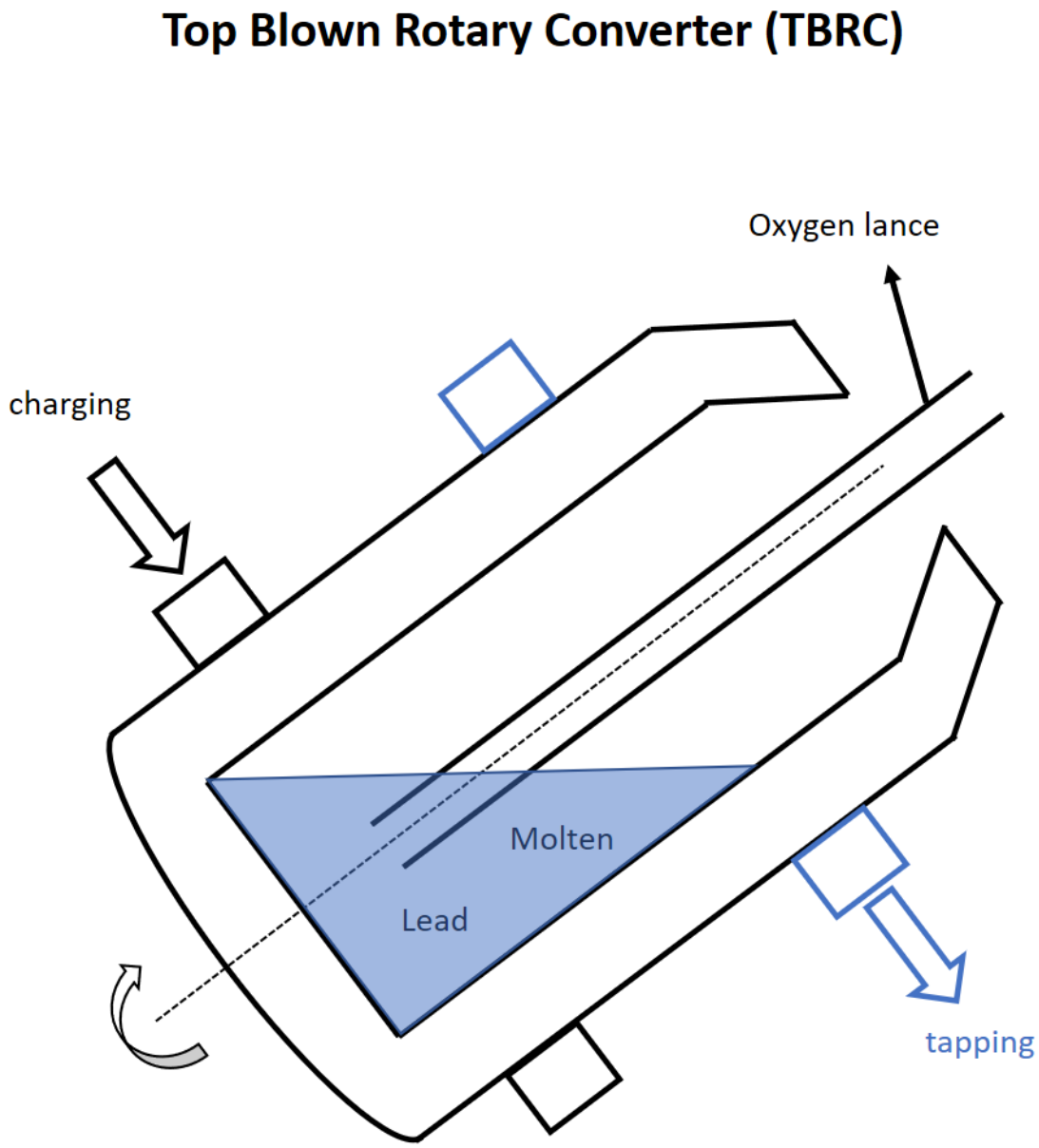

Figure 2.6 Schematic diagram of a TBRC. Redrawn based on Reference.[37]

2.2.1.2.3 ISASMELT or AUSMELT process

The ISASMELT (or AUSMELT) process was initially developed at Mount Isa Mines in 1983 and the process was used for secondary lead smelting in 1991 by a company "Britannia Refined Metals".[38] A schematic diagram of the ISASMELT smelting furnace is shown in Figure 2.7.

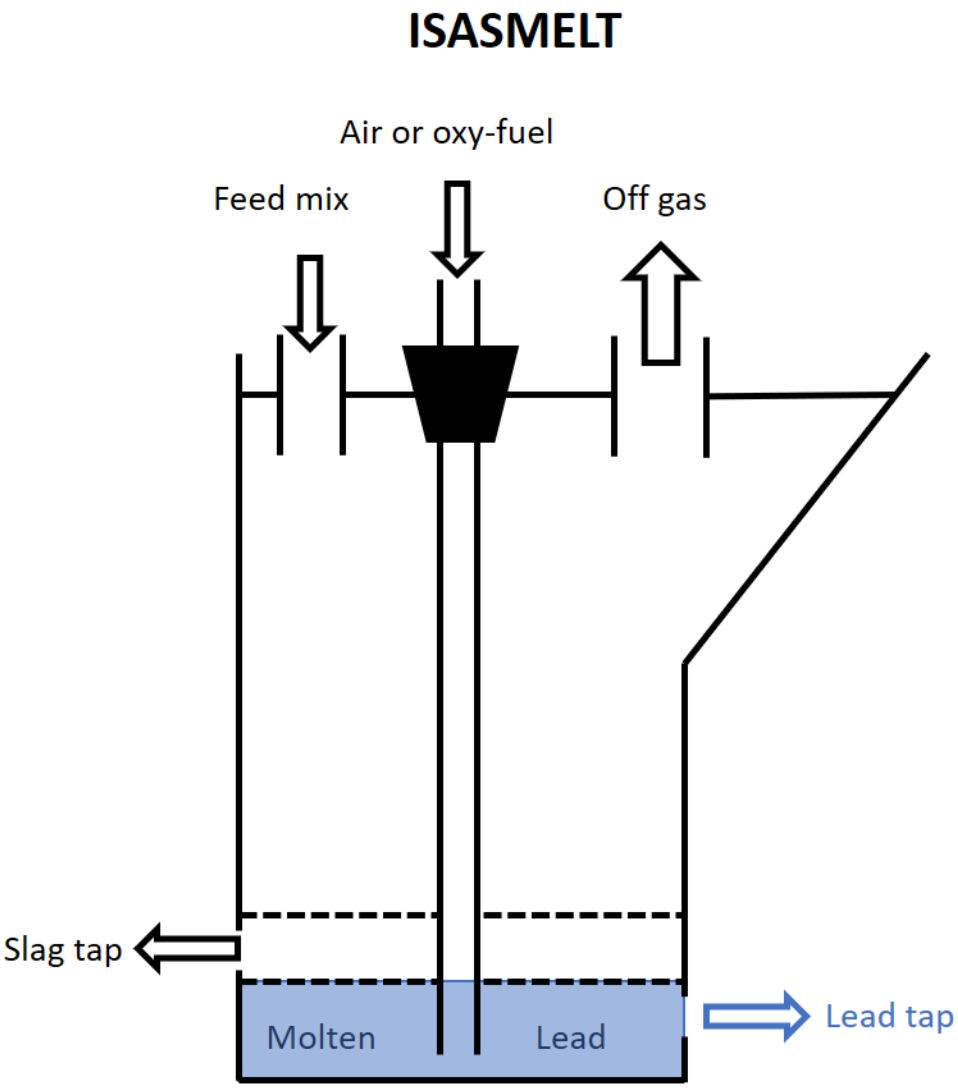

Figure 2.7 Schematic diagram of a ISASMELT smelting furnace. Redrawn based on Reference.[39]

First, a molten slag bath is produced and stays at the bottom of the furnace. Feed materials including lead concentrates and coke, are fed from the top of the furnace to the molten slag. A steel lance is inserted to the bottom of the molten slag layer, through another entrance hole from the roof of the furnace. A conventional ISASMELT smelting furnace has an inner diameter of 4-5 m and the lance used for fuel feeding has a diameter of 0.25- 0.5 m.[40] O_2 or

O_2-enriched air fuel is fed through the steel lance to the molten slag to smelt lead. The feed of fuel and lead concentrates leads to turbulence in the molten bath. The bath turbulence and agitation within the molten bath accelerates the reaction rate.

During the ISASMELT smelting process, soft lead bullion with an Sb content of lower than 0.1 wt% is tapped out from the furnace and then collected for refining.[38] With continuous tapping of soft lead bullion, the molten lead bath becomes Sb rich. The Sb-rich lead slag is then tapped through another hole of the furnace and sent into a rotary furnace to produce hard lead bullion which has an Sb content of up to 20 wt% along with slags.[41] The off-gases generated during the smelting process are cooled to 200 ^oC and vented through a third hole from the roof of the furnace. [38]

2.2.1.2.4 Queneau Schumann Lurgi (QSL) process

The QSL process was initially invented by P. E. Queneau and R. Schuhmann and improved by Lurgi.[42] There are 3 QSL plants globally, situated in Stolberg in Germany, Onsan in South Korea, and Xi'an China. A schematic diagram of the QSL furnace is shown in Figure 2.8. The furnace of the South Korea plant is 41.1 m in length and consists of an oxidation zone and a reduction zone. The oxidation zone has an inner diameter of 4.5 m and a length of 14.4 m, while the reduction zone has an inner diameter of 4 m and a length of 26.7 m.[43]

Lead concentrates, flux and flue dust are thoroughly mixed and then fed into the oxidation zone of the furnace. The feed mix is rapidly dissolved in the molten bath, the temperature of which is around 1000 ^oC. Oxygen is blown into the oxidation zone from the bottom of the furnace. Primary lead bullion, PbO-rich slag, and off-gases are formed in the oxidation zone. Primary lead bullion is tapped out via a siphon at one end of the furnace. Off-gases, which are enriched by SO_2, are cooled to 200 ^oC, emitted via the gas outlet from the oxidation zone and collected in a baghouse to produce sulfuric acid.[42] PbO-rich slag is flowed to the reduction zone.

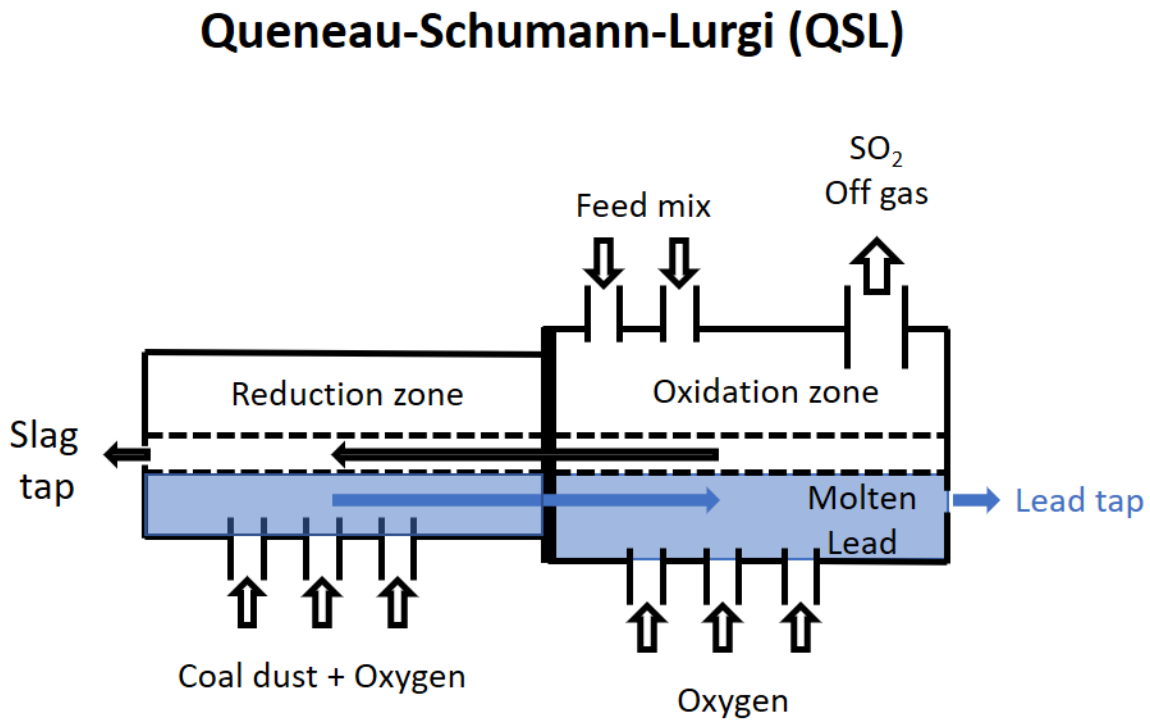

Figure 2.8 Schematic diagram of a QSL furnace. Redrawn based on Reference.[44]

In German plant, the slag has a lead content of 20-30 wt%, while in Korea's plant the slag has a lead content of 35 to 40 wt%.[43] Once the slag is flowed to the reduction zone, oxygen and coal are blown into the reduction zone from the bottom of the furnace. PbO slag is reduced to secondary lead bullion and low Pb content slags. The furnace has a controlled temperature and oxygen level gradient. The temperature in the oxidation zone is around 1000 ^{o}C and increases gradually to 1250 ^{o}C in the reduction zone.[44] Secondary lead bullion and off-gas produced in the reduction zone flow counter-currently, meaning that they flow back to the oxidation zone and are treated the same as products produced from the oxidation zone. Slags is tapped out from another end of the furnace. In German plant, the lead content in the final slag contains 1.6 wt% of lead, while in Korea's plant, the lead content in the final slag contains 5 wt% of lead.[43]

During the process, the off-gas produced from the furnace has a small volume with a high concentration of sulfuric acid. The plant in Germany produces 15,000 Nm^3 off-gas per hour

with a SO_2 concentration of 20 wt%, while the plant in Korea produces 18,000 Nm^3 off-gas per hour with a SO_2 concentration of 24 wt%.[45]

The power consumption in German plant is 115 kWh per tonne of lead produced.[43]

2.2.1.2.5 KIVCET process

KIVCET is an acronym of oxygen cyclone vortex and electrothermic smelting in Russian. The KIVCET process was invented by the VNIITSVETMET Institute in Kazakhstan and installed in 1985.[46] There are 2 KIVCET smelters globally. One is built in Portovesme, Italy (Enirisorse) and another is built in Trail, Canada (TeckCominco Metals). [47] A schematic diagram of a KIVCET furnace is shown in Figure 2.9.

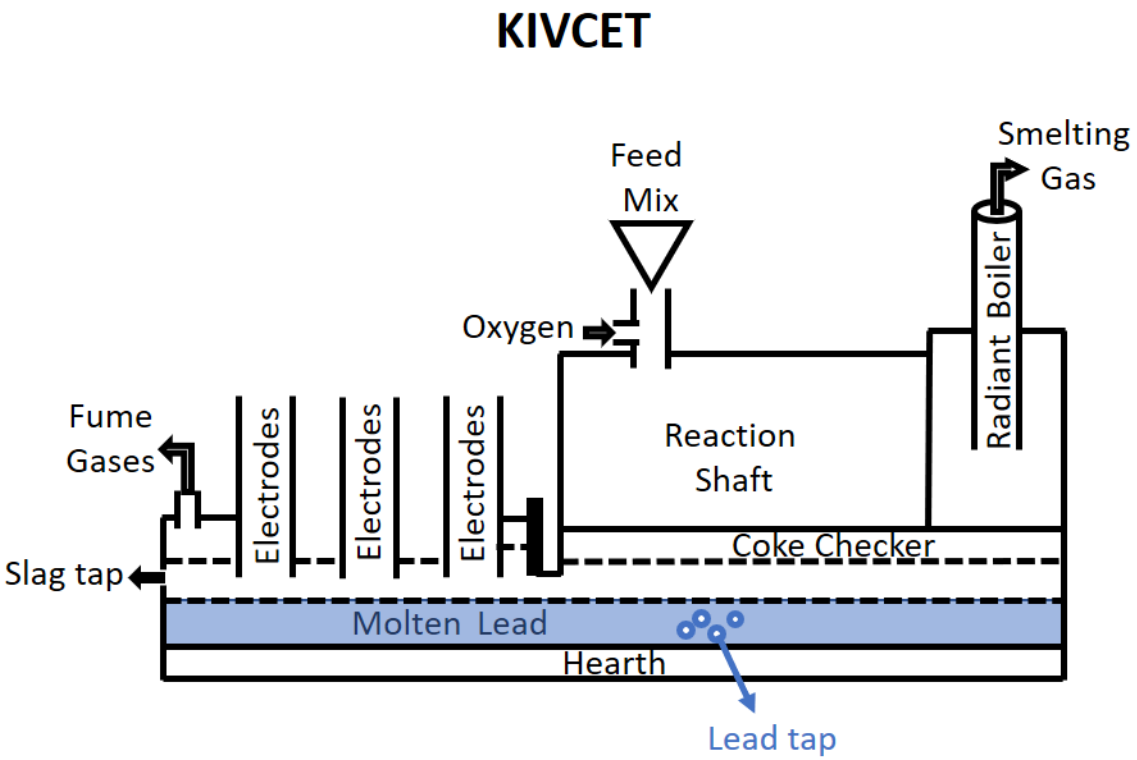

Figure 2.9 Schematic diagram of a KIVCET furnace. Redrawn based on Reference.[48]

Prior to the smelting process, the feed mix, which contains lead concentrates, recycled dust, limestone, coarse coke and coal, needs to be pre-dried to a moisture content of less than

1 wt%.[47] The dried feed mix is then charged to the reaction shaft with oxygen. The weight ratio of oxygen to feed mix determines the lead content in the final products. If the oxygen percentage is too high, this results in a high lead content in the slag, thus, resulting in a lower recovery rate; if the oxygen percentage is too low, then the feed cannot be thoroughly decomposed to form lead bullion, thus, resulting in a lower yield.

Lead concentrates are desulfurized to PbO, which reacts with the coarse coke in the feed mix. The coke can form a layer on the molten slag. The molten slag, which is enriched with PbO, is converted to molten lead by the reduction of coke. The thickness of the coke layer determines the quality of the reduction. The coke layer is called "coke checker" as its thickness can be controlled by temperature. The "coke checker" temperature is maintained at 1100-1200 ^{o}C to achieve an optimum thickness of 0.1 to 0.15 m.[47] A higher "coke checker" temperature leads to a thinner layer while a lower "coke checker" temperature leads to a thicker layer. This procedure is critical to control the lead content in the slag.

Slags and lead bullion flow into the electric furnace where three in-line electrodes are to provide heat to keep them in the molten state. During the flow process, the heavy molten lead sinks to the bottom of the furnace, and the molten lead and slags can be tapped separately.

The off-gas is cooled to 350 ^{o}C and exits via a radiant boiler. The volume of off-gas is 21,000 Nm^3 per hour in Italian plant and an output of 12,000 Nm^3 per hour in Canadian plant.[45] Both output off-gases have an SO_2 concentration from 12-15 wt%.

2.2.1.3 Refining

After the lead is smelted, a refining process is required to remove impurities from the lead bullion. The main impurities of lead bullion from LAB smelting are Sb, Cu, and Sn with limited As, Bi, Ag, and Zn.[49] These impurities can be removed by pyrometallurgical refining processes, which consist of a sequence of treatments to remove different elements.[45]

2.2.1.3.1 Decoppering

For Cu-rich lead bullion, the majority of Cu is removed by temperature control. As the temperature of the molten lead bath decreases, Cu floats on top of the lead bath and forms a layer of Cu-rich dross. After the Cu-rich dross is removed, the residual copper in the lead bullion can be removed by adding sulphur to the lead bath. Cu is sulphurized to form CuS and CuS_2 at 350 ^oC, lowering the Cu content in the lead bath to lower than 0.001 wt%.[49]

2.2.1.3.2 Sn, As, and Sb removal

After Cu is removed, oxygen or oxygen-rich air is injected into the lead bath. The lead bath is heated to 593-649 ^oC.[50] At this stage, Sn and As is oxidized and removed from the molten lead. Then the molten lead is heated further to 750 ^oC to oxidize Sb.[49]

Alternatively, Sn, As and Sb can be removed through the Harris process, where a molten lead bath is stirred with a molten mixture of of NaOH and $NaNO_3$ at a temperature between 400-450 ^oC.[49] The molten NaOH and $NaNO_3$ are added in a stoichiometric ratio so that they preferentially react with impurities.[50] Sn, As, and Sb are removed from the lead bath as oxides or oxysalts.

2.2.1.3.3 Ag, Zn, and Bi removal

The removal of Sn, As, and Sb is called the “softening” process. Subsequently, Ag is removed by the Parkes process, where zinc (<1 wt%) is added to the lead bath.[51] During the process, Ag reacts with Zn and forms an intermetallic layer on top of the molten lead. The mixture is then cooled to 370 ^oC at which point the intermetallic forms a crust and can be removed from the molten lead. Then the lead bath is heated to 500 ^oC to remove residual Zn (0.5 to 0.6 wt%) through vacuum distillation.[49,51] Finally, Bi is removed through the Kroll-Betterton process, where Ca and Mg are added.[49] During this process, Bi is converted to Ca_3Bi_2 and Mg_3Bi_2. $NaNO_3$ is used to remove residual Ca and Mg. The refined lead has a Bi content of lower than 0.005-0.01 wt%.[51]

2.2.1.4 Drawbacks of pyrometallurgy

Though pyrometallurgy is a mature process for LAB recycling in industry, the pollution issue of SO_2 and lead particulates to the environment cannot be ignored. A study in Taiwan has shown that workers exposed to a lead environment over a long period of time have a blood lead level (BLL) of 36.2 ± 12.4 μg/dl which is 3 times higher than the standard level of 10 μg/dl in adults,[52] even if the workers followed the safety protocols during working. The situation is significantly worse for informal LAB recycling. In an informal LAB recycling plant, the recycling process are carried out without safety and health protocols due to limited knowledge of the toxicity of lead. In these working environments, workers are at high risks of lead exposure and the informal battery recycling plant also brings hazards to local people. A community in the suburbs of Dakar, Senegal reported 18 deaths of children from November 2007 to March 2008 due to lead exposure from LAB recycling.[53] The study also showed that the BLL in adults from that community were as high as 55.5 ± 19.0 μg/dl, and 129.5 ± 92.4 μg/dl in children. Lead exposure comes not only from particulates inhalation but also comes from soil and water due to improper treatment of waste streams from the recycling plant. The dust containing lead is blown into the air and settles down in the soil, contaminating the local environment, including areas where young children play. Young children thus often have a higher BLL than adults due to ingestion of lead from hand-to-mouth behaviour on these lead-contaminated areas. The report has also shown that the lead level in soil in Dakar has achieved 14,000 mg/kg indoors and 302,000 mg/kg outdoors.[53] Moreover, food grown on this lead-rich soil is also lead contaminated. While people consume these foods, they unknowingly consume lead as well. Additionally, the informal recycling company may pour the lead-rich water from the waste stream directly into the local water bodies or ground,[54] increasing the lead level in drinking water.

From the drawback of pyrometallurgy described above, hydrometallurgy, an alternative process, has been also used for LAB recycling.

2.2.2 Hydrometallurgy

Hydrometallurgy is a method which uses an aqueous solution to dissolve lead materials (mainly lead paste) from LABs. $PbSO_4$ and PbO_2 are the main components of lead paste.[24]

Dissolving $PbSO_4$ and PbO_2 with an aqueous solution is the main challenge in hydrometallurgy processes. After lead goes into the solution, it will be recovered to metallic lead through an electrochemical process from the lead-bearing solution.

2.2.2.1 Revere smelting refining (RSR) process

The RSR process was developed in 1980 by Raymond D. Prengaman and Herschel B. McDonald from the RSR Corporation.[55] In the RSR process, the main component, $PbSO_4$ is firstly desulfurized with $(NH_4)_2CO_3$. The reaction can be described as shown in Equation 2.10.

$$PbSO_4(s) + (NH_4)_2CO_3(aq) \rightarrow PbCO_3(s) + (NH_4)_2SO_4(aq) \quad \textbf{Equation 2.10}$$

Another component of lead paste, PbO_2 can be reduced via two methods. The first method is to heat the battery sludge in a reducing atmosphere (by adding a reducing agent or blast reducing flame to the reaction shaft) to 290-300 ^oC.[56] As PbO_2 is a strong oxidizing material, it can react rapidly with the reducing components to form PbO, which can be easily dissolved in an electrolyte for further processing. Temperature control is the most important issue during PbO_2 reduction, as it can also easily be reduced to Pb_2O_3 and Pb_3O_4, which are not easily dissolved in an electrolyte making electrowinning or electrodeposition difficult.[56] Moreover, the temperature also needs to be controlled to below 325 ^oC to avoid the formation of metallic lead and volatile dust.[56]

The second method is to reduce PbO_2 through a chemical reaction, which is easier to control than the first method. PbO_2 is reduced with ammonium or alkali (abbreviated as Alk) carbonates aqueous solution with addition of SO_2.[55] The Alkali material can be lithium, sodium or potassium, but preferable aqueous solutions are sodium and ammonium carbonate.[56] The reaction can be described as shown in Equation 2.11 and Equation 2.12.[55]

$$2PbO_2(s) + (Alk)_2CO_3(aq) + 2(Alk)HSO_3(aq) + H_2O(l) \rightarrow PbCO_3 \cdot Pb(OH)_2(s) + 2(Alk)_2SO_4(aq)$$

Equation 2.11

$$PbO_2(s) + PbSO_4(s) + (Alk)_2CO_3(aq) + (Alk)_2SO_3(aq) + H_2O(l) \rightarrow PbCO_3 \cdot Pb(OH)_2(s) + 2(Alk)_2SO_4(aq)$$

Equation 2.12

After the paste is desulfurized to PbO, $PbCO_3$ or $PbCO_3 \cdot Pb(OH)_2$, they are separated from the battery sludge. They are then dissolved in an electrolyte, which can either be H_2SiF_6 or HBF_4.[56] The concentration of the electrolyte is adjusted to 120-300 g/L and the concentration of lead is adjusted to 50 to 200 g/L to maximize the recovery rate and electrowinning performance.[56] H_3BO_3 is added to the electrolyte to prevent the production of HF during the electrowinning process.

During the electrowinning process, the electrolysis is operated at a voltage of 2-4 V and a current density of 15-50 A/m^2.[56] Although a higher current density provides faster lead deposition on the cathode, PbO_2 is deposited on the anode and impurity ions are deposited as its corresponding metal on the cathode, affecting the electrowinning performance. With the addition of As in the electrolyte, the formation of PbO_2 on the anode can be prevented.[55]

Although optimal conditions for electrolysis are chosen to minimize the deposition of impurity ions, this cannot be prevented. The cathode which contains limited amounts of Sb, As Cu and Fe could lead to failure of the electrode in a battery.[55] Thus, in industrial applications, the cathode obtained from the RSR process needs to be purified for further uses.

2.2.2.2 Bureau of Mines process

The Bureau of Mines process was invented by E.R. Cole, A.Y. Lee and D.L. Paulson from the Bureau of Mines Rolla Research Center in 1981.[55] This process, which is similar to the RSR process, utilizes $(NH_4)_2CO_3$ and $(NH_4)HSO_3$ to desulfurize the lead paste. The desulfurized lead

paste, which mainly consists of $PbCO_3$ and unreacted PbO_2, is then added to an electrolyte, H_2SiF_6, with the addition of lead powder. The lead powder comproportionate with unreacted PbO_2 at 50 °C as shown in Equation 2.13 to form PbO, which can be dissolved in H_2SiF_6.[57] The reaction of $PbCO_3$ and PbO with H_2SiF_6 can be shown in Equation 2.14 and Equation 2.15, respectively.[57]

$$PbO_2(s) + Pb\ (s) \xrightarrow{H_2SiF_6(aq)} 2PbO(aq\ in\ H_2SiF_6) \quad \textbf{Equation 2.13}$$

$$PbCO_3(s) + H_2SiF_6(aq) \rightarrow PbSiF_6(aq) + H_2O(l) + CO_2(g) \quad \textbf{Equation 2.14}$$

$$PbO(s) + H_2SiF_6(aq) \rightarrow PbSiF_6(aq) + H_2O(l) \quad \textbf{Equation 2.15}$$

The solution, which contains 100 g/L Pb in the form of $PbSiF_6$ and 90/L free H_2SiF_6, will then be electrowon at conditions of 35-40 °C, a voltage of 60-100 mV and a current density of 170-180 A/m^2 to recover lead.[58]

During the electrowinning process, PbO_2 forms on the anode while Pb is deposited on the cathode. In the Bureau of Mines process, a phosphorus (P) compound at a concentration of 0.75-3 g/L of P, preferably 1.5-2.5 g/L, is added to the electrolyte to prevent the formation of PbO_2 on the anode.[57] Though H_3PO_4 is most commonly used, other phosphorus compounds such as $(NH_4)_3PO_4$, organic phosphorus compounds and phosphorus oxides can also be used. A study from the Bureau of Mines Research Centre has shown that the ratio of Pb deposited on the cathode to the ratio of PbO_2 deposited on the anode is 1 : 1 in an electrolyte without phosphorous, while this ratio is decreased to 1 : 100 when 1.5 g/L P was added to the electrolyte.[59]

Additionally, a study has shown that during the electrowinning process a current density exceeding 200 A/m^2 results in the growth of dendrites, knobs or wires on the cathode.[60] The phenomenon is referred to as “cathode polarization”. The “cathode polarization” can be minimized by the addition of levelling agents such as animal glue, aloes, or calcium lignin. In this case, a combination of 0.6 g/L animal glue and 4.0 g/L calcium lignin sulfonate[58] or a

combination of 0.02-0.04 g/L bone gelatin and 4.0 g/L calcium lignin sulfonate [59] were added to the electrolyte as levelling agents to provide smooth deposition.

The overall electrowinning chemical reaction on both electrodes and corresponding electrode potential are summarized as Equation 2.16, Equation 2.17 and Equation 2.18.[59]

$$\text{Cathode: } 2PbSiF_6(aq) + 4H^+(aq) + 4e^- \rightarrow 2Pb(s) + 2H_2SiF_6(aq) \qquad E_c^\circ = -0.126\ V$$

Equation 2.16

$$\text{Anode: } 2H_2O(l) \rightarrow O_2(g) + 4H^+(aq) + 4e^- \qquad E_a^\circ = -1.23\ V$$

Equation 2.17

$$\text{Total: } 2PbSiF_6(aq) + 2H_2O(l) \rightarrow 2Pb(s) + O_2(g) \qquad E_t^\circ = -1.356\ V$$

Equation 2.18

The purity of the deposited lead can achieve 99.99 % at an average recovery rate of 92% using the above conditions with an energy consumption of the procedures is 0.7 kWh per 1 kg lead produced.[58]

2.2.2.3 Engitec process

The Engitec process was invented in 1988 by Marco Olper and Pierluigi Fracchia from the Engitec Technologies.[61] The process desulfurizes the lead pasted using a method similar to that described in the desulfurization of the indirect smelting process. $PbSO_4$ from the sulfurized paste is converted to $PbCO_3$ or $PbCO_3{\cdot}Pb(OH)_2$ as shown in Equation 2.6 and Equation 2.7. The solution mixture is maintained at 30-40 °C in order to separate lead compounds from the solution through hot filtration without crystallisation of Na_2SO_4.[61] Then the desulfurized lead paste is leached with an electrolyte, H_2BF_4. All lead compounds except PbO_2 and Pb can be dissolved in HBF_4. A reducing agent, H_2O_2, needs to be added to dissolve PbO_2 and Pb. The redox reaction can be described as shown in Equation 2.19 and Pb undergoes comproportionation reaction with PbO_2 as shown in Equation 2.20.[55] The sign of

completion of the reaction is that the paste turns from brown/red to grey.[62] The residual paste contains 25% of lead and other impurities such as Ag, Sb and Bi.[61,62] Through these reactions, 75% of Pb from lead paste converts into the electrolyte solution, which can be then electrolysed to recover lead.

$$PbO_2(s) + H_2O_2(aq) + 2HBF_4(aq) \rightarrow Pb(BF_4)_2(aq) + 2H_2O(l) + O_2(g) \quad \textbf{Equation 2.19}$$

$$Pb(s) + PbO_2(s) \xrightarrow{H_2O_2(aq)} 2Pb^{2+}(aq) \quad \textbf{Equation 2.20}$$

The recovery rate of lead was found to be 96 % without the formation of PbO_2 on the anode when the electrolysis was operated at a current of 7.4 A, a voltage of 2.9 V, and a cathodic current density of 300 A/m^2.[62] The excessive H_2O_2 helps the redissolution of PbO_2 generated on the anode back into the electrolyte solution.

The energy consumption of the electrowinning process is 0.8 kW·h per kg of lead produced, which is slightly higher than the Bureau of Mines process.[63]

2.2.2.4 Ginatta process

The Ginatta process was developed by Marco Ginatta in 1984 using a similar method as described in the Engitec process but with additives in the electrolyte. The process uses (1) Co in the electrolyte as a PbO_2 deposition inhibitor on the anode and (2) Triton X-100 polymer (C_8H_{17}-(C_6H_4)-(OCH_2)$_{9\text{-}10}$OH) and phenolphthalein as levelling agents to allow operation at a higher current density.[64]

Under electrowinning processes, the reaction happening at the anode is the same as shown in Equation 2.17. In real applications, the anode potential is higher than the theoretical value that is required to drive the reaction. The difference between the actual value and the theoretical value is referred to as “overpotential” of the anode. If the overpotential is too high, PbO_2 is preferably deposited on the anode.[65] A study has shown that the addition of 20 mg/L Co in the electrolyte can lower the overpotential by 0.117 Volt.[65] The decrease in the overpotential of the anode is possibly due the change in reaction at the anode. Co^{2+} in the

reaction is oxidised to Co^{3+}, which acts as a catalyst for the oxidation of water at the anode as shown in Equation 2.21 and Equation 2.22.[66]

$$Co^{2+}(aq) \rightarrow Co^{3+}(aq) + e^{-} \quad \textbf{Equation 2.21}$$

$$4CoOH^{2+}(aq) \rightarrow 4Co^{2+}(aq) + O_2(g) + 2H_2O(l) \quad \textbf{Equation 2.22}$$

Another problem during the electrowinning process is the deposition of Sb from Sb^{3+} on the cathode, which affects the purity of the deposited lead. To solve this issue, a small amount of PbO_2 can be added near the anode area to oxidize Sb^{3+} to Sb^{5+}.[67] The excess PbO_2 is consumed by the excess H_2O_2 in the solution. Sb is stabilized as Sb^{5+} to avoid deposition on the cathode The optimal concentration of Sb is maintained at 250-1000 mg/L and cannot exceed 3000 mg/L to avoid precipitation of Sb.[64,67]

Using the above conditions, the electrowinning process can be operated at 40 °C at a cell voltage of 2.7 V, cathodic current density of 400 A/m^2 and an anodic current density of 800 A/m^2 with the addition of levelling agents at a concentration of 0.2 g/L Trition X-100 and 0.1 g/L phenolphthalein to achieve a Pb cathode with 99.99 % purity.[64]

2.2.2.5 Ammoniacal ammonium sulfate (AAS) process

The AAS process was developed by William B. Moure Jr. and Thomas H. Etsell in 1993.[68] The process uses an aqueous solution, AAS, which is a mixture of NH_4OH and $(NH_4)_2SO_4$, to dissolve $PbSO_4$ from the lead paste. Then lead is recovered from the solution via electrolysis or a steam distillation method.

The concentrations of NH_4OH and $(NH_4)_2SO_4$ in the AAS are 140 g/L and 210 g/L, respectively.[69] The ratio is selected to achieve the highest solubility of lead (100 g/L Pb in solution). The lead species in solution are of the form $[Pb(OH)SO4]^-$. The chemical reaction in the solution can be expressed as shown in Equation 2.23.

$$PbSO_4(s) + NH_4OH(aq) \rightarrow (NH_4)[Pb(OH)SO_4](aq) \quad \textbf{Equation 2.23}$$

However, the AAS solution itself cannot dissolve PbO_2. PbO_2 needs to be converted to $PbSO_4$ with concentrated H_2SO_4 aqueous solution (>50 wt%) at over 80 °C.[68] Then the $PbSO_4$ can be dissolved in AAS solution. Excessive H_2SO_4 can be neutralized by the AAS solution.

After the lead is dissolved in the solution, it can be recovered via electrolysis methods. The electrolysis is operated at a current density of 350 A/m^2 to achieve a current efficiency of above 95%.[68,69]

Alternatively, Pb can be recovered from the Pb-bearing AAS solution using a steam distillation method. During distillation, Pb species in the solution are crystallized in the form of $PbSO_4{\cdot}(NH_4)_2SO_4$ or $PbO{\cdot}PbSO_4$. The chemical reactions occurring during distillation are shown in Equation 2.24 and Equation 2.25, and the mixture of crystals can be converted to $PbSO_4$ when heated between 110 °C to 120 °C as shown in Equation 2.26.[69]

$$(NH_4)[Pb(OH)SO_4](aq) + (NH_4)_2SO_4(aq) \rightarrow PbSO_4 \cdot (NH_4)_2SO_4(aq) + NH_3(g) + H_2O(l)$$

Equation 2.24

$$2(NH_4)[Pb(OH)SO_4](aq) \rightarrow PbO \cdot PbSO_4(s) + (NH_4)_2SO_4(aq) + H_2O(l)$$

Equation 2.25

$$PbO \cdot PbSO_4(s) + PbSO_4 \cdot (NH_4)_2SO_4(s) \rightarrow 3PbSO_4(s) + 2NH_3(g) + H_2O(l)$$

Equation 2.26

2.2.2.6 Plomo Acido (Placid) process

The Placid process is a commercialized process to dissolve lead compounds in the lead paste using HCl and brine solution instead of using H_2SiF_6 or HBF_4. The dissolution of the main lead compounds ($PbSO_4$, PbO, PbO_2 and Pb) is shown in Equation 2.27, Equation 2.28, and Equation 2.29.[55,70] PbO can be dissolved directly in HCl solution, PbO_2 and Pb are dissolved via

comproportionation reaction and $PbSO_4$ is dissolved in brine solution at a maximum temperature of 80 °C.[70] The impurities from other metals are also dissolved in the solution in the form of $MeCl_2$(aq), where Me represents all other metal impurities. $MeCl_2$(aq) can be converted to metallic form by a displacement reaction with lead powder as shown in Equation 2.30.[41]

$$PbO(s) + 2H^+(aq) + 2Cl^-(aq) \rightarrow PbCl_2(s) + H_2O(l) \quad \textbf{Equation 2.27}$$

$$Pb(s) + PbO_2(s) + 4H^+(aq) + 4Cl^-(aq) \rightarrow 2PbCl_2(aq) + 2H_2O(l) \quad \textbf{Equation 2.28}$$

$$PbSO_4(s) + 2Na^+(aq) + 2Cl^-(aq) \rightarrow PbCl_2(aq) + 2Na^+(aq) + SO_4^{2-}(aq) \quad \textbf{Equation 2.29}$$

$$Me^{2+}(aq) + Pb(powder) \rightarrow Me(s) + Pb^{2+}(aq) \quad \textbf{Equation 2.30}$$

Na_2SO_4 obtained in the solution as shown in Equation 2.29 can be converted to brine solution and $CaSO_4$ with the use of $Ca(OH)_2$. Then the solution can be electrolysed to recover Pb and HCl solution. HCl and brine solutions can be re-used to dissolve a new batch of lead paste. The electrolysis is operated at a current density of 1000 to 1200 A/m^2 with 5 electrode cells in a plant near Madrid, Spain, the yield of which can achieve 730 tonnes of lead per year at an energy cost of 1300 kWh/tonne of lead produced.[70]

2.2.2.7 Aqua Metals process

The process was developed by Aqua Metals Inc. in 2014, which uses methane sulfonic acid (MSA, CH_3SO_3H) and a chelator, ethylenediaminetetraacetic acid (EDTA), to dissolve waste battery materials including $PbSO_4$, PbO, PbO_2.[71] PbO can be rapidly dissolved in MSA solution, the chemical reaction of which can be shown in Equation 2.31.[71] $PbSO_4$ does not have a high solubility in pure MSA solution, thus, EDTA is added to improve the solubility. It has been reported that a solution which contains 330 $\pm$ 60 g/L MSA and 45 g/L Na_2(EDTA) can dissolve around 75 g waste battery materials per 1 L of solution used.[72] Na_2(EDTA) is used as it has a higher solubility in MSA in solution than EDTA. Alternative chelators such as NTA, IDA, DTPA and its corresponding salt can also be used.[73] After lead is dissolved in the solution, it can be

recovered by electrochemical processes. The reaction of electrolysis at the cathode is shown in Equation 2.32.[74]

$$PbO(s) + 2CH_3SO_3H(aq) \rightarrow Pb(CH_3SO_3)_2(aq) + H_2O(l) \quad \textbf{Equation 2.31}$$

$$Pb(CH_3SO_3)_2(\text{aq}) + 2e^- \rightarrow Pb(s) + 2CH_3SO_3{}^-(aq) \quad \textbf{Equation 2.32}$$

The electrolysis is operated at a current density of between 100 A/m^2 to 1000 A/m^2 at a maximum temperature of 80 ^{o}C with purity of 99.5%.[71,73] Lead is deposited on the cathode in a soft nanoporous form instead of in a sheet/film form and can be easily removed from the cathode.[73] The nanoporous form is preferrable as removal of sheets/films is labour intensive and may cause deposit to break.[72]

2.2.2.8 Drawbacks of Hydrometallurgy

Although hydrometallurgy does not emit any hazardous particulates and gases into the environment and has eliminated the major drawback of pyrometallurgy, the energy cost, mainly from the electrolysis process in hydrometallurgy, is much higher than pyrometallurgy. A study has shown that the energy cost for pyrometallurgy is $43.9-59.2 per ton of lead produced, while the energy cost for hydrometallurgy is $72.4-103.9 per ton of lead produced.[75] Pyrometallurgy is now still more economically favourable in industry due to the higher energy cost in hydrometallurgy. Moreover, the use of strong acids such as H_2SiF_6 and HBF_4 is also a potential risk for workers. HF and SiF_4 gases may also be produced during hydrometallurgy processes when the reaction temperature is above 60 ^{o}C.[76] HF can penetrate deeply the human skins and cause irreversible damage to bones and tissues. The consequence of HF exposure for industrial workers is as severe as exposure to lead particulates. These strong acids are also corrosive to metal components. As a result, this leads to higher capital cost as the metallic parts from either the leaching or electrolysis equipment needs to be replaced regularly due to corrosion or dissolution from the strong acid electrolytes.[75] Additionally, all hydrometallurgy leaching/dissolution processes require a large amount of water. This leads to higher resource consumption for hydrometallurgy processes.

Based on the drawbacks discussed above, it is clear that a greener process needs to be developed, which is both less toxic and requires lower energy consumption. Vasant Kumar from Cambridge University has developed a method to dissolve and leach the waste battery materials followed by a low-temperature calcination procedure. This is known as the Aurelius process, and it has been commercialized as the company "Aurelius Technologies Ltd.".

2.2.3 Leaching followed by precipitation method – the Aurelius process

The Aurelius process involves the use of a carboxylic acid aqueous solution to dissolve lead compounds from a waste LAB. Lead compounds (PbO, PbO_2 and $PbSO_4$) are leached out from the solution as a lead organic precipitate, which will then be calcined at a temperature lower than 500 ^oC to form PbO.[77,78] Initial leaching studies were done on individual pure lead compounds to analyse their corresponding leaching product. PbO is leached out as $PbC_6H_6O_7{\cdot}H_2O$(mono-lead citrate) with the use of pure $C_6H_8O_7{\cdot}H_2O$ (citric acid hydrate) aqueous solution as shown in Equation 2.33, while PbO_2 is leached out as the same product ($PbC_6H_6O_7$) with a mixture of $C_6H_8O_7{\cdot}H_2O$ and H_2O_2 aqueous solution as shown in Equation 2.34.[78] $PbSO_4$ is leached out as $Pb_3(C_6H_5O_7)_2{\cdot}3H_2O$ (tri-lead citrate) with the use of a mixture of $C_6H_8O_7{\cdot}H_2O$ and $Na_3C_6H_5O_7{\cdot}2H_2O$ (trisodium citrate dihydrate) as shown in Equation 2.35.[77] A subsequent study was conducted on actual battery paste containing 64.5 wt% $PbSO_4$, 29.5 wt% PbO_2, 4.5 wt% PbO, 1.0 wt% Pb and 0.5 wt% impurity) in Li's study.[79] In the study, the battery paste was leached out through a solution of $C_6H_8O_7{\cdot}H_2O$, $Na_3C_6H_5O_7{\cdot}2H_2O$ and H_2O_2. $Pb_3(C_6H_5O_7)_2{\cdot}3H_2O$ is converted to mono-lead citrate at excessive $C_6H_8O_7{\cdot}H_2O$ as shown in Equation 2.36.[79]

$$PbO(s) + C_6H_8O_7 \cdot H_2O(aq) \rightarrow Pb(C_6H_6O_7) \cdot H_2O(s) + H_2O(l)$$

Equation 2.33

$$PbO_2(s) + C_6H_8O_7 \cdot H_2O(aq) + H_2O_2(aq) \rightarrow Pb(C_6H_6O_7) \cdot H_2O(aq) + O_2(g) + 2H_2O(l)$$

Equation 2.34

$$3PbSO_4(s) + 2Na_3C_6H_5O_7 \cdot 2H_2O(aq) \rightarrow Pb_3(C_6H_5O_7)_2 \cdot 3H_2O(s) + 3Na_2SO_4(aq) + H_2O(l)$$

Equation 2.35

$$Pb_3(C_6H_5O_7)_2 \cdot 3H_2O(s) + C_6H_8O_7 \cdot H_2O(aq) \rightarrow 3Pb(C_6H_6O_7) \cdot H_2O(s) + H_2O(l)$$

Equation 2.36

Both $PbC_6H_6O_7$ and $Pb_3(C_6H_5O_7)_2 \cdot 3H_2O$ obtained from battery paste can be calcined at around 380 °C to PbO in an O_2-enriched air, and to Pb in N_2 atmosphere.[79,80] This initial process is simple and has low energy consumption, but it requires a long reaction time for precipitating lead citrate. The addition of acetic acid increases the reaction rate significantly.[81]

The lead compounds can be leached out with the use of a mixture of acetic acid (CH_3COOH or HAc), $Na_3C_6H_5O_7 \cdot 2H_2O$, and H_2O_2. The dissolution of PbO and PbO_2 in HAc is similar to $C_6H_8O_7 \cdot H_2O$, but with replacement by HAc as shown in Equation 2.37 and Equation 2.38, lead acetate is then converted into tri-lead citrate as shown in Equation 2.39.[82] As lead acetate is more soluble, it can stay in the solution without contaminating the precipitates. The role of HAc and $C_6H_8O_7 \cdot H_2O$ in $PbSO_4$ dissolution is similar with both functioning as a buffer function.

$$PbO(s) + 2CH_3COOH(aq) \rightarrow Pb(CH_3COO)_2(aq) + H_2O(l)$$

Equation 2.37

$$PbO_2(s) + 2CH_3COOH(aq) + H_2O_2(aq) \rightarrow Pb(CH_3COO)_2(aq) + O_2(g) + 2H_2O(l)$$

Equation 2.38

$$Pb(CH_3COO)_2(\text{aq}) + 2Na_3C_6H_5O_7 \cdot 2H_2O(s) \rightarrow Pb_3(C_6H_5O_7)_2 \cdot 3H_2O(s) + 6NaCH_3COO(aq) + H_2O(l)$$

Equation 2.39

The use of acetic acid also leads to less consumption of reagents when dissolving actual lead paste. The consumption of HAc and $Na_3C_6H_5O_7 \cdot 2H_2O$ are 0.0092 mol and 0.0048 mol,

respectively, for each gram of lead paste, while the consumption of $C_6H_8O_7 \cdot H_2O$ and $Na_3C_6H_5O_7 \cdot 2H_2O$ are 0.011 mole and 0.0064 mol, respectively.[82] Additionally, the leaching time when using acetic acid decreases from 8 hours to 2 hours when dissolving 10 grams of lead paste.

This dissolution followed by a low-temperature calcination process is both environmental-friendly and energy-saving as it costs 0.25 kWh per kilogram of Pb produced.[81] However, this process still requires a large amount of water to dissolve reactants. Therefore, to overcome this issue, a non-aqueous system such as ionic liquids (ILs) can be considered as an alternative medium to dissolve lead paste.

2.3 Solvent Development

2.3.1 Ionic liquids (ILs)

Ionic liquids are molten salts which consist of cations and anions. ILs, with a melting temperature lower than 100 ^oC, are classified as room temperature ionic liquids (RTILs).[83] The cation of an IL is normally imidazolium, and the anion of an IL is normally a quaternary ammonium salt. Although ILs have saved large amounts of water as an alternative potential medium for dissolving lead, the viscosity of ILs is normally higher than conventional aqueous solvents. The viscosity of ILs ranges from 10-1000 cp which is much higher than that of water (viscosity = 0.89 cP at 25 ^oC).[84,85] High viscosity results in poor mass transport of the ions, thus, affecting the reaction rate when it will be used for dissolving lead paste. Additionally, the synthesis of an IL is complicated making the production cost economically uncompetitive. Moreover, ILs are toxic to aquatic species which is a potential problem for waste stream treatment.[86]

A greener solvent with optimized fluidity is required as a medium to dissolve lead paste. In 2001, a new type of solvents, deep eutectic solvents (DESs) were developed as a derivative of ILs. The components of a DES are normally biodegradable, and DESs can be synthesized via simple mixing and heating.[87] These make DESs a potential green solvent for dissolving lead paste.

2.3.2 Deep Eutectic Solvents (DESs)

A eutectic composition is the composition at which the melting temperature is the lowest among all mixing ratios of the components. A DES is a solvent for which the melting temperature is lower than its individual components.[88,89]A schematic phase diagram of two mixed components is shown in Figure 2.10. It is similarly to that of an alloy system. The components of DES are normally non-symmetric. The mixture is not ordered like crystalline materials but through a weak interaction between molecules, thus, resulting in low lattice energy, which leads to a lower melting point.[88,90] In particular, the melting point of a DES at eutectic point is much lower than that expected for the case of ideal mixing as shown in Figure 2.11, due to the strong intermolecular interactions between DESs. [91]

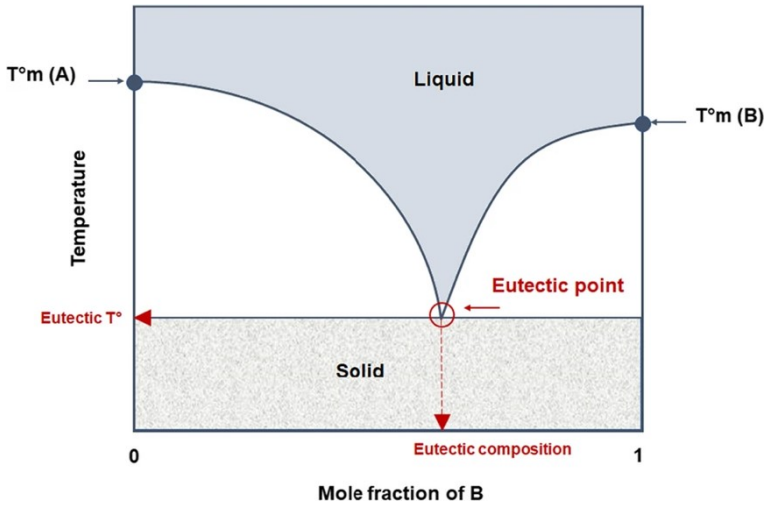

Figure 2.10 Schematic phase diagram of melting temperature of two mixed components. Adapted from Reference.[91]

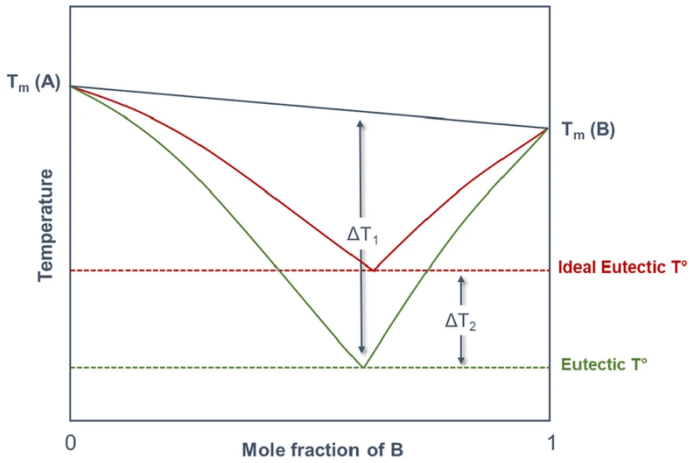

Figure 2.11 Melting point of a DES versus an ideal mixture. Adapted from Reference.[91]

The weak interaction which links two components to form a DES remains unclear. It is assumed that hydrogen bonding is the main intermolecular force between two components and makes the main contribution to the significant decrease in the melting point.[88,92] Other intermolecular interactions such as ionic interactions between cationic and anionic species or steric effects between molecules may also be present.[92]

The general form of a DES can be written as $[Cat]^+[X]^- \cdot zY"$.[88] $[Cat]^+$ represent an organic cation and is typically an ammonium or phosphonium salt. $[X]^-$ is a Lewis base which forms an organic salt with the organic cation. It acts as a hydrogen bond acceptor (HBA) in DES formation. Y represents a Lewis or Bronsted acid and acts as a hydrogen bond donor (HBD) in DES formation. z represents the molar ratio of the species. Based on different compositions, DESs are divided into four types.

Type I DES is formed between a quaternary ammonium salt and a metal chloride such as $AlCl_3$, $FeCl_3$, $ZnCl_2$, $SnCl_2$, etc. In 2001, Andrew Abbott's group developed a range of type I DESs by mixing of a series of quaternary ammonium salts with $ZnCl_2$ or $SnCl_2$.[93] Though the lowest melting point among these DESs is 15 ^oC from acetylcholine and $SnCl_2$, the majority have a melting point higher than 25 ^oC, among which the highest melting point achieved was 200 ^oC. This means that most type I DESs are solid at room temperature, resulting in limited applications. The high melting point is possibly due to the high lattice energy from the non-hydrated metal chloride.

Type II DESs, the metal chloride is replaced by hydrated metal chloride. The formula can be written as $[Cat]^+[X]^- \cdot zY \cdot yH_2O"$. Typical metals in this category are Cu, Fe, Ni, Co and Cr. An example of this type of DES is formed by choline chloride and $CrCl_3 \cdot 6H_2O$. At a molar ratio of 1 : 1.5, the mixture gives the lowest melting temperature of 17.3 ^oC, while the mixture at a molar ratio of 1 : 3 gives the highest melting temperature of 48.5 ^oC.[94] This is considerably lower than that of type I DESs. The water molecules act as a ligand and their existence changes the coordination environment of the Cr charge centre. This leads to a reduction in melting temperature.

While type I and and type II DESs are formed from a HBA and a Lewis acid, in type III and type IV DESs, the Lewis acid is replaced by a Bronsted acid. Type III is formed from a quaternary ammonium halide salt as HBA, among which the most common one is choline chloride, and a Bronsted acid as HBD, which can be amides, carboxylic acids, and alcohols.[88] Typical examples of the HBD used in type III DESs are urea (H_2NCONH_2), oxalic acid (HOOCCOOH) and ethylene glycol ($HOCH_2CH_2OH$). The physical properties including viscosity and ionic mobility can be changed according to different functional groups and the substituent of the HBD.[87] As a wide range of organic compounds can be selected as HBD candidates to form a room temperature liquid DES, it offers the possibility that a wide range of DESs can be formed to satisfy specific applications and performance. The components of type III DESs are metabolites. Though these components are more economic to synthesize from natural source, these components (carboxylic acid, amides, and alcohols) are currently prepared from petrochemicals.

In type I-III DESs, the cations selected for the HBA are generally organic molecules as inorganic cations normally have a lower void size and higher charge density resulting in a limited amount of DESs can be formed which are liquid at room temperature.[95] Andrew Abbott's group has explored a range of inorganic compounds such as $ZnCl_2$, $SnCl_2$ and $FeCl_3$ as HBA to form a DES with an HBD. This type of DESs is classified as Type IV DES. The general formula of a type IV DES can be written as $MeCl_x \cdot zY$, where Me represents a metal. In the example of $ZnCl_2$, DESs can be formed with urea, acetamide and ethylene glycol with a melting point of 9 ^oC, -16 ^oC and -30 ^oC, respectively.[95] The difference between type IV and type I-II DESs is the form of the metal species. For example, in the $ZnCl_2$-based DESs, in type I DESs, $ZnCl_2$ acts as a HBD and exists in solution as a zinc complex anion such as $[ZnCl_3]^-$, $[Zn_2Cl_5]^-$, and $[Zn_3Cl_7]^-$, while in type IV DESs, $ZnCl_2$ acts as a HBD and exists in the solution both as a zinc complex anion and cation.[95,96] The complex zinc cation exists as $[Zn(HBD)]^+$ depending on the HBD used in DESs.

Among all four types of DESs, type I and type II DESs are more commonly used for electrodeposition. Since type I and type II DESs have high viscosity and thus low ion mobility,[93] they are not ideal media to dissolve lead paste. Moreover, type I, II and IV DESs are all formed with the use of a metal salt, which might be a potential hazard and requires extra post-

treatment when it comes to processing LABs. Type III DESs are less toxic and some of them are used for food additives, thus, they are more environmentally friendly. As type III DESs also have higher adaptability, they have widely been studied for various applications.

2.3.3 Applications of DESs

2.3.3.1 Metal Electrodeposition

DESs can be used as electroplating solutions owing to their high capacity to dissolve metal salts. Gas evolution has been observed using normal aqueous electroplating solutions which can lead to hydrogen-embrittlement of the electrodeposits. DESs have a better chemical stability during electrodeposition processes which can lead to a better overall performance than ILs. A range of metals including Al, Cu, Zn, and Ni have been successfully electrodeposited using DESs.[97–100]

2.3.3.2 Metal Electropolishing

Metal electropolishing is a process which removes a thin layer of a metal part to provide a smooth surface to prevent it from corrosion. In traditional methods, the metal is immersed in an electrolyte and the metal ions from the top layer are removed using an electric current. The electrolytes of this traditional method are strong acids, normally a mixture of phosphorous acids and sulfuric acids, which are corrosive. Abbott's group has developed the possibility of using DES formed from choline chloride (ChCl) and ethylene glycol (EG) in a molar ratio of 1 : 2 as the electrolyte to electropolish stainless steel 316.[101] This DES is also known as Ethaline. The current efficiency using DES was 92% which is 3 times higher than normal aqueous electrolyte. Research on the possibility of using DESs to electropolish other metals including aluminium, titanium, nickel and cobalt has also been studied.[102–104] Ethaline has also been used as an electrolyte to electropolish the Ni superalloy from turbine blades.[105] It has successfully removed the casting scale, a metal oxide layer formed during initial casting of turbine blade components. These casting scales could lead to incipient melting of the turbine blades components during further heat treatment process, affecting the mechanical property of the turbine blade. Results from this study have shown that incipient melting have not been observed on the DES-electropolished turbine during heat treatment. This proves that DESs are a promising candidate for metal alloy surface etching.

2.3.3.3 Dissolution/Extraction of metal compounds

DESs can be used in electrochemical processing owing to their higher electron conductivity and metal salts solubility than other non-aqueous solutions (e.g., ionic liquids). Metal oxides such as V_2O_5 or MnO can only be dissolved in strong acids solutions such as HCl and are hardly soluble in normal aqueous solutions. Abbott's group explored the solubility of a range of metal oxides in various DESs including oxides of Ti, V, Cr, Mn, Fe, Co, Ni, Zn and Co in a range of valence states.[106] Studies have shown that the solubility of these oxides in the DES formed from choline chloride and malonic acid in a molar ratio of 1 : 1 is comparable to that in HCl solution. The DES formed from choline chloride and urea at a molar ratio of 1 : 2 shows a 4-time higher solubility for CrO_3 than HCl solution though it only shows limited solubility for other metal oxides. It is assumed that different DESs may have different solvation ability targeting different metal oxides. Different DESs can then be tailored for different application requirements.

A study on DESs has investigated their ability to preferentially to extract heavy toxic metal compounds (oxides, chlorides, acetates and phosphates) from incinerated sewage sludge ash (ISSA).[107] Results from this study have shown that urea-based DESs preferentially dissolve metal chlorides and phosphates, while carboxylic acid-based DESs preferentially dissolve metal oxides, and choline chloride-based DESs preferentially dissolve metal acetates.

Another study has found that DESs formed from choline chloride with urea or ethylene glycol were able to extract zinc and lead from steel production waste with the use of DESs.[108] After extraction, zinc and lead were recovered from the DESs either using an electrowinning process or leached out from the solution via a complexing agent.

Both the extraction study on metal and metal compounds are based on the high solubility of target metal compounds in DESs. From the perspective of using DESs to recycle LAB paste, the focus would be first to find out DESs which can dissolve lead paste components efficiently, then to investigate the possible mechanism of the reaction to explore more selective DESs. A

range of studies have been done using DESs to dissolve lead compounds and possible lead species formed during the reaction have been investigated.

2.3.4 Lead Recycling in DESs

Previous studies have shown the possibility of the dissolution of metal compounds in DESs. There have been various studies on the solubility of lead compounds and the corresponding mechanism in DESs.

Yang and Reddy have investigated the solubility of PbO in a Reline, a DES formed from choline chloride and urea in a molar ratio of 1 : 2. They showed that the solubility of PbO can achieve 26.7 g/L.[109] However, the viscosity of the solution increases and thus leads to a decrease in electrical conductivity when the PbO loading exceeds 17.8 g/L. The increase in viscosity may be attributed to the radius of lead complexes which blocks the mobile movement of ions in the solution. The solvation mechanism of the Pb complexes formed in Reline can be described as shown in Equation 2.40. [109] It is suggested that in this Pb complexation structure, the sp^3 hybrid orbitals from Pb^{2+} are filled with the electron pair from Cl^- from choline chloride, O from urea and O^{2-} from PbO and a lone pair from Pb. This structure forms a stable Pb^{2+} complexation structure in Reline.

$$PbO(s) + CO(NH_2)_2(urea)(aq) + Cl^-(aq) \rightarrow \{Pb^{2+}O^{2-} \cdot CO(NH_2)_2 \cdot Cl\}^-(aq) \quad \textbf{Equation 2.40}$$

After PbO is dissolved in Reline, high-purity Pb can be electrodeposited on a Cu substrate at electrode potentials from -0.5 to -1.1 Volts. Results have shown that the more negative the electrode potential is, the more dendrites can be observed in the electrodeposits.[110]

Research has also shown that the solubility of $PbSO_4$ and PbO_2 in Reline can also achieve 22.7 g/L and 17.9 g/L, respectively.[111] This study has shown that the recovery rate of lead from electrodeposition process can achieve 90-93 wt% for a lead-bearing Reline, which has dissolved a mixture of $PbSO_4$, PbO_2 and PbO. This result indicates that Reline can be a good candidate for dissolving lead battery paste.

Ru has used Ethaline to dissolve a PbO pellet on a stainless-steel mesh. The PbO dissolved in Ethaline to form a 0.4 g/L Pb solution and Pb was recovered at a current efficiency of 87.8% at an energy consumption of 0.736 kWh per kilogram of lead produced.[112,113] The amount of PbO dissolved in this study does not reflect the maximum solubility of PbO in Ethaline as the study more focused on the electrochemical behaviour of the DES during the electrodeposition process. Though the amount of PbO dissolved is small, it offers the possibility of using DES to dissolve lead materials. The solvation mechanism of PbO in Ethaline can be described as shown in Equation 2.41, the mechanism of lead deposition on the cathode can be shown in Equation 2.42 and the gas evolution on the anode during deposition can be shown in Equation 2.43.[113]

$$PbO(s) + (CH_2OH)_2(l) + Cl^-(aq) \rightarrow \{Pb^{2+}O^{2-} \cdot (CH_2OH)_2 \cdot Cl\}^-(aq)$$

Equation 2.41

$$Cathode: \{Pb^{2+}O^{2-} \cdot (CH_2OH)_2 \cdot Cl\}^-(aq) + Ch^+(aq) + 2e^- \rightarrow Pb^0(s) + [ChCl \cdot O \cdot (CH_2OH)_2]^{2-}(aq)$$

Equation 2.42

$$Anode: 2Cl^-(aq) \rightarrow Cl_2(g) + 2e^-$$

Equation 2.43

Ethaline can also be used to dissolve a range of lead perovskite materials including formamidinium lead triiodide ($FAPbI_3$), methylammonium lead triiodide ($MAPbI_3$) and a mixed halide perovskite ($MAPbCl_{3-x}I_x$).[114] EXAFS results from the study from Payne's group have shown that the lead species formed in Ethaline of all three lead perovskite materials are identical and confirmed to be $[PbCl_3]^-$. $[PbCl_3]^-$ also exist in a $PbCl_2$-based IL.[115] The solubility of these perovskites in Ethaline was found to be ranging from 0.4-0.6 g/L and lead in the solution was recovered via an electrochemical process with an extraction efficiency of at least 98.7%.[114]

Another study in my research group has investigated the solubility of individual components of lead paste ($PbSO_4$, $PbCO_3$, PbO and PbO_2). The solubility of $PbSO_4$, $PbCO_3$, PbO and PbO_2 in Ethaline was found to be 1.8 g/L, 5.9 g/L, 4.4 g/L and 12.2 g/L respectively,[116] the solubility which is much higher than the solubility of transition metal oxides in a urea-based DES reported by Abbott's group.[106] It is assumed that the speciation of these lead compounds in Ethaline is similar to that the speciation of lead perovskite materials. To understand the potential of recovery of lead from the lead-bearing DES, an electrochemical process was carried out from a $PbCl_2$ dissolved Ethaline solution. The results showed that Pb can be electrodeposited on a Pt electrode with small nuclei ranging from 80-200 nm in diameters and some large aggregates ranging from 600-1000 nm in diameters.[116]

This study from Payne's group has demonstrated the possibility of recycling lead paste using DES Ethaline, however, a weak signal of $PbCl_2$ was observed in X-ray photoelectron spectroscopy (XPS) on the Pb deposits.[116] The $PbCl_2$ contamination may either comes from a side reaction of the electrodeposition process or precipitates from the DES. The formation of $PbCl_2$ on the deposits cannot be avoided as most of DESs are formed based on choline chloride. Therefore, it is essential to find chloride-free DESs, which can resolve this issue. A subcategory of DESs which are called natural deep eutectic solvents (NADESs) can satisfy this requirement.

2.3.5 Natural deep eutectic solvents (NADESs)

NADESs are a derivative of DESs, the components of which are primary metabolites such as carboxylic acids, amino acids, amines, alcohol and sugars.[117] Compared to novel ionic liquids and DESs, the components of NADESs are mostly natural products, thus, they are less toxic and mostly biodegradable. The functional groups of these organic molecules can easily form hydrogen-bonding supramolecular forces between each other,[118] thus, various of NADESs can be formed. In a water-free NADES system, the hydrogen-bonding interaction in NADESs leads to a highly ordered network nature, resulting in a high viscosity of the system.[119] Therefore, water is added and becomes an essential part of the NADES system to weaken the hydrogen bonding interactions and to increase the entropy of the system, thus reducing the viscosity of

the liquid.[120] Too much water in the system destroys the NADESs which becomes a diluted aqueous solution of organic compounds. Dai's group has investigated the effect of water content on the supramolecular forces, viscosity, and conductivity of the NADES system. The study has found that in most NADESs 25 wt% of water can cause a dramatic decrease in hydrogen bonding and a 50 wt% water content will leads to a break-down of hydrogen bonding.[121]

NADESs have been widely used in the extraction of organic compounds from plants.[122] An example of this application is the extraction of phenolic metabolites from a plant, Safflower, with the use of lactic acid/glucose, proline/malic acid, and fructose/glucose/sucrose based NADESs.[123] Recently several studies have been reported on the extraction of metal or metal compounds using NADESs. Osowaska and Ruzik have developed the extraction of trace metals including Zn, Cu, Mn, and Mo from young barley powder using a range of NADESs. Different NADESs have different extraction efficiencies on metals. Results have shown that choline chloride/carboxylic acid NADESs is preferential in Mn extraction, fructose/citric acid-based NADESs are preferential in Zn and Cu extraction and the ability of Mo extraction among all NADESs studied remains similar.[124,125] Shikov et al. have investigated the extraction efficiency of Al and Cr from a seeweed *Fucus vesiculosus* with the use of a NADES.[126] Chen's group has shown that the extraction efficiency of Cd from rice flour can reach 96% using a choline chloride/tartaric acid-based NADES.[127] The group has also developed a high extraction efficiency (>78%) for Pb, Cd, As, Cu and an acceptable extraction (~49 %) for Cr from a red algae *Porphyra haitanensis* with the use of NADESs.[128] The extraction of Pb offers the possibility of recycling lead compounds using NADESs.

2.4 Perspective of lead recycling with new solvents

Though pyrometallurgy is the most economic and dominant process in the LAB recycling industry, the pollution of hazardous particulates has raised concerns for public health. Hydrometallurgy, as an alternative method for pyrometallurgy, also poses safety concerns due to the use of strong acids.

The leaching followed by precipitation method proposed by Aurelius is a good approach for LAB recycling. However, the leaching solution used by the Aurelius method requires a large amount of water, which does not meet the requirements for resource saving and sustainability. Under this circumstance, a non-aqueous solvent – deep eutectic solvent (DES) has been introduced to dissolve lead components. Though the DES based on choline chloride and urea produce $PbCl_2$ contaminants on the Pb electrodeposits, the use of this non-aqueous solvent is a good start for finding a greener, economic and effective method to recycle LABs.

This thesis will initially focus on finding a suitable chloride-free solvent from the subcategory of DESs – NADESs to dissolve LAB waste components. The NADESs used in this thesis are based on a hydrogen bond acceptor, carboxylic acids, and water. Though water is also an essential part of NADESs, the amount required is much less than in the Aurelius process. After the lead is dissolved in NADESs, the lead can be either leached out as corresponding lead carboxylate, which can be calcined to PbO as value product. Alternatively, the lead in NADESs can be leached out as lead oxalate with the addition of oxalic acid dihydrate as the precipitation agent, enabling reuse of the solvent. A schematic diagram of these two procedures can be shown in Figure 2.12.

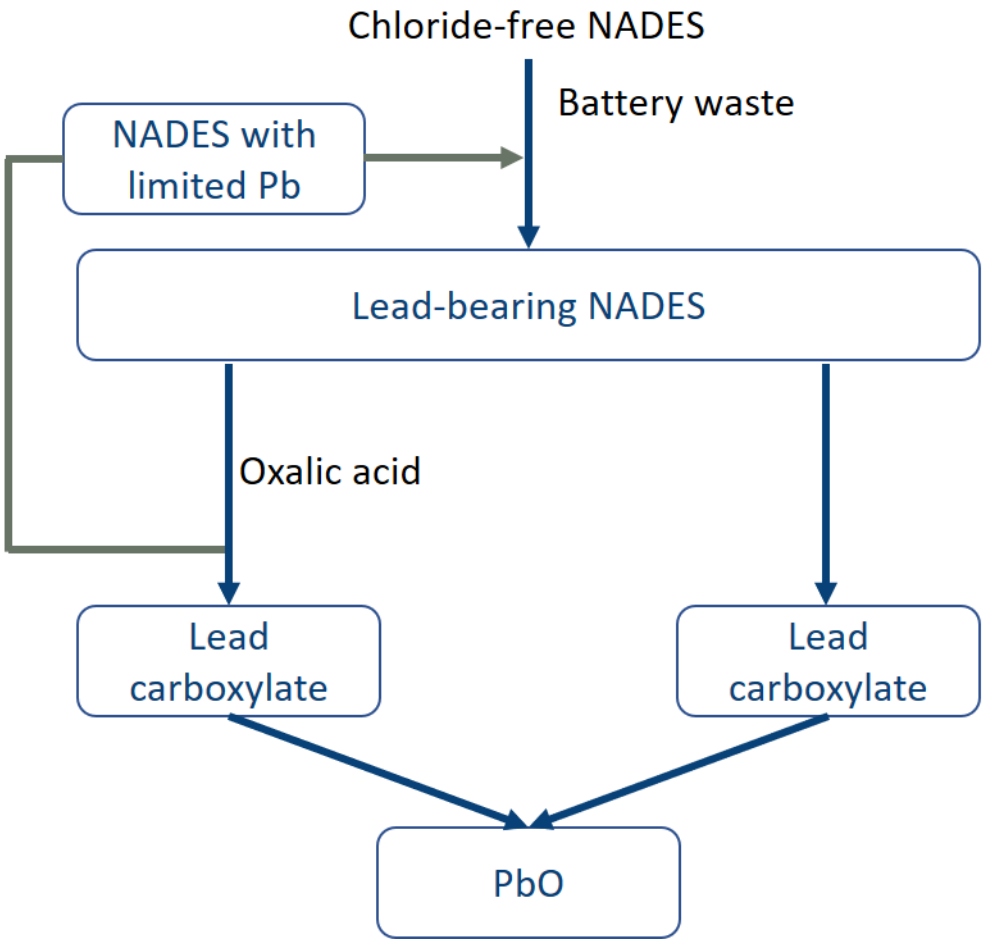

Figure 2.12 Schematic diagram of a proposed recycling route of LAB waste with the use of a chloride free NADES.

Chapter 3 Experimental methods

3.1 Inductively Coupled Plasma – Optical Emission Spectroscopy (ICP-OES)

ICP-OES is a quantitative analysis technique which determines the presence and quantity of a wide range of metal elements (such as Na, Ca, Pb, Mn, etc.) and inorganic elements (such as Si and P) in a solution at the same time. The technique uses an inductively coupled plasma (ICP), the source of which is typically argon gas, is generated under a strong magnetic field with a high-frequency electric current. [129] The plasma is surrounded by silica tubes. The whole unit is considered as a plasma torch, the excitation temperature of which can achieve 5000 to 9000 K as a result of collisions between electrons and argon atoms.[130] Then the solution sample is delivered through a peristaltic pump into an aerosolizer using a nebulizer. The resulting aerosol is fed through a spray chamber to the plasma torch. The high temperature of the plasma torch allows the atomization of the sample and excites electrons of the atom into a higher energy state. When the electrons fall to the initial state, it is accompanied by the relaxation of photons. The wavelength of the emitted photons is characteristic for different elements. The signal intensity of the element of interest is proportional to the concentration of the element.[131] More specifically, the concentration of an unknown sample is determined by comparison of the intensity of the signal with a set of reference samples with known concentrations.

In some cases, there might be multiple elements present in the sample. The signal of different characteristic wavelengths may overlap, causing potential quantification problems. Therefore, a diffraction grating device can be used in a wavelength dispersive function to separate signals from different elements. The diffraction grating device is a surface-etched mirror which disperses incident light into different diffraction angles according to their wavelengths. The diffracted wavelengths then exit through different slits to the detector so that they do not interfere with each other. The light signal can be recorded by several types of detectors, such as a photomultiplier or a charge-coupled device. A photomultiplier converts the light signal into an electrical signal. The stronger the light signal the larger the electrical signal, and the higher the concentration of the elements. A charge-coupled device consists of a Si substrate and a SiO_2 layer. When the Si substrate is exposed to the incident light signal, the Si-Si bond

breaks leaving an electron and a hole pair in the structure. When an outer voltage is applied, electrons move towards the SiO_2 substrate, and the holes move away from the SiO_2. The movement of the electrons and holes generate an electrical current within the device. The strength of the current is proportional to the strength of the light or the concentration of the elements.

The ICP-OES in this thesis was carried out via a Thermo-Fisher 6000.

3.2 X-ray Diffraction (XRD)

XRD is a non-destructive characterisation technique which has been commonly used to identify the crystallographic information for crystalline materials. The XRD pattern is unique for each crystalline material. Therefore, an unknown crystalline material can be identified through comparison to the International Centre for Diffraction Data (ICDD), which is a diffraction pattern database of known crystal materials.

XRD can be used to obtain the lattice parameters of a crystalline material is because the wavelength of X-rays is in the same order as the lattice spacing of a crystal structure. The principle of the technique is based on Bragg's law: $n\lambda = 2dsin\theta$, where n is the order of diffraction (normally equals to 1), λ is the wavelength of the X-ray, d is the spacing between two lattice planes, and θ is the incident angle.

During the XRD analysis, the incident X-ray beam is generated through the bombardment of accelerated electrons from a filament towards a target material, commonly Cu ($\lambda = 1.5418$ Å). Inner-shell (K shell) electrons from the target material are knocked out to a higher energy state. Electrons from the out-shell drop down to fill the hole left in the K-shell. When these electrons fall from the outer shell (higher energy state) to K shell (initial ground state), characteristic X-rays are produced. When the electrons fall from the L shell, M shell or N shell, corresponding Kα, Kβ and Kγ X-ray lines are produced, respectively. As all these subshells have more than 1 subshell, and X-rays with more than 1 energy level in each X-ray lines are produced. As an example, the L shell has two subshells ($2p_{3/2}$ and $2p_{1/2}$), Kα X-ray lines with two different energies are produced, namely Kα_1 ($\lambda = 1.5405$ Å for Cu source) and Kα_2 ($\lambda =$

1.5443 Å for Cu source). Kβ and Kγ can be eliminated by a filter. The filter material depends on the target material that is being used. For example, a Ni filter is used for a Cu source and Zr is used for Mo source.

3.2.1 Powder X-ray Diffraction (PXRD)

PXRD is carried out on powder samples. The X-ray beam and the X-ray detector are positioned in the same plane, which is perpendicular to the plane where the sample is placed as shown in Figure 3.1.[132] During measurement, the sample is fixed on the sample stage, while the X-ray tube and the X-ray detector move towards each other at the same step size. Due to the immobility of the sample, only planes that are parallel to the sample surface can diffract the X-ray beam.[133] In other words, only planes that are parallel to the sample surface can be detected. Crystallites are randomly orientated in powdered samples, therefore, there are likely to be different planes parallel to the sample surface, which can then produce a Bragg diffraction peak. In this study, samples were ground before the analysis, in order to produce more randomness in the crystallite orientations.

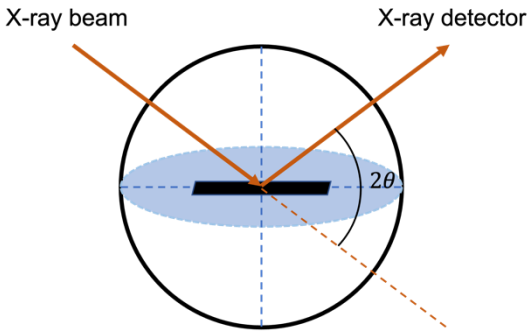

Figure 3.1 Schematic diagram of PXRD.

PXRD is convenient and useful in crystalline phase identification by matching the diffraction pattern of the sample to the ICDD reference. However, one drawback of PXRD is that it cannot identify phases of a material which is not present in the database. It is therefore difficult to identify phases of an unknown or new substance using ICDD. In this situation, single crystal X-ray diffraction is more useful to determine the structure information of an unknown or new substance.

The PXRD analysis in this thesis was carried out with a Panalytical X-ray diffractometer with Cu-Kα source and nickel filter at a current of 40 mA and a voltage of 40 mV. A 7.6-µm thick Kapton film (LGC standards) was covered on the precipitate during analysis to prevent exposure to lead.

3.2.2 Refinement of PXRD

As phases from a powdered sample are determined through comparison between its diffraction pattern with ICDD reference, the structural information provided on the reference often does not reflect the precise lattice information of the actual powdered sample. In this situation, structural refinement of the powdered XRD pattern is used to obtain precise lattice parameters. Software Topas 4.0 with jEdit software package was used for refinement in this thesis.

Two refinement methods were used, Pawley and Rietveld refinement. During powder sample data collection, a Kapton film was covered to prevent spillage, the pattern of which contributes to the overall diffraction pattern. Background correction was carried out for both refinement methods.

For the Pawley refinement, only the unit cell dimensions (a, b, c and α, β, γ), crystal system and space group of a phase are required. The software uses the least-squares method to fit the actual pattern based on these parameters until a minimum difference is obtained between the calculated pattern and the actual pattern. In Pawley refinement, peak intensity cannot be refined as it lacks structural information.

For the Rietveld refinement, detailed structure information of a phase is required. This includes atomic positions, the site occupation number of and the thermal factor of atoms which constitutes a unit cell. The pseudo-Voigt profile, which is a linear relationship between Lorentz and Gauss distribution is used to refine the peak shape. At lower angles, peaks tend to be more Gaussian distributed, while at higher angles, peaks tend to be more Lorentzian distributed. [134]

A weight-profile R_{wp} as shown in Equation 3.1, where y_i is the intensity and w_i is the weight percentage, can be used to define the quality of the refinement. [135]

$$R_{wp} = \sqrt{\frac{\sum_i w_i[y_i(observed) - y_i(calculated)]^2}{\sum_i w_i[y_i(observed)]^2}} \qquad \textbf{Equation 3.1}$$

3.2.3 Single Crystal X-ray Diffraction (SCXRD)

The X-ray tube, the X-ray detector and the sample stage of a single crystal diffractometer have more mobility than a powder X-ray diffractometer. The diffraction pattern of the single crystal is related to the electron density of the atoms. The electron density of a unit can be expressed as Equation 3.2, where V is the volume of the unit cell, (hkl) is the lattice plane, (abc) is the lattice parameter, $F(hkl)$ is the structure factor of a lattice plane. $F(hkl)$ can be expressed as Equation 3.3, where f_j is the atomic scattering factor and x_j, y_i, z_j is the positional coordinates of atom j.

$$\rho(x,y,z) = \frac{1}{V}\sum_h \sum_k \sum_l F(hkl)\, e^{-2\pi i(\frac{hx}{a}+\frac{kl}{b}+\frac{lz}{c})} \qquad \textbf{Equation 3.2}$$

$$F(hkl) = \sum_j^N f_j\, e^{-2\pi i(hx_j+ky_i+lz_j)} \qquad \textbf{Equation 3.3}$$

After the data collection, the pattern was modelled and refined to solve the structure of the single crystal.

The single crystals in this thesis were all analysed using an Agilent Xcalibur PX Ultra A with Mo source at 173 K for structure information and crystallographic data. All single crystal data were collected, modelled, and refined by Dr. Andrew White, Department of Chemistry, Imperial College London.

3.3 Scanning Electron Microscopy (SEM)

SEM is a characterisation technique which reflects the surface morphology and chemical composition of a sample through the interaction between a focused electron beam and atoms within the sample. The electrons are generated under high vacuum through emission from a thermionically heated tungsten filament, the energy of which can achieve up to 50 keV, and the electrons are condensed through condenser lenses into the electron beam with a focused spot size of 1 to 5 nm.[136] The condensed electron beam then passes through scanning coils and a final lens aperture to the samples. Various signals are generated as a result of interaction between primary electrons from the electron beam and atoms of the sample. These signals include secondary electrons (SE), backscattered electrons (BSE), and characteristic X-rays.

SE are generated as a result of inelastic collisions between the incident electron beam and valence electrons of in the sample. The excited valence electrons escape from the sample towards the SE detector. These excited electrons normally have a kinetic energy of lower than 50 keV.[136] Due to the low kinetic energy, only electrons from the top few nm can escape from the sample and reach the detector. The electrons pass through a scintillator and convert to a light signal through a photomultiplier. The brightness of the signal depends on the number of electrons that reach the detector. The steep features of a sample have a higher incident angle than the flat features of a sample, resulting in a shorter mean free path length to the detector. This means that more electrons can reach the detector from steep features than flat features, resulting in brighter areas in steep features. Therefore, this brightness contrast of the image reflects the surface topography of a sample.[137]

BSE are generated as a result of elastic collisions between the incident electron beam and the nucleus. When the incident electron beam (negatively charged) encounters the positively charged nucleus, some of the electrons will circle the nucleus and escape out of the sample rather than being attracted by the nucleus. These electrons are of high-speed and have higher kinetic energy than SE. The number of electrons backscattered depends on the atomic number of the atom.[138] The larger the atomic number, the larger the nucleus, therefore, more electrons are backscattered. Heavier atoms produce a brighter area than the lighter atoms. A

BSE image is commonly used to identify phases and crystallography. Moreover, this brightness contrast of a BSE image only gives relative atomic number of the elements present. To identify the actual elements present, an energy-dispersive X-ray analysis is needed.

When the incident electron beam hits the inner-shell electrons of the sample, an outer-shell electron moves to the hole where the inner-shell electron has been knocked out, and a characteristic X-ray is generated. The energy of the characteristic X-rays is measured by an energy-dispersive spectrometer; thus, the chemical composition of the sample can be detected.

The SEM in this thesis was carried out with a Zeiss Leo Gemini 1525 SEM. The powdered sample was mounted on an aluminium stub with carbon tape. Then Cr with a thickness of 15 nm was coated on the the powder to minimize charging effects during analysis. All images were taken with an In-lens detector at an accelerating voltage of 5 kV and a working distance of around 7 cm.

3.4 X-ray Photoelectron Spectroscopy (XPS)

XPS is surface-sensitive technique which measures the chemical composition and chemical state of a material based on the excitation of electrons upon bombardment of incident X-rays (normally an Al source, $h\nu = 1486.6\ eV$). When the binding energy of an electron in a core level is smaller than the energy of the incident X-rays, the electron can escape from the core level. The emitted electrons are considered as photoelectrons. The number of electrons that can escape from the sample is inversely proportional to sample depth. Beer's law defines the relationship between the number of photoelectrons emitted from the sample and the sample depth as shown in Equation 3.4, where d is the sample depth, I_0 is the initial intensity (number) of electrons generated from a sample at the depth of d, I is the intensity (number) of electrons emitted from the sample and λ is the attenuation length of photoelectrons.[139] λ is also considered as the inelastic mean free path (IMFP), which is defined as the average distance of electrons can travel until they are inelastically scattered.[140]

$$I = I_0 e^{-\frac{d}{\lambda}}$$ **Equation 3.4**

To get 95% of electrons emitted from the sample without scattering, the sample depth d should be equal to 0.0513λ. For a monochromatic Al $K\alpha$ source, the inelastic mean free path is in the range of 16-200 nm as shown in Figure 3.2.[141] Consequently, the sample depth d should be in the range of 0.8-10 nm.

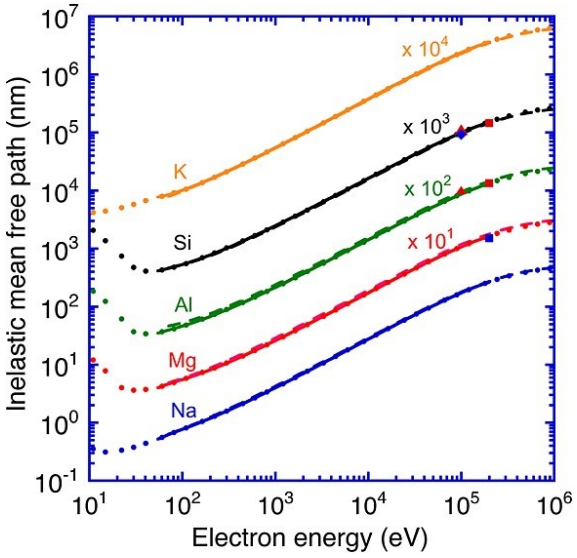

Figure 3.2 Inelastic mean free path (IMFP) as a function of electron energy. Adapted from Reference.[141]

When the photoelectrons are emitted from the sample, it reaches the detector with a certain kinetic energy. The relationship between the kinetic energy (E_{KE}), binding energy (E_{BE}), the energy of incident X-rays ($h\nu$) and work function (W), which is a fixed constant, is described in Equation 3.5. The kinetic energy of the emitted electron is measured by the detector and the binding energy of the electron is calculated using Equation 3.5. As the binding energy is characteristic for an electron of a core level of a specific element, while the kinetic energy of the electrons changes as the energy of incident energy of X-ray changes, the calculated binding energy gives information on chemical composition and chemical state of the sample.

$$E_{BE} = h\nu - E_{KE} - W$$ **Equation 3.5**

Upon excitation of electrons, a sample becomes positively charged. The subsequent electrons are more difficult to emit from the sample as they are attracted by the positively charged site. These electrons need to overcome the attractive force to emit from the sample, resulting in lower kinetic energy. Based on Equation 3.5, this leads to a higher "apparent" binding energy. This phenomenon is known as the charging effect. The charging effect can be minimized or eliminated using a flood gun, which delivers electrons to the sample to maintain electron neutrality. A peak shift may still be seen with the use of a flood gun, and corrections are made to align the binding energy using the adventitious carbon (C-C) peak set to 284.8 eV.

All core levels except the *s* core level exhibit a doublet due to spin-orbit coupling effects. Electrons have a spin quantum number of $s = 1/2$, while the angular momentum quantum number ℓ depends on the orbital that the electron is in. ℓ equals to 0,1,2 and 3 for *s,p,d* and *f* orbitals respectively. The interaction between the two angular momenta of the electron spin and orbit can be parallel or anti-parallel. This different orientation alignment of two momentum results in different interaction energy of spin-orbit coupling. As a result, a doublet can be seen from the XPS spectrum. The total quantum number j equals to $\ell \pm s$. The relative intensity of the doublets equals to $2j + 1$. For example, for a 2*p* core level, two peaks $2p_{1/2}$ and $2p_{3/2}$ with a relative ratio of $\left(2 \times \frac{1}{2} + 1\right) : \left(2 \times \frac{3}{2} + 1\right) = 1 : 2$ can be seen.

The XPS in this thesis was carried out with a Thermo Scientific Al-Kα (hν=1486.6 eV) system, a 180^{o} double focussing hemispherical analyser with a 2D-detector at a pressure of lower than 2x10^{-8} mbar, and a flood gun to minimize the charging effect during the excitation of electrons from the X-ray. The sample was mounted on a Tantalum strip with carbon tape. The spot size of the sample has a maximum of 400 μm^{-2}. Core level spectra of all elements were obtained at a passing energy of 20 eV and a step size of 0.1 eV. The data was analysed using Thermo Avantage software. The binding energy (BE) of all elements was adjusted according to the adventitious carbon (C-C) peak, which should be aligned at 284.8 eV.

3.5 Thermal Gravimetric Analysis - Differential Scanning Calorimetry (TGA-DSC)

TGA is a technique which measures the mass change of a material subjected to an variation in temperature. The sample is loaded in a pan, which is placed on an isolating rod. They are placed on a thermo-micron balance which is connected to the temperature controller. [142] This allows measurement of mass change and temperature of the sample at the same time. During the analysis, purge gas is fed from the bottom towards the sample and exits from the top of the analysis chamber. The purge gas can be inert gas such as N_2 or an oxidising gas such as O_2 or air. In the experiment in this thesis, the analyses were done in air.

During the heating process, the density of the atmosphere decreases with the change in temperature. This change leads to an increase in the apparent mass of the sample. This phenomenon is considered as "buoyancy effect". To minimize this effect, a blank run with the conditions (purge gas, flow rate, heating rate, pan) but without any sample is carried out to subtract the buoyancy.

Though TGA can measure the mass change during heating, it cannot identify reactions such as phase transitions where the mass of the sample does not change. Therefore, DSC coupled with TGA can be used to record any heat capacity changes. DSC is a technique which measures the heat absorbed or released from the sample in the pan in order to keep the temperature the same as the reference pan as a function of temperature.[143] In this work, DSC helps to identify the temperature at which a phase change occurs. A phase change can be identified from either an exothermic or endothermic peak.

TGA coupled with DSC in this thesis was carried out in a NETZSCH STA 449 C on 10 to 15 mg of powdered samples in an aluminium crucible under air.

3.6 Fourier Transform Infrared Spectroscopy (FTIR)

FTIR is an analytical technique which measures the absorption of energy as a function of frequency due to vibration and rotation of chemical bonds. Though the frequency of infrared

ranges from 10−12800 cm^{-1}, the infrared region used in this thesis falls in the mid-infrared region from 400−4000 cm^{-1}. As specific functional groups have a characteristic absorption at a certain frequency, FTIR can be used to identify the functional group present in a chemical compound. When the incident infrared light with certain radiation energies hits the sample, the molecule in the sample absorbs the radiation energy and the vibrational energy level transfer from the initial state energy level to higher energy levels. Different functional groups have different absorption energies which are equal to the energy required for a vibrational energy level transition. The relationship between the vibrational energy and frequency can be described in Equation 3.6, where n is an integer, h is Planck's constant and υ is the vibrational frequency. Moreover, not all transitions can be studied, only transitions where a dipole moment in a molecule is changed, can be captured.[144]

$$E_{vib} = \left(n + \frac{1}{2}\right) h\upsilon \qquad \textbf{Equation 3.6}$$

The vibrational mode of a molecule depends on the number of atoms in the molecule. Assuming that a molecule has N atoms, then each atom has $3N$ degree of freedom movement in 3 dimensions x, y and z. Of these, translation movement where the atoms move along one of the axes in the same direction, and rotation movement around axes, are not considered as vibrational movement of atoms. Excluding these $3 + 3 = 6$ movements, a molecule with N atoms has $3N - 6$ vibrational modes. For a linear molecule, the atoms can only rotate around two axes, therefore, a linear molecule with N atoms will have $3N - 5$ vibrational modes.

An example of vibrational modes in water is shown in Figure 3.3. The vibrational modes include symmetric and asymmetric stretching, in-plane bending (scissoring and rocking) and out-of-plane bending (wagging and twisting).

The FTIR in this thesis was carried out via a Thermo-Scientific Nicolet iS10 with an attenuated total reflection (ATR) optics at a wavenumber range of 400-4000 cm^{-1}. An air background was collected before all measurements.

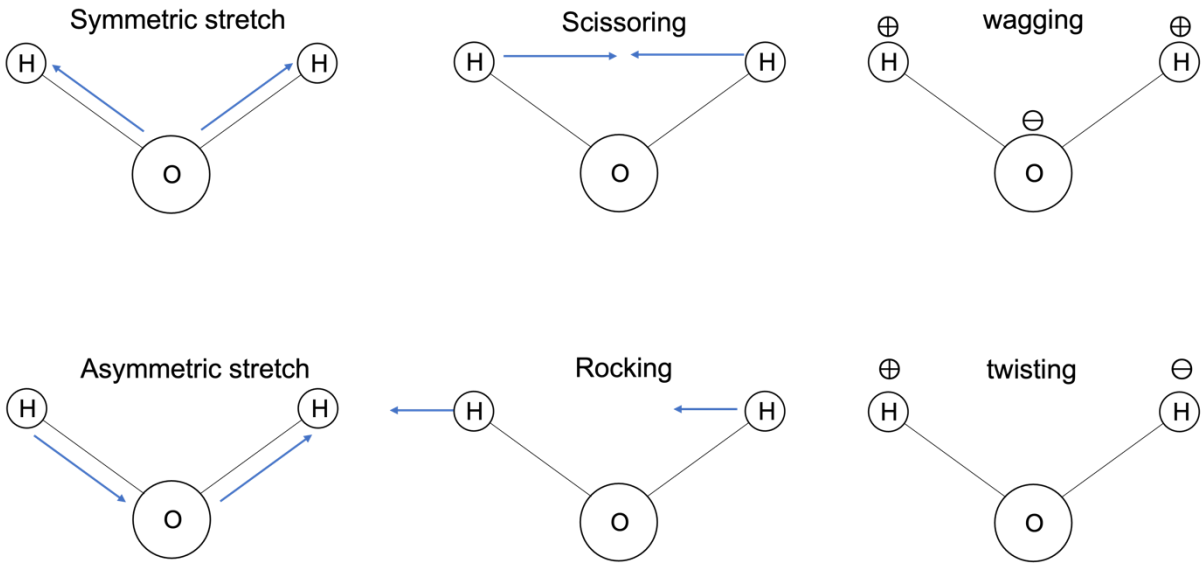

Figure 3.3 Vibrational modes of water molecules.

3.7 Nuclear Magnetic Resonance (NMR)

NMR is an analytical technique which can be used to gain structural information about a chemical compound based on the magnetic properties of its atomic nuclei. When the sample is exposed to an external magnetic field, it forces the atomic nuclei to align in a certain orientation. The alignment of a nuclei has $2s + 1$ possible orientations, where s is the spin quantum number of the nuclei.[145] ^{1}H, also known as a proton, it has a spin quantum number of $\frac{1}{2}$, and two possible orientation alignments. One of the two ($m_s = +\frac{1}{2}$) aligns parallel to the external magnetic field and has a lower energy level, while the other ($m_s = -\frac{1}{2}$) aligns anti-parallel to the external magnetic field and has a higher energy level. The energy gap (ΔE) between the two energy levels is proportional to the strength of external magnetic field (B_0) as shown in Equation 3.7, where s is the spin quantum number of the nuclei and μ is the magnetic moment of the nuclei. In the case of a proton, $s = \frac{1}{2}$, therefore, $\Delta E = 2\mu B_0$.

$$\Delta E = \frac{\mu B_0}{s} \qquad \textbf{Equation 3.7}$$

When nuclei are positioned in an external magnetic field, they have not yet aligned parallel or anti-parallel to the external magnetic field. In order to be aligned parallel or anti-parallel, the nuclei would spin around the axis of the external magnetic field. This rotation is called "Larmor precession". The frequency of the precession is called the "Larmor frequency" (ν_0), which is proportional to the strength of external magnetic field (B_0) as shown in Equation 3.8 , where γ is the gyromagnetic ratio of the nucleus.

$$\nu_0 = \frac{\gamma}{2\pi} B_0 \qquad \textbf{Equation 3.8}$$

Most of the nuclei aligns in the lower energy state. If an applied electromagnetic field excites the nuclei from a lower energy state to a higher energy state, magnetic resonance can occur between nuclei. Different nuclei have different resonance frequencies. The energy of the applied electromagnetic field is equal to the energy gap of two energy states and the resonance frequency equals to the Larmor frequency.

The resonance frequency not only depends on the type of nuclei, but it also depends on the environment it is in. For example, the protons in CH_4 have a different resonance frequency than the protons in CH_3OH. This difference makes it possible to use NMR to differentiate protons or other nuclei in different chemical compounds. The difference occurs due to the presence of electrons surrounded by the magnetic nucleus. The motion of the electrons generates an induced magnetic field, which augments or counters the external magnetic field. The augmentation to the external magnetic field is called "de-shielding effect", while the counter effect to the external magnetic field is called "shielding effect". The higher the electron density is present around the nucleus of interest, the greater the shielding effect the electrons have to the nucleus.

The frequency of a nucleus from different molecules may only differs slightly, therefore, to denote this frequency more precisely a chemical shift (δ) is used. δ is defined as shown in

Equation 3.9, where ν_o is the Larmor frequency of the nucleus, ν_{TMS} is the Larmor frequency of reference tetramethysilane [$Si(CH_3)_4$] and ν_s is the frequency of the spectrometer.

$$\delta = \frac{\nu_o - \nu_{TMS}}{\nu_s} \times 10^6\ ppm \qquad \textbf{Equation 3.9}$$

The ^1H NMR carried out in this thesis via a Joel – 400 MHz machine.

Chapter 4 Synthesis, Characterisation and Decomposition of Lead Malate Dihydrate

4.1 Introduction

LABs play a critical role in the automobile industry and are also the most recycled batteries among all battery technologies. The most mature LAB recycling process – pyrometallurgy - has raised concerns both for the environment and key workers due to the production of hazardous particulates and SO_2. Though efforts such as the use of bag houses at the end line of the process have been used to reduce pollutions, the leakage of hazardous particulates is always a potential risk. In countries with low environmental regulations, the pollution control of lead is significantly worse.

Commendable advances have been made in hydrometallurgy processes to minimize the pollution of hazardous particulates. Due to the high cost and energy consumption of the electrowinning process in hydrometallurgy, an alternative method involving leaching, precipitation or cementation followed by calcination has been used for LAB recycling. Typical examples of these reactions are the synthesis of lead citrate with the use of a mixture of citric acid and acetic acid solution (also known as the Aurelius process) and the synthesis of lead acetate with the use of urea acetate solution and metallic iron.

These two leaching/cementation processes both require a large amount of water which is problematic both in terms of resource minimization and the economics of decontaminating large quantities of solvent. In this chapter, a green type of solvent, NADES, which requires significantly less water consumption in synthesis than normal aqueous solutions, has been investigated to resolve the water issue. In parallel, the formation of new organic lead compounds as LAB precursors through the reaction of lead paste components (mainly $PbCO_3$) has also been developed.

In this chapter, a NADES formed from malic acid, beta alanine and water, has been used to dissolve $PbCO_3$, the main component of desulfurized lead paste. The precipitate achieved

through this reaction was found to be lead malate dihydrate. Lead malate dihydrate, to date, has only been reported once by C. N. R. Rao who published limited structural characterisation. No existing works reported the structural changes and thermal degradation of this organic lead compounds. To understand the degradation behavior of lead malate dihydrate, it has been first calcined in a furnace at various temperatures and then a detailed analysis including XRD, SEM and XPS has been investigated on pure lead malate dihydrate and all calcined products. It has been found in this work that lead malate dihydrate can be decomposed to pure lead oxide at 550 ^{o}C. This result has shown the promising possibility of using NADES to recycle LAB waste based on a leaching, precipitation, and calcination method.

4.2 Experimental

4.2.1 Chemical Reagents

Chemical reagents used in this chapter along with their chemical formula, chemical structure, purity and supplier are shown in Table 4.1.

Table 4.1 Chemical reagents

Chemical Name	Chemical Formula	Chemical Structure	Purity	Supplier
DL-malic acid	$C_4H_6O_5$	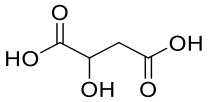	99 %	Sigma Aldrich
β-alanine	$C_3H_7NO_2$	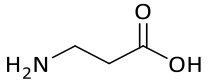	99 %	Sigma Aldrich
Lead (II) carbonate	$PbCO_3$		99 %	EMSURE

4.2.2 Synthesis of NADES and precipitates

4.2.2.1 Synthesis of NADES

MABA5 was prepared through the mixing of DL-malic acid, β-alanine and de-ionized water (conductivity = 18.2 MΩ^{-2}) in a molar ratio of 1 : 1 : 5 at 50 ^{o}C until a clear liquid was formed.

4.2.2.1.1 Justification for the use of MABA5

The ratio of DL-malic acid and β-alanine was referred to the reference.[146] In the reference, the ratio of malic acid or β-alanine to water was 1 : 3. The NADES formed at this ratio was too viscous. In this experiment, water was added to 5 part to reduce the viscosity. The density of MABA5 was measured through the following method. 100 μL of MABA5 was dispensed and the mass of which was measured. The density of MABA5 was calculated through mass divided by volume. The density of MABA5 was 1.309 g/mL (equivalent to 1309 g/L). The concentration of malic acid in MABA5 is 560 g/L. The solubility of malic acid in water is 363 g/L. The concentration of malic acid in MABA5 is higher than the solubility of water, meaning that MABA5 is still a NADES rather than a mixed aqueous solution. A NADES can achieve a higher concentration of malic acid than aqueous solution. This is the main reason why NADES rather than a concentrated malic acid aqueous solution was used.

4.2.2.2 Synthesis of precipitates

25 g $PbCO_3$ (99 %, EMSURE) was added to 100 mL of MABA5 and stirred at room temperature for a period of days until the formation of white precipitates was observed. The loading was chosen based on the experiment conducted in Chapter 6 (section 6.2.4). The mixture was centrifuged at 6000 rpm at room temperature for 30 minutes to separate the precipitate and the solution. The precipitate was then washed via a Buchner funnel using de-ionized water and acetone and dried in a Büchi-586 glass oven under vacuum at 60 ^{o}C overnight.

4.2.3 Crystallisation and characterisation of a single crystal

The above precipitate was dissolved in hot acetic acid solution (5 wt% in water). Single crystals were formed after weeks through slow evaporation of the solution. SXRD was carried out and crystallographic information was obtained.

4.2.4 Characterisation of precipitates

To identify the crystal structure and confirm the crystallinity of the precipitate, PXRD was carried out on the precipitates The analysis was carried out in the 2θ range of 10^{o} to 90^{o} with a step size of 0.034^{o} and step length of 149.86 seconds/step. SEM was carried out to identify

the surface morphology of the precipitates. XPS was carried out to identify the chemical state of each element in the precipitates and confirm the elemental composition of the precipitates. TGA coupled with DSC was carried out to identify the thermal decomposition behaviour of the precipitates. The TGA analysis was carried out from 25 ^{o}C to 550 ^{o}C at a heating rate of 10 ^{o}C/minute. FTIR and ^{1}H NMR were carried out to identify the organic part of the compounds.

4.2.5 Calcination of precipitates and characterisation of calcined products

The precipitates were calcined at 116 ^{o}C, 222 ^{o}C, 335 ^{o}C, 384 ^{o}C, 414 ^{o}C and 550 ^{o}C according to the endothermic or exothermic peaks from the DSC curve in a 10 mL alumina crucible and a glass tube in an Elite Thermal Furnace under air at a heating rate of 10 ^{o}C/minute. All calcined products were held at the designated temperature for 2 hours before cooling to room temperature. The calcined products were then analysed by XRD, SEM and XPS using the same conditions as the precipitates.

4.3 Results and Discussion

4.3.1 Structure identification of the precipitate

White precipitates were formed from a precipitation reaction of $PbCO_3$ and MABA5. PXRD was initially carried out on the precipitates, however, the XRD pattern of the white precipitate failed to match any XRD pattern from the ICDD database. To identify the compound of the precipitate, a single crystal needs to be formed. This was achieved by slow recrystallisation of the precipitate from a hot acetic acid solution. The single crystal was confirmed by SXRD to be lead malate dihydrate, Pb(D,L -$C_4H_4O_5{\cdot}2H_2O$). Lead malate dihydrate has a triclinic crystal shape with lattice parameters of $a = 6.5381(5)$ Å$, b = 7.5187(5)$Å$, c = 7.9923(6)$Å$, \alpha = 75.416(6)^{\circ}$, $\beta = 85.194(6)^{\circ}$ and $\gamma = 84.017(6)^{\circ}$ and lead has a coordination number of nine. An asymmetric unit of lead malate dihydrate is shown in Figure 4.1. Crystallographically, a lead malate dihydrate molecule contains 1 lead atom, 8 hydrogen atoms, 4 carbon atoms and 7 oxygen atoms. Of these 7 oxygen atoms, 5 come from a malic acid molecule and 2 come from two water molecules. It can be seen from Figure 4.1 that lead

malate dihydrate forms a zigzag structure through Pb-O-Pb chains rather than forming individual independent single molecules. The Pb-O-Pb chains are extended along the b axis of

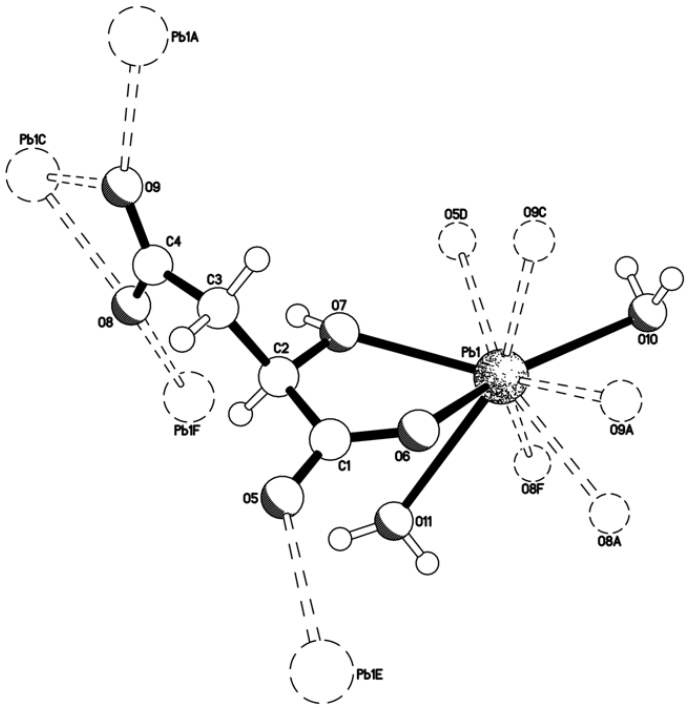

Figure 4.1 Asymmetric unit of lead malate dihydrate.

the unit cell as shown in Figure 4.2. From Figure 4.1, the oxygen (O7) of the hydroxyl group and the oxygen (O6) of carbonyl from its nearer carboxyl group form an intermolecular bonding with the lead atom. Other oxygens (O5, O8 and O9) from malic acid molecules act as bridging atoms to link lead from another molecule to form a zig-zag structure. From the crystallographic data of the single crystal, the Pb-O-Pb linkage is formed from three different types of Pb-O bonds, which are Pb to O from water with bond lengths of 2.735(8) and 2.882(6) Å, Pb to O from hydroxyl with a bond length of 2.581(8) Å and Pb to O from carboxylate with bond lengths from 2.495(12) to 2.667(12) Å. The bond length of C to C and C to O from malic acid sites in the structure ranges from 1.24(2) to 1.54(3) Å. The structure of lead malate dihydrate obtained matches the structure reported by C. N. R. Rao, which is prepared through crystallisation of $Pb(NO_3)_2$ from malic acid solution.[147]

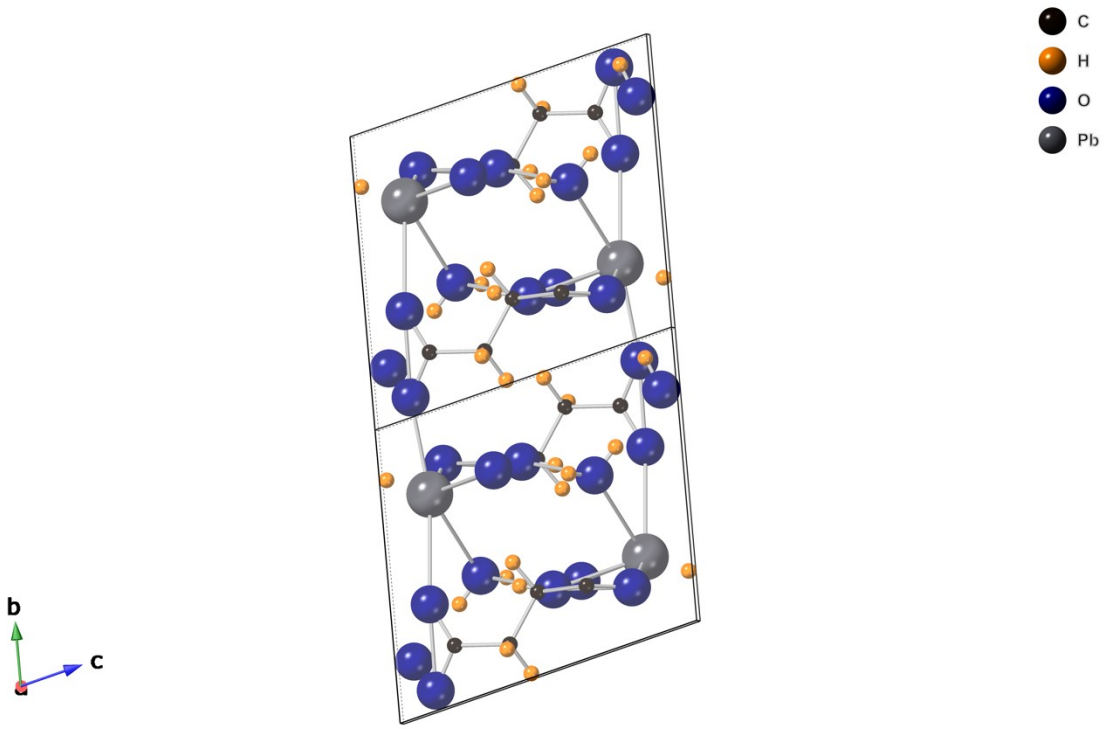

Figure 4.2 Extended version of lead malate dihydrate.

In the preparation of bulk precipitates, precipitation took a period of days. The reason for the long formation time of the precipitates may be attributed to the complex structure of lead malate dihydrate. The zigzag structure is formed from a large amount of lead malate dihydrate molecules through Pb-O-Pb bonds. The Pb-O-Pb bonds between each molecules need time to form a chain-like structure, then the chain must reach a certain size, the nuclei of which needs to reach the critical nuclei size for precipitation, to stabilize as bulk precipitates. Another reason may be attributed to the viscosity of the solvent. NADES has a higher viscosity than aqueous solution, the ions thus have a lower mobility in NADES than in aqueous solution. The formation of Pb-O-Pb bonds may take longer in NADES. These two reasons may explain the slow formation of lead malate dihydrate. In terms of recycling LAB paste, the slow precipitation would allow separation of plastic impurities from the precipitates. If the precipitation happens straight away when LAB paste is added to the NADES, then it is harder to separate the plastics or other metal impurities from the precipitate. In this case, the plastics

or metal impurities can be filtered when the Pb compounds are fully dissolved in the solution, then further stirring can be carried out to obtain pure lead malate dihydrate precipitate.

4.3.2 Characterisation of lead malate dihydrate

4.3.2.1 ^{1}H NMR of lead malate dihydrate

^{1}H NMR reflects the chemical environment of protons, and it be used to determine the chemical composition of the precipitate. Figure 4.3 a) shows the ^{1}H NMR spectrum of lead malate dihydrate dissolved in deuterated acetic acid solution and b) shows the corresponding protons from malate to the ^{1}H NMR peaks. The NMR spectrum reveals a quartet between 4.66-4.68 ppm and a doublet of doublet of doublets between 2.85-3.00 ppm. The integration ratio of these two multi-peaks is 1 : 2.12, which matches the number of protons present. According to the (n+1) empirical splitting rule, proton H_3 as shown in Figure 4.3 is present as a quartet attributed to 3 protons attached to the neighbouring atoms that H_3 is attached to, namely C2. Of these 3 protons, two of them (H_1 and H_2) are attached to C3 and one of them is attached to O7. The multiplicity of H_1 and H_2 does not match the (n+1) splitting rule. When the rule is used to predict the multiplicity of the protons, it assumes that the chemical environment of these two protons is the same. However, spatially, one of the protons is closer to the alcohol group (O_7H) and one of the protons is further away from the alcohol group. Therefore, these two protons are non-equivalent. One of the protons (assumed to be H_1 in Figure 4.3) is coupled to H_3 resulting in a doublet. As H_2 also has a coupling effect on H_1 resulting in a splitting of the doublet to a doublet of doublets. Protons H_1 and H_3 have the same coupling effect on H_2, and so H_2 also appears as a doublet of doublets. The chemical environment of H_1 and H_2 are similar, therefore, they should have a similar chemical shift. On the ^{1}H NMR spectrum, the multiplicity of these two protons appears as an overlapping of two doublet of doublets, which is called a doublet of doublet of doublets.

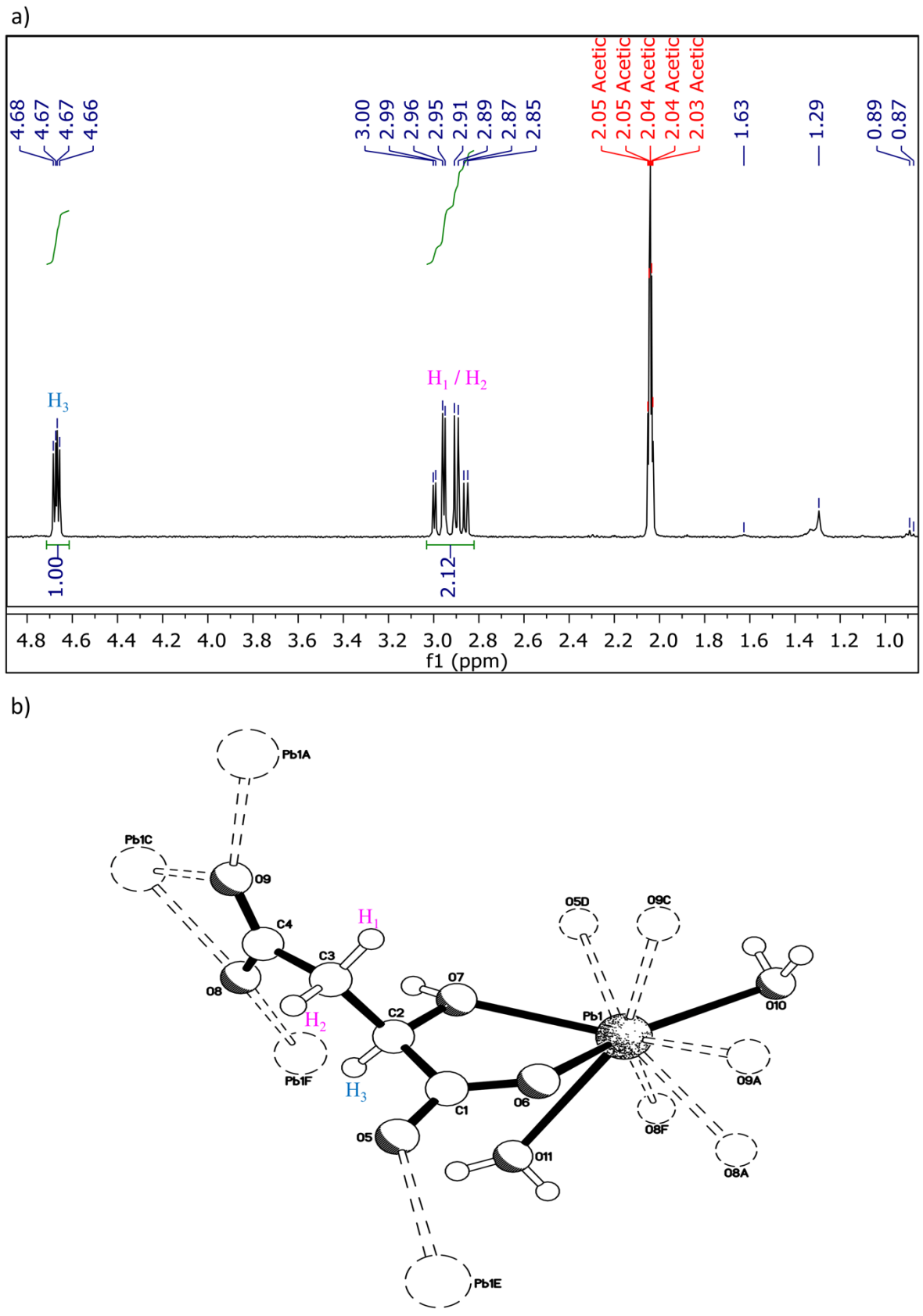

Figure 4.3 a) ^{1}H NMR (CD_3COOD) spectrum of lead malate dihydrate and b) corresponding protons of the ^{1}H NMR peaks.

4.3.2.2 FTIR of lead malate dihydrate

Figure 4.4 shows the FTIR spectrum of lead malate dihydrate and it reflects the vibration modes of the organic part of the compounds. From the FTIR spectrum, a broad O-H stretching peak can be seen at 3154 cm^{-1}, which reveals the O-H group of the carboxylic acid, alcohol and water molecules of the compound. A sharp C=O and C-O stretching peak can be seen at 1544 cm^{-1} and 1100 cm^{-1}, respectively, which reveal the presence of C-O and C=O from carboxylic groups. A medium-strong peak at 1406 cm^{-1} reflects the water adsorption of the hydrated molecules.[148] The peak at 675 cm^{-1} within the fingerprint region reflects the Pb-O-Pb bonds.[149]

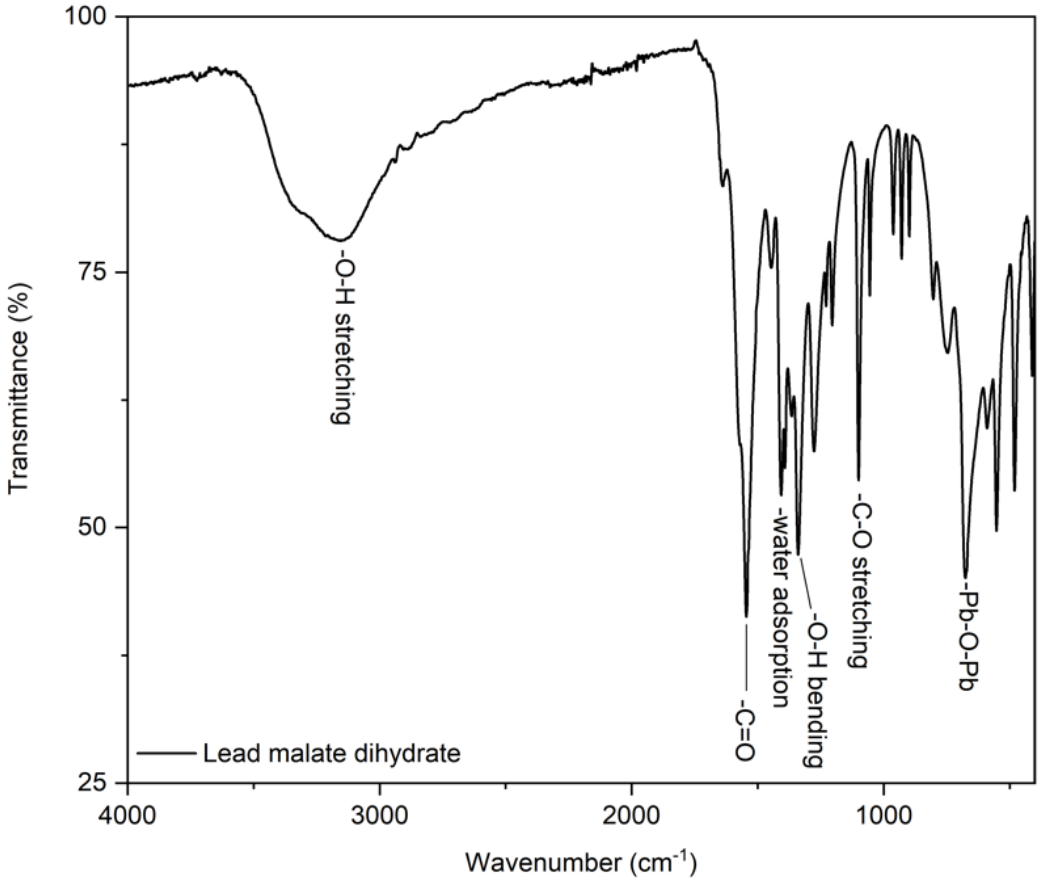

Figure 4.4 FTIR of lead malate dihydrate.

4.3.2.3 XRD, SEM and XPS analysis

PXRD was carried out on the bulk precipitate. As no reference pattern can be found in the database, Rietveld refinement was done based on the crystal structure obtained from the single crystal. The experimental and the calculated XRD pattern along with Bragg's position from the refinement can be shown in Figure 4.5. The biggest difference between the experimental and the calculated XRD pattern comes from the peak at 11.4°. The difference in the intensity of peaks may be due to preferential orientation within the bulk precipitate when being precipitated from the NADES.

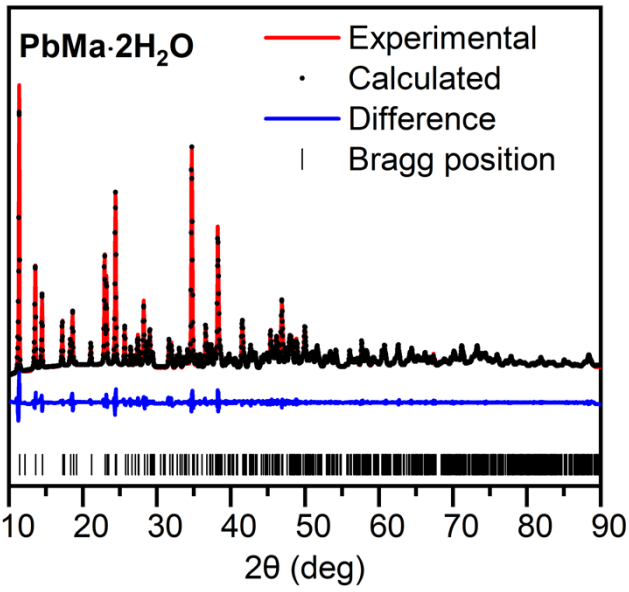

Figure 4.5 Rietveld refinement for lead malate dihydrate including the experimental and calculated XRD patterns along with difference and Bragg positions.

The preferred orientation can be confirmed by the secondary electron image of lead malate dihydrate as shown in Figure 4.6. From the SEM image shown in Figure 4.6 (a), the precipitates formed in a thin platelet shape. This platelet shape may be due to capillary force of the DESs,[150] which pushes the growth of the precipitates in a preferred orientation. It can also be seen from the image that small thin plates are stacked on larger plates. At a higher magnification of the SEM image as shown in Figure 4.6 (b), some pores can be seen on larger plates. The pores might be the nucleation sites to accommodate smaller thin plates, and thus the precipitate clusters can grow bigger to exist stably as precipitates from the solution. The

growth of these small thin plates may be slower in a viscous NADES, which would explain the slow bulk precipitation formation of lead malate dihydrate.

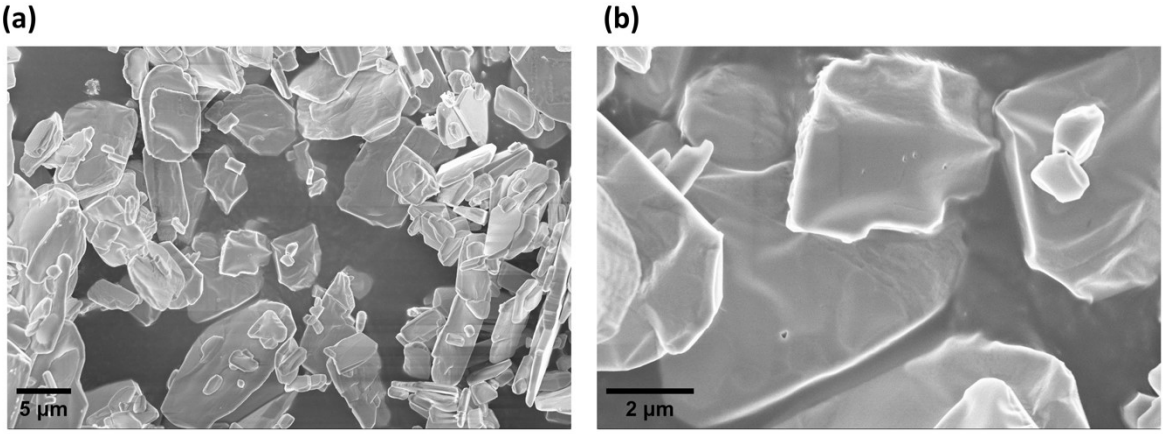

Figure 4.6 SEM images of lead malate dihydrate at a low (a) and high (b) magnification.

Lead malate dihydrate is a non-conductive material, and so a conductive Cr layer is coated on the sample prior to the analysis. However, the platelet-shaped structure has an uneven surface so that the Cr conductive layer cannot be covered on the whole surface area. As a result, charging effects were observed on the SEM images.

XPS analysis was conducted on the precipitates to identify the elemental compositions of the precipitates. From the survey (shown in Figure A. 1), only carbon, oxygen and lead were detected. Nitrogen was not detected meaning that β-alanine from the residual solvent was not present in the precipitate. It is then assumed that the NADES had been washed away completely and was not trapped between the precipitates. This confirms the purity of the precipitates analysed without the presence of residual solvent. From the elemental core levels as shown in Figure 4.7, Pb 4*f* shows two set of $f_{5/2}$ and $f_{7/2}$ doublets. Both have a spin orbit splitting (SOS) of 4.9 eV, which is similar to the value reported in the literature.[151] The Pb $4f_{7/2}$ peak at 136.5 eV and 138.7 eV are attributed to the Pb metal and organic Pb, respectively. The Pb $4f_{7/2}$ core level peak at 138.7 eV refers to the organic lead from lead malate dihydrate with an atomic concentration of 7.28 % of all elements being detected, while the weak peak at 136.5 eV refers to metallic lead with an atomic concentration of 0.98 at%. The metallic lead did not exist as a metal in the raw precipitate, it results from the reduction

of lead malate by X-rays during analysis. C 1*s* shows three singlets at 284.8 eV for C-C single bond, 286.2 eV for C-O single bond and 288.2 eV for C=O double bond, respectively. O 1*s* shows two singlets at 531.9 eV and 531.1 eV for the presence of O-H bond and O=C bonds, respectively. The total atomic ratio of C 1*s* : O 1*s* : Pb 4*f* was found to be 51.31 : 40.43 : 8.26 (equivalent to 6.21 : 4.89 : 1). Based on the chemical formula of $PbC_4H_4O_5 \cdot 2H_2O$, the atomic concentration of C is higher, and the atomic concentration of O is lower than the theoretical value. The difference might be attributed to the adventitious carbon materials being adsorbed on the surface of the sample.

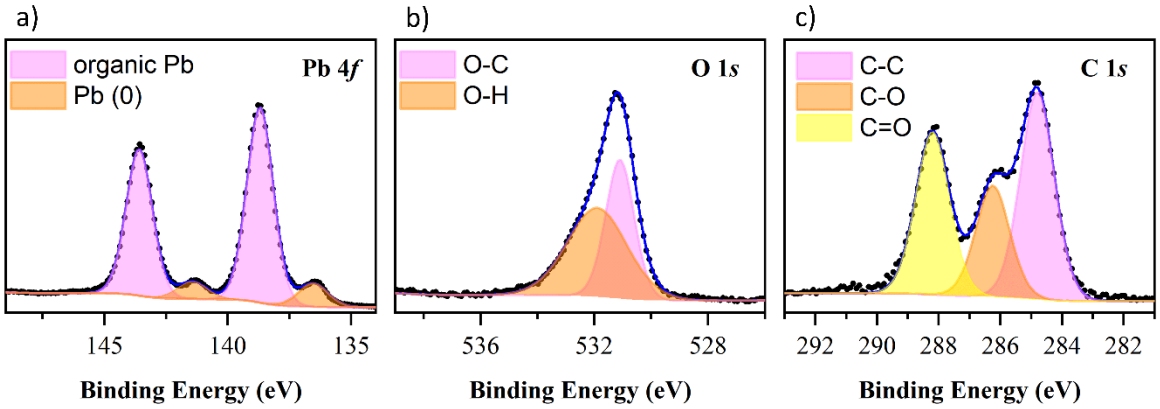

Figure 4.7 XPS core levels of lead malate dihydrate precipitate a) Pb 4*f*, b) O 1s and c) C 1s.

4.3.2.4 TGA analysis

To understand the thermal degradation behaviour of lead malate dihydrate, TGA/DSC analysis was carried out, the result of which is shown in Figure 4.8. The initial decomposition step starts from 94 °C and ends at 140 °C along with a phase change based on the exothermic peak of the DSC curve at 116 °C. The weight loss during this step was found to be 7.3 % and is referring to the loss of water molecules from lead malate dihydrate. After the initial water loss step, a plateau is reached until 190 °C, from which the mass of the powder decreases gradually as temperature increases until another plateau is achieved. The final plateau indicates a stable final product is achieved. A total mass loss of 39.5% was observed, which matches the calculated value of 40.5% assuming PbO as the final stable compound. The DSC curve exhibits one endothermic peak at 222 °C and three exothermic peaks at 335 °C, 384 °C and 414 °C. This indicates that 4 phase change reactions occurred during this gradual

decomposition step. However, it is difficult to determine the chemical compounds present at each phase change step from the TGA graph. Therefore, lead malate dihydrate powder was calcined in a furnace at these corresponding temperatures to identify the chemical compounds present at each reaction. Several analysis techniques including XRD, SEM and XPS were carried out on these calcined products to identify the composition and chemical evolution of lead malate dihydrate.

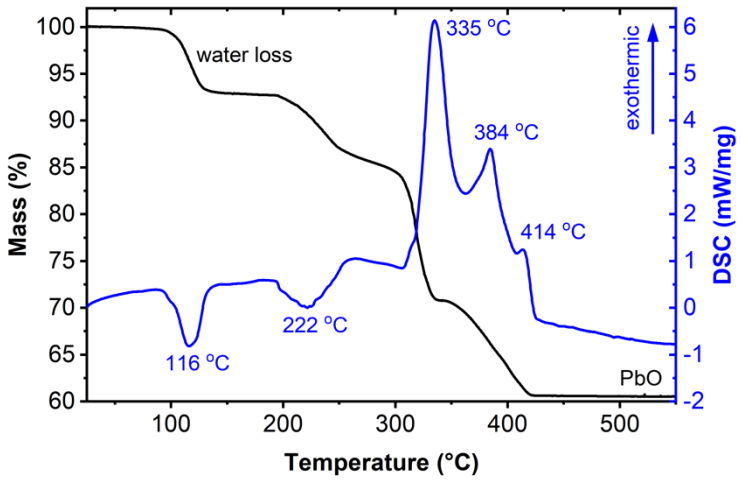

Figure 4.8 TGA and DSC analysis of lead malate dihydrate under air flow.

4.3.3 Chemical composition evolution upon thermal decomposition of lead malate dihydrate

4.3.3.1 Water loss

From the TGA analysis of lead malate dihydrate, the initial step involves the loss of water molecules. The peak positions (a quartet and a doublet of doublet of doublets) of ^{1}H NMR (shown in Figure A. 2) of the calcined product at 116 °C presents at the same chemical shift of lead malate dihydrate. It was used to prove the intactness of the malate group. The integration ratio of these two multi-peaks is 1 : 2.18 which matches the stoichiometric ratio of malate. This proves that the malate group remains after calcination at 116 °C.

The FTIR spectrum as shown in Figure 4.9 reveals that most peaks remain similar as the FTIR spectrum of lead malate dihydrate (Figure 4.4). The O-H stretching peak 3163 cm^{-1} is less intense than that of lead malate dihydrate due to the loss of water molecules. The peak at

1406 cm^{-1} referring to water adsorption is lost after calcination at 116 °C. The characteristic peaks including O-H alcohol bending, C-O stretching and Pb-O-Pb remain after calcination at 116 °C. Both ^{1}H NMR and FTIR analysis has confirmed that only water molecules are lost, and malate group remains after calcination at 116 °C for two hours.

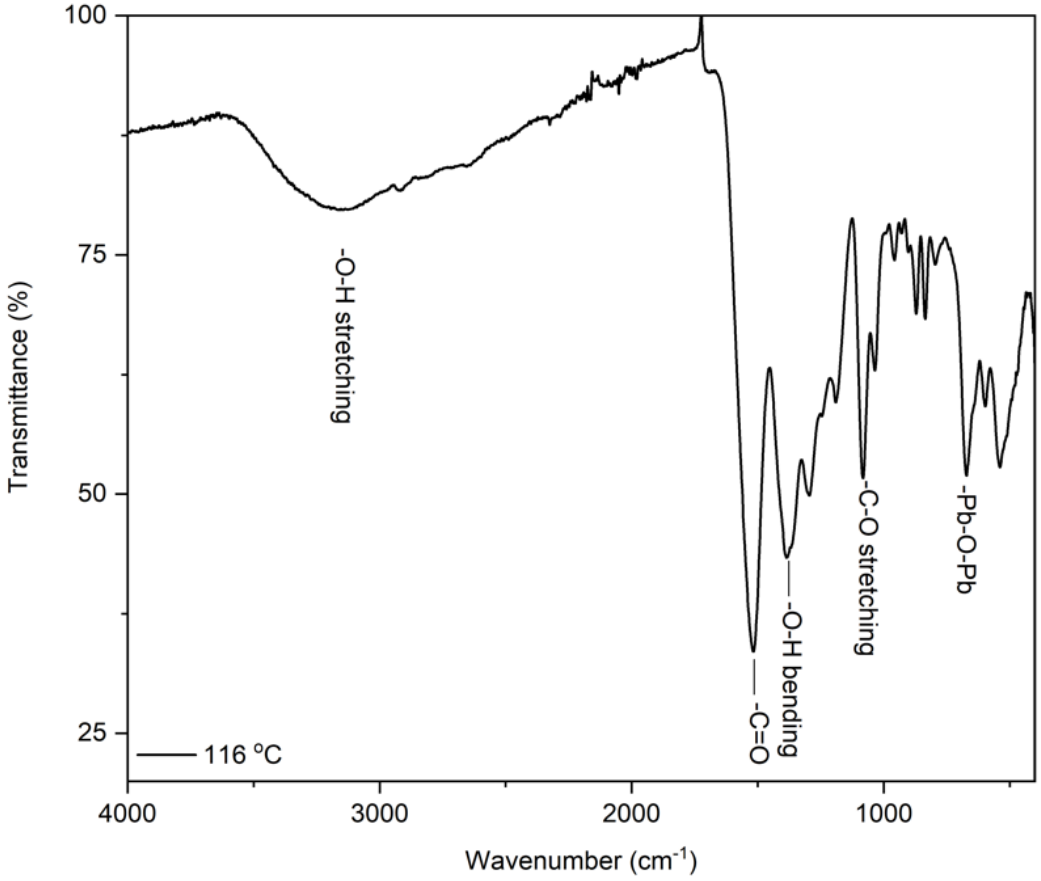

Figure 4.9 FTIR of lead malate dihydrate calcined at 116 °C for 2 hours.

Figure 4.10 shows the XRD pattern of the calcination product at 116 °C. As only water is lost at 116 °C, the chemical formula of this product should be Pb(D,L -$C_4H_4O_5$). The XRD pattern indicates that Pb(D,L -$C_4H_4O_5$) is not a structured compound. This indicates that the loss of water results in the loss of crystallinity of the structure. Thus, it is assumed that water molecules are essential in the crystal structure formation of lead malate dihydrate.

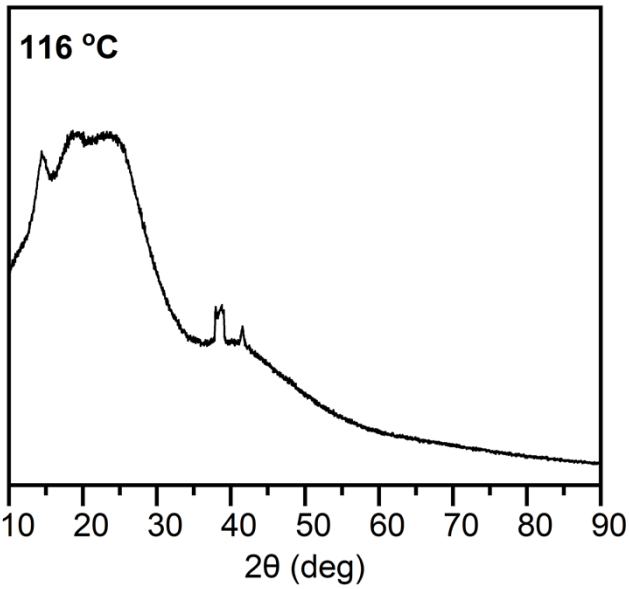

Figure 4.10 XRD pattern of lead malate dihydrate calcined at 116 °C for 2 hours.

4.3.3.2 Gradual decomposition

Figure 4.11 (a) to (f) shows the XRD patterns of lead malate dihydrate calcined from 116 °C to 550 °C. With the increase in calcination temperature, further decomposition occurs from anhydrous lead malate (product found at 116 °C). The product remains in the amorphous phase when the calcination temperature reaches 222 °C, thus, it is hard to determine the exact chemical formula of this product. As the calcination temperature reaches 335 °C, a mixture of β-PbO, α-PbO and $2PbO{\cdot}PbCO_3$ (lead oxide carbonate) forms as shown in Figure 4.11 (c). With the calcination temperature further increasing to 384 °C, a new compound, $PbO{\cdot}PbCO_3$, is formed as shown in Figure 4.11 (d). At 384 °C, $PbO{\cdot}PbCO_3$ is formed along with the increase of β-PbO at the consumption of $2PbO{\cdot}PbCO_3$ as shown in Figure 4.12, where the weight fraction of each compound was present at different calcination temperatures. The weight fraction of these compounds remains similar when the calcination temperature reaches 414 °C. $2PbO{\cdot}PbCO_3$, $2PbO{\cdot}PbCO_3$**,** α-PbO have all converted to β-PbO when the calcination temperature reaches 550 °C.

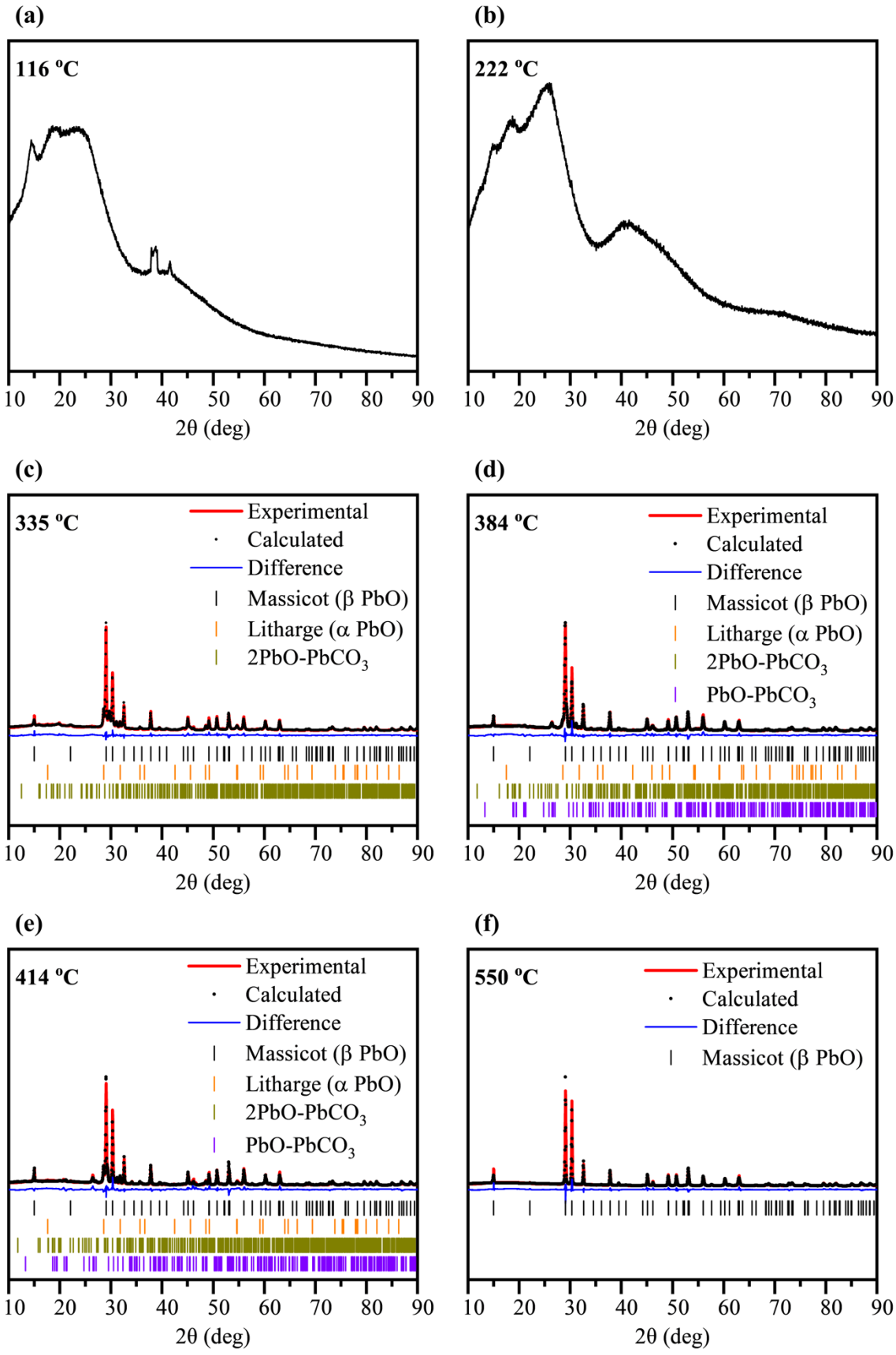

Figure 4.11 XRD pattern of lead malate dihydrate calcined for 2 hours at (a) 116 °C, (b) 222 °C, (c) 335 °C, (d) 384 °C, (e) 414 °C and (f) 550 °C.

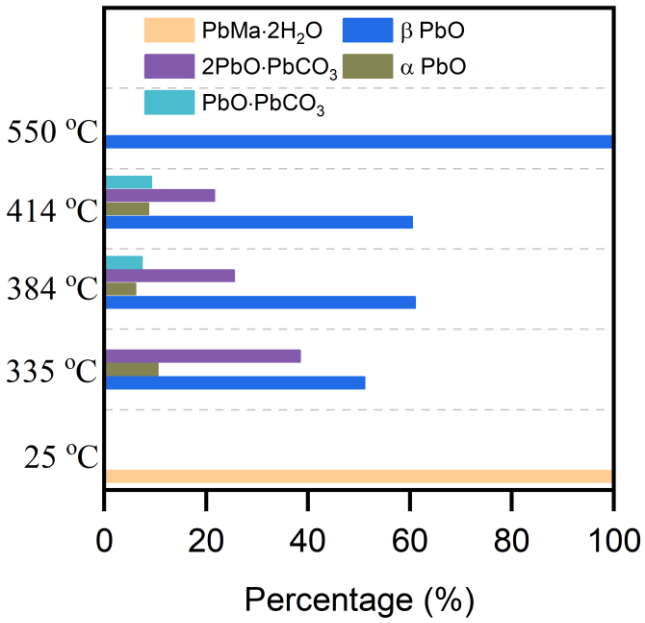

Figure 4.12 Weight percentage of $PbMa{\cdot}2H_2O$, $2PbO{\cdot}PbCO_3$, $2PbO{\cdot}PbCO_3$, α-PbO and β-PbO at room temperature as pristine precipitate and at different calcination temperatures.

4.3.3.2.1 Summary of chemical formula conversion of lead malate dihydrate

From the discussion of ^1H NMR, FTIR and XRD patterns, the evolution of chemical compounds at various calcination temperatures can be summarized as shown in Equation 4.1.

$$Pb(D,L\ -C_4H_4O_5{\cdot}2H_2O\ (s) \rightarrow Pb(D,L\ -C_4H_4O_5)(s) \rightarrow 2PbO\cdot PbCO_3(s) \rightarrow PbO(s) + PbO\cdot PbCO_3(s) \rightarrow \beta\cdot PbO(s)$$

Equation 4.1

4.3.4 XPS analysis of calcined products from lead malate dihydrate

To prove the chemical composition of calcinated products, XPS analysis was carried out on all the calcinated powder. Figure 4.13 (a-c) has shown the Pb 4*f*, C 1*s* and O 1*s* core levels evolution from calcination temperature from 116 °C to 550 °C. All peaks were normalised to Pb $4f_{7/2}$ organic Pb components to observe the changes in quantities. At 116 °C, all peaks from core level C 1*s* and Pb 4*f* remain almost unchanged compared to that of lead malate dihydrate.

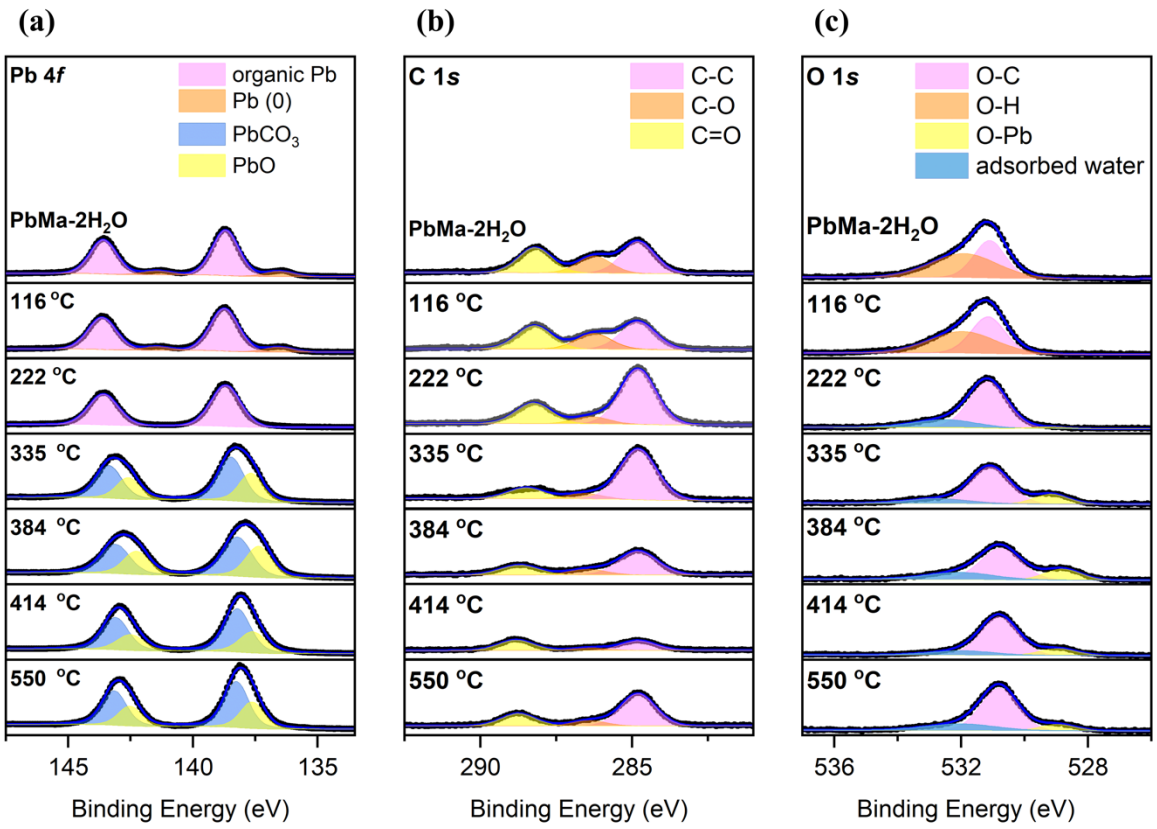

Figure 4.13 Evolution of XPS core levels (a) Pb 4*f*, (b) C 1*s* and (c) O 1*s* upon decomposition of lead malate dihydrate from as-received precipitate to calcination from 116 °C to 550 °C.

In the O 1*s* core level, the peak position of O=C and O-H peak, but the atomic ratio of O-H to Pb has decreased from 2.8 to 2.54 due to the loss of water molecules.

When the calcination temperature reaches 222 °C, the peak position of all peaks in C 1*s* remains the same as that of the calcined product at 116 °C. The atomic ratio of the C-O single bond decreases from 1.39 to 0.75 indicating the loss of C-O bond from the carboxyl group. In the O 1*s* core level, the O-H peak shifts to higher binding energy for 0.6 eV as its atomic ratio to Pb decreased to 1. The peak decrease or loss indicates that O-H hydroxyl and C-O carbon oxygen bonds break earlier than the C=O carbonyl group during calcination. The breakup of these chemical groups has changed the chemical environment in neighbouring atoms of C=O group, which causes a shift towards to higher binding energy. More interestingly, a tiny O-Pb peak in O *1s* has been found at a binding energy of 529.3 eV indicating the initial formation of PbO. As the atomic percentage of this O-Pb only shows 0.81 at%, the amount of PbO formed is too small to be detected by XRD.

When the calcination temperature reaches 335 °C, Pb 4*f* shows one doublet for PbO at 137.7 eV and 142.6 eV and another doublet for $PbCO_3$ at 138.5 eV and 143.4 eV. No organic Pb peak has been found in the Pb 4*f* core level indicating the conversion of lead malate to a mixture of $PbCO_3$ and PbO. From the quantitative analysis, $PbCO_3$ has shown a higher atomic percentage among all peaks identified in comparison to PbO (PbO : $PbCO_3$ = 0.6), though the major compound identified from XRD analysis is PbO. This is attributed to the reaction of PbO on the surface with atmospheric CO_2.[116,152,153] The O=C peak at 531.1 eV and O-Pb peak at 529.2 eV in the O 1*s* core level were assigned to the presence of $PbCO_3$ and PbO, respectively. The peak at 532.7 eV in O 1*s* core level may be attributed to the presence of adsorbed water from the atmosphere.

With further increases in the calcination temperature, the peaks did not change significantly. Although from the chemical composition analysis by XRD the main composition above calcination temperature of 500 °C is β-PbO, in the XPS analysis $PbCO_3$ dominates the surface. This could be attributed to the reaction between PbO with atmospheric CO_2 on the surface layer.

4.3.5 Morphology analysis of calcined products from lead malate dihydrate

From the SEM image after calcination at 116 ºC as shown Figure 4.14 (a), the platelet shape of the structure remains unchanged compared to that of lead malate dihydrate precipitate. However, many pores can be observed on the surface of each plate. From the discussion of chemical conversion at 116 ºC, it is assumed that these pores are the result of water loss. These pores might also be the reason for the loss of crystallinity. When the calcination temperature reaches 222 ºC, the calcined product loses its platelet shape and result in a porous structure. The pores of the calcined product at 222 ºC are much bigger than that at 116 ºC as shown in Figure 4.14 (b). When the calcination temperature reaches 335 ºC, the porous morphology remains with the formation of some square-shaped crystals. As the calcination temperature increases to 384 ºC, more small sphere-shaped crystals form. When the calcination temperature further increases to 414 ºC, the sphere-shaped crystals grow slightly bigger compared to that at 384 ºC along with a slight loss of square-shaped crystals. When the calcination temperature reaches 550 ºC, the crystals has formed a homogenous

morphology with an uneven surface. From the XRD result, it is confirmed that β-PbO is the only phase present in the calcined product. It is assumed that the homogenous structure represents the morphology of β-PbO.

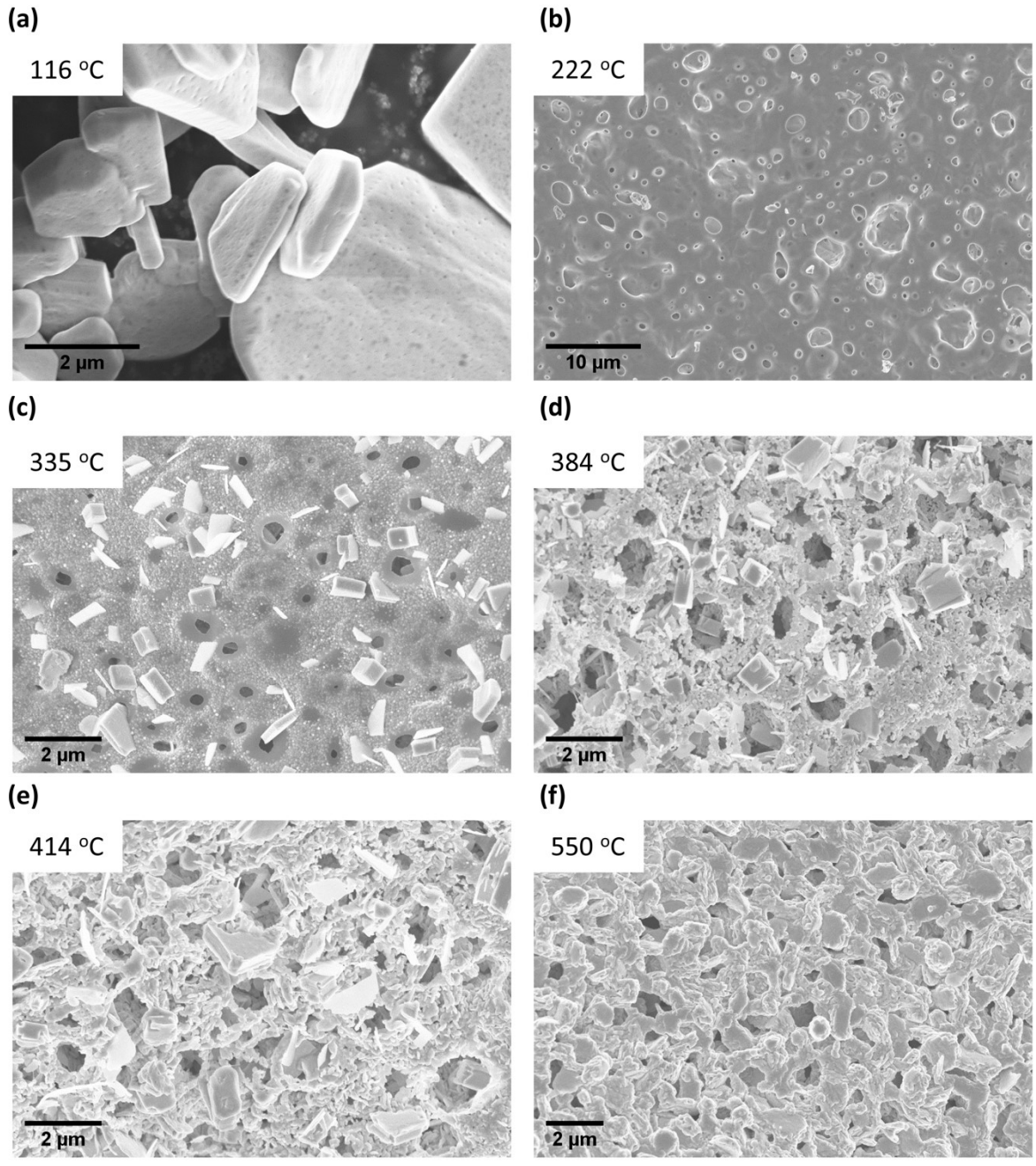

Figure 4.14 SEM images of lead malate dihydrate calcined for 2 hours at (a) 116 °C, (b) 222 °C, (c) 335 °C, (d) 384 °C, (e) 414 °C and (f) 550 °C.

4.4 Conclusions

A green solvent NADES (malic acid/β-alanine/de-ionized water) has been used to convert $PbCO_3$, the main component of desulfurized lead paste, to an organic lead precipitate. Recrystallisation of the powder precipitate in hot acetic acid aqueous solution (5 wt% in water) produced single crystals, later confirmed to be lead malate dihydrate. PXRD has confirmed that the bulk powder precipitate is also lead malate dihydrate. Lead malate dihydrate has been the subject of limited study, only the crystal structure of which has been reported by C. N. R. Rao. A series of analysis techniques in this study including powder XRD, ^{1}H NMR, FTIR, XPS and SEM were carried out to investigate the structure and morphology of lead malate dihydrate. In terms of conversion of organic lead precipitate to PbO, a thermal degradation behaviour analysis TGA/DSC was carried out to investigate the degradation of lead malate dihydrate. It was found that lead malate dihydrate can be decomposed to PbO through several gradual degradation steps between 116 ^oC to 550 ^oC. To identify the degradation products at each step, lead malate dihydrate was calcined in a furnace at certain temperatures based on the endothermic/exothermic peaks observed from the DSC curve. Techniques including powder XRD, XPS and SEM have been carried out to analyze the calcined products. High purity of β-PbO has formed at a calcination temperature of 550 ^oC.

In conclusion, this chemical process has explored the possibility of recycling Pb paste components, $PbCO_3$, through a leaching and calcination method with the use of a NADES. The dissolution of $PbCO_3$ and conversion to lead malate dihydrate precipitate both can happen at room temperature, meaning that the leaching method is economically promising relative to more energy-intensive methods.

It has been found that the formation of an organic lead precipitate is mainly attributed to the carboxylic acid component of NADES. Therefore, the leaching and calcination method can be extended to the use of other carboxylic acid-based NADES if the constituent carboxylic acid of which can form an organic lead compound. However, only limited organic lead compounds are available making the selection of NADESs more difficult. Future work should focus on the exploration of new organic lead compounds. In the next chapter, a new lead compound, lead lactate, has been formed through the reaction of $PbCO_3$ and a NADES (lactic

acid/betaine/deionized water). This has promoted the diversity of organic lead compounds precipitated through this leaching method.

Chapter 5 Synthesis, Characterisation and Decomposition of Lead Lactate

5.1 Introduction

To overcome the limitation of pyrometallurgy and hydrometallurgy in the LAB recycling process, an advanced process (leaching followed by calcination) has been developed to offer an improvement from both economic and environmental perspectives. The process was developed by Sonmez and Kumar, in which a citric acid aqueous solution was to leach battery paste to lead citrate, which then can be calcined at a temperature lower than 500 ^{o}C to obtain PbO as the recovered product.[77,78] In the last chapter (chapter 4), a greener solvent, a NADES, was used to replace the aqueous solution as the leaching solvent to dissolve battery paste components, minimizing the water use in the solvent. Progress has been made with the use of NADES; however, only limited NADES can be used with this method due to the limited organic lead compounds that can precipitate. In this chapter, a new compound, lead lactate, has been formed as a precipitate through the reaction of $PbCO_3$ (the main component of desulfurized lead paste) and a lactic acid-based NADES. This offers more solvent flexibility for the leaching/calcination method.

5.2 Experimental

5.2.1 Chemical Reagents

Chemical reagents used in this chapter along with their chemical formula, chemical structure, purity, and supplier are shown in Table 5.1.

Table 5.1 Summary of Chemical Reagents in Chapter 5.

Chemical Name	Chemical Formula	Chemical Structure	Purity	Supplier
DL-Lactic acid solution (85 wt% in water)	$C_3H_6O_3$	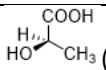 (D-lactic acid) 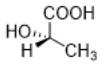 (L-lactic acid)	85 %	Sigma Aldrich
betaine	$C_5H_{11}NO_2$	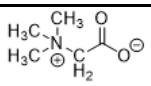	98 %	Sigma Aldrich
Lead (II) oxide	PbO		99.999 % (Trace metal basis)	Sigma Aldrich

5.2.2 Synthesis of NADES and precipitates

5.2.2.1 Synthesis of NADES

LABet5 was prepared by mixing of lactic acid (LA) solution, betaine and de-ionized water (conductivity = 18.2 $M\Omega^{-2}$) in a molar ratio of 2 : 1 : 5 at 50 ^oC until a clear liquid is formed. The ratio of lactic acid and betaine was referred to the reference.[154] In the reference, the ratio of betaine to water was 1 : 2. The NADES formed at this ratio was too viscous. In this experiment, water was added to 5 part (to betaine) to reduce the viscosity.

5.2.2.2 Synthesis of precipitates

To two vials containing 10 mL of LABet5 were added 5g and 9 g PbO, respectively. Both vials were stirred at 50 ^oC for 4 days. The selection of the loadings is based on the experiments conducted in Chapter 7 section 7.2.2.1 and 7.2.3.1.

After 4 days, the LABet5 with a loading of 5 g/10 mL PbO forms a clear solution without precipitation. Single crystals were formed in the vial several months later. The LABet5 with a loading of 9 g/10 mL PbO forms a cloudy solution with white precipitates. This loading was chosen to be able to collect significant number of precipitates for a series analysis.

Both mixtures were centrifuged at 6000 rpm at room temperature for 30 minutes to separate the precipitate and the solution. The precipitate was then washed via a Buchner funnel using de-ionized water and acetone and dried in a Büchi-586 glass oven under vacuum at 60 ^oC.

5.2.3 Crystallisation and characterisation of a single crystal

The single crystals analysed in this chapter were formed unintentionally along with the conduction the experiments in Chapter 7. The experimental conditions for the formation of the single crystals refer to the conditions of specific samples in Chapter 7 where the single crystals were formed and analysed. No optimisation experiments for the single crystal formation were done.

5.2.3.1 LABet5 with 5 g/ 10 mL PbO loading – Pb dilactate $Pb(LA)_2$

The clear solution was left for over 8 months and single crystals formed from the solution. The single crystal was analysed using SXRD to obtain crystallographic data.

5.2.3.2 LABet5 with 9 g/ 10 mL PbO loading – Pb mono-lactate PbLA

To form a single crystal, a loading of 9 g/10 mL PbO was added to LABet5 and stirred at RT for 72 hours. The solution was filtered through a 0.2 μm PES filter and was left for weeks to months to form single crystals.

To shorten the single crystal formation time, 9 g PbO was added to LABet10 formed from lactic acid : betaine : water in a molar ratio of 2 : 1 : 10. The mixture was stirred at 50 ^{o}C for 2 hours. The solvent was then filtered, and single crystals were formed after 1 day. SXRD has confirmed that these two single crystals are enantiomers of each other (Figure 5.3 and Figure 5.3 Asymmetric unit of Pb(D-$C_3H_4O_3$).Figure 5.4).

5.2.4 Characterisation of precipitates

PXRD was carried out on the precipitates to identify the crystal structure and confirm the crystallinity of the precipitates. The analysis was carried out in the 2θ range of 5^{o} to 90^{o} with a step size of 0.034^{o} and step length of 149.86 seconds/step. SEM was carried out on the precipitates to identify the surface morphology of the precipitates. XPS was carried out to identify the chemical state of each element in the precipitates and confirm the elemental composition of the precipitates. FTIR and ^{1}H NMR were carried out to identify the organic part of the compounds.

5.2.5 Calcination of precipitates and characterisation of calcined products

The precipitates were calcined at 100 °C, 200 °C, 300 °C, 400 °C, 550 °C in a 10 mL alumina crucible and a glass tube in an Elite Thermal Furnace under air at a heating rate of 10 °C/minute. All calcined products were held at the designated temperature for 2 hours before cooling to room temperature. The calcined products were then analysed by XRD, SEM and XPS using the same conditions as the precipitates.

5.3 Results and Discussion

5.3.1 Analysis of single crystals

5.3.1.1 Analysis of a single crystal – $Pb(LA)_2$

The single crystal formed from LABet5 with a loading of 5 g/10 mL PbO was confirmed to be lead dilactate $Pb(C_3H_5O_3)_2$ as shown in Figure 5.1.

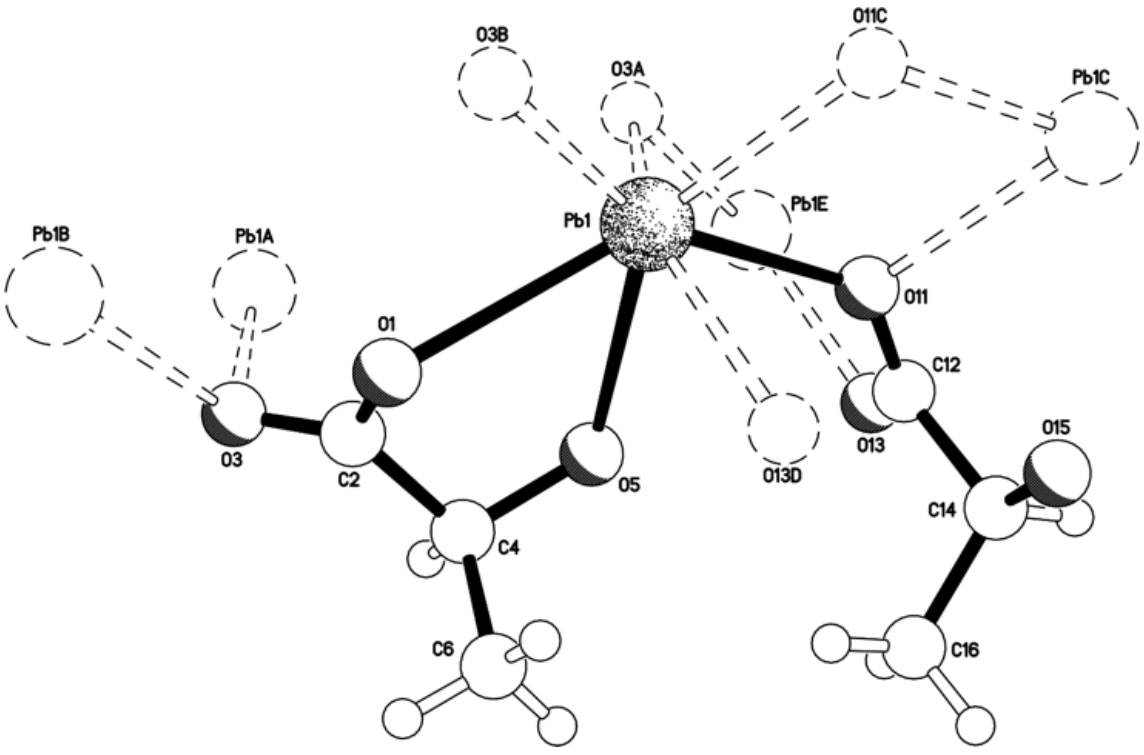

Figure 5.1 Asymmetric unit of lead dilactate $Pb(C_3H_5O_3)_2$.

Though the formation of the single crystal took over 8 months, the single crystal formed was of poor quality with twinned plates. As a result, the crystallographer was not able to locate

the H atom on O5 and O15 due to high background noise. The sum of the chemical formula of this single crystal $Pb(C_3H_5O_3)_2$, which assumes that these two H atoms are present. Lead dilactate has a monoclinic crystal structure with lattice parameters of $a = 10.8445(5)$ Å, $b = 4.6937(2)$ Å, $c = 17.2710$ Å and $\beta = 97.801(4)°$. The crystal structure of $Pb(C_3H_5O_3)_2$ is shown in Figure 5.2. It can be seen that the crystal formed is a racemate, which refers to Pb(D,L- $C_3H_5O_3$). Similar to lead malate dihydrate, lead dilactate also forms a zigzag structure through Pb-O-Pb chains rather than forming a single molecule. The Pb-O-Pb linkage is formed from three different types of Pb-O bonds, which are Pb to O (O5) of the hydroxyl group and Pb to O (O1) of carboxyl group from the same lactic acid molecule with bond lengths of 2.662(5) Å and 2.706(5) Å, respectively. The third Pb-O bond is formed between Pb to O (O11) of carboxyl group from another lactic acid molecule with bond length of 2.517(5) Å. These three O atoms form intermolecular bonds with the Pb atom. In particular, the O11 also acts as a bridging atom along with other O atoms (O3 and O13) to link lead from other molecules. These extended Pb-O-Pb linkage then form a zigzag structure. Other types of bonds including C-O bonds and C-C bonds ranging from 1.257(9) Å to 1.532(11) Å. These are the first data to reveal the structure of lead dilactate.

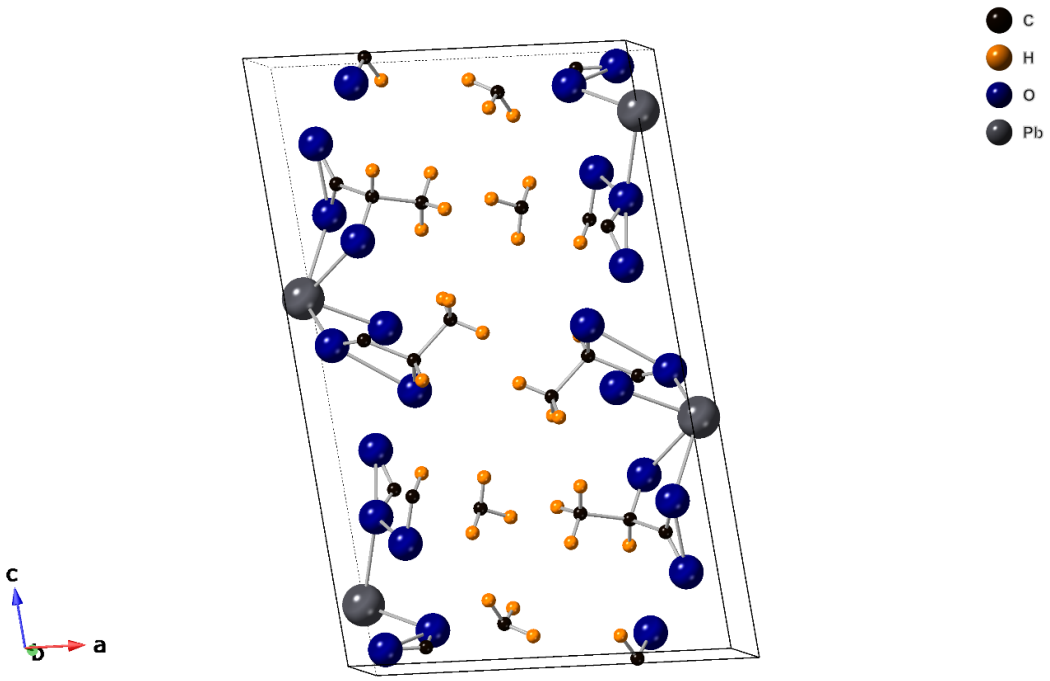

Figure 5.2 Crystal structure of Pb(D,L-$C_3H_5O_3)_2$.

5.3.1.2 Analysis of a single crystal – PbLA

The single crystal formed from LABet5 with a loading of 9 g/10 mL PbO has been confirmed to be lead mono-lactate [Pb(D-$C_3H_4O_3$)] as shown in Figure 5.3.

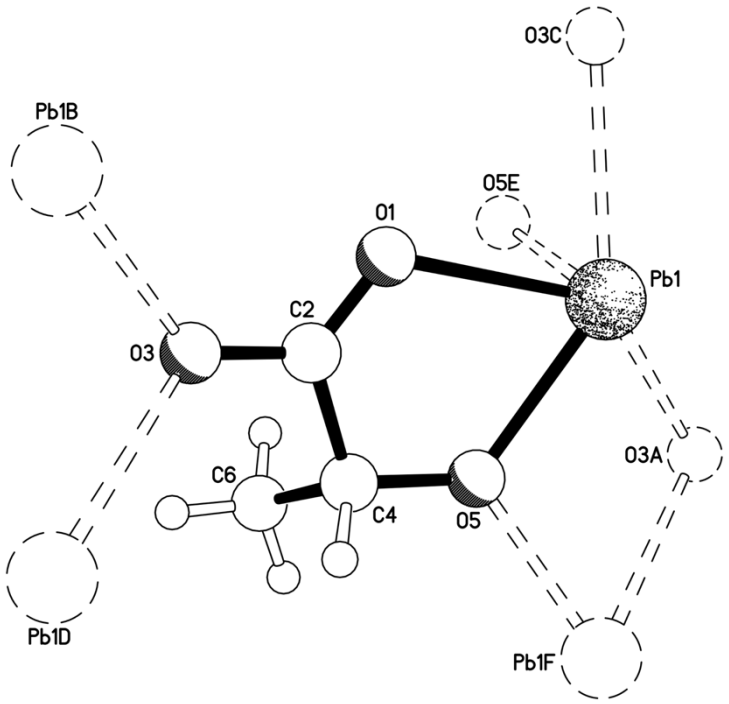

Figure 5.3 Asymmetric unit of Pb(D-$C_3H_4O_3$).

Lead D-lactate has a tetragonal crystal structure with lattice parameters of $a = b = 6.16213(12)$ Å, $c = 12.6875(4)$Å $and\ \alpha = \beta = \gamma = 90°$. From in Figure 5.3, the oxygen (O1) from the carboxyl group and the oxygen (O5) from the alcohol group forms an intermolecular bond with Pb with bond lengths of 2.481(6) Å and 2.317(6) Å, respectively. Other types of bonds including C-O bonds and C-C bonds are present with lengths ranging from 1.227(11) Å to 1.544(13) Å. Another oxygen (O3) from the carboxyl group and the oxygen (O5) link individual lead lactate molecule to form indefinite Pb-O-Pb chains. The bond lengths of these two Pb-O bonds are 2.751(7) Å and 2.278(6) Å, respectively. It is assumed that a single lead lactate molecule is not able to crystallise from the solution. When the Pb-O-Pb chain is extended to a critical length, the structure is big enough to crystallize from the solution. The crystallisation of Pb(D-lactate) in LABet5 requires at least two months. The slow crystallisation of lead lactate may be attributed to the complex formation of the

Pb-O-Pb linkage. Another reason for the slow crystallisation may be attributed to the high viscosity of the solvent.

Therefore, water was added to LABet5 to modify the viscosity. This solvent with higher water content was used to accelerate the crystallisation of lead lactate. The new solvent (LABet10) comprised lactic acid, betaine and water at a molar ratio of 2 : 1 : 10. 9 g PbO was added to 10 mL of LABet10 and left at 50 ^{o}C for for 2 hours. The solvent was then filtered, and single crystals were formed after 1 day. The single crystal formed in this new solvent was confirmed by SXRD to be Pb(L-$C_3H_4O_3$) as shown in Figure 5.4, which is an enantiomer of the single crystal formed in LAbet5.

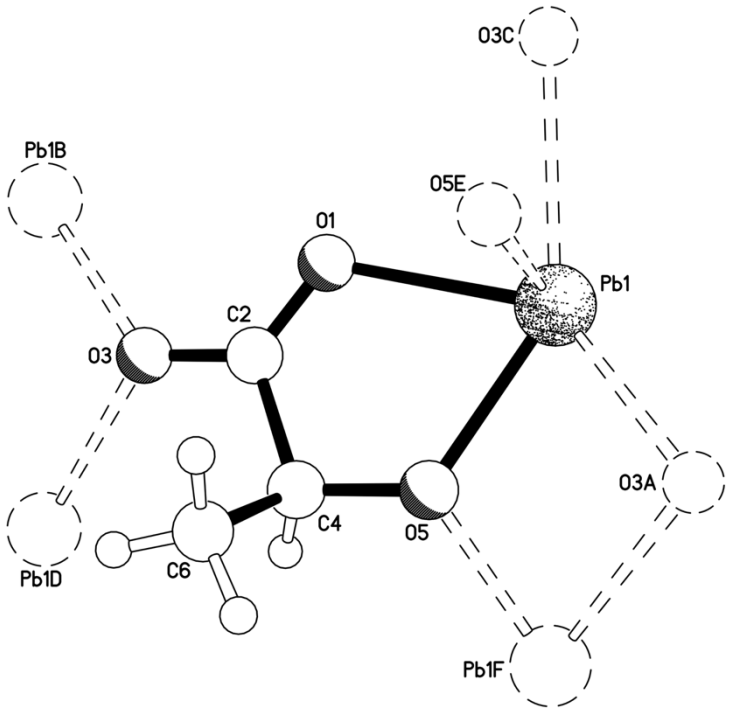

Figure 5.4 Asymmetric unit of Pb(L-$C_3H_4O_3$).

The crystal structures and lattice parameters of these two enantiomers, as shown in Figure 5.5 and Figure 5.6, are otherwise identical. Though Pb(D-$C_3H_4O_3$) and Pb(L-$C_3H_4O_3$) were formed with NADESs differencing in water content, no evidence has suggested that the water content has an impact on the formation of different isomers as the paired isomers normally have similar chemical and physical properties. It might be a coincidence that two different isomers (D- and L-) were formed using NADESs with different water content.

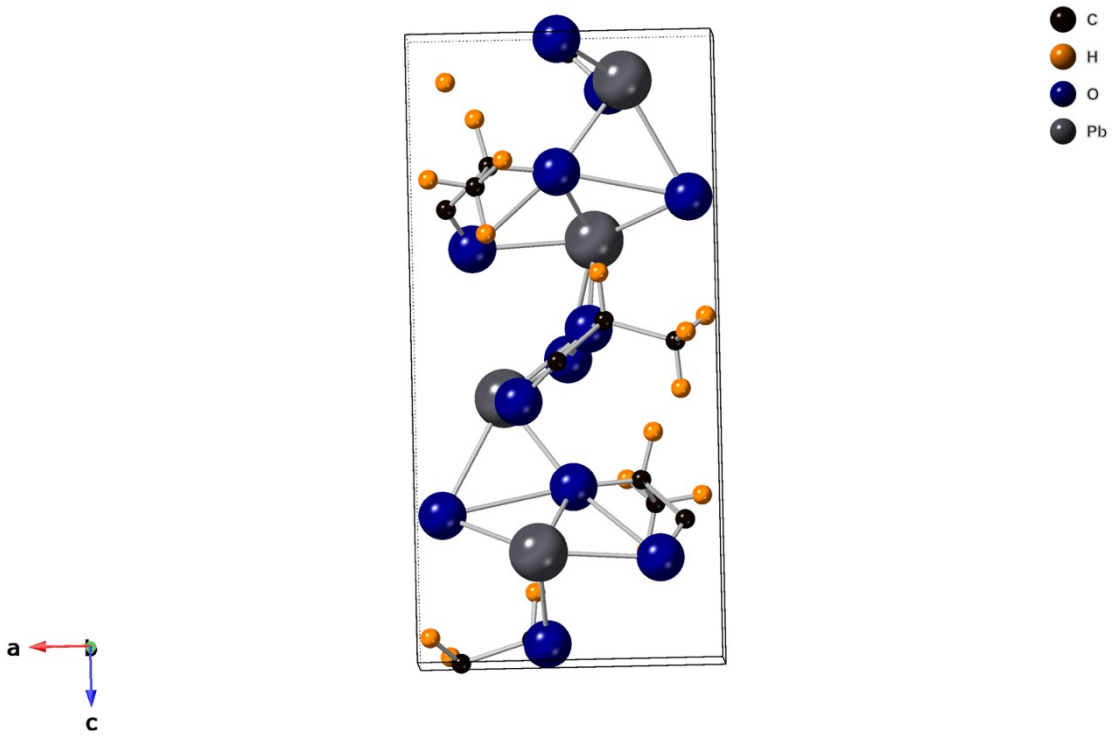

Figure 5.5 Crystal structure of Pb(D- $C_3H_4O_3$).

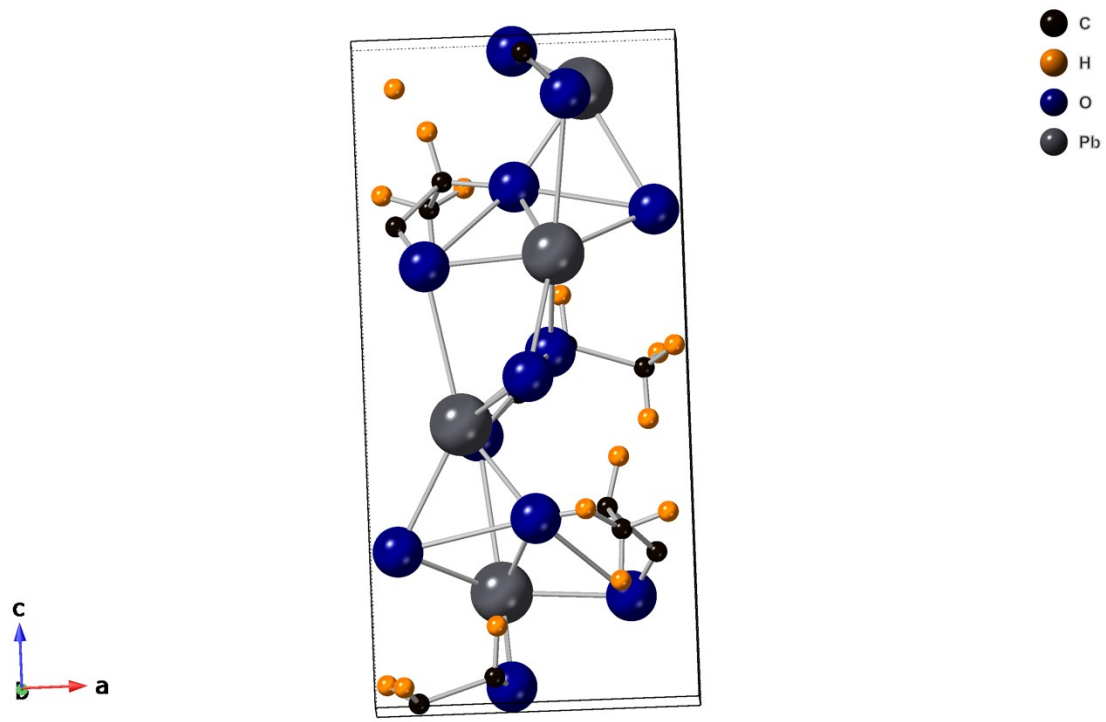

Figure 5.6 Crystal structure of Pb(L- $C_3H_4O_3$).

5.3.2 Identification of the precipitate

Bulk white precipitates were formed from 10 mL LABet5 with 9 g PbO after reacting at 50 °C for 4 days. Powder XRD was carried out on the precipitate as shown in Figure 5.7, which did not match any XRD patterns from the ICDD database. Three types of single crystals were identified based on Pb atoms and lactic acid. Analysis of the single crystals was initially done, and calculated powder XRD patterns based on the single crystals were compared with the XRD pattern of the precipitate.

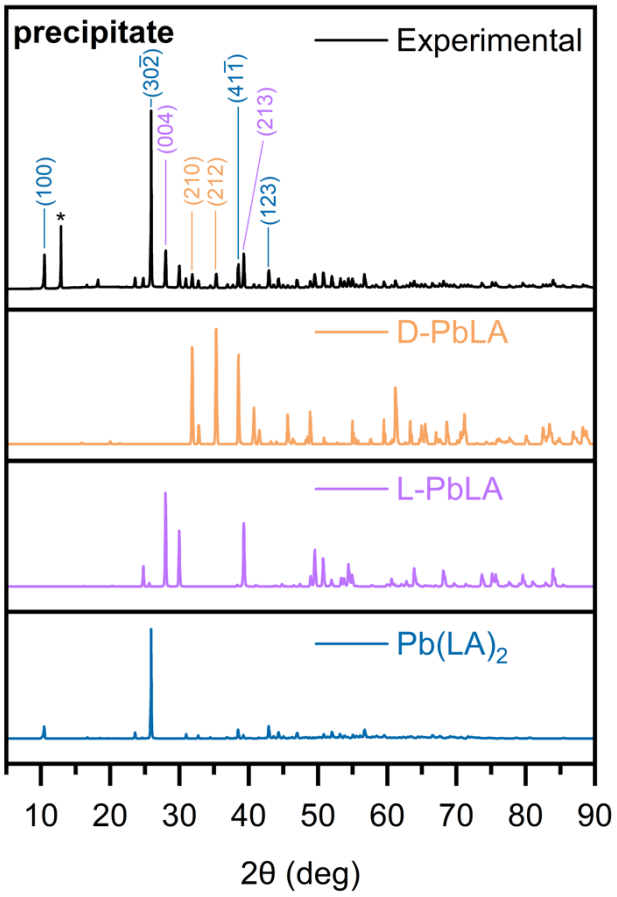

Figure 5.7 XRD pattern of the precipitate.

5.3.2.1 Powder XRD

As shown in Figure 5.7, the precipitate contains a mixture of $Pb(LA)_2$, D-PbLA and L-PbLA. As two H atoms in $Pb(LA)_2$ cannot be located from SXRD data, it is not possible to carry out Rietveld refinement to determine the weight fraction of each compound. Instead, Pawley refinement was done based on the lattice parameters and space group given from the single

crystal XRD. A peak at $2\theta = 12.83°$ (marked as * in Figure 5.7) cannot be identified. It does not match the XRD pattern of the starting lead material, PbO, and it is difficult to identify the compound from this peak. With this exception, most of the peaks can be assigned to one of three lead compounds identified. Further analysis and calcination processes have been carried out based on the precipitate, however, due to its complexity, lead lactate or $Pb(LA)_x$ was used as a representative model.

5.3.2.2 FTIR

Figure 5.8 shows the FTIR spectrum of lead lactate. Two sharp peaks can be seen at 2968 cm^{-1} and 2849 cm^{-1}, ascribed to C-C stretching,[155] and the sharp peak at 1564 cm^{-1} confirms the presence of C=O from carboxylic acid groups.[156] Peaks in the range of 1380 – 1300 cm^{-1}, 1120 – 1080 cm^{-1} and 480 – 430 cm^{-1} reflect the C-H bending, C-O stretching, and C-OOR vibration, respectively.[156,157] The peak at 675 cm^{-1} within the fingerprint region reflects the Pb-O-Pb bonds.[149,157]

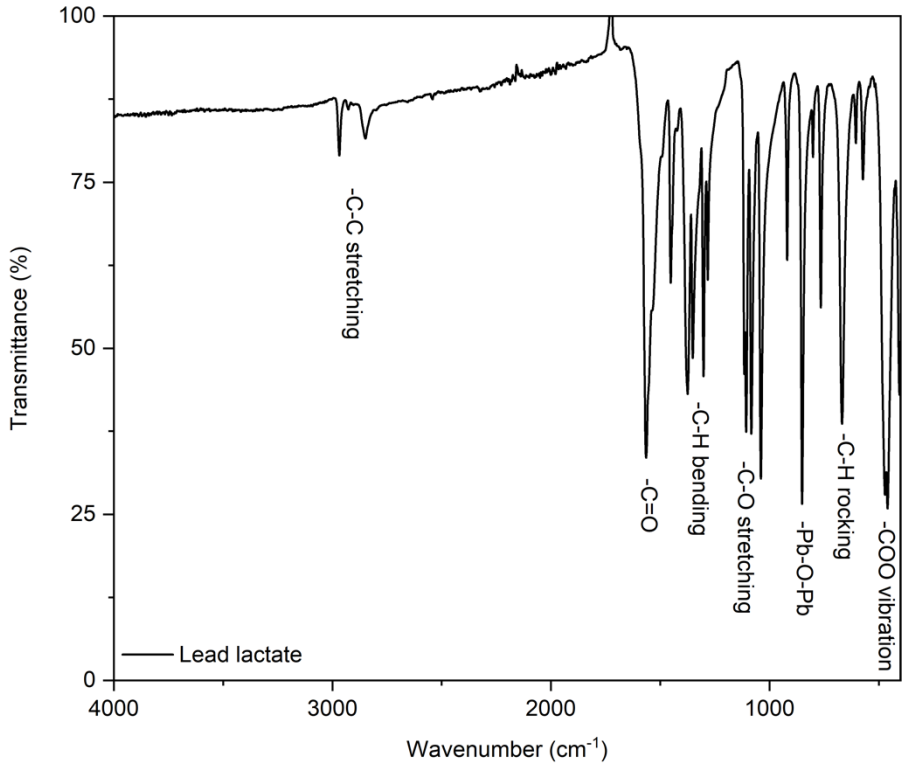

Figure 5.8 FTIR of the precipitate, lead lactate.

5.3.2.3 ^{1}H NMR

^{1}H NMR reflects the chemical environment of protons, and it can be used to study the organic part (lactate) of the lead lactate precipitate. The ^{1}H NMR (400 MHz, CD_3COOD) peak positions of the lead lactate are: δ = 1.45 (3H, CH_3, d, J = 8 Hz), 4.41 (1H, CH, q, J = 8 Hz). The original ^{1}H NMR spectrum with assignment of can be shown in Figure A. 3. Ideally the C-H or CH_3 group from PbLA and $Pb(LA)_2$ would have different chemical shifts. As the chemical environments of the protons in PbLA and $Pb(LA)_2$ are so similar, they overlap at a close chemical shift so that they cannot be separated on the spectrum.

5.3.2.4 XPS

XPS analysis was carried out on the precipitates to identify the elemental composition. From the survey (shown in Figure A. 4) only carbon, oxygen, and lead have been detected. Nitrogen was not detected, meaning that betaine was not present in the precipitate. Accordingly, it is assumed that the NADES was successfully removed during the washing steps. For the elemental core levels, as shown in Figure 5.9 (a), Pb 4*f* shows two set of $f_{5/2}$ and $f_{7/2}$ doublets. Both doublets have a SOS of 4.9 eV, which is similar to the value reported in the literature.[151] The Pb $f_{7/2}$ peak at 136.5 eV and 138.5 eV are attributed to Pb metal and organic Pb, respectively.

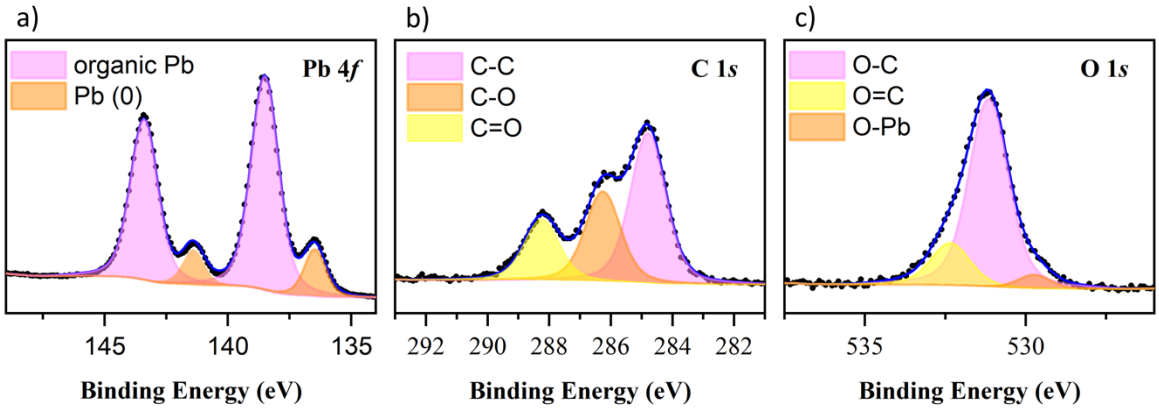

Figure 5.9 XPS core levels of precipitated lead lactate a) Pb 4*f*, b) C 1*s* and c) O 1*s*.

The organic Pb refers to lead lactate, while the metallic Pb is present due to the reduction of lead lactate during analysis. C 1*s* (Figure 5.9 b)) shows three singlets at 284.8 eV for the C-C

single bond, 286.2 eV for the C-O single bond and 288.2 eV for the C=O double bond. O 1*s* (Figure 5.9 c)) shows three singlets at 532.4 eV for the O=C double bond, 531.2 eV for the O-C single bond and 529.7 eV for the O-Pb bond. The O=C and O-C bonds are present in the lactate, while the O-Pb bond corresponds to PbO, which comes from unreacted PbO being adsorbed on the surface of the precipitate.

5.3.2.5 SEM

Figure 5.10 shows the SEM image of the precipitated lead lactate [$Pb(LA)_x$]. It can be seen from the figure that the crystals of the precipitate are of different sizes. This is possibly caused by the presence of multiple compounds in the precipitate. Additionally, the reaction takes around 96 hours and precipitates are crystallized gradually from the solvent. As a result, fresh precipitates are of smaller crystal size and older precipitates have grown to larger crystal size.

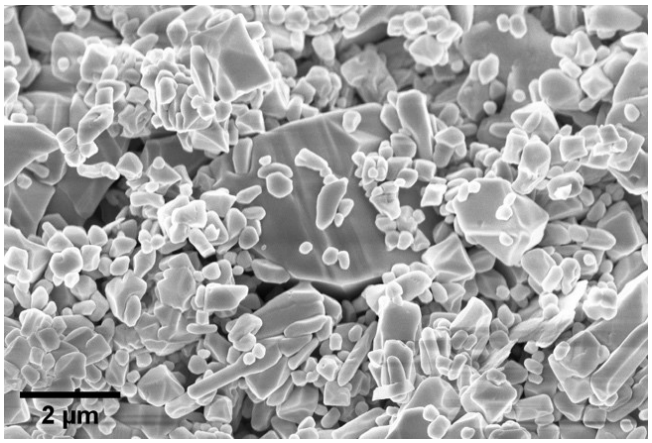

Figure 5.10 SEM image of precipitate lead lactate.

5.3.3 Analysis of calcined products

5.3.3.1 XRD

Figure 5.11 (b) to (f) shows the XRD patterns of lead lactate calcined from 100 ^{o}C to 550 ^{o}C. When the calcination temperature is set at 100 ^{o}C and 200 ^{o}C, the XRD patterns are almost identical to the as-synthesized precipitate. The peak difference at around 10^{o} may possibly be due to preferred orientation when the powder is pressed into the XRD holder. Further analysis including FTIR and ^{1}H NMR will be presented later to confirm the intact organic group.

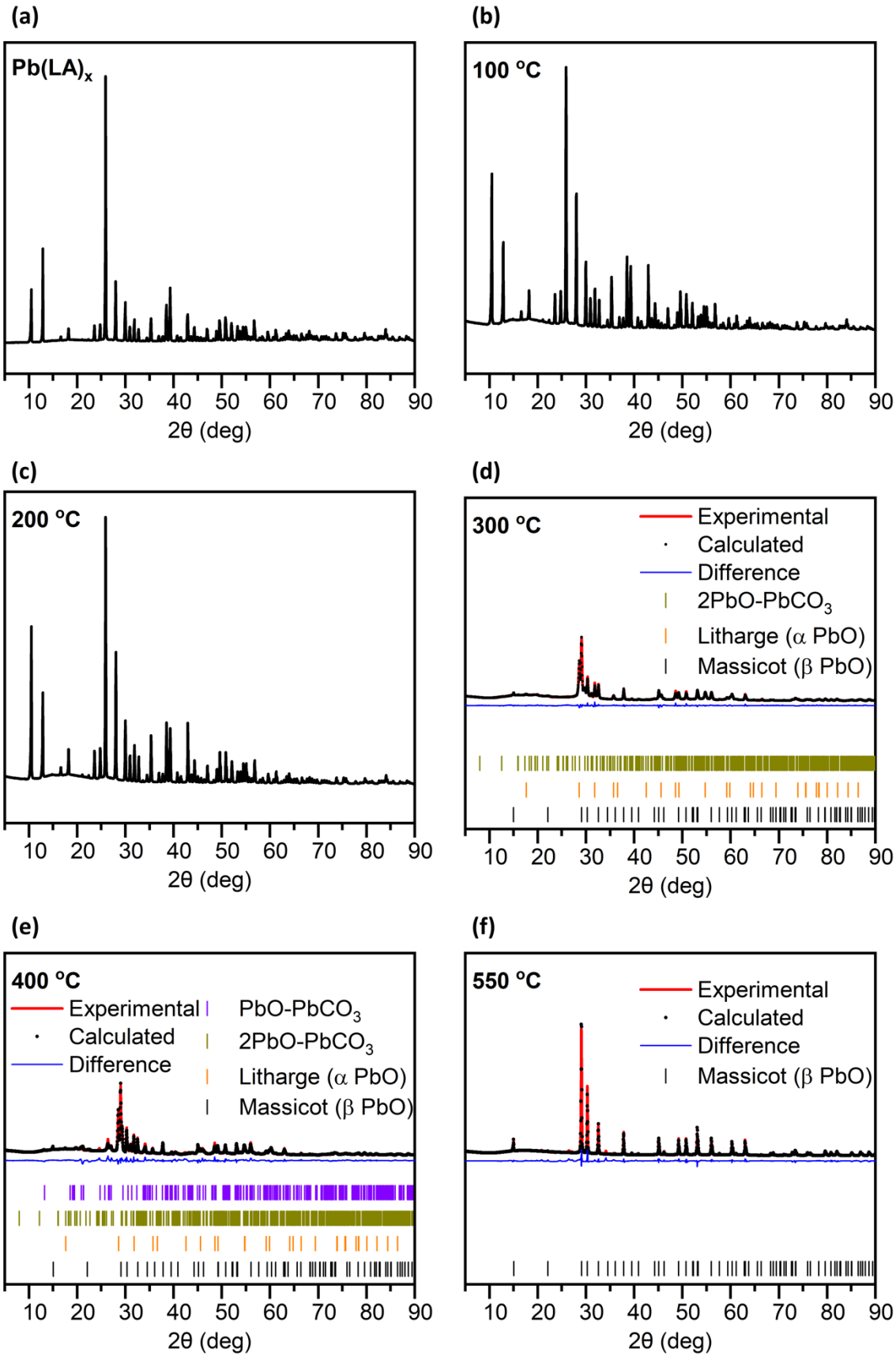

Figure 5.11 XRD patterns of lead lactate from (a) as-synthesized precipitate and calcined products for 2 hours at (b) 100 °C, (c) 200 °C, (d) 300 °C, (e) 400 °C and (f) 550 °C.

When the calcination temperature is set to 300 °C, a mixture of β-PbO, α-PbO and $2PbO \cdot PbCO_3$ (lead oxide carbonate) are formed as shown in Figure 5.11 (d). When the calcination temperature is further increased to 400 °C, a new compound, $PbO \cdot PbCO_3$ is formed from the consumption of $2PbO \cdot PbCO_3$, as shown in Figure 5.11 (e). The weight fraction of these compounds is shown in Figure 5.12. When the calcination temperature reaches 500 °C, all compounds are converted to β-PbO. The decomposition steps of lead lactate above 300 °C shows a similar pattern as that of lead malate dihydrate. It is, therefore, assumed that other lead carboxylates may also be decomposed in a similar pattern as lead malate dihydrate and lead lactate. This assumption may widen the selection of organic lead precursors for LAB paste recycling using precipitation/calcination methods.

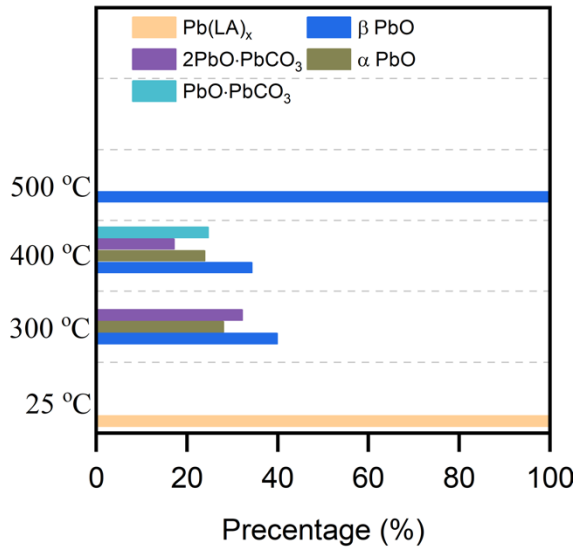

Figure 5.12 Weight percentage of $Pb(LA)_x$, $2PbO \cdot PbCO_3$, $2PbO \cdot PbCO_3$, α-PbO and β-PbO at toom temperature as the as-synthesized precipitate and at different calcination temperatures.

5.3.3.2 FTIR

Figure 5.13 shows the FTIR comparison of lead lactate and its calcined products at 100 °C and 200 °C. No significant differences can be observed in the FTIR spectrum between these three samples. This indicates that the organic part of lead lactate remains intact when the calcination temperature is lower than 200 °C.

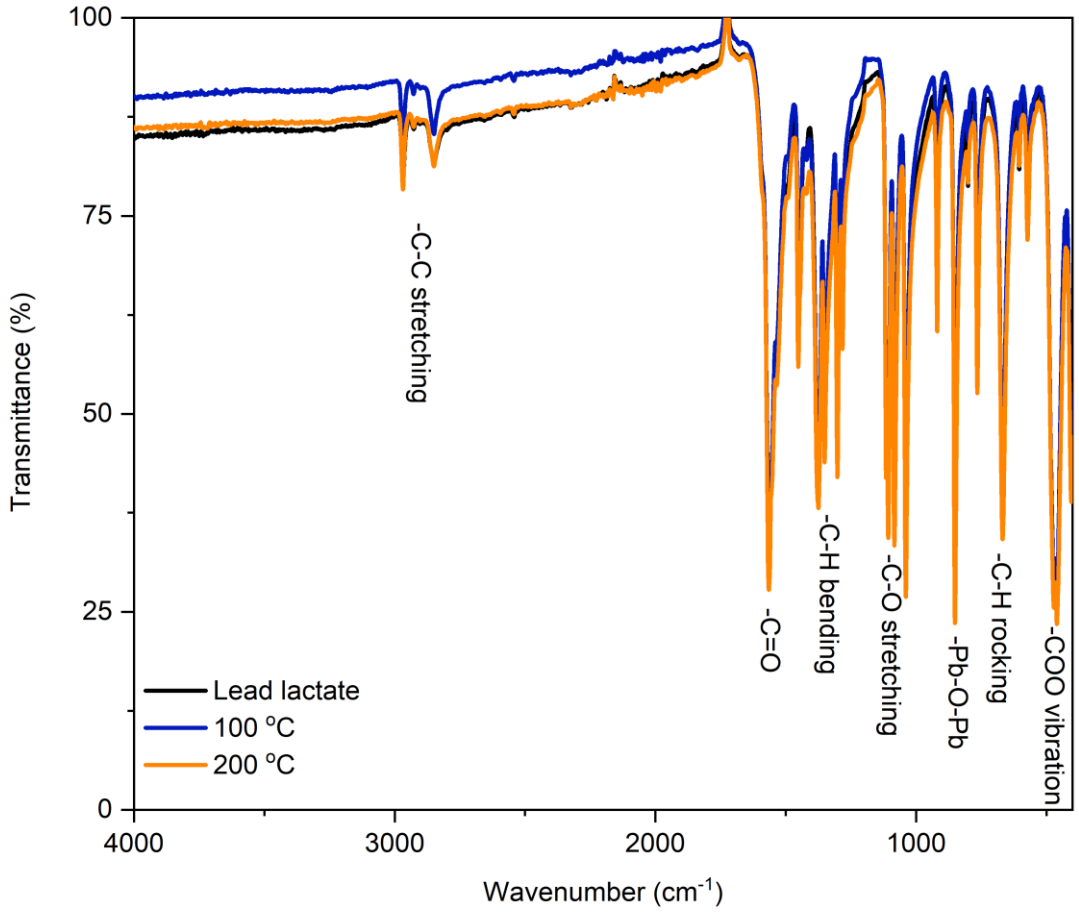

Figure 5.13 FTIR spectra of lead lactate and its calcined products at 100 °C and 200 °C for 2 hours.

5.3.3.3 ^{1}H NMR

The ^{1}H peaks of lead lactate calcined at 100 °C and 200 °C did not shift according to the ^{1}H NMR spectrum (shown in Figure A. 5). The quartet and doublet are present at the same chemical shift of the lead lactate precipitate. The integration ratio of the doublet to quartet is also identical. Based on the result of XRD, FTIR and ^{1}H NMR, it is concluded that no decomposition step occurs when the calcination temperature is lower than 200 °C.

5.3.3.4 XPS analysis

To prove the chemical composition of the calcinated products, XPS analysis has been carried out on all the calcinated powders. Figure 5.14 (a-c) shows the Pb 4*f*, O 1*s* and C 1s core levels' evolution from calcination temperatures from 100 °C to 550 °C. All peaks were normalized to

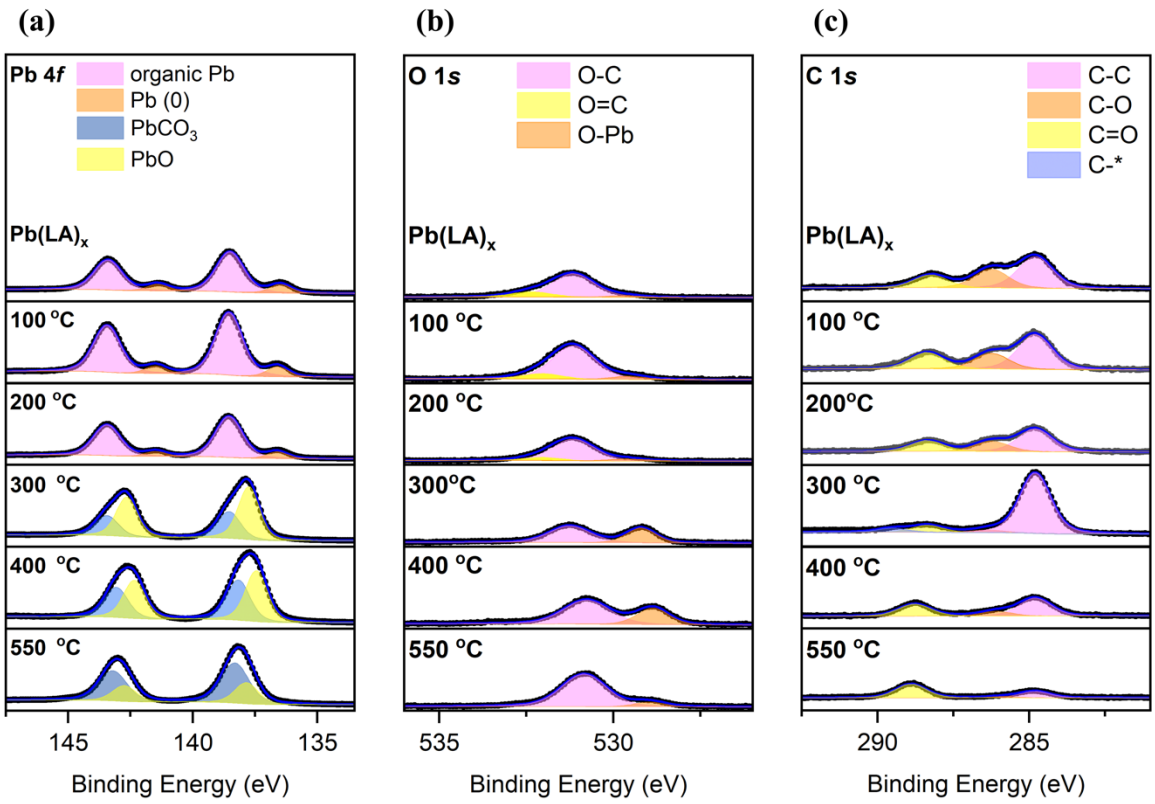

Figure 5.14 Evolution of XPS core levels (a) Pb 4*f*, (b) O 1*s* and (c) C 1*s* upon decomposition of lead lactate from as-synthesized precipitate to calcination from 100 °C to 550 °C.

Pb $4f_{7/2}$ to observe the changes in quantities. At 100 and 200 °C, all peaks from core level Pb 4*f*, O 1*s* and C 1*s* remained almost unchanged compared to that of lead lactate. From the discussion of its XRD pattern and SEM images, it is thus assumed that lead lactate is not decomposed if the calcination temperature is lower than 200 °C.

When the calcination temperature reaches 300 °C, Pb 4*f* shows one doublet for PbO at 137.8 eV and 142.7 eV and another doublet for $PbCO_3$ at 138.5 eV and 143.4 eV. No organic Pb peak was found in the Pb 4*f* core level indicating the conversion of lead lactate to a mixture of $PbCO_3$ and PbO. From the quantitative analysis, the majority of the mass was PbO, which matches the result of XRD. For the O 1*s* core level, the O-C peak at 531.2 eV and O-Pb peak at 529.2 eV in O 1s core level were assigned to the presence of $PbCO_3$ and PbO, respectively. The O 1*s* O-C to Pb 4*f* $PbCO_3$ ratio is 2.97 and the O 1*s* O-Pb to Pb 4*f* PbO is 1. This matches the stoichiometric ratio of O to Pb in $PbCO_3$ and PbO. For the C 1*s* core level, an additional

peak at 289.5 eV was observed, which may be due to surface contamination of the product being analysed.

Upon further increasing the calcination temperature to 400 °C, no significant changes in the composition were observed. However, the ratio of $PbCO_3$ to PbO did increase from 1 : 2 to 1 : 1. From the XRD results, $PbCO_3$·PbO started to form from 2PbO·$PbCO_3$ between 300 °C to 400 °C. One possible reason is that $PbCO_3$·PbO might formed more on the surface as the sample depth of XPS is normally within 10 nm. Another reason might be that the PbO reacted with atmospheric CO_2 at surface level.[152]

With calcination temperature further increased to 550 °C, $PbCO_3$ to PbO ratio further increased to 2.25 : 1. This suggests that at higher calcination temperatures there is more $PbCO_3$ relative to PbO. This XPS result is contradictory to the XRD result (Figure 5.12), which suggested that the precipitate all converted to PbO at 550 °C. The presence of $PbCO_3$ in XPS analysis may also be attributed to the reaction of CO_2 and PbO.

XPS reflects more the information of sample at the surface level. The $PbCO_3$ formed at the surface level was too limited to be detected by XRD.

5.3.3.5 Morphology analysis

Figure 5.15 (a-f) shows the SEM image of the as-synthesized precipitate and the calcined products from 100 °C to 550 °C. From Figure 5.15 (a-c), the morphology of the powder does not change significantly. Along with the analysis from the XRD pattern, it is then assumed that the powder remains unchanged after calcination at 200 °C. When the calcination temperature reached 300 °C, square-shaped crystals started to form along with some small crystals. When the calcination temperature was further increased to 400 °C, more square-shaped crystals have formed with larger crystal sizes. When the calcination temperature reached 550 °C, the crystals has formed a homogenous morphology (β-PbO) with even larger crystal sizes. The larger crystals are possibly formed through agglomeration of β-PbO due to heat accumulation during combustion.

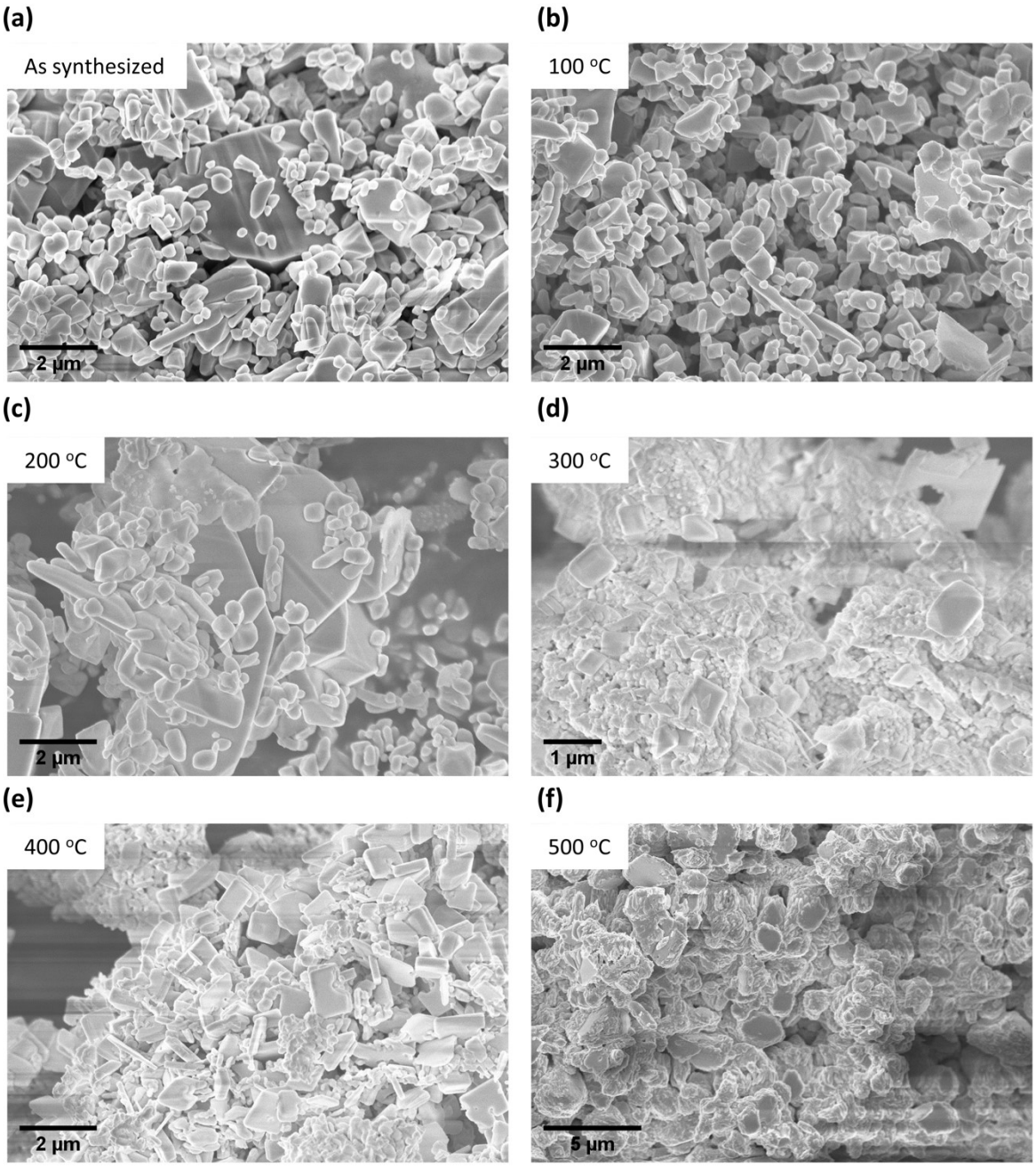

Figure 5.15 SEM images of lead lactate from (a) as-synthesized precipitate to calcined products for 2 hours at (b) 100 °C, (c) 200 °C, (d) 300 °C, (e) 400 °C and (f) 550 °C.

A comparison of β-PbO received from this work and from lead citrate from the literature is shown in Figure 5.16. The particle shape of PbO is similar to that from the reference. Agglomeration behaviour has also been observed from J. Yang's work using lead citrate. In Yang's work, lead citrate was calcined at a lower temperature (450 °C) for less time (1 hour).[80] As a result, the β-PbO obtained in this work has larger crystal sizes due to crystal growth at

higher temperatures. Improvements can be made in this experiment on comparing the features of PbO obtained from this work at higher magnification (at similar magnitude) with the PbO from the reference using lead citrate.

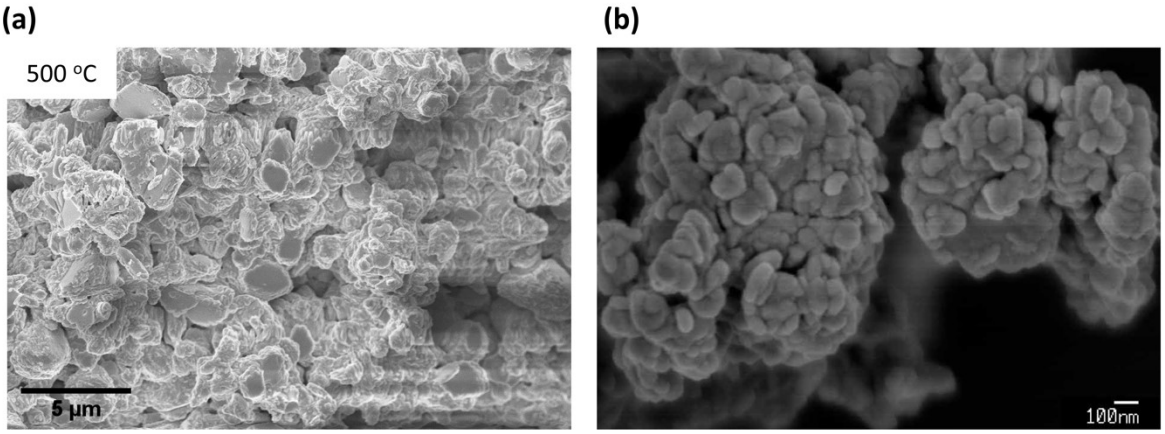

Figure 5.16 SEM images of β-PbO obtained from (a) this work and (b) referenced work using lead citrate.[80]

5.4 Limitations

5.4.1 Limitation in analysis of lead lactate

Due to the poor quality of the obtained $Pb(LA)_2$ single crystals, not all atoms have been located for this crystal structure. As the precipitate obtained from the NADES contains a mixture of $Pb(LA)_2$, D-PbLA and L-PbLA, a thorough analysis of the precipitate is difficult and a weight percentage of each compound cannot be given. The identification of compounds by XRD was refined by the Pawley method, which is less accurate than Rietveld refinement which could not be done due to the incompleteness of the crystal structure of $Pb(LA)_2$.

5.4.2 Limitation in precipitation followed by calcination methods

This study has investigated the possibility of using NADES to convert a lead paste component, PbO, to an organic lead precipitate, which can then be calcined at a moderate temperature (550 °C) to be recovered as β-PbO. Compared to normal pyrometallurgical and hydrometallurgical processes, the method in this study neither emits any hazardous particulates to the environment nor requires aqueous solutions containing large amounts of

water. This method still, however, has its own limitations. As the components of NADESs are in reality made from petrochemicals and the energy or cost of making NADESs and calcination was not calculated. An energy or cost comparison with currently used process such as pyrometallurgy and hydrometallurgy needs to be made before it can be applied as an industrial recycling route.

Furthermore, improvements can also be made in the starting lead components. The process in this thesis uses pure PbO as starting lead component, though actual desulfurized lead paste contains mixed lead components and other metal impurities. The solubility of other lead components (PbO_2) needs to be investigated. Other metallic compounds may also be soluble in NADES, and indeed precipitated simultaneously with the lead compounds. This organic precipitate would then be converted to corresponding metal oxide during calcination and would be an impurity in the final product of β-PbO. Further processes would thus be required to purify β-PbO.

Additionally, though the formation of NADES used does not require a large amount of water, the washing of precipitates to remove residual NADESs does. The washing water contains lead and thus is required to be treated as hazardous waste. This can cause additional costs in the waste stream treatment when it comes to real-world applications.

Moreover, the carboxylic acids used in the NADES are consumed from the solvent in the form of the precipitated organic lead compound. Therefore, once the NADES has been used to convert the lead component to organic lead precipitate, it can no longer be re-used to dissolve fresh lead components. Additional carboxylic acid needs to be added to form fresh NADES. However, in actual application, the quantity of carboxylic acid required to make fresh NADES is hard to control as the carboxylic acid that is consumed during the reaction would need to be monitored. Therefore, improvement needs to be made to increase the re-usability of NADES. As the organic lead precipitate may take days to form, precipitation agents such as oxalic acid can be added to the solution before lead malate dihydrate or lead lactate is precipitated. The precipitate obtained will then be lead oxalate as it is less soluble than lead malate dihydrate and lead lactate. The addition of oxalic acid as a precipitation agent can both reduce the reaction time and improve the recycle ability of the solvent.

5.5 Conclusions

This study uses a lactic acid-based NADES to recycle lead battery paste components through precipitation and calcination method. A mixture of several different lead lactate compounds has been formed as precipitates for a calcination precursor. None of the three types of lead lactate identified in this study has had crystal structures reported in the literature. The lead lactate precipitate was calcined at 550 ^{o}C to β-PbO, which can then be used for new LAB manufacturing. The new compound widens the use of carboxylic acid-based NADESs for precipitation and calcination LAB recycling routes.

However, the limitation of this precipitation method is clear in terms of recycling of the solvent. An improved method using precipitation agent oxalic acid has been proposed. Before this can be put into practice, the solubility of all Pb components in lead paste in NADES needs to be investigated, and this is the subject of further work in Chapters 6 and 7.

Chapter 6 Solubility behaviour of lead compounds in malic acid-based NADESs

6.1 Introduction

In Chapter 4 & 5, a precipitation followed by calcination method using NADES to recycle one of the LAB components, $PbCO_3$, was proposed to overcome the drawbacks of pyrometallurgy and hydrometallurgy. Preliminary results have proved the success of this new proposed green route. A precipitate is, however, formed from the reaction between $PbCO_3$ with the constituent carboxylic acid of NADES. This means that NADES is consumed and cannot be re-used for every new batch. Considering the sustainable use of NADES and the phenomenon of the precipitation behaviour, an improved recycling route has been proposed. This recycling route consists of two steps. First, it involves the dissolution of LAB components in a malic acid-based NADES. This is followed by the addition of a precipitation agent (oxalic acid dihydrate would be used throughout this thesis) before the precipitation of lead malate dihydrate occurs. Ideally, the precipitate is formed as corresponding organic lead compounds. For example, the precipitate should be lead oxalate if oxalic acid dihydrate is used as the precipitation agent. With the use of a precipitation agent, the NADES can be re-used to recycle new batch of LAB components. The most challenging part of this improved green route is the amount of precipitation agent required to precipitate all lead species and the time frame when the precipitation can to be added to the solution after the dissolution of LAB components. To make the usage of the precipitation agent in industrial applications more controllable, this chapter will focus on the maximum lead concentration levels and the solubility behaviours of individual LAB components ($PbCO_3$, $2PbCO_3{\cdot}Pb(OH)_2$, PbO, PbO_2) in malic acid-based NADESs.

6.2 Experimental

6.2.1 Chemical Reagents

Chemical Name	Chemical Formula	Chemical Structure	Purity	Supplier
DL-malic acid	$C_4H_6O_5$	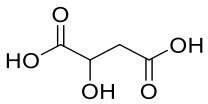	99 %	Sigma Aldrich
β-alanine	$C_3H_7NO_2$	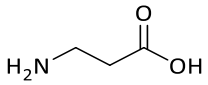	99 %	Sigma Aldrich
L-proline	$C_5H_9NO_2$	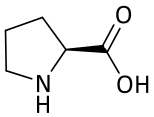	99 %	Sigma Aldrich
Lead (II) carbonate	$PbCO_3$		99 %	EMSURE
Lead (II) carbonate basic	$2PbCO_3{\cdot}Pb(OH)_2$		Pb % (78-82 %)	Sigma Aldrich
Lead (II) oxide	PbO		99.999 % (Trace metal basis)	Sigma Aldrich
Lead (IV) oxide	PbO_2		99.995 % (metal base)	Alfa Aesar

6.2.2 Synthesis of Natural deep eutectic solvents (NADESs)

MABA5 was prepared by mixing of DL-malic acid, β-alanine, and de-ionized water (conductivity = 18.2 $M\Omega^{-2}$) in a molar ratio of 1 : 1 : 5 at 50 ^oC for hours until a homogenous liquid was formed.

MALP5 was prepared through the mixing of DL-malic acid, L-proline and de-ionized water in a molar ratio of 1 : 1 : 5 at 50 ^oC for hours until a homogenous liquid was formed.

The ratio of malic acid/L-proline : β-alanine : water used in the reference was 1 : 1: 3.[146] The NADES formed at this ratio was too viscous. In this experiment, water was added to 5 part to reduce the viscosity.

6.2.3 Analysis of lead paste

XRD was carried out on two batches of lead paste (Lead paste 2017 and lead paste 2019, both provided by Envirowales, Ltd) to identify the phases present. The analysis was carried out by Panalytical XRD at a scan range from 5^{o} to 90^{o}. XPS was carried out to identify the chemical state of different lead compounds and non-crystalline materials such as plastics and fibres.

6.2.4 Dissolution of lead compounds in NADESs

6.2.4.1 MABA5

One of the lead compounds ($PbCO_3$, $2PbCO_3{\cdot}Pb(OH)_2$ or PbO), ranging from 0.5 to 3.5 g at an interval of 0.5 g, were added into glass vials each containing 10 mL of MABA5, respectively. This makes up a total of 21 samples. Similarly, PbO_2, ranging from 0.5 to 5.0 g at an interval of 0.5 g, were added into glass vials each containing 10 mL of MABA5. This makes up a total of 10 samples. Two batches of such vials were prepared, each containing 31 samples of the above mixture. One batch was stirred at room temperature and another at 50 ^{o}C both on a magnetic hotplate (VW, VMS-C7 advanced) for 4 days. The mixtures were then centrifuged at 6000 rpm for 30 minutes. The liquid was filtered through a 0.2 μm PES vacuum filter (Thermo Fisher) and then diluted with 1M nitric acid, which was diluted from 67% nitric acid (Fisher Scientific, analysis grade). The concentration of lead in the diluted liquid was measured via ICP-OES at a transition wavelength of 220.353 nm through comparing a set of 0, 1, 5, 10, 20 ppm lead standard solution, which was prepared via dilution from 1000 ppm Pb stock solution (Sigma). The initial lead concentration in the liquid was calculated by multiplying corresponding dilution factor.

6.2.4.1.1 Optimisation experiments for choosing the range of lead components

The loading used in this experiment was initially based on the loading used in the literature from my research group[116], where to each 5 mL DES was added 0.2 g $PbCO_3$ (equivalent to 0.4 g/10mL DES). The reaction was carried out at room temperature. $PbCO_3$ was found to be all dissolved. The selected loading was therefore increased to 0.5 g/10 mL. $PbCO_3$ was found to be all dissolved again. The selected loading was further increased to 2.5 g/10 mL and the mixture was given 4 days to ensure enough time for the dissolution reaction. During the 4-day reaction, it was found that the $PbCO_3$ was initially dissolved and then precipitates were

formed. It was proposed that the reaction might be a slow precipitation reaction and the lead concentration in the solution might change as the change of loadings. An experiment of lead concentration versus loading curve was proposed. The maximum loading chosen for lead compounds ($PbCO_3$ or PbO) was 3.5 g (per 10 mL NADES) to identify what will happen at a higher loading. The lead components per 10 mL at an interval of 0.5 g were chosen to conduct the experiment. For PbO_2, the maximum loading was further increased to 5.0 g/10 mL NADES based on the ICP results during the experiment.

6.2.4.2 MALP5

$2PbCO_3{\cdot}Pb(OH)_2$, ranging from 0.5 to 2.5 g at an interval of 0.5 g, were added into glass vials each containing 10 mL of MALP5. This makes up a total of 5 samples. Two batches of such vials were prepared. One batch was stirred at room temperature and another at 50 ^oC for 4 days. The mixtures were then centrifuged at 6000 rpm for 30 minutes. The liquid was treated by the same procedure as described in MABA5 to measure lead concentration.

6.2.5 Dissolution and precipitation behaviour of lead compounds in MABA5

Dissolution and precipitation behaviour of lead compounds were analysed by conducting the experiments with a fixed loading with different stirring time. 2.5g one of the lead compounds ($PbCO_3$, $2PbCO_3{\cdot}Pb(OH)_2$ or PbO), were added into glass vials each containing 10 mL of MABA5, respectively. Ten batches of such vials were prepared. Five batches were stirred at room temperature and the others at 50 ^oC for 6, 24, 48, 72, or 96 hours, respectively. The mixtures were then centrifuged at 6000 rpm for 30 minutes. The liquid was prepared following the same procedure as described in dissolution of lead compounds in MABA5 to measure lead concentration evolution upon stirring time.

6.2.6 Analysis of MABA5

6.2.6.1 FTIR

FTIR was carried out on all initial components (DL-malic acid, β-alanine, and de-ionized water) and MABA5.

6.2.7 ^{1}H NMR

All initial components and MABA5 were dissolved in D_2O (VWR, 99.96%) for ^{1}H NMR analysis. A further analysis was done on decomposed MABA5, which was heated at 80 ^{o}C, to compare with the NADESs before the analysis. Lead compounds with a loading of 50 g/L reacted at room temperature and at 50 ^{o}C and lead compounds with a loading of 350 g/L reacted at 50 ^{o}C were dissolved in D_2O for ^{1}H NMR analysis. All ^{1}H NMR data was processed and exported from MestroNova software.

6.3 Results and Discussion

6.3.1 Characterisation of lead paste

The work in this chapter aims at understanding the dissolution behaviour of individual lead components from lead paste in malic acid-based NADESs. An analysis on the industrial lead paste supplied by company "Envirowales Ltd." was carried out to identify the lead compounds. The company has provided two batches of lead paste, one in Year 2017 and the other in Year 2019. Analysis was carried out on both batches. From the refinement on the XRD results of lead paste as shown in Figure 6.1, the two batches have the same crystalline phases, which are $NaOH{\cdot}(PbCO_3)_2$ (ICSD 261807), $PbCO_3$ (ICSD 36554), PbO_2 (ICSD 8491), and β-PbO (ICSD 15402). Most phases in the lead paste match the result of de-sulphurised lead paste reported in the literature.[158] In the literature, Pb was present in the de-sulphurised paste instead of PbO. Though the two batches have presented the same phases, the relative quantification of each phase is not the same. Figure 6.2 shows the relative quantification of each phase present in both batches of lead paste. The quantities of PbO_2 and β-PbO were almost the same, but significant differences in the relative quantity of $NaOH{\cdot}(PbCO_3)_2$ and $PbCO_3$ could be observed. As these two phases are the result of desulfurization reaction from $PbSO_4$ and Na_2CO_3 solution,[30,31] the relative quantity changes may possibly be due to the difference in reaction conditions such as pH or the concentration of Na_2CO_3 solution during the desulphurisation process.

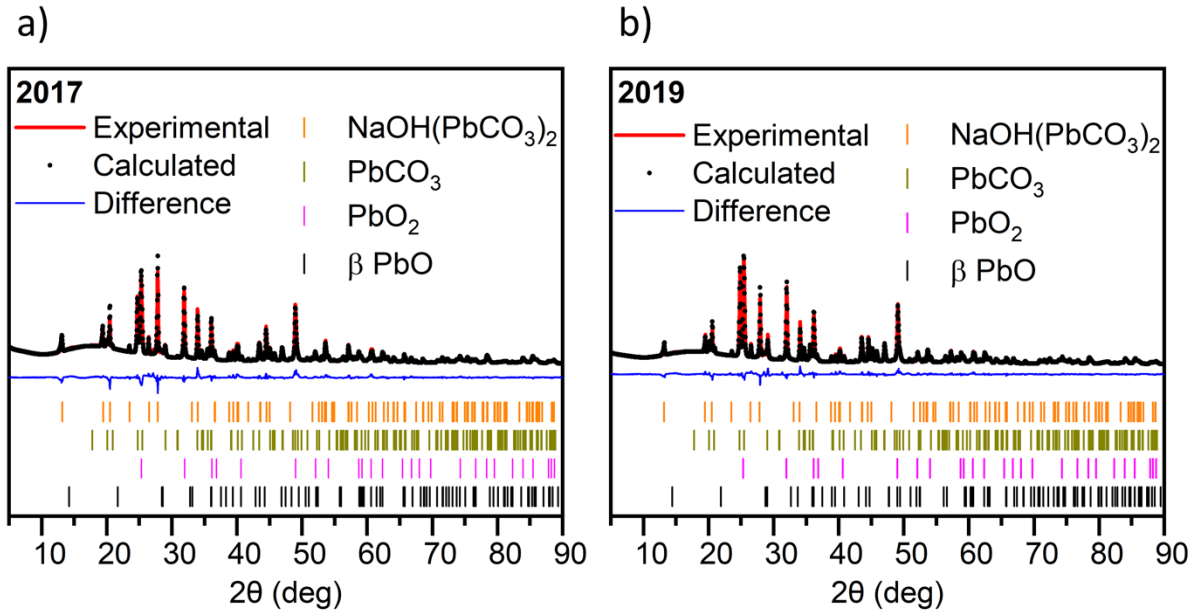

Figure 6.1 XRD analysis of lead paste from a) Year 2017 and b) Year 2019.

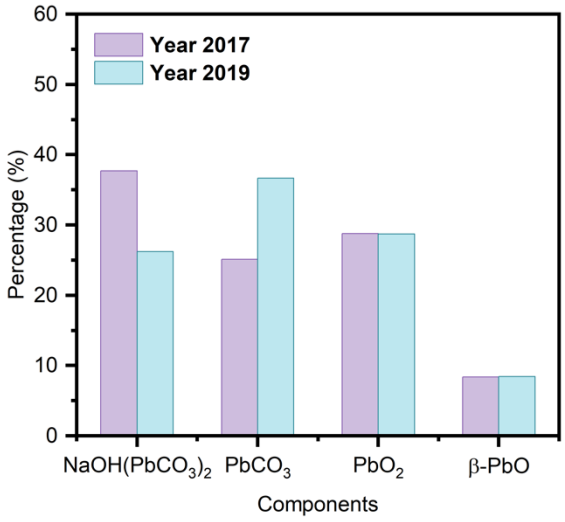

Figure 6.2 Relative quantification of each phase present in two batches of lead paste.

XPS analysis was also carried out to confirm the result obtained by XRD refinement. From the full spectrum survey of XPS (shown in Figure A. 6), an additional element, Si, in addition to Na, Pb, O, and C, has been identified. Si may have come from the silicon fibres within the lead paste. As fibres are non-crystalline, they cannot be identified by XRD. Figure 6.3 and Figure 6.4 show the core levels of Pb paste of Year 2017 and 2019, respectively. The peaks identified from XPS core levels matches the relevant bonds of compounds identified in XRD.

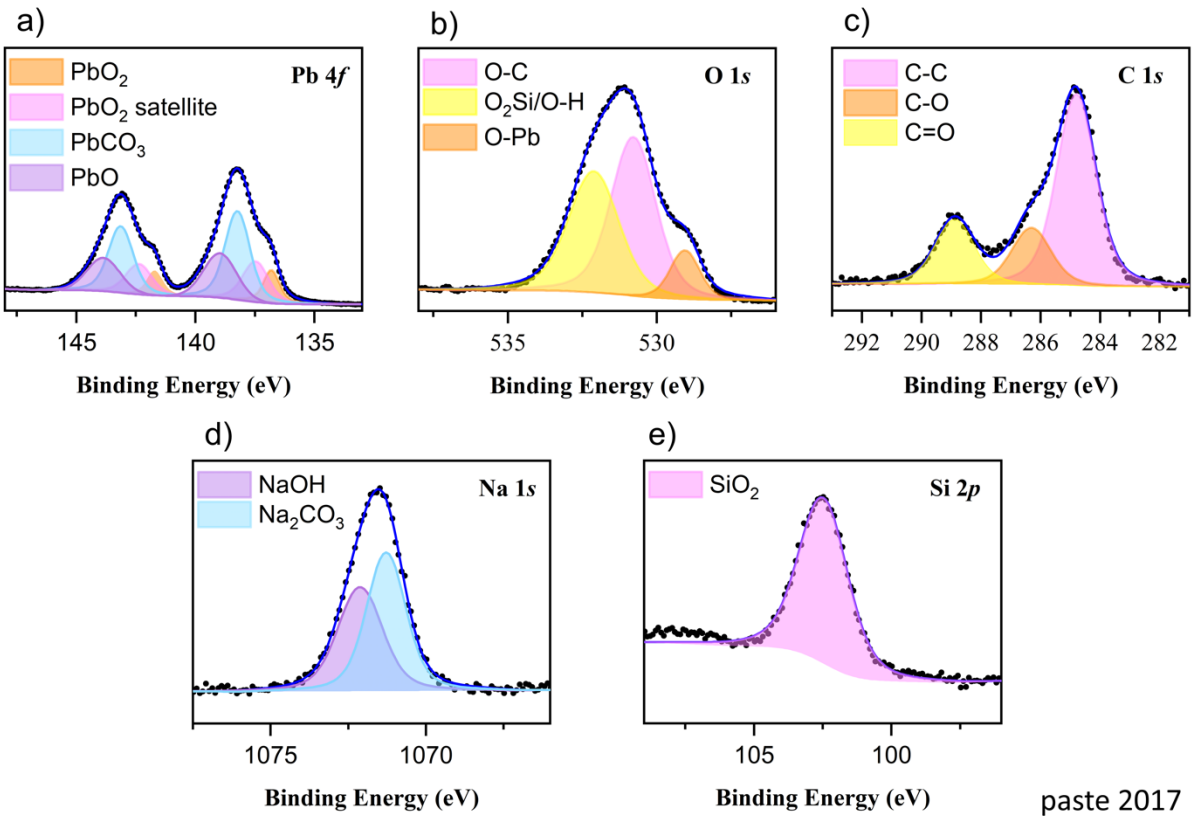

Figure 6.3 XPS core levels of Pb paste from Year 2017 a) Pb 4*f*, b) O 1*s*, c) C 1*s*, d) Na 1*s* and e) Si 2*p*.

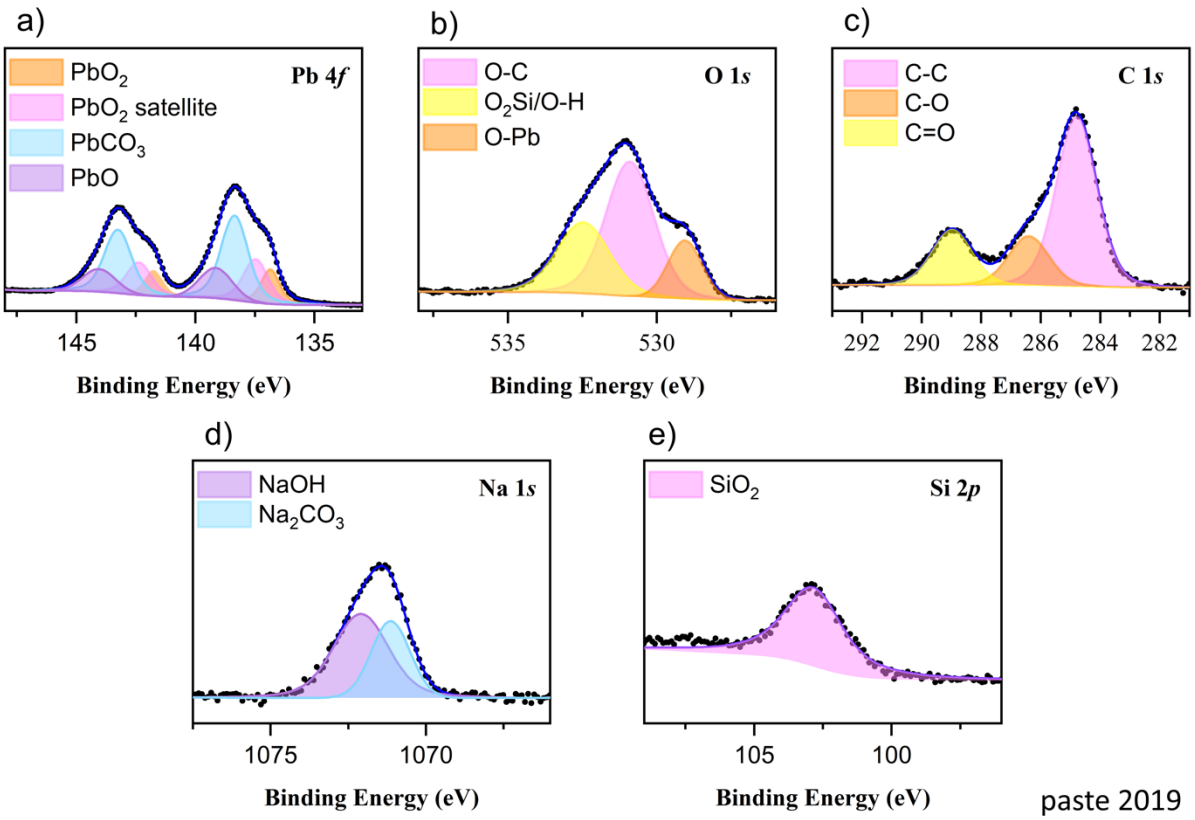

Figure 6.4 XPS core levels of Pb paste from Year 2019 a) Pb 4*f*, b) O 1*s*, c) C 1*s*, d) Na 1*s* and e) Si 2*p*.

6.3.2 Justification for the use of individual lead compounds

Pure $PbCO_3$, PbO_2, and β-PbO will be used as individual lead compounds in further solvent chemistry study. Ideally, $NaOH{\cdot}(PbCO_3)_2$ should be used as one of the individual lead compounds. To reduce the complexity and prevent the interference of Na in ICP analysis of solvent chemistry, $Pb(OH)_2{\cdot}(PbCO_3)_2$ will be used as an alternative of $NaOH{\cdot}(PbCO_3)_2$ in further studies.

6.3.3 Characterisation of MABA5

6.3.3.1 ^{1}H NMR

Figure 6.5 a) to c) shows the ^{1}H NMR of pure malic acid, β-alanine, and MABA5, respectively. In the ^{1}H NMR of malic acid, the spectrum reveals a doublet of doublets (4 peaks) between 4.61-4.64 ppm and a doublet of doublet of doublets (8 peaks) between 2.85-2.98 ppm. The integration ratio of these two multiplets is 1 : 2.14, which matches the number of protons present. The multiplets between 2.85-2.98 ppm occur as a result of coupling effect of two non-equivalent protons on the CH_2 group. These two non-equivalent protons have similar coupling effect on the proton on its neighbouring carbon, resulting in a doublet of doublets. In the ^{1}H NMR of β-alanine, the spectrum has shown two triplets at 3.18-3.21 ppm and 2.55-2.59 ppm, respectively. The integration ratio of these two triplets is 1 : 1, which matches the number of protons present in β-alanine. In the ^{1}H NMR spectrum of MABA5, all protons from malic acid and β-alanine have a slight chemical shift compared to that of pure compounds. The chemical shift may possibly be due to the change in chemical environment from the mixture. No additional peaks have been observed after the formation of MABA5, meaning that no additional compounds have formed through the formation of MABA5. In particular, the peaks of CH_2 group from β-alanine shifted a lot. The chemical shift of can also be due to the esterification between malic acid (MA) and β-alanine (BA). To prove this, MA and BA at a molar ratio of 1 : 1 were dissolved in D_2O and ^{1}H NMR was carried out on as shown in Figure A. 7. Results suggested that the chemical shift of the aqueous solution presented at similar position of NADES. It means that the chemical shift of CH_2 group β-alanine may be due to the change in chemical environment caused by the addition of malic acid rather than esterification.

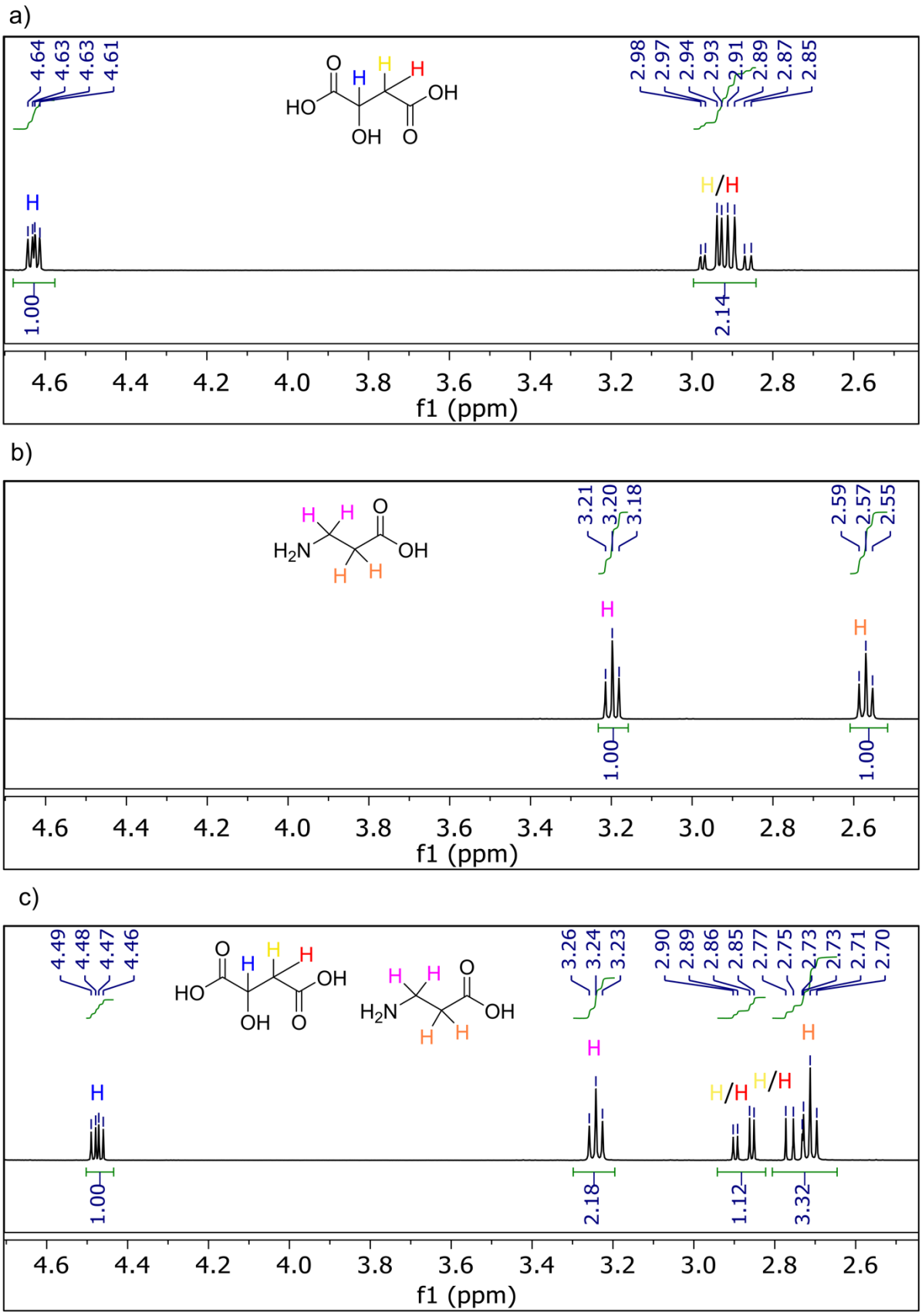

Figure 6.5 ^{1}H NMR (D_2O) of a) malic acid, b) β-alanine and c) MABA5.

As D_2O is added through preparation of ^1H NMR, the dilution of water may break down the hydrogen bonding. As a result, the hydrogen bonding may not show any evidence on the ^1H NMR spectrum.

6.3.3.2 FTIR

Figure 6.6 shows the FTIR spectrum of malic acid, β-alanine, and MABA5. The characteristic functional groups of MABA5 are a sum of the functional groups from malic acid and β-alanine. The positions of functional groups in MABA5 all shift towards higher wavenumbers. This indicates the formation of the hydrogen bonding between malic acid and β-alanine in MABA5.[121]

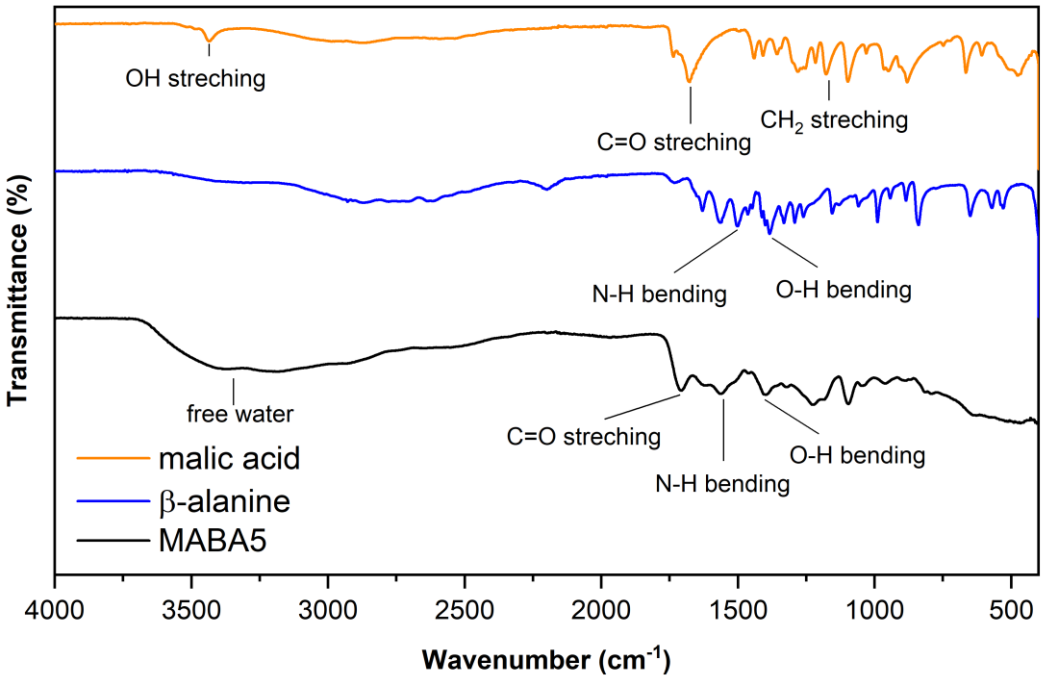

Figure 6.6 FTIR of malic acid, β-alanine and MABA5.

6.3.4 Maximum lead concentration in solution of lead compounds ($2PbCO_3 \cdot Pb(OH)_2$, $PbCO_3$, PbO and PbO_2)

6.3.4.1 Lead concentration vs loading of individual components ($2PbCO_3 \cdot Pb(OH)_2$, $PbCO_3$ and PbO)

MABA5 was reacted with different lead compounds $2PbCO_3 \cdot Pb(OH)_2$, $PbCO_3$ and PbO at an increased loading for 4 days. With the increase of loading, precipitates started to form from the solution. The precipitates have been confirmed as lead malate dihydrate, the analysis of which has been discussed in Chapter 4. Figure 6.7 a) to c) shows the maximum lead concentration in solution of different lead compounds and illustrates the precipitation starting point of different lead compounds.

At RT, NADES achieves 101.9 g Pb^{2+}/L at the loading of 150 g $2PbCO_3 \cdot Pb(OH)_2$/L, 146.8 g Pb^{2+}/L at the loading of 200g $PbCO_3$/L, and 171.7 gPb^{2+}/L at the loading of 200g PbO/L. For $2PbCO_3 \cdot Pb(OH)_2$, the precipitation happens at lower loading than the other two lead compounds, whose possible reaction mechanism will be discussed later. For $PbCO_3$ and PbO, they achieved different Pb concentration at the same loading due to different Pb percentage of the compounds. With the increase of loading for all lead compounds, the lead concentration drops to below 30 g Pb^{2+}/L due to precipitation, the concentration of which has been considered as a stable concentration of the solution at room temperature.

At 50 ^oC, the dissolution behaviours of these three lead compounds followed the same trend as at room temperature. The precipitation, however, lagged at 50 ^oC for $PbCO_3$ and PbO. The critical loading when the lead concentration starts to drop significantly, turns from 250 g/L at RT to 300 g/L at 50 ^oC, respectively, for both lead compounds. At 50 ^oC, the NADES achieves the maximum lead concentration of 194.3 g Pb^{2+}/L for $PbCO_3$ and 224.0 g Pb^{2+}/L for PbO, respectively. The maximum lead concentration of $2PbCO_3 \cdot Pb(OH)_2$ at 50 ^oC is 104.0 g Pb^{2+}/L, which remains similar to the concentration at room temperature. Meanwhile, the stable Pb^{2+} concentration of the solution at 50 ^oC remains around 50 g/L, which is 20 g/L higher than that at room temperature.

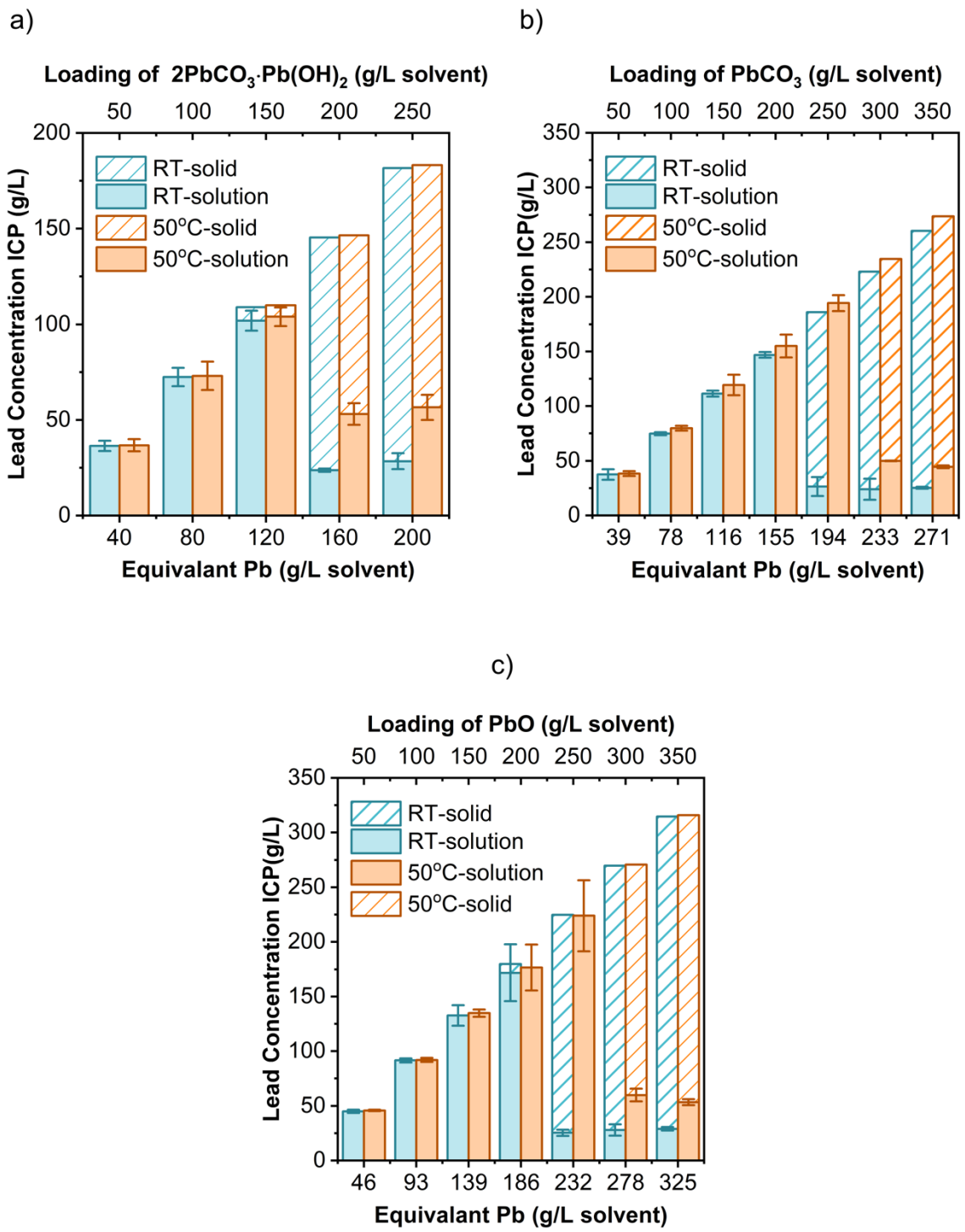

Figure 6.7 Lead concentration in solution and in precipitate with a variety of a) $2PbCO_3 \cdot Pb(OH)_2$, b) $PbCO_3$ and c) PbO loading at RT and 50 °C after reaction for 4 days.

6.3.4.2 Lead concentration vs loading of PbO_2

Figure 6.8 shows the lead concentration trend in solution of different PbO_2 and illustrates the starting point of the precipitation. The overall lead concentration in the NADES as the increase of PbO_2 loading shows an upward trend followed by a downward decrease, behaving similarly to other lead compounds. The Pb concentration in solution, however, is higher at 50 °C than at room temperature with loadings ≤ 200 g/L, unlike the behaviour of $PbCO_3$ or PbO. This may contribute to the dissolution speed of PbO_2 and could be explained as following.

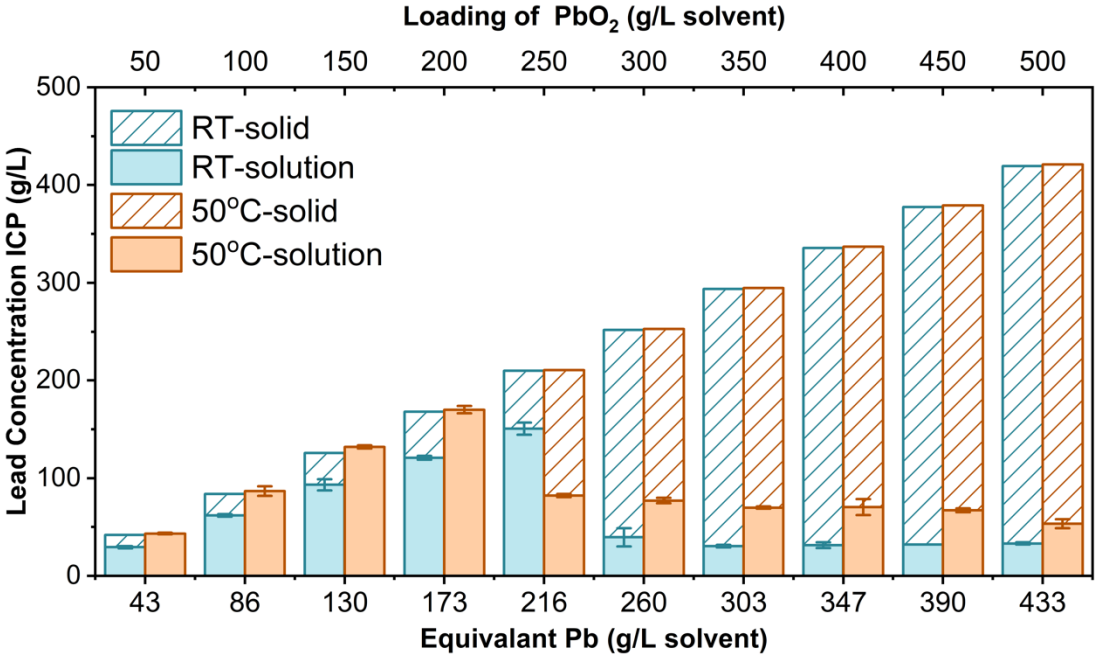

Figure 6.8 Lead concentration in solution and as solid with a variety of PbO_2 loading at RT and 50 °C after reaction for 4 days.

After the solutions were stirred at RT for 4 days, PbO_2 cannot be completely dissolved. The solid part in the graph refers to the undissolved PbO_2 at loadings lower than 250 g/L. Only 60% of the PbO_2 was dissolved, while the rest 40% of the loading was left over as residue. The NADES, however, shows an upward trend until the maximum Pb concentration of 150.7 g/L at the loading of 250 g/L, indicating the ability of dissolving more PbO_2 until the dropping point. When the PbO_2 reaches the dropping point (≥300 g/L), the solid is a mixture of undissolved PbO_2 and precipitate. With the increase of loading, the Pb concentration drops and reaches a plateau at around 30 g/L at room temperature.

At 50 °C, all the PbO_2 with loadings lower than 200 g/L, has been dissolved visually, which explains the higher Pb concentration than that at room temperature with the same loading. This indicates that the dissolution of PbO_2 is faster at 50 °C than at room temperature. The less concentrated Pb solution at room temperature lagged the precipitation. As a result, the precipitation happens at a higher loading at room temperature than at 50 °C. With the increase of PbO_2 loading, the Pb concentration drops gradually to around 50 g/L at 50 °C.

6.3.4.3 Solubility comparison of lead compounds in various solvents

Table 6.1 summarizes the solubility of different lead compounds in malic acid-based NADES and compares it with other solvents. One of the most successful solvents for sulfurized lead paste extraction is Methane sulfonic acid (MSA) used by Aquametals. The concentration of lead compounds in different solvents refers to Pb^{2+} concentration and it was measured by ICP. The solubility of Pb paste in MSA was given in g Pb paste/ L solution as stated in the literature.[71] The NADES used in this paper was malic acid, β-alanine and DI water with a molar ratio of 1:1:5. It has a high solubility of individual de-sulphurised lead paste components, thus, making it ideal for dissolving desulfurized paste with competitiveness against MSA.

Table 6.1 Maximum lead concentration comparison among various solvents. The concentrations of lead compounds are given in g Pb^{2+} /L solution, which are measured from the ICP. The solubility of Pb paste in MSA was given in g Pb paste/ L solution as stated in the literature.

	$2PbCO_3 \cdot Pb(OH)_2$ (g Pb^{2+}/L)	**$PbCO_3$ (g Pb^{2+}/L)**	**PbO (g Pb^{2+}/L)**	**PbO_2 (g $Pb^{2+/4+}$/L)**	**$PbSO_4$ (g Pb^{2+}/L)**	**Pb paste (g/L)**
MABA5 (Room temperature)	101.9	146.8	171.7	150.7	N/A	N/A
MABA5 (50 °C)	104.0	194.3	224.0	170.0	N/A	N/A
Ethaline 200 [159]	N/A	5.9	4.4	12.2	1.8	N/A
Methanesulfonic acid (MSA)[73]	N/A	N/A	N/A	N/A	N/A	73.3 (Sulphurised paste)
Urea acetate solution[160]	N/A	N/A	N/A	N/A	44.7	N/A

6.3.4.4 Possible reaction mechanism

As the trend of lead concentration versus loading behaves similarly at room temperature and 50 °C. It is assumed that the reaction mechanism at room temperature would be similar to at 50 °C apart from reaction rate. Therefore, the discussion around the mechanism would be mainly based on the reaction at room temperature unless otherwise stated.

6.3.4.4.1 $2PbCO_3 \cdot Pb(OH)_2$

Effervescence was seen immediately once $2PbCO_3 \cdot Pb(OH)_2$ was added into the NADES, indicating the formation of CO_2. Gas evolution showed that the reaction between $2PbCO_3 \cdot Pb(OH)_2$ began instantaneously after the addition of lead compound. The solution remained clear at the loadings of 50 g/L and 100 g/L after being stirred for 4 days. Precipitates started to form at a loading of 150 g/L $2PbCO_3 \cdot Pb(OH)_2$ after 4 days, as the solution became slightly cloudy. More precipitates have formed when the loading achieved 200 g/L. These solutions with precipitates were then centrifuged with the liquid collected and filtered. After the filtration, the liquid remained clear. ICP was done immediately. Results showed that the Pb concentration in the solutions achieved 101.9 g/L (for the loading of 150 g/L) and 23.7 g/L (for the loading of 200 g/L). After a few days, the filtered solution with an initial loading of 150 g/L became cloudy again. This indicates further formation of precipitates within the solution. This also proves that this solution is a super-saturated solution. After a few weeks, tiny white precipitates were observed in the solution with an initial loading of 100 g/L. This also indicates further precipitation. Drawing from the evidence above, it is assumed that precipitation happens gradually within the solvent and depends on the concentration of Pb^{2+} in the solution. A possible reaction mechanism can be described as in Equation 6.1 (1) and (2).

$$2PbCO_3 \cdot Pb(OH)_2(s) + 6H^+(aq) \rightarrow 6Pb^{2+}(aq) + 3H_2O\ (l) + 2CO_2(g) \quad \text{fast} \quad \textbf{(1)}$$

$$Pb^{2+}(aq) + MA^{2-}(aq) + 2H_2O\ (l) \rightarrow PbMA \cdot 2H_2O(s) \quad \text{slow} \quad \textbf{(2)}$$

Equation 6.1

The precipitates were confirmed as lead malate dihydrate. Given that effervescence was seen immediately, so Equation 6.1 (1) should be a fast reaction. From the observance, precipitation could happen after a few days to a few weeks, indicating that the precipitation reaction

(Equation 6.1 (2)) happened slowly. The clear solution obtained is a super-saturated solution, thus appearing as a comparatively high Pb concentration. When the initial loading achieves the critical loading, Pb^{2+} accumulates in the solution and is more likely to react with malic acid species (MA^{2-}). This accelerates the precipitation reaction.

Another assumption for the solvation mechanism can be descried as shown in Equation 6.2 (1) to (3). At the start of the reaction, the solvent system is considered to have excessive NADES or malic acid species. Pb^{2+} would form soluble species $Pb(MA)_2^{2-}$ in an excessive MA^{2-} environment. At lower loadings (≤50 g/L), the system would always have an excessive MA^{2-} environment; thus, no precipitation would be observed. At higher loadings (≥200 g/L), excessive Pb^{2+} would react with soluble $Pb(MA)_2^{2-}$ to form precipitate. For those solutions, from which precipitation has been observed after a few days or a few weeks, the mechanism can be explained as following. As the solvent is quite viscous, the species within the solution may not be homogeneously distributed. There might be a localized area with excessive Pb^{2+}. Over time, these Pb^{2+} have the chance to encounter $Pb(MA)_2^{2-}$ and thus resulting in precipitation.

$2PbCO_3 \cdot Pb(OH)_2\,(s) + 6H^+(aq) \rightarrow 6Pb^{2+}(aq) + 3H_2O(l) + 2CO_2(g)$		**(1)**	**Equation 6.2**
$Pb^{2+}(aq) + 2MA^{2-}(aq) \rightarrow Pb(MA)_2^{2-}(aq)$	Excessive MA	**(2)**	
$Pb^{2+}(aq) + Pb(MA)_2^{2-}(aq) + 4H_2O\,(l) \rightarrow 2PbMA \cdot 2H_2O(s)$	slow	**(3)**	

6.3.4.4.2 $PbCO_3$

A Similar phenomenon has been observed during the reaction of $PbCO_3$ and MABA5. As $2PbCO_3 \cdot Pb(OH)_2$ can be considered as a mixture of $PbCO_3$ and $Pb(OH)_2$, it is assumed that the reaction of $PbCO_3$ with malic acid is a simplified reaction of $2PbCO_3 \cdot Pb(OH)_2$. Ideally, they should have a similar reaction mechanism. It has been observed that at a loading of 200 g/L, the MABA5 still remains clear after 4 days when reacting with $PbCO_3$. Significant precipitation, however, has been observed for $2PbCO_3 \cdot Pb(OH)_2$ at the same loading. This means that precipitation happens slower when MABA5 reacts with $PbCO_3$. According to Equation 6.3 (1), during the reaction, 1 part of $Pb(OH)_2$ can generate 2 parts of H_2O while 1 part of $PbCO_3$ can only generate 1 part of H_2O. To form the precipitate, 1 part of Pb would need 2 parts of H_2O.

This means that $PbCO_3$ would need to gain 1 part of H_2O from the solvent system to form the precipitate. As the NADES system has limited water content and water may form hydrogen bonding with the NADES components, there might only be limited free water in the NADES system. The reaction between the free water from the NADES and Pb^{2+} may be slow, which might also contribute to the slow reaction of the precipitation. This slow combination of water and Pb species may cause the lag of the precipitation for the reaction of NADES and pure $PbCO_3$.

$$Pb(OH)_2\,(s) + 4H^+\,(aq) \rightarrow Pb^{2+}(aq) + 2H_2O(l) \quad (1)$$

$$PbCO_3\,(s) + 2H^+\,(aq) \rightarrow Pb^{2+}(aq) + H_2O\,(l) + 2CO_2(g) \quad (2)$$

Equation 6.3

6.3.4.4.3 PbO

No effervescence has been observed for the reaction of PbO and MABA5. A slight temperature increase can be felt when touching the bottom of the glass vial. This indicates that this reaction is an exothermic reaction. Ideally, temperature of the solution should be measured to monitor the temperature variance. However, the thermal couple may be considered as an inhomogeneous site within the solution, which may trigger the precipitation. To avoid inconsistence of the reaction, temperature measurement was not carried out.

Similar reaction mechanism has been assumed for the reaction of PbO and malic acid as shown in Equation 6.4. Similar to $PbCO_3$, 1 part of PbO needs to gain 1 part H_2O from the solvent system. Therefore, for PbO, significant precipitation has been observed at the same loading of $PbCO_3$, which is 250 g/L.

$$PbO\,(s) + 2H^+\,(aq) \rightarrow Pb^{2+}(aq) + H_2O(l)$$

Equation 6.4

6.3.4.4.4 PbO_2

Colour change of the solutions has been observed during the reaction between MABA5 with PbO_2 as shown in Figure 6.9. With the addition of PbO_2, the colour of the solution becomes darker than the pure MABA5. By comparing sample (ii) (MABA5 + 10 g/L PbO_2 + 10 g/L Pb) and sample (iii) (MABA5 + 10 g/L PbO_2) in Figure 6.9, the colour of sample (iii) is darker. This

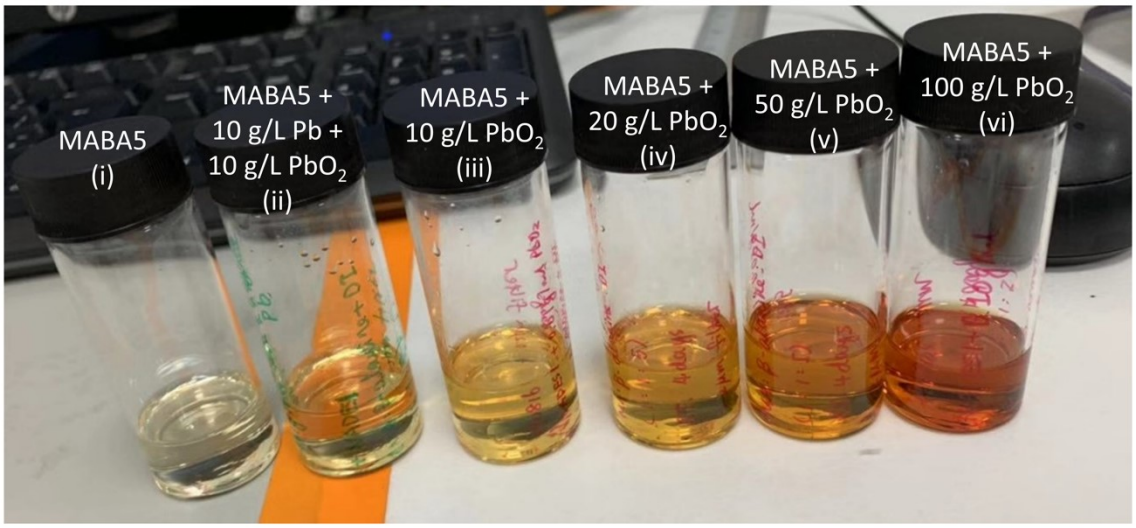

Figure 6.9 Appearance of solution from left to right: (i) pure MABA5, (ii) MABA5 + 10 g/L PbO_2 + 10 g/L Pb, (iii) MABA5 + 10 g/L PbO_2, (iv) MABA5 + 20 g/L PbO_2, (v) MABA5 + 50 g/L PbO_2, (vi) MABA5 + 100 g/L PbO_2.

may be due to the comproportionation reaction of Pb and PbO_2 to form Pb^{2+} in the solution in sample (ii). It is thus assumed that the colour change of the solvent is caused by the reaction of PbO_2 with MABA5. The reaction mechanism of PbO_2 with MABA5 may be different from other Pb(II) compounds with MABA5. Two possible assumptions of the reaction mechanism have been made. The first assumption is that the Pb species formed in the solution is Pb(IV). Pb(IV) is coloured. The more concentrated the Pb(IV), the darker the colour of the solution. The second assumption is based on the oxidizing property of PbO_2. PbO_2 acts as an oxidizing product, which oxidizes the malic acid in the MABA5. The oxidized product is coloured. The more PbO_2 added in the MABA5, the more oxidized products formed. As a result, the colour of the solution is darker. The Pb species formed in the solution is still Pb(II). Due to the limitation of instrument, the oxidised product of the Pb solvation state cannot be confirmed.

6.3.4.5 Stability of solution after reaction

The solution was not decomposed after the reaction with lead compounds based on the results from ^{1}H NMR. The ^{1}H NMR spectrum in shown in the Appendix A.

6.3.4.5.1 Decomposed MABA5

MABA5 was heated at 80 ^{o}C for 4days. ^{1}H NMR was carried out on this solvent. The spectrum is shown in Figure A. 8. Additional peaks have been observed at the chemical shift around 2.6,

indicating the decomposition of the solvent. This solvent has been considered as decomposed MABA5, the ^{1}H NMR of which has been compared with the ^{1}H NMR of other solutions after the reaction with lead compounds.

6.3.4.5.2 ^{1}H NMR of solutions reacting at room temperature

Figure A. 9 shows the ^{1}H NMR of MABA5 reacting with different lead compounds at room temperature. The representative decomposed peaks have not been observed on these solutions. It is assumed that MABA5s have not decomposed after reacting with lead compounds at room temperature. In Figure A. 9, the peaks at a chemical shift around 2.7 are slightly different from other solutions. This is due to the overlapping of protons from CH_2 of malic acid and CH_2 of β-alanine.

6.3.4.5.3 ^{1}H NMR of solutions reacting at 50 ^{o}C – low Pb compounds loading

Figure A. 10 shows the ^{1}H NMR of MABA5 reacting with different lead compounds at a loading of 50 g/L at 50 ^{o}C. Though the decomposed peaks have been observed for $2PbCO_3{\cdot}Pb(OH)_2$, $PbCO_3$ and PbO, the decomposition is not severe. The decomposition of MABA5 after reacting with PbO_2 is more obvious. Possible reasons for this result include both high temperature and the oxidation from PbO_2.

6.3.4.5.4 ^{1}H NMR of solutions reacting at 50 ^{o}C – high Pb compound loading

Figure A. 11 shows the ^{1}H NMR of MABA5 after reacting with different lead compounds at a loading of 350 g/L at 50 ^{o}C. A decrease in the malic acid peak has been observed. Theoretically, the integration ratio of proton from CH from malic acid to the protons from CH_2 from β-alanine should be 0.5 to 1. In all three lead compounds ($PbCO_3$, PbO, and PbO_2), the integration ratio of these two protons is less than 0.5 to 1. The loss of malic acid is due to the conversion to the malate as precipitate.

6.3.5 Dissolution and precipitation behaviour of lead compounds

6.3.5.1 Room temperature

Lead concentration in the solution drops when the loading exceeds the critical point. It has been observed during the reaction that the precipitation did not happen immediately after the dissolution, but after a certain period. To understand the precipitation behaviour of lead compounds in the NADES, the lead concentration in solution with different stirring times was measured. The experiments were initially carried out using $2PbCO_3 \cdot Pb(OH)_2$ with five vials, all of which containing 10 mL NADES and 2 g $2PbCO_3 \cdot Pb(OH)_2$. They were stirred for 6, 24, 48, 72, and 96 hours, respectively. Similar experiments were carried out on a loading of 2.5 g/10 mL (=250 g/L) $2PbCO_3 \cdot Pb(OH)_2$ with the same experimental protocol. Figure 6.10 shows the lead concentration in solution with 200 g/L and 250 g/L $2PbCO_3 \cdot Pb(OH)_2$ as a function of stirring time. As $2PbCO_3 \cdot Pb(OH)_2$ has not been observed in the precipitate at both loadings from the XRD analysis, all $2PbCO_3 \cdot Pb(OH)_2$ would have been converted either to the precipitate or to the lead ions in solution. It is thus assumed that the drop of the lead concentration in solution is resulted from precipitation. From Figure 6.10, for both curves, the maximum lead concentration peaks at 6 hours. After 6 hours, the lead concentration starts to drop. This means that the dissolution of $2PbCO_3 \cdot Pb(OH)_2$ is completed within 6 hours for both loadings. The lead concentration drops gradually for both loadings from 6 hours until 48 hours. The lead concentration then drops significantly between 48 hours and 72 hours. For 250 g/L $2PbCO_3 \cdot Pb(OH)_2$, lead concentration remains stable around 30 g/L between 72 hours to 96 hours, while for 200 g/L $2PbCO_3 \cdot Pb(OH)_2$, lead concentration keeps dropping until a stable concentration (~30 g/L) is achieved.

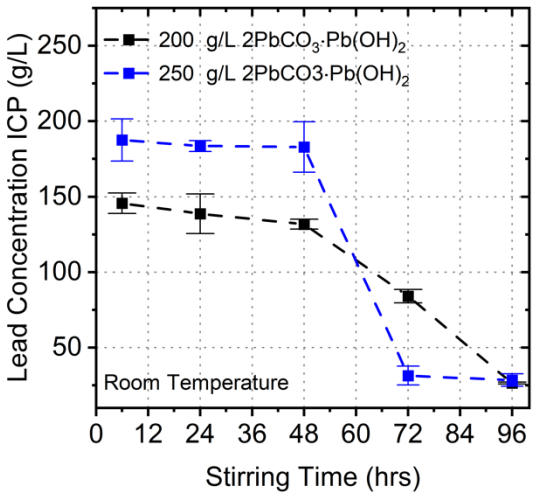

Figure 6.10 Lead concentration in MABA5 with 200 g/L and 250 g/L $2PbCO_3 \cdot Pb(OH)_2$ as a function of stirring time for reaction at room temperature.

From the precipitation curve of $2PbCO_3 \cdot Pb(OH)_2$, it can be concluded that the precipitation speed is proportional to the lead concentration in the solution or the initial loading. The higher the initial loading, the more Pb can be dissolved in the solution. The higher the lead concentration in the solution, the more likely is Pb to agglomerate together to form precipitates, thus resulting in faster precipitation.

Similar experiments were done on other lead components ($PbCO_3$ and PbO). The lead concentration in solution curves of these components are shown in Figure 6.11. The dissolution of $PbCO_3$ and PbO is slower than that of $2PbCO_3 \cdot Pb(OH)_2$. For $PbCO_3$ and PbO, the maximum lead concentration peaks at 24 hours. Only 63.5 % of PbO and 78.2 % of $PbCO_3$ have been dissolved for the first 6 hours. From the dissolution behaviour of $2PbCO_3 \cdot Pb(OH)_2$, Pb can stay in the solution without significant precipitation for a minimum of 42 hours. The precipitation of $PbCO_3$ and PbO, thus, starts to happen from 72 hours. Between 24 hours and 72 hours, Pb^{2+} remains stablely in the solution. In the reaction with $PbCO_3$ and PbO, the mixture starts to form precipitates from 72 hours until a stable Pb concentration is achieved at 96 hours.

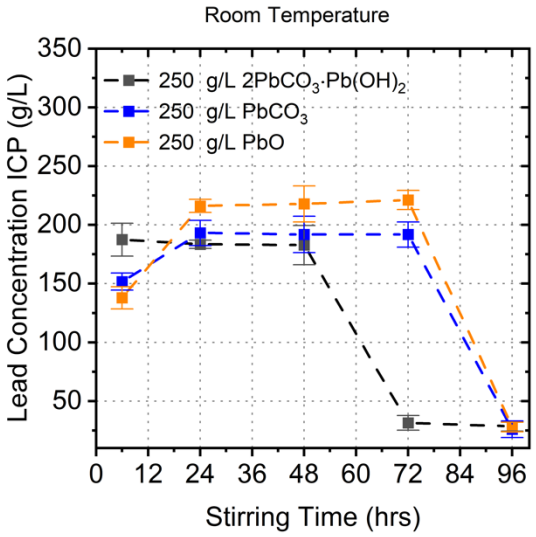

Figure 6.11 Lead concentration in MABA5 with 250 g/L $2PbCO_3 \cdot Pb(OH)_2$, $PbCO_3$ and PbO as a function of stirring time for reaction at room temperature.

6.3.5.2 50 °C

To understand the dissolution and precipitation behaviour of lead components thoroughly, similar experiments with the same loading were done on $2PbCO_3 \cdot Pb(OH)_2$, $PbCO_3$, and PbO at 50 °C. The lead concentration curves of these components are shown in Figure 6.12.

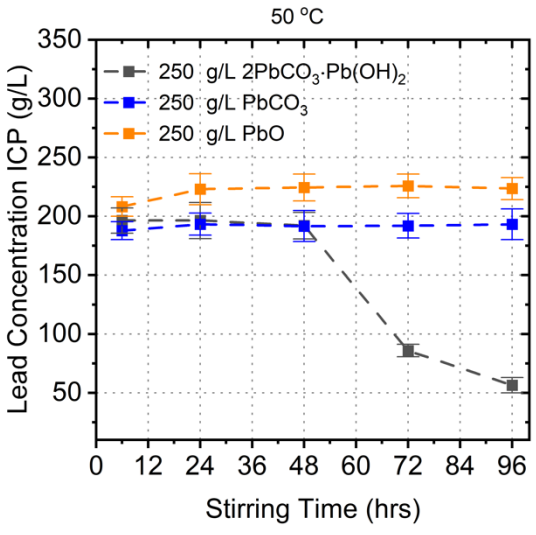

Figure 6.12 Lead concentration in MABA5 with 250 g/L $2PbCO_3 \cdot Pb(OH)_2$, $PbCO_3$ and PbO as a function of stirring time for reaction at 50 °C.

For $2PbCO_3 \cdot Pb(OH)_2$, all components were dissolved within the first 6 hours. For $PbCO_3$ and PbO, the components were completely dissolved after 24 hours. The dissolution speeds of $PbCO_3$ and PbO at 50 °C are higher than that at room temperature. For the first 6 hours, 92.1 % of PbO and 97.2 % of $PbCO_3$ were dissolved. At 50 °C, precipitation behaviour has not been observed for $PbCO_3$ and PbO at a loading of 250 g/L after 96 hours. For $2PbCO_3 \cdot Pb(OH)_2$, precipitation occurs after 48 hours. Unlike the precipitation behaviour of $2PbCO_3 \cdot Pb(OH)_2$ at RT, whose precipitation finishes at 72 hours, the precipitation behaviour of $2PbCO_3 \cdot Pb(OH)_2$ finishes at 96 hours at 50 °C. This means that the precipitation behaviour at 50 °C is slower than that at room temperature. Two assumptions were made for the slower precipitation at higher temperature. The first is that the precipitation speed is inversely proportional to the temperature. The proof of this assumption, however, requires further studies. The second assumption is related to the water content. As discussed in Equation 6.4, water is an essential part to form precipitates. At higher temperature, water is lost gradually during heating. The water loss may possibly be due to that these vials do not have a good sealing property. Another reason might be that the water was heated and built up close to top of the cap. Though the water still existed in the vial, it did not stay in the NADES mixture. More water was built up close to top of the vial at higher temperature, more water was lost to the NADES system at higher temperature. As shown in Equation 6.2 (3), water is an essential part to form the precipitate. The loss of water content in the MABA5 system slows down the formation of precipitates.

6.3.6 Replacement of β-alanine by another amino acid – L-proline

During the discussion of reaction mechanism of MABA5 with lead compounds, it is assumed that β-alanine did not anticipate much in reacting with lead compounds. β-alanine forms a hydrogen bonding with malic acid in MABA5. The hydrogen bonding leads to a higher viscosity of MABA5, which slows down the precipitation. This allows the lead stays in the MABA5 in a super-saturated state, resulting in a higher lead concentration in the solvent. In order to expand available NADES candidates for lead paste dissolution, the idea to replace β-alanine by other amino acids has been proposed. L-proline was initially used to prove this. MALP5 was formed from malic acid, L-proline and water in a molar ratio of 1 : 1 : 5. Reactions between MALP5 and $2PbCO_3 \cdot Pb(OH)_2$ were conducted at room temperature. Figure 6.13 shows the

lead concentration in solution as a variety of $2PbCO_3 \cdot Pb(OH)_2$ loadings in MALP5 with comparison to that in MABA5. The maximum lead concentration in MALP5 (94.0 g/L) is slightly lower than that of MABA5 (101.9 g/L). The lead concentration trend versus lead compound loading in MALP5 is similar to that in MABA5 with both having the same critical loading point after which significant precipitation has been observed. This further proves that the malic acid in MABA5 and MALP5 is mainly responsible for reacting with lead compounds. It is also assumed that MALP5 would have a similar trend on other lead compounds.

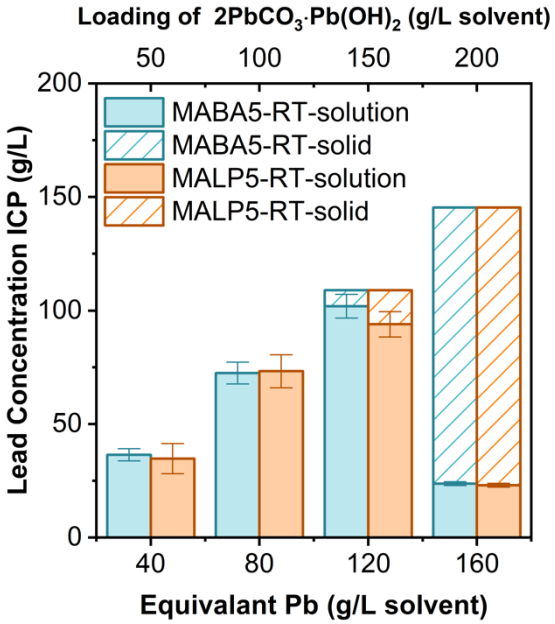

Figure 6.13 Lead concentration in solution and as precipitate of $2PbCO_3 \cdot Pb(OH)_2$ in MABA5 and MALP5 after reaction at room temperature for 4 days.

6.4 Advantages, Limitation and Future work

6.4.1 Advantages

In terms of a solvent-based recycling route, lead paste can be recycled either via an electrochemical method or a precipitation method. For both methods, the quality and purity of the final products are essential. In an electrochemical method, control on the working voltage and the working electrodes can yield high purity lead whilst other dissolved metal species including zinc and iron can remain in the solution. In a traditional precipitation

method, the precipitation starts virtually instantaneously. In this case, the precipitates are mixed with the undissolved particles, it would therefore be a challenge to separate the precipitate and the impurities. Unless they are of different particle sizes, a range of filter of different sizes should be used.

The advantage of using the malic acid based-NADESs in this chapter is based on the slow precipitation. From the analysis of precipitation behaviour, Pb^{2+} can stay stably in the solution for at least 42 hours with a controlled loading of Pb compounds. In the industrial application, the slow precipitation allows enough time frame to separate the undissolved impurities and the precipitates. Once the undissolved impurities are removed, precipitates can form from further stirring. With the use of the malic acid based-NADESs, precipitate obtained should be high purity lead malate dihydrate. Thus, high purity PbO will be obtained after the calcination.

6.4.2 Limitations and future work

6.4.2.1 Starting components

Pure Pb compounds have been used in this study. Industrial (desulfurized) lead paste, however, contains lots of plastics or metal impurities, which may be considered as an heterogenous site to induce the precipitation. As a result, a precipitation reaction using the industrial lead paste may happen at a lower loading and at less stirring time than pure lead compound. Future work can be conducted on the (desulfurized) lead paste provided by Envirowales Ltd. using the same experimental protocols.

Desulfurized lead paste was referenced and the main component of which $2PbCO_3 \cdot Pb(OH)_2$ and $PbCO_3$ were used. The work in this thesis therefore mainly focuses on the dissolution of desulfurized lead paste component. The main component of lead paste, $PbSO_4$, is however more difficult to dissolve than $2PbCO_3 \cdot Pb(OH)_2$ or $PbCO_3$. Future work can be switched to the dissolution of $PbSO_4$ to save the cost and energy consumption during the desulfurization process.

6.4.2.2 Precipitation behaviour

6.4.2.2.1 Time span

For all individual lead compounds in this chapter, it took at least 42 hours to form significant number of precipitates with continuous stirring. This time can be longer when the reaction happens at 50 ^{o}C. Though the long precipitation time frame allows the removal of undissolved plastics or fibres, the removal requires more time and energy. It is suggested that a precipitation agent can be used to shorten the precipitation time. Future work can be focused on the use of a precipitation agent, oxalic acid dihydrate, to form the precipitate, lead oxalate, after the individual lead compounds are fully dissolved in the NADESs.

6.4.2.2.2 Data point at room temperature

From the precipitation behaviour as shown in Figure 6.10, the precipitation of $2PbCO_3{\cdot}Pb(OH)_2$ happened between 48 to 72 hours, while the precipitation of $PbCO_3$ and PbO happened between 72 to 96 hours. The precipitation behaviours between this 24-hour time span were not captured. More data points between the 72- 96 hours can be selected to analyse the precipitation behaviour in future work.

6.4.2.2.3 Data point at 50 ^{o}C

To compare the precipitation behaviour of the Pb compounds, the same loadings of these Pb compounds were selected for 50 ^{o}C and room temperature. For $PbCO_3$ and PbO, the precipitation was not observed after 96 hours. To capture the precipitation behaviour of $PbCO_3$ and PbO, a higher loading of $PbCO_3$ and PbO or longer reaction time needs to be carried out in future work.

6.5 Conclusions

The study in this chapter has shown that a malic acid, β-alanine, and water-based NADES can achieve a maximum lead concentration of 104.0 g/L Pb for $2PbCO_3{\cdot}Pb(OH)_2$, 194.3 g/L Pb for $PbCO_3$, 224.0 g/L Pb for PbO and 170.0 g/L Pb for PbO_2 at 50 ^{o}C. The high maximum lead concentration is due to the over-saturation state of Pb in the solution caused by slow precipitation. From the precipitation behaviour study, all Pb compounds ($PbCO_3$,

$2PbCO_3 \cdot Pb(OH)_2$ and PbO) can stay stably in the solution for at least 42 hours. The slow precipitation offers the feasibility of removal of undissolved plastics or fibres in lead paste from the solution in industrial applications.

From the precipitation study in previous chapters (Chapter 4 & Chapter 5), the loading of Pb compounds in lactic acid based NADESs is approximately 4 times higher than in malic acid based NADESs. Therefore, the next chapter (Chapter 7) would study the dissolution and precipitation behaviour of lead compounds in a lactic acid based-NADES to identify if a higher maximum Pb concentration in the solution can be achieved.

Chapter 7 Solubility behaviour of lead compounds in lactic acid-based NADESs

7.1 Introduction

In Chapter 4 & 5, preliminary results have shown the possibility of using a precipitation followed by calcination method to recycle lead paste. The precipitation in both malic acid-(Chapter 4) and lactic acid-based NADES (Chapter 5) was observed to be slow in terms of reaction time. Based on the unique precipitation behaviour of NADESs and in consideration of their re-using, the idea of using a precipitation agent to leach out the lead from the solution has been proposed.

To confirm the feasibility of the use of precipitation agent, the precipitation behaviour of lead compounds in NADESs needs to be studied. Chapter 6 has analysed the maximum Pb concentration and precipitation behaviour of lead compounds in malic acid based NADESs.

Similarly, this chapter will focus on the maximum Pb concentration and precipitation behaviour of PbO and PbO_2 in lactic acid/betaine/water based NADESs. From previous results, lactic acid-based NADES can bear a higher PbO loading when forming precipitates than malic acid-based NADES. It is thus assumed that lactic acid-based NADES may have a higher maximum Pb concentration in solution. Additionally, effect of water content on reactions and results will be studied. Water content does not only change the concentration of individual NADESs components (lactic acid and betaine), but also influences the viscosity of the solvents. The viscosity of the solvents may further affect the reaction rates of lead compounds. Therefore, 3 NADESs with various water contents (23.2 wt%, 31.2 wt% and 37.7 wt%) will be used and their viscosity will also be studied.

7.2 Experimental

7.2.1 Synthesis of NADESs

The organic chemical components used to make NADESs in this chapter were the same as outlined in Chapter 5 (section 5.2.1 Table 5.1) and the lead compounds used were the same as outline in Chapter 6 (section 6.2.1 Table 6.1).

LABet5, LABet7.5 and LABet10 were prepared by mixing lactic acid solution (85 wt% in water, Sigma Aldrich), betaine (98%, Sigma Aldrich) and de-ionized water in a molar ratio of 2 : 1 : 5, 2 : 1 : 7.5 and 2 : 1 : 10, respectively, at 50 ^{o}C for hours until a homogenous liquid was formed.

7.2.1.1 Justification for the use of NADESs

The ratio of lactic acid and betaine was referred to the reference.[154] In the reference, the ratio of betaine to water was 1 : 2. The NADES formed at this ratio was too viscous. In this experiment, water was added to 5 part (to betaine) to reduce the viscosity. To analyse the effect of water content on the lead concentration and dissolution/precipitation behaviour of lead compounds in NADESs. 3 NADESs with different water ratio was chosen.

Though the ratio of carboxylic acid to amino acid used in MABA5 was 1 : 1, the ratio of carboxylic acid (lactic acid) to amino acid (betaine) in this chapter was 2 : 1 and was not adjusted because the purpose of the project is to dissolve as many lead compounds as possible and the carboxylic acid in the NADES is the main component used to dissolve lead compounds.

7.2.2 Solubility of Lead compounds in NADESs

7.2.2.1 PbO

To each 10 mL of LABet5, LABetT7.5 and LABet10 were added 5 g to 10 g PbO at an interval of 1 g PbO. The mixtures were stirred both at RT and at 50 ^{o}C respectively for 4 days. The mixtures were then centrifuged at 6000 rpm for 30 minutes. The solid (precipitate) has been discussed in Chapter 5. The liquid was filtered through a 0.2 μm PES vacuum filter. To measure the lead concentration in the liquor, ICP-OES was carried out on the liquid after dilution with

1 M nitric acid through comparison of a set of standard solutions with known concentrations (0, 1, 5, 10, 20 ppm) at a transition wavelength of 220.353 nm.

7.2.2.2 PbO_2

To each 10 mL of LABet5 and LABet7.5 were added 5 g to 10 g PbO_2 at an interval of 1 g PbO_2. The mixture was stirred both at RT and at 50 ^oC respectively for 4 days. The mixture was then centrifuged at 6000 rpm for 30 minutes. The liquid was treated and analysed following the same steps as PbO as described.

7.2.3 Precipitation behaviour analysis

7.2.3.1 PbO

9 g PbO was added to each of 10 mL LABet5, LABet7.5 and LABet10. The mixture was stirred both at RT and at 50 ^oC, respectively, for 2h, 6h, 24h, 48h, 72h and 96h. The mixture was centrifuged at 6000 rpm for 10 minutes. The liquid was filtered through a 0.2 μm PES vacuum filter. The liquid was then diluted and measured through ICP-OES.

7.2.3.2 PbO_2

9 g PbO_2 was added to 10 mL of LABet5. The mixture was stirred both at RT and at 50 ^oC, respectively, for 2h, 6h, 24h, 48h, 72h and 96h. The mixture was centrifuged at 6000 rpm for 10 minutes. The liquid was filtered through a 0.2 μm PES vacuum filter. The liquid was then diluted and measured through ICP-OES.

7.2.4 Analysis of NADESs

7.2.4.1 Viscosity

Viscosity of the solvents (LABet5, LABet7.5 and LABet10) was measured through a Discovery hybrid rheometer with a 40 mm geometry under an applied force of 0.1 MPa at a velocity of 0.1 rad/second over a temperature range of 20 ^oC to 60 ^oC at a heating rate of 3 ^oC/ minute.

7.2.4.2 FTIR

FTIR was carried out on all initial components (lactic acid solution, betaine) and LABet5-10.

7.2.4.3 ^{1}H NMR

All initial components and NADESs were dissolved in D_2O for ^{1}H NMR analysis. A further analysis was done on decomposed LABet5, which was heated at 80 °C to compared with qualified NADESs before the analysis. LABet5 with PbO loading from 5 g/10 mL to 10 g/10 mL reacted at RT and at 50 °C, and LABet5 with PbO_2 loading from 5 g/ 10 mL to 10 g/10 mL reacted at RT were dissolved in D_2O for ^{1}H NMR analysis. All ^{1}H NMR data was processed and exported through MestroNova software.

7.3 Results and Discussion

7.3.1 Characterisation of NADES

7.3.1.1 Viscosity

Figure 7.1 shows the viscosity of LABet5-10 as an increase of temperature. The viscosity of solvent decreases significantly with the increase of water content and the temperature. The change in viscosity might affect the maximum lead concentration in different NADESs as well as the dissolution and precipitation behaviour.

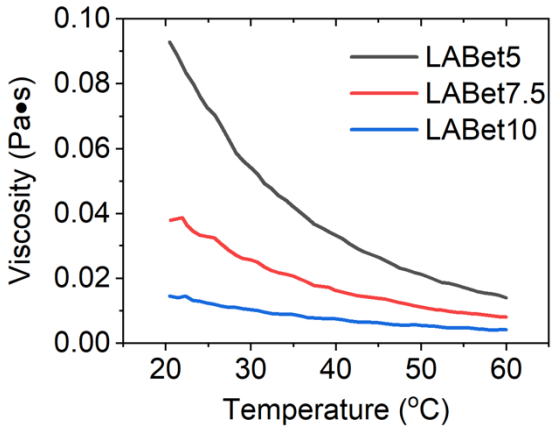

Figure 7.1 Viscosity of LABet5-10 as an increase of temperature.

7.3.1.2 ^{1}H NMR

Figure 7.2 a) and b) shows the ^{1}H NMR spectrum of betaine and lactic acid solution, respectively. In the molecule of betaine, the neighbouring atom (nitrogen) of the carbon atoms that all protons are attached to, has no proton attached. According to the "n+1", all

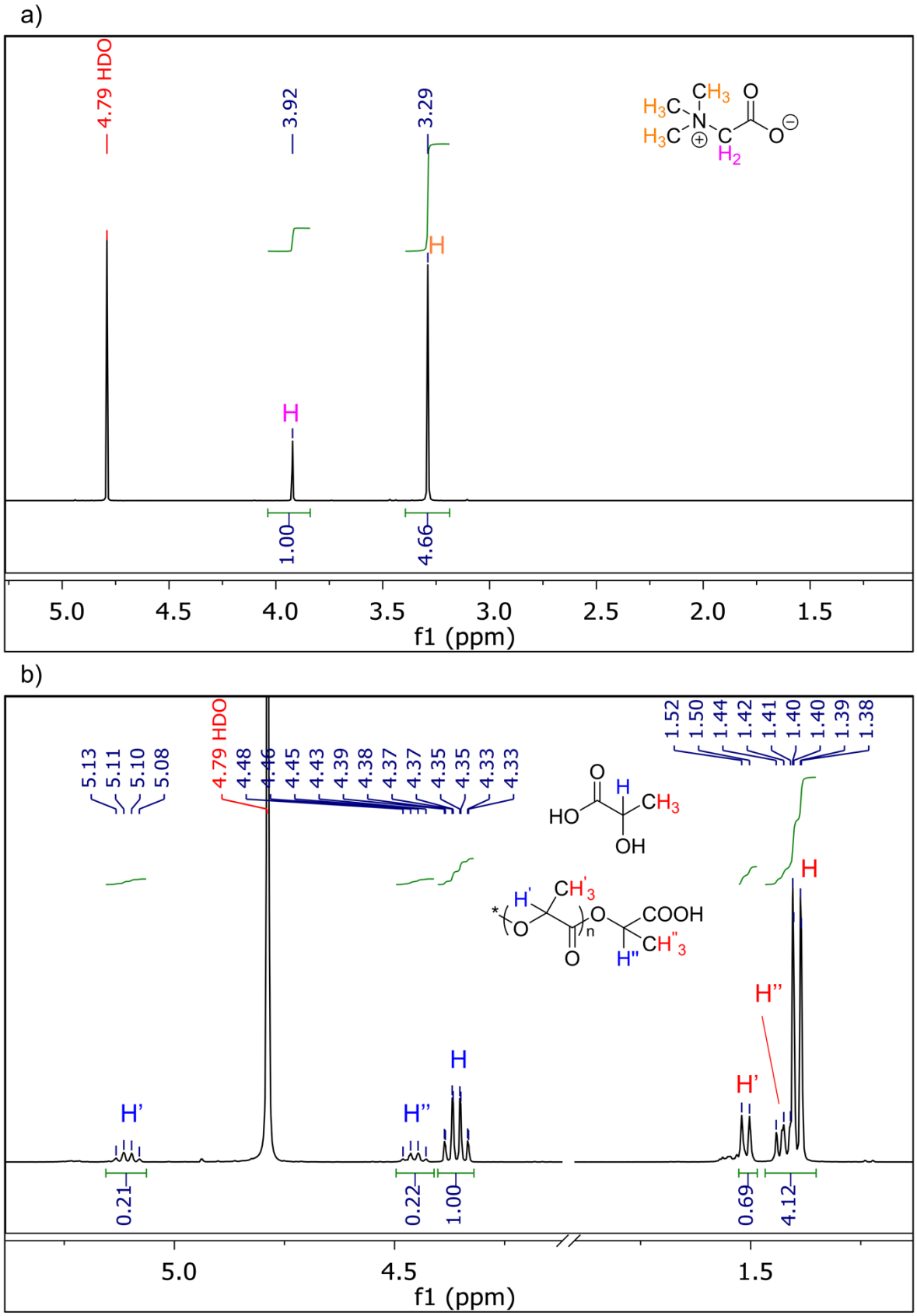

Figure 7.2 ^{1}H NMR (D_2O) of a) betaine and b) lactic acid solution.

protons in betaine should be present as singlet. In betaine, protons with two different chemical environments are present. Thus, two singlets have been observed at chemical shift of 3.92 and 3.29 ppm as shown in Figure 7.2 a). The integration ratio of these two singlets is around 1 : 4.66, corresponding to the number of protons present. In the lactic acid solution, according to the "n+1" rule, the protons should be present as a doublet and a quartet. As shown in Figure 7.2 b), the corresponded protons in lactic acid present as two quartets at chemical shift between 4.39-4.33 ppm and two doublets at chemical shift between 1.40-1.38 ppm. As the lactic acid solution used is a racemic mixture of D-lactic acid and L-lactic acid, the chemical shift of protons in D- and L-lactic acid might be slightly different. As a result, they appear as two quartets and doublets in ^{1}H NMR. Some sub-peaks have been observed at higher chemical shift due to the presence of poly-lactic acid (PLA) oligomers.[161] Figure 7.3 shows the ^{1}H NMR spectrum of LABet5, no additional peaks have been observed.

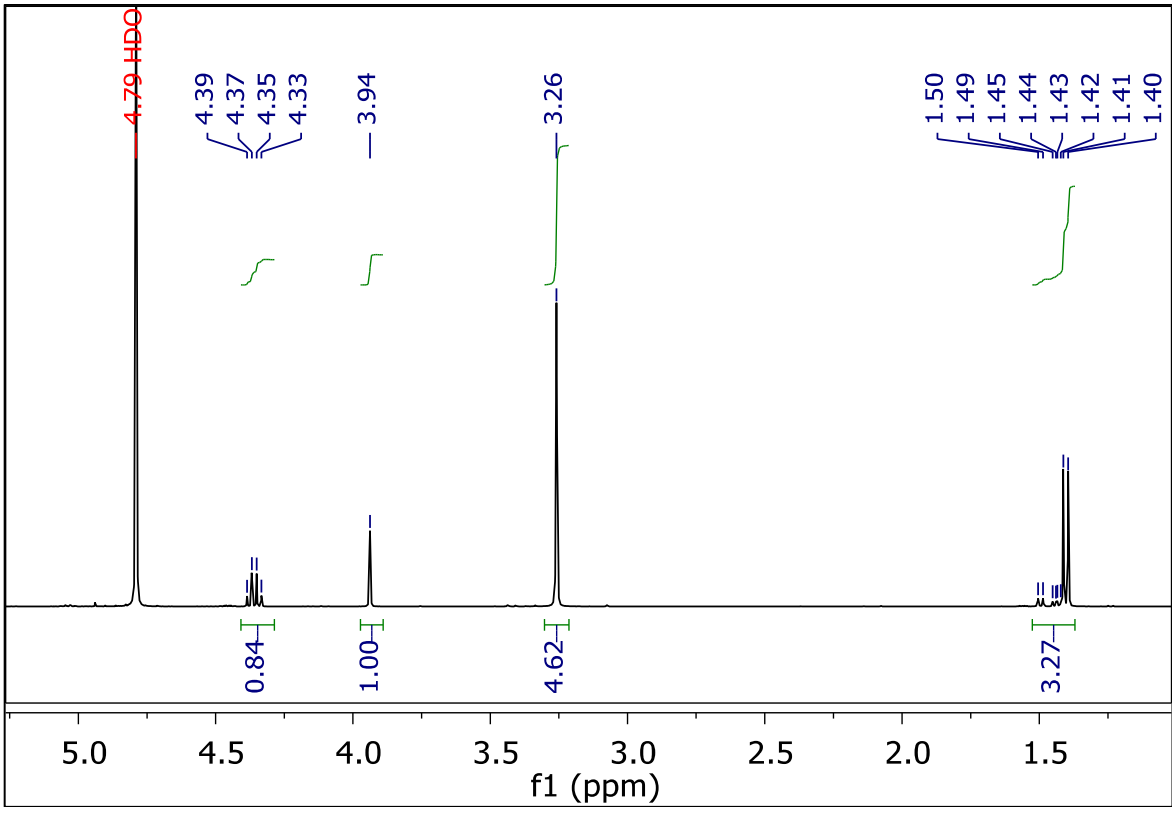

Figure 7.3 ^{1}H NMR (D_2O) of LABet5.

This indicates that no new compounds have been formed during the formation of LABet5. Some proton peaks from PLA were missing due to low amount of PLA oligomers. Peaks of D- and L-lactic acid may overlap so that only one doublet and one quartet have been observed. All peaks present in LABet5 have shifted towards higher chemical shift. This may possibly be due to the change in the chemical environment from the mixture.

Only ^{1}H NMR of LABet5 has been carried out. The main difference of LABet5, LABet7.5 and LABet10 lies in water content. Excessive D_2O was added to LABet5 during the preparation of ^{1}H NMR solution, which changes the water content of the solvent. No difference would be expected in ^{1}H NMR of LABet7.5 and LABet10.

7.3.1.3 FTIR

Figure 7.4 shows the FTIR spectrum of betaine, lactic acid solution, LABet5, LABet7.5 and LABet10. From the FTIR spectrum of betaine, a C=O stretching peak corresponding to carboxylic acid group can be seen at 1618 cm^{-1}. Two medium strong peaks at 1388 and 1340 cm^{-1} reveal the vibration and bending of N-C peak, respectively.[162] From the FTIR spectrum of lactic acid solution, the broad peak at 3387 cm^{-1} reflects the free water and OH from alcohol group. Peaks present in 1716 and 1122 cm^{-1} reflect the vibration of C=O and C-O, respectively. These characteristic peaks have all been observed in FTIR spectrum of LABet5 to LABet10. All peaks except the peak corresponding to the N-C bending from betaine has shifted towards higher wavenumber. The position of these peaks presents similarly in LABet5 to LABet10. The N-C peak has shifted towards lower wavenumber (higher frequency). The higher the water content, the more the N-C bending peak is shifted. The chemical shift indicates the formation of hydrogen bonding.[121] With more water added to the NADES system, water may break down the hydrogen bonding within the NADES; thus, less peak shift has been observed at higher water content.

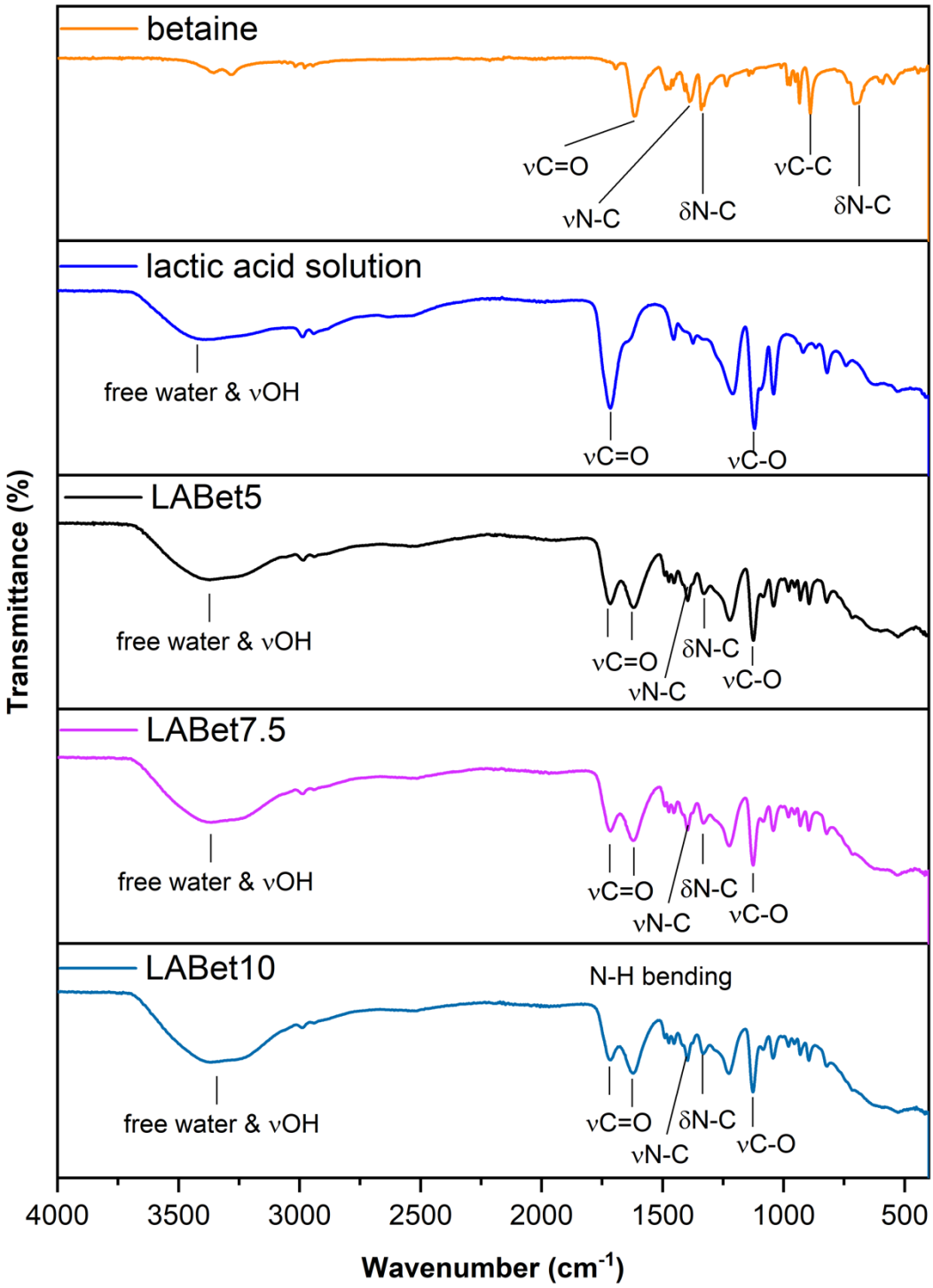

Figure 7.4 FTIR of betaine, lactic acid solution, LABet5, LABet7.5 and LABet10.

7.3.2 Maximum lead concentration in solution versus loading of lead compounds (PbO and PbO_2)

7.3.2.1 Justification the use of lead compounds

Theoretically, pure $Pb(OH)_2{\cdot}(PbCO_3)_2$ or $PbCO_3$, PbO and PbO_2 should be used as individual lead compounds in this study. Only PbO and PbO_2 have been studied in this study with the failure of using $Pb(OH)_2{\cdot}(PbCO_3)_2$ and $PbCO_3$ due to carbonation. When adding $Pb(OH)_2{\cdot}(PbCO_3)_2$ or $PbCO_3$ to LABet5-10, effervescence was immediately observed. Due to the high viscosity of the solvents and high loading of the lead compounds, the effervescence could not be removed from the solvent quickly. As a result, the solvent spilled outside the glass vial. Attempts were made to solve this issue by adding the $PbCO_3$ to the solvent slowly and by using a larger beaker rather than a glass vial. Both attempts have failed.

The spillage has caused potential hazardous safety issue and would result in inaccuracy of the results. From the discussion in Chapter 6 (section 6.3.4 and 6.3.5), the dissolution behaviour of $Pb(OH)_2{\cdot}(PbCO_3)_2$ or $PbCO_3$ and PbO in MABA5 has shown a similar trend. It is thus assumed that the dissolution behaviour of $Pb(OH)_2{\cdot}(PbCO_3)_2$ or $PbCO_3$ would also show a similar trend in lactic acid-based NADESs as PbO. Therefore, the study in this chapter would be more focused on the use of PbO.

7.3.2.2 PbO

3 NADESs differentiating in water content, LABet5, LABet7.5 and LABet10 have reacted with PbO at an increased loading for 4 days. Figure 7.5 a) to c) shows the maximum lead concentration in solution and precipitates with an increased loading of PbO. With the increase of loading, precipitates started to form from the solution. The precipitates have been confirmed to be a mixture of D-, L-lead lactate and lead dilactate, the analysis of which has been discussed in Chapter 5. Figure 7.5 also shows the starting point of precipitation in NADESs with different water content.

At RT, the overall trend of maximum lead concentration in solution with the increase of PbO loading exhibits similarly in LABet5-10, but the precipitates started to form at different PbO loadings. The critical loading point, at which the precipitate started to form, and the maximum

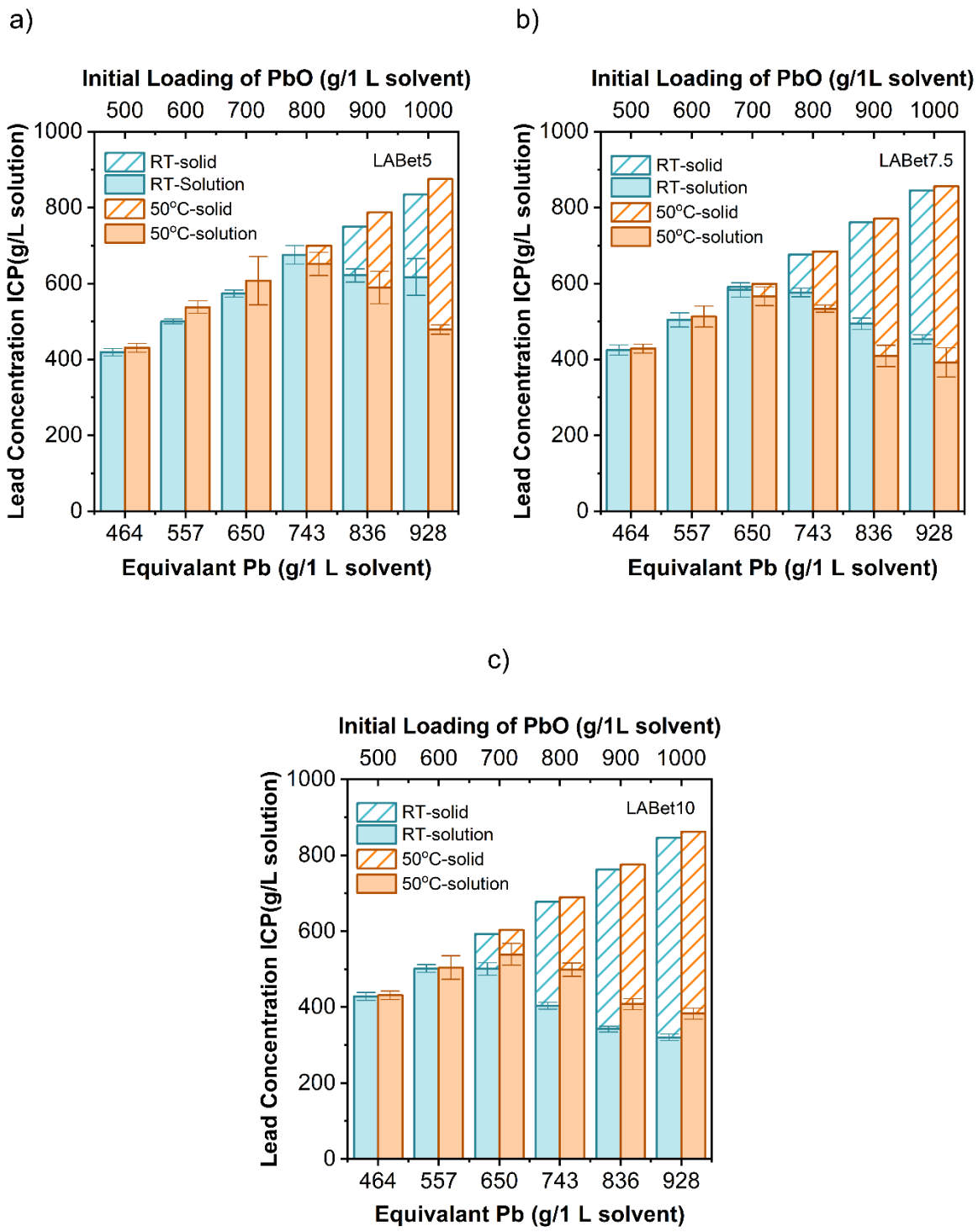

Figure 7.5 Lead concentration in solution and in precipitate with a variety PbO loading at RT and 50 °C after reaction in a) LABet5, b) LABet7.5 and c) LABet10 for 4 days.

lead concentration in solution decreases with the increase of water content. At RT, LABet5 with the lowest water content among 3 solvents, exhibits the maximum lead concentration

of 675 g/L at the loading of 800 g/L PbO. LABet7.5 exhibits the maximum lead concentration of 583 g/L at the loading of 700 g/L PbO. LABet10 with the highest water content among 3 solvents, exhibits the maximum lead concentration of 502 g/L at the loading of 600 g/L PbO. With the PbO loading further increasing to 1000 g/L, the amount of the solid (a mixture of undissolved PbO and precipitates) formed is higher in the NADESs with higher water content. It is thus assumed that NADESs with lower water content can bear with higher Pb in the solution.

At 50 ^{o}C, the dissolution behaviours of PbO in all 3 NADESs follow the same trend as at RT. The precipitation, however, started to form at a lower critical loading. This may possibly be due to that PbO dissolves quicker and thus precipitates quicker at 50 ^{o}C than at RT. Both LABet5 and LABet7.5 exhibits an approximate 20 g/L lower maximum lead concentration at 50 ^{o}C than at RT. The maximum lead concentration in LABet10 is around 35 g/L higher than that at RT. As the solid is a mixture of undissolved PbO and precipitates, LABet10 may have dissolved more PbO at this loading (700 g/L) at 50 ^{o}C than at RT. As a result, the lead concentration in solution appears higher at 50 ^{o}C than at RT.

7.3.2.2.1 Water loss

Ideally columns at RT and 50 ^{o}C at each loading should be of the same height. However, the column at 50 ^{o}C is slightly higher than that at RT due to more water loss at 50 ^{o}C. To confirm this, pure LABet5-10 have been stirred at some condition at RT and 50 ^{o}C for 4 days. Water content on pristine and post-reaction solvents have been detected with a Karl Fischer volumetric titration method. Due to the limitation of the Karl Fischer equipment, only pure solvents can be added to the titration solvent. Results are shown in Table 7.1. The volume change has been calculated as shown in Table 7.2. Water loss and volume change are more significant at 50 ^{o}C than at RT.

Table 7.1 Change in water content of LABet5-10 after stirring at RT and 50 °C for 4 days.

	wt% water (pristine)	wt% water (RT)	wt% water (50 °C)
LABet5	22.22 ± 0.62	21.46 ± 0.76	18.95 ± 0.46
LABet7.5	30.65 ± 0.33	29.68 ± 0.24	26.60 ± 0.22
LABet10	36.31 ± 1.05	35.22 ± 0.29	32.07 ± 0.36

Table 7.2 Volume change of LABet5-10 at RT and 50 °C.

	Δ_{vol}(RT) mL	Δ_{vol}(50 °C) mL
LABet5	-0.008	-0.082
LABet7.5	-0.015	-0.096
LABet10	-0.016	-0.127

The volume change in Table 7.2 was measured by noting the difference of volume through the mass over density pre- and post- reaction. Density was measured through a portable density meter. The mass was measured by weighing the whole vial (containing NADESs and stirring bar) subtracting the mass of glass vial and stirring bar. It was noted that mass of the whole vial decreased after stirring for 4 days at 50 °C. Given that the mass of stirring bar and glass vial would not change, the decrease in the mass was attributed to the water loss of NADESs. The water loss may possibly be due to that these vials do not have a good sealing property.

Another phenomenon has been noted that the water was heated and built up close to top of the cap after reaction. While measuring the water content as shown in Table 7.1, the water around the cap was not tapped back into the NADESs. When the NADESs would have reacted with lead compounds later, the water built up around the cap would not involve in the reaction. Therefore, the water content was measured without counting the water around the cap.

While measuring the mass of the whole vial (Table 7.2) post reaction, the water around the cap was counted. There might be some inconsistency in the data in Table 7.1 and Table 7.2.

7.3.2.2.2 Estimated reaction mechanism

The maximum lead concentration trend versus PbO loading shows a similar pattern at RT and at 50 °C. Similar to the reaction in malic-based NADESs, the reaction mechanism here in lactic acid-based NADESs is also assumed to be similarly at RT and at 50 °C but with different dissolution rate. The dissolution rate and corresponding precipitation behaviour will be analysed later. Based on the dissolution and precipitation phenomenon, the whole reaction is assumed to have two steps, dissolution as shown in Equation 7.1 followed by precipitation. Based on the single crystal of the precipitate analysed in chapter 5, the precipitation reaction can be described as shown in Equation 7.2.

$$PbO(s) + 2CH_3CH(OH)COOH(aq) \rightarrow Pb^{2+}(aq) + 2CH_3CH(OH)COO^-(aq) + H_2O(aq) \quad \textbf{Equation 7.1}$$

$$Pb^{2+}(aq) + 2(D,L\text{-})\ CH_3CH(OH)COO^-(aq) \rightarrow Pb(D,L\text{-}C_3H_5O_3)_2(s) \quad (1) \quad \textbf{Equation 7.2}$$

$$Pb^{2+}(aq) + (D\text{-}/L\text{-})\ CH_3CH(OH)COO^-(aq) \rightarrow Pb(D\text{-}/L\text{-}C_3H_4O_3)(s) + H^+(aq) \quad (2)$$

A mixture of three types of precipitates can be obtained from XRD results from Figure 5.7. However, due to imperfect crystal structure of Pb(D,L-$C_3H_5O_3)_2$, the fraction of each type of precipitates cannot be calculated from XRD Rietveld refinement.

7.3.2.2.3 Stability of solvents after reaction

The LABet5 proves to be stable after reacting with PbO. Figure A. 12 and Figure A. 13 compares the ^{1}H NMR of LABet5 after reacting with PbO at RT and at 50 °C, respectively. PLA peaks have not been observed after reacting with PbO. Depolymerization of PLA might occur as a side-effect when PbO is reacted with lactic acid. No additional peaks have been observed after reaction either at RT or at 50 °C, indicating that LABet5 was not decomposed. Slight shift of the ^{1}H peaks may be caused by the change in chemical environment of lactate due to the speciation of lactate with Pb species.

7.3.2.3 PbO_2

Figure 7.6 shows the maximum lead concentration trend in solution of different PbO_2 in LABet5 and LABet7.5 at RT and 50 °C. While the PbO_2 loading increases from 500 g/L to 1,000 g/L, the maximum lead concentration in LABet5 and LABet7.5 increases from 405 g/L to 540 g/L and 399 g/L to 500 g/L, respectively, after stirring at RT for 4 days. Though the maximum lead concentration in both LABet5 and LABet7.5 shows an upward trend within the loading range being analysed, remaining solids have been observed at all loadings.

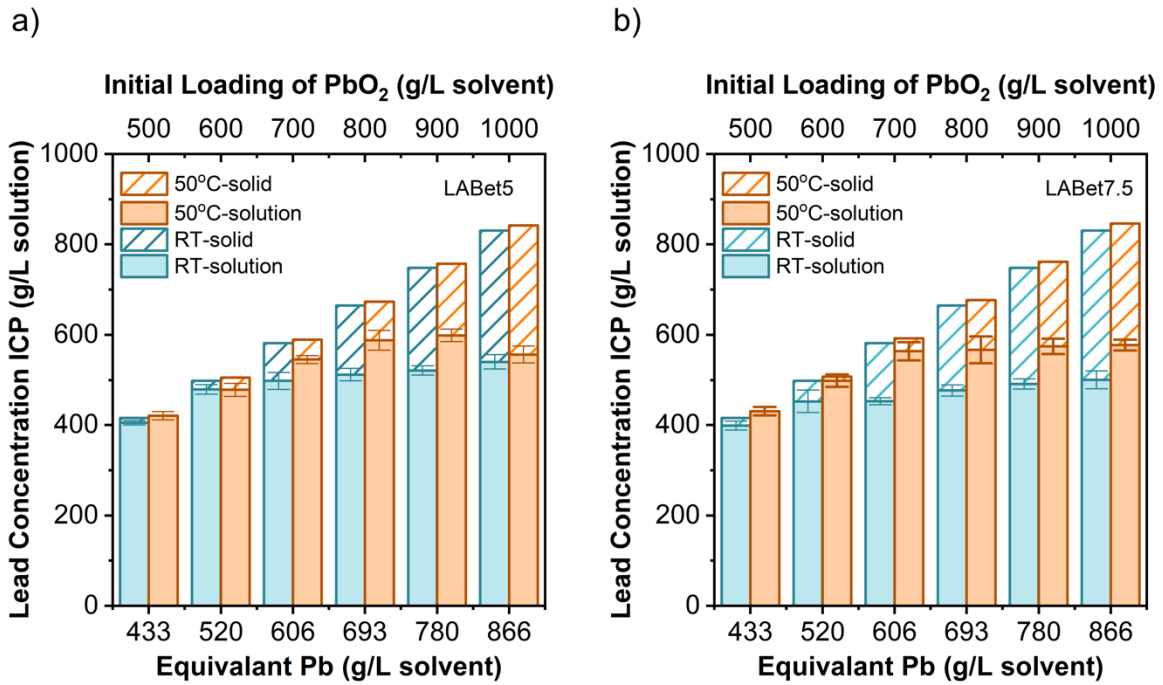

Figure 7.6 Lead concentration in solution and in solid with a variety PbO_2 loading at RT and 50 °C after reaction in a) LABet5 and b) LABet7.5 for 4 days.

After stirring at 50 °C for 4 days, PbO_2 can be completely dissolved in both LABet5 and LABet7.5 at the loading of 500 g/L. With the further increase of PbO_2, the lead concentration shows an upward trend in LABet7.5 from 430 g/L to 577 g/L within the loading range being analysed. The lead concentration in LABet5 also shows an upward trend to 599 g/L at the loading of 900 g/L, but the lead concentration drops to 556 g/L at the loading of 1,000 g/L due to precipitation. At loadings higher than 600 g/L, remaining solids have been observed and the number of solid increases with the increased loading. Two estimations have been made for this behaviour. The first estimation is that with further increase loading of PbO_2, PbO_2

cannot be further dissolved. The more PbO_2 is added, the more undissolved PbO_2 is remained. The second estimation is that with further increase loading of PbO_2, NADESs can dissolve more PbO_2, but precipitation has occurred. The amount of PbO_2 can be further dissolved is slightly higher than the Pb leaches out from the solution as precipitate. As a result, the lead concentration in NADESs still increases and the remained solid is a mixture of undissolved PbO_2 and precipitate.

7.3.2.3.1 Proposed reaction mechanism

Colour change of the solutions has been observed under the reaction of LABet5 and LABet7.5 with PbO_2 at RT as shown in Figure 7.7 and Figure 7.8. With the addition of PbO_2, the colour of the solution becomes darker than pure NADESs. The colour of these solutions is similar to the PbO_2 solution with MABA5. In Chapter 6, two estimations have been proposed to explain the colour change. One is due to the formation of Pb(IV) in the solution and the other is due to the decomposition product from oxidation of malic acid. As similar colour has been observed in lactic acid-based NADESs as well, it is more likely that the colour change is caused by the formation of Pb(IV). EXAFS study is required to confirm the Pb(IV) estimation. This was not completed due to the limitation of time.

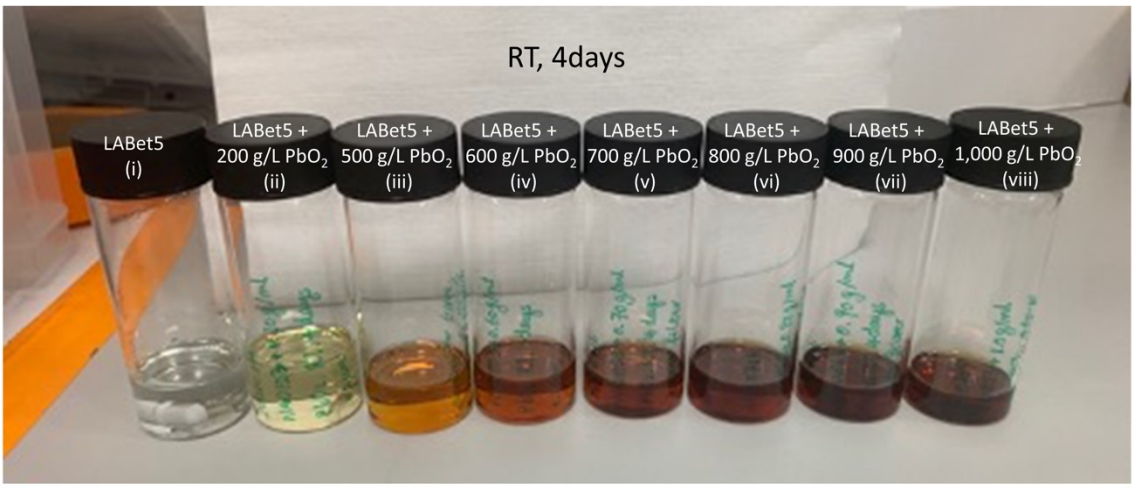

Figure 7.7 Appearance of solution from left to right: (i) pure LABet5, (ii) LABet5 + 200 g/L PbO_2, (iii) LABet5 + 500 g/L PbO_2, (iv) LABet5 + 600 g/L PbO_2, (v) LABet5 + 700 g/L PbO_2, (vi) LABet5 + 800 g/L PbO_2, (vii) LABet5 + 900 g/L PbO_2, (viii)LABet5 + 1,000 g/L PbO_2 reacted at RT for 4 days.

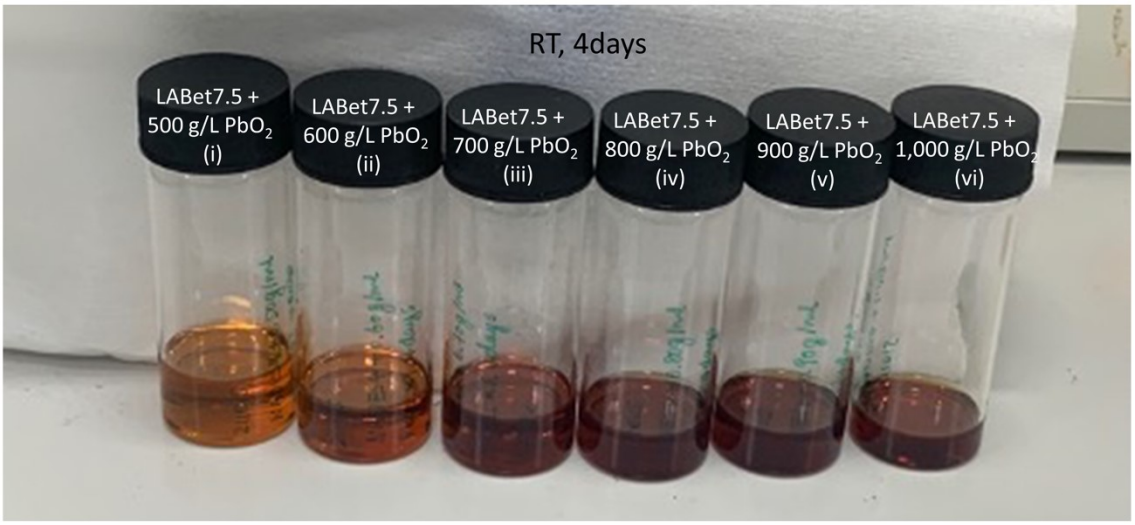

Figure 7.8 Appearance of solution from left to right: (i) LABet7.5 + 500 g/L PbO_2, (ii) LABet7.5 + 600 g/L PbO_2, (iii) LABet7.5 + 700 g/L PbO_2, (iv) LABet7.5 + 800 g/L PbO_2, (v) LABet7.5 + 900 g/L PbO_2, (vi) LABet7.5 + 1,000 g/L PbO_2 reacted at RT for 4 days.

7.3.2.3.2 Reduction of solvents by PbO_2 oxidation

^{1}H NMR was used to identify if the solvent has been oxidized by PbO_2. Figure A. 14 compares the ^{1}H NMR of pure LABet5 and LABet5 after reacting with increased PbO_2 loading at RT for 4 days. From the integration ratio of proton peaks, the integration of lactic acid peaks keeps decreasing as the PbO_2 loading increases, indicating the loss of lactic acid after reaction. An additional peak at chemical shift around 2 ppm has been observed. The integration of this additional peak increases as the increase of PbO_2 loading. It is estimated that this peak might be attributed to the oxidation product of lactic acid. One of the oxidation products of lactic acid can be acetic acid.[163] At PbO_2 loadings of 500 g/L, the chemical shift of the additional peak appears at around 2.03 ppm, which is close to the chemical shift (=2.08 ppm) of pure acetic acid in D_2O.[164] The additional peak is a singlet, which matches the peak type of protons from acetic acid. These indicate that the oxidation product is highly likely to be acetic acid.

7.3.3 Dissolution and precipitation behaviour of lead compounds

7.3.3.1 PbO

Similar as the reaction behaviour of PbO in malic acid-based NADES, the lead concentration in solution drops as the PbO loading increases in all 3 lactic acid-based NADESs due to

precipitation. The critical loading, at which the lead concentration in solution drops, varies with the water content of the solution due to different dissolution and precipitation rate. To understand the effect of water content on the dissolution and the precipitation behaviour of of PbO, lead concentration in solution with different stirring times was measured for 3 lactic acid-based NADESs with different water content at a fixed loading of 900 g/L PbO. The experiments have been carried out at both RT and at 50 °C.

7.3.3.1.1 Room temperature

Figure 7.9 shows the lead concentration in solution with 900 g/L PbO in LABet5-10 as a function of stirring time at RT. For the first 2 hours, NADES with the lowest water content had the least lead concentration. It means that NADES with the lowest water content has the lowest dissolution rate at the start of the dissolution. For these 3 NADESs, the viscosity decreases with the increase of water content. At the initial start of the dissolution, high viscosity of the solvent limits the diffusion of PbO within the solution, leading to a lower dissolution rate. Between 2 to 6 hours, the dissolution rate remains similarly in 3 NADESs. The dissolution rate then slowed down after 6 hours until precipitation occurs.

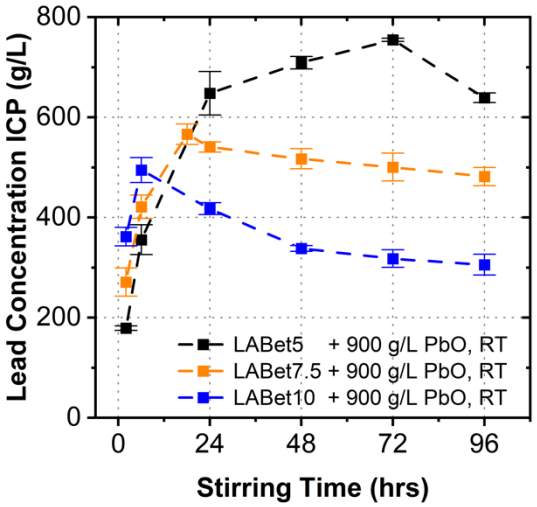

Figure 7.9 Lead concentration in LABet5-10 with 900 g/L PbO as a function of stirring time at RT.

The lower the water content, the later the precipitation occurs as higher viscosity leads to a lower diffusion rate of Pb species within the solution. Thus, the Pb species are less likely to

cluster together to form precipitate so that the longer Pb can stay within the solution with lower water content. Additionally, as NADES with lower water content has a higher lactic acid concentration, its ability of dissolving PbO is stronger. As a result, the lower the water content, the higher the maximum lead concentration solution can be achieved. With further stirring, precipitation occurs. The effect of water content on the precipitation rate cannot be determined as more experiments need to be carried out to determine a more accurate point where precipitation started. The time intervals used to calculate the precipitation rate between different samples also need to be the same for comparison. This is one of the improvements can be made in future work.

7.3.3.1.2 50 °C

The dissolution and precipitation behaviour of PbO at 50 °C has also been analysed. Figure 7.10 shows the lead concentration in solution with 900 g/L PbO in LABet5-10 as a function of stirring time at 50 °C.

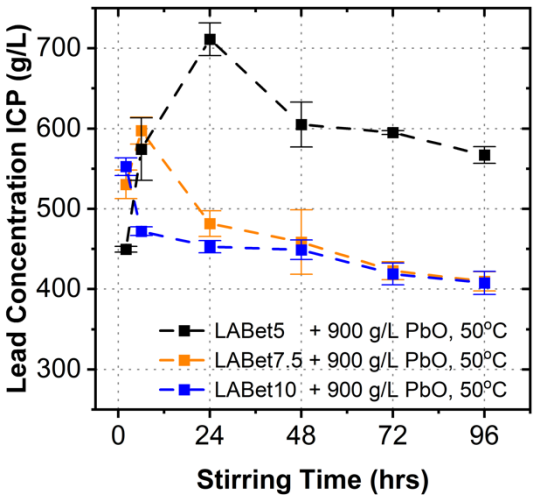

Figure 7.10 Lead concentration in LABet5-10 with 900 g/L PbO as a function of stirring time at 50 °C.

For the first 2 hours, NADES with the lowest water content still has the least lead concentration, the value of which is higher than that at RT comparatively. As the increased temperature lowers the viscosity of the solution and increases the kinetic energy of the reactants, PbO can be more easily dissolved at 50 °C. The dissolution rate has also slowed down with further stirring. Due to lower viscosity and increased kinetic energy, the

precipitation happens earlier in all NADESs than at RT. Additionally, water content may also affect the precipitation. As NADES with higher water content has a lower viscosity, Pb species cluster easier together to form precipitates at an increased temperature. As a result, NADES with higher the water content precipitated earlier at the same loading. To compare the actual precipitation rate between samples with different content, more experiments will be required to determine a more accurate point where precipitation started. Time intervals between different samples also need to be the same.

7.3.3.2 PbO_2

Figure 7.11 shows the lead concentration in solution with 900 g/L PbO_2 in LABet5 as a function of stirring time at RT and at 50 °C.

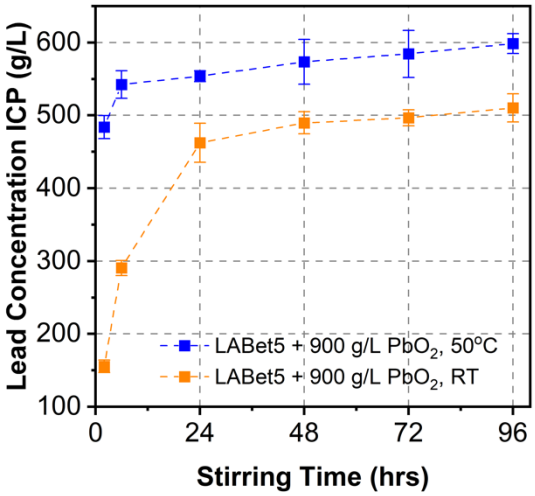

Figure 7.11 Lead concentration in LABet5 with 900 g/L PbO_2 as a function of stirring time at RT and at 50 °C.

For the first 2 hours, the reaction rate of PbO_2 in LABet5 has increased significantly at increased temperature. As higher temperature lowers both the viscosity of the solvent and activation energy of the reaction, PbO_2 dissolves quicker at 50 °C. The dissolution then slows down between 2-24 hours. After 24 hours, the lead concentration in solution only increases gradually both at RT and at 50 °C. From the discussion in section 7.3.2.3, precipitation may occur throughout the reaction. To prove this estimation, XRD has been carried out on these left-over solids from reaction between LABet5 and 900 g/L PbO_2 at 50 °C. Figure 7.12 a) shows the XRD analysis of the left-over solids as a function of reaction time. Around $2\theta = 25^{o}$, an

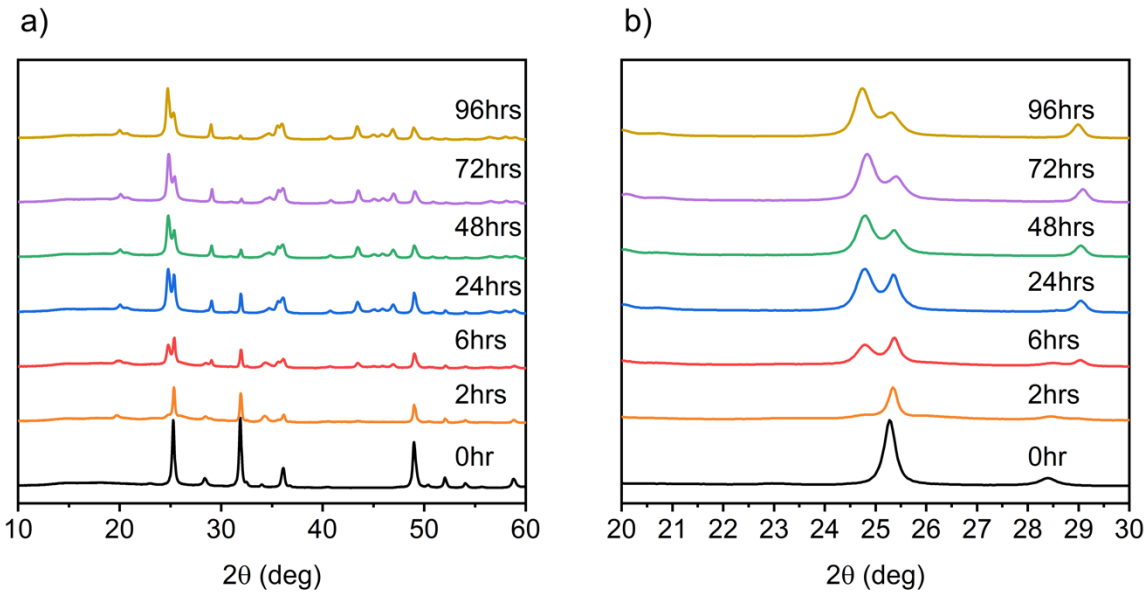

Figure 7.12 a) full pattern and b) focused range of XRD analysis of left-over solids from reaction between LABet5 + 900 g/L PbO_2 at 50 °C.

additional peak has appeared, and the peak intensity increases as the reaction time increases. Figure 7.12 b) focuses the XRD peak around 2θ = 25°. It is assumed that the peak at higher diffraction angle belongs to PbO_2 and the peak at lower diffraction angle belongs to the precipitate. Over reaction time, the PbO_2 peak decreases and the precipitate peaks increases. This suggests that more PbO_2 has been dissolved, meanwhile, more precipitate is generated over reaction time. As the lead concentration in solution keeps increasing over reaction time, it is suggested that the amount PbO_2 dissolved is larger than the amount of Pb precipitated from the solution.

7.4 Advantages, Limitation and Future work

7.4.1 Advantages

The maximum lead concentration in lactic acid-based NADES achieved 675 g/L for PbO and 599 g/L for PbO_2. The value is at least 3 times higher than it can achieve in malic acid-based NADESs. In terms of battery recycling, this means that by using lactic acid-based NADESs, more lead can be recovered per cycle. In the precipitation behaviour study, the precipitation took at least 24 hours to reach a comparatively steady state. In terms of actual lead battery

paste recycling, there is still a chance for the removal of undissolved impurities such as plastics or fibre.

7.4.2 Limitations

7.4.2.1 Starting components

Due to the viscosity of the solvents and the size of the container, $PbCO_3$ or $Pb(OH)_2{\cdot}(PbCO_3)_2$ cannot be used as one of the reactants. As $PbCO_3$ is the main component of desulfurized lead paste, the issue with the effervescence must be solved. Water can be added to the solvent to reduce the viscosity at the compensation of maximum lead concentration. A large-sized container could be used at the compensation of space.

7.4.2.2 Precipitation behaviour

7.4.2.2.1 Loading

Lead concentration in solution versus stirring time has been compared in NADESs with different water content at a fixed loading. Different starting loading may also affect the time when precipitation starts. To thoroughly understand the precipitation behaviour, comparison with different loadings of lead compounds in the same NADES can be made.

7.4.2.2.2 Time span

For the precipitation behaviour study of PbO in NADESs at RT, the lead concentration almost achieves a plateau in LABet7.5 and LABet10 between 48 to 96 hours. Such plateau has not been observed in LABet5. It is estimated that the lead concentration would continue to drop in LABet5 after 96 hours. The lead concentration can be further analysed in LABet5 when stirring time is longer than 96 hours until a steady concentration is achieved.

7.5 Conclusions

This chapter has shown that lactic acid, betaine-based NADESs can achieve a maximum lead concentration of 675 g/L Pb for PbO (800 g/L loading, RT, 4 days) and 599 g/L Pb for PbO_2 (900 g/L loading, 50 ^{o}C, 4 days). The maximum lead concentration in lactic acid-based NADESs is around 3 times higher than that malic acid-based NADES can achieve. Similar to malic acid-

based NADES, the dissolution of Pb compounds in lactic acid-based NADES also has slow precipitation behaviour, which results in an over-saturated state Pb in the solution. Therefore, the solution exhibits a higher maximum lead concentration.

The precipitation behaviour and the effect of water on the overall reactions have been analysed. It has been found that NADES with lower water content has higher viscosity. As a result, NADES with lower water content has lower initial dissolution rate of lead compounds. Due to higher viscosity, the precipitation happens slower in NADES with lower water content. As viscosity of the solution decreases with the increase of temperature, the initial dissolution rate of lead compounds increases, and the precipitation happens faster at 50 ^{o}C than that at RT.

As the precipitation took at least 24 hours to complete, it offers the probability to remove undissolved impurities from the solution when using industrial lead paste as starting component.

Chapter 8 Industrial application – Re-usability test of NADESs

8.1 Introduction

Chapter 4 and Chapter 5 have successfully converted $PbCO_3$ and PbO, the main components of lead paste, respectively, using carboxylic acid-based NADESs to organic lead compounds precipitate, which can be calcined to β-PbO for new LAB manufacturing. These results have proved the idea of using NADESs to recycle lead paste through a precipitation followed by calcination method. While actual lead paste is used, the separation of undissolved fibres or plastics from the precipitates is a potential issue. Chapter 6 and Chapter 7 have analyzed the dissolution and precipitation behaviour of lead paste components ($PbCO_3$, PbO and PbO_2) in two different carboxylic acid based-NADESs. Results have shown that both NADESs have high lead concentration of lead components due to slow precipitation. These results have proven the possibility of using NADESs in recycling lead paste. The main issue with the industrial lead paste is that it may contain SiO_2 fibres and undissolved plastics, which may be mixed with the precipitates during precipitation. While the precipitation of lead paste components in both NADESs is a slow process, this allows the removal of undissolved fibres or plastics before the precipitation occurs. Therefore, high-purity precipitates can be obtained.

During the precipitation reaction, the carboxylic acid component from the NADES is reacted with lead components to form precipitates. This means that the NADES cannot be re-used as fresh carboxylic acid which needs to be added to the solvent per cycle to dissolve new lead paste batch. In this chapter, the idea of using a precipitation agent, oxalic acid dihydrate, has been proposed to overcome this drawback. Industrial desulfurized lead paste will be dissolved using malic acid, β-alanine based NADES. The precipitation agent, oxalic acid dihydrate, will then be added to the solution to form lead oxalate, which can be calcined to PbO. Through this method, the NADES can be re-used to recycle new lead paste batch.

8.2 Experimental

8.2.1 EDX characterization of lead paste

Lead paste 2019 provided by Envirowales Ltd. was characterized using EDX mapping. Elemental compositions were identified.

8.2.2 Re-usability test of MABA5

The procedure of re-usability test on MABA5 for recycling lead paste is shown in Figure 8.1. This experiment in this thesis was conducted before conducting the experiment using LABet (Chapter 5 and Chapter 7). Though the lactic acid-based NADES can dissolve more lead compounds, MABA5 was used in the recycling process.

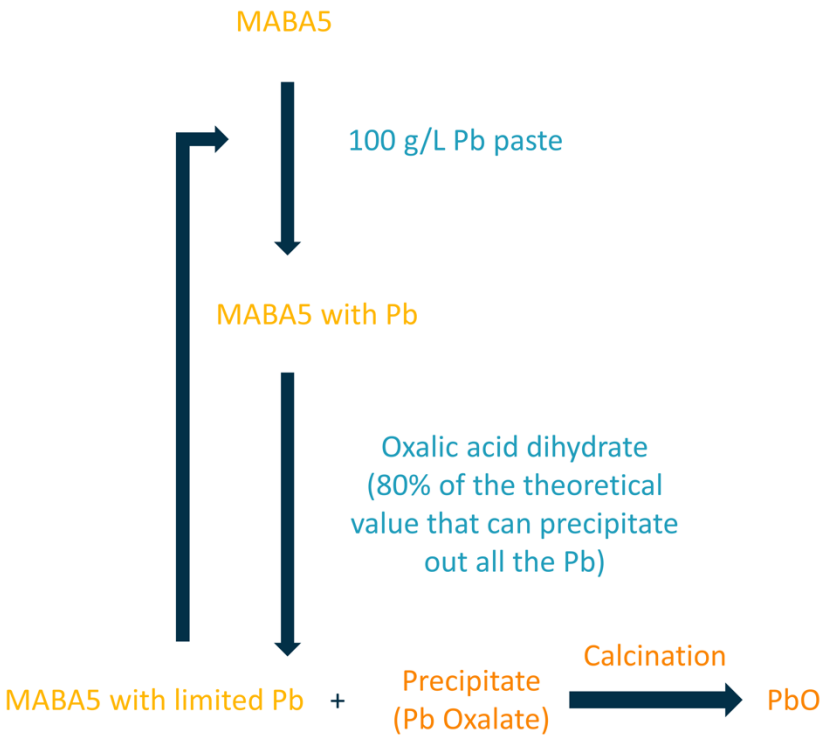

Figure 8.1 Process flow chart of re-usability test on MABA5 for lead paste recycling.

To 200 mL of MABA5 was added 20 g lead paste 2019. The mixture was stirred at 300 rpm using 3 conditions (RT for 5 hours, RT for 48 hours and 50 ^{o}C for 5 hours) respectively. After the reaction, the mixture was filtered via a vacuum filter through a 0.45μm PES filter. 1 mL of

the filtered liquid was taken from the filtered liquid and diluted by 1M nitric acid for ICP-OES analysis to measure the lead concentration. Oxalic acid dihydrate (Sigma, 99 %) was then added to the bulk liquid and mixed at room temperature at 300 rpm for 3 days. The amount of oxalic acid dihydrate added was 80 % of the theoretical value which can precipitate all lead from the bulk solvent. Only 80 % oxalic acid was chosen is to ensure that oxalic acid would not remain in the solution due to uncomplete reaction with Pb species. After 3 days, the mixture was centrifuged at 6000 rpm for 30 minutes to separate the precipitate from the liquor. The precipitate was washed via a Buchner funnel with de-ionized water and acetone. The precipitate was then dried in a glass oven at 60 ^{o}C under vacuum overnight. The precipitate was analysed by PXRD, SEM and XPS. The precipitate was subsequently calcined at 550 ^{o}C. The calcined product was analysed by PXRD, SEM and XPS. The liquor after centrifugation was filtered via a vacuum filter with 0.2μm PES filter. 1mL of the filtered liquid was taken from the filtered liquid and diluted by 1M nitric acid for ICP-OES analysis to measure the lead remained in the solution. 0.1 g lead paste 2019 was then added to each 1 mL bulk solution. The total amount (in grams) of lead is dependent on the volume of each solution. Next, the mixture was stirred and treated using the same conditions as last cycle. After dissolution of lead paste and filtration, 1 mL of the liquid was taken again and diluted by 1M nitric acid for ICP-OES to measure the lead concentration. This concentration subtracts the lead remained in the solution from last cycle would be the solubility of lead paste for this cycle. Then the mixture was processed using the same conditions and procedures as last cycle. All processes were repeated for 3 cycles to identify the re-usability of MABA5 through this leaching method.

8.2.3 Characterisation and calcination of precipitate

The precipitate obtained from each cycle was washed with DI water via a Buchner funnel and dried at 60 ^{o}C overnight in a Buchi-oven. The precipitate was then characterized by XRD and XPS. The precipitate was next calcined at 550 ^{o}C in a furnace for 2 hours. The calcined product was characterized by XRD and XPS.

8.3 Results and Discussion

8.3.1 Characterisation of lead paste

Previous results (Chapter 6 Figure 6.1) have shown that the main crystalline components of lead paste provided by Envirowales Ltd are $NaOH{\cdot}(PbCO_3)_2$, $PbCO_3$, PbO_2 and β-PbO based on XRD results. The non-crystalline components cannot be identified by XRD. Long fibres have been observed from the SEM image as shown in Figure 8.2. EDX mapping from Figure 8.3 has confirmed the majority elements of the paste to be Pb. The compositions of the fibres have been identified as Si and O. It is estimated that the fibres are mainly composed of SiO_2. The Pb content around the fibre area is significantly lower than other area from the EDX spectrum. The average weight percentage of all elements of the lead paste 2019 has been shown in Table 8.1. Pb accounts for 71 wt% of the paste materials.

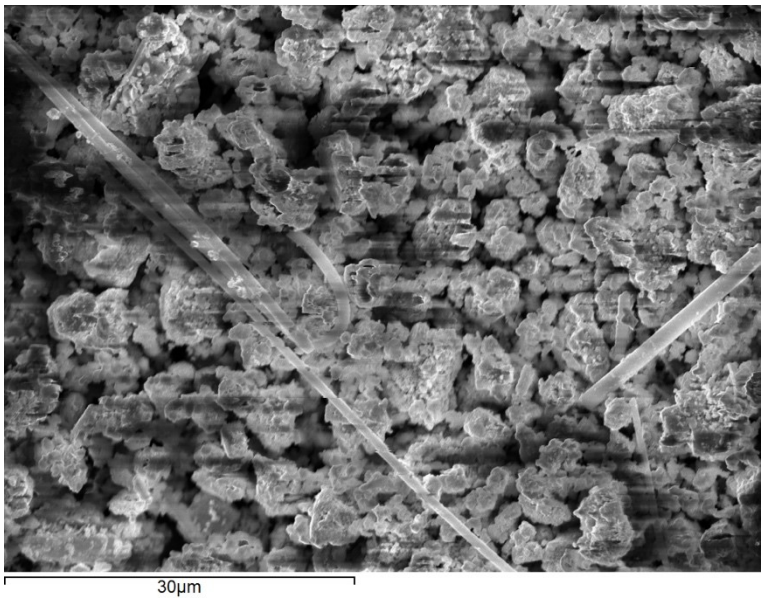

Figure 8.2 SEM image of lead paste 2019 provided by Envirowales Ltd.

Table 8.1 Weight percentage of all elements from the lead paste 2019.

Pb paste 2019 elements	C	O	Na	Mg	Al	Si	K	Ca	Pb
wt%	5.91	18.44	1.18	0.17	0.22	2.84	0.1	0.46	70.67

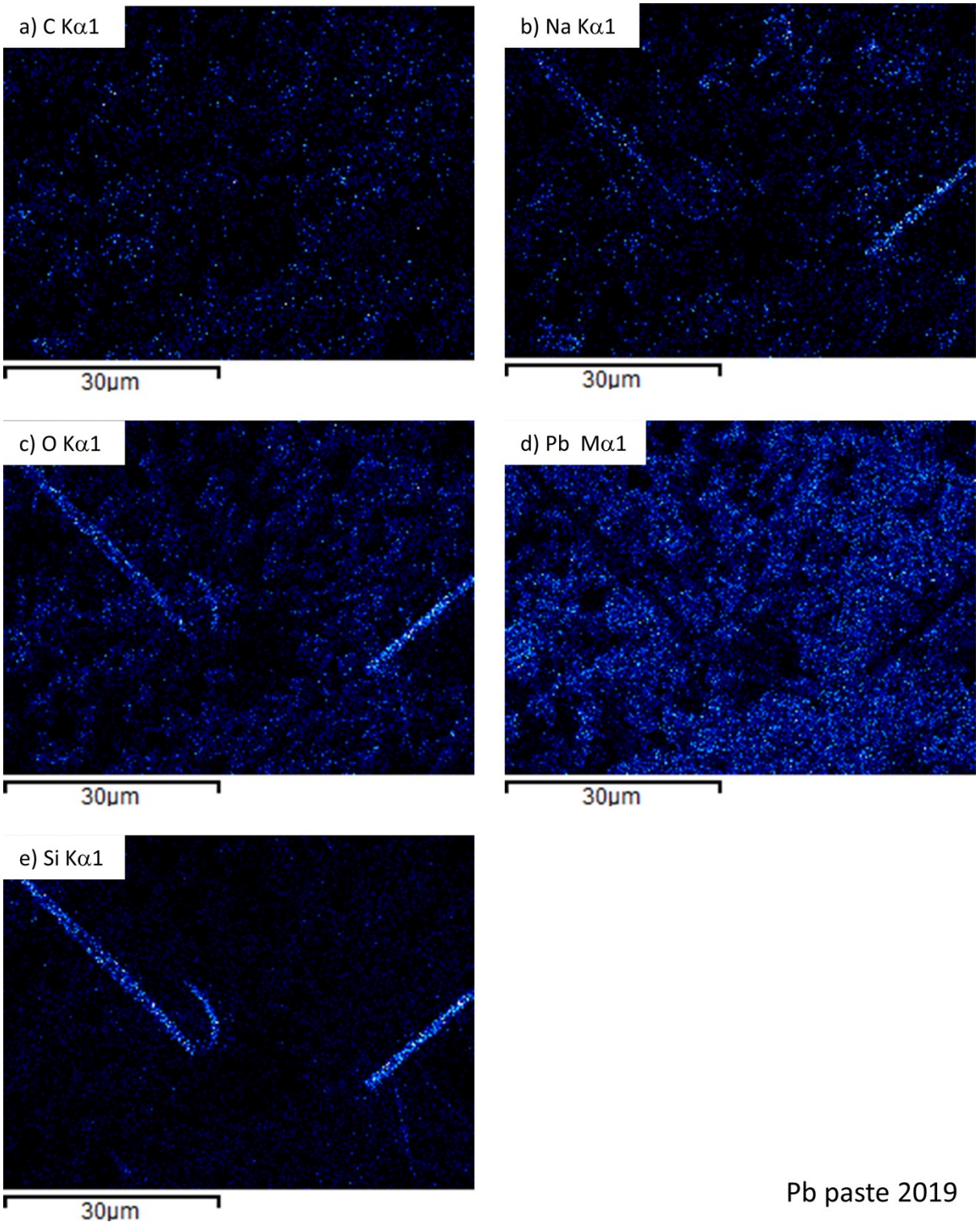

Figure 8.3 EDX images of lead paste 2019 provided by Envirowales Ltd.

8.3.2 Re-usability test of MABA5

3 different conditions (RT 2days, RT 5 hours and 50 ^{o}C 5 hours) were used to recycle lead paste. Figure 8.4 shows the lead concentration in each MABA5 cycle for all 3 recycle

conditions. 80 % of the lead from the paste can be dissolved, when the lead paste is stirred in MABA5 at RT for 5 hours. The dissolution efficiency can be increased significantly when increasing the temperature or stirring time. When the lead paste is stirred at RT for 2 days, almost all lead can be dissolved. The concentration remains similar for each cycle when lead paste is reacted at RT. When lead paste is reacted at 50 °C for 5 hours, the dissolution efficiency can achieve 94 % for the first cycle. However, the lead concentration decreases 1 g/L every further cycle. This may possibly be due to the oxidation of MABA5 from PbO_2 or due to the water loss. Based on the amount of lead dissolved in the solution, 50 °C for 5 hours or RT 2 days may be an optimum condition for lead paste recycling efficiency. To identify which one suits better for large scale applications, an energy calculation for the whole process will be required.

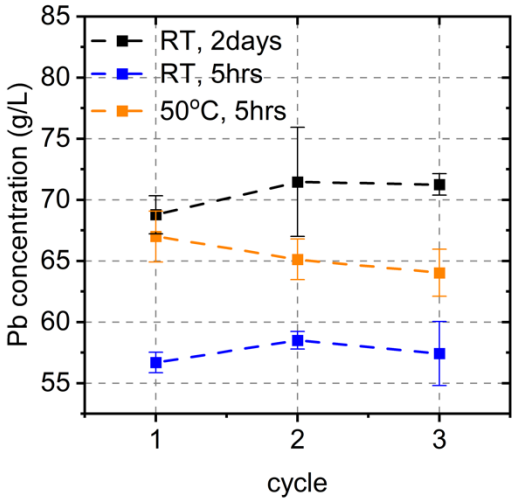

Figure 8.4 Lead concentration of MABA5 recycling lead paste under different conditions upon cycles.

8.3.3 Characterisation of precipitate

The XRD pattern shown in Figure 8.5 has confirmed that the precipitate is lead oxalate (ICSD 109830). From the XPS survey (shown in Figure A. 15) only Pb, C and O have been detected. Si has not been detected. As Si was detected in the raw Pb paste (Figure A. 6), this means that fibres were not present in the precipitate as they have been removed before precipitation agent is added. Figure 8.6 shows the core levels of Pb 4*f*, C 1*s* and O 1*s*. The atomic ratio of Pb : C (C=O) : O (O-C) is 1 : 2.93 : 3.78. The Pb : O ratio matches the elemental composition of

lead oxalate (PbC_2O_4). C is slightly higher, possibly due to the adventitious carbon materials from the environment being adsorbed on the surface of the precipitate.

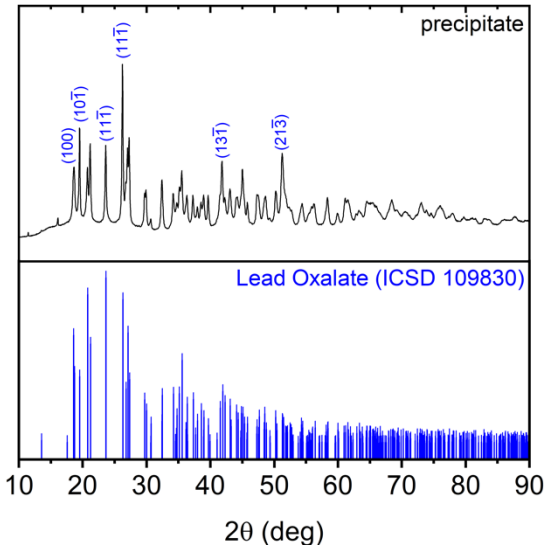

Figure 8.5 XRD pattern of precipitate.

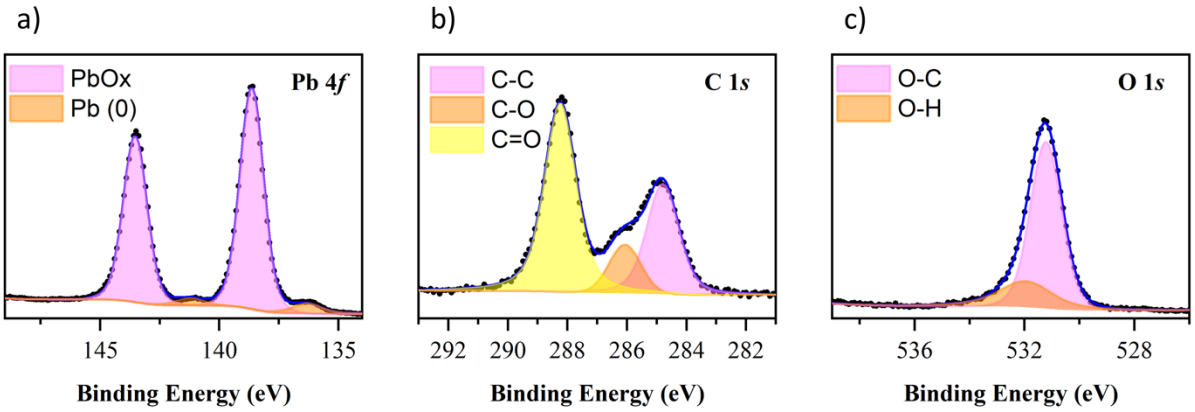

Figure 8.6 XPS core levels a) Pb 4*f*, b) C 1*s* and c) O 1*s* of precipitate.

8.3.4 Calcination of the precipitate

The precipitate is calcined at 550 °C for 2 hours to recover to PbO. XRD as shown in Figure 8.7 has confirmed that the calcined product is a mixture of α-PbO and β-PbO. This result matches the result from literature,[165] though the conversion temperature from α-PbO to β-PbO is 486.5 °C. From the result from literature, pure α-PbO can be achieved if the calcination

temperature is lower than 500 °C, while pure β-PbO can be achieved if the calcination temperature is higher than 600 °C.[165]

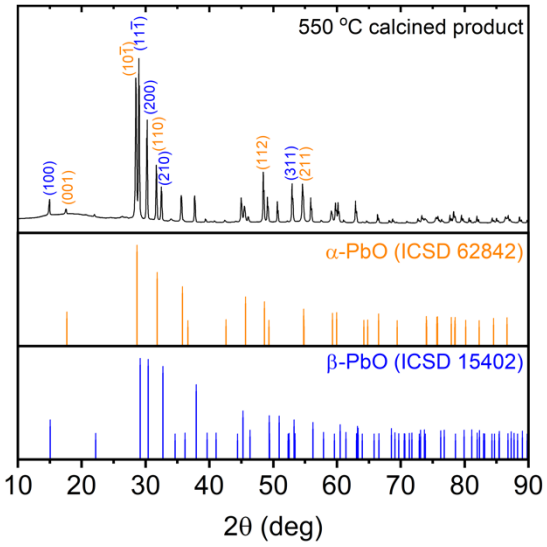

Figure 8.7 XRD pattern of calcined product.

From the XPS survey (shown in Figure A. 16), the main elements of the calcined product are Pb, C and O. Figure 8.8 a) – c) present the core levels for these elements, respectively. Pb 4*f* shows a doublet at 137.9 eV with a SOP of 4.9 eV, which matches the peak position of $PbCO_3$/PbO from literature.[166] O 1*s* shows two peaks at 528.9 eV for PbO and 530.7 eV for O-C, respectively. The results from O 1*s* core level shows that the majority components from the calcined product is $PbCO_3$. The reason for this is that XPS is sensitive to the surface of the sample. $PbCO_3$ is formed from the reaction between PbO from the surface with the atmospheric CO_2.[152]

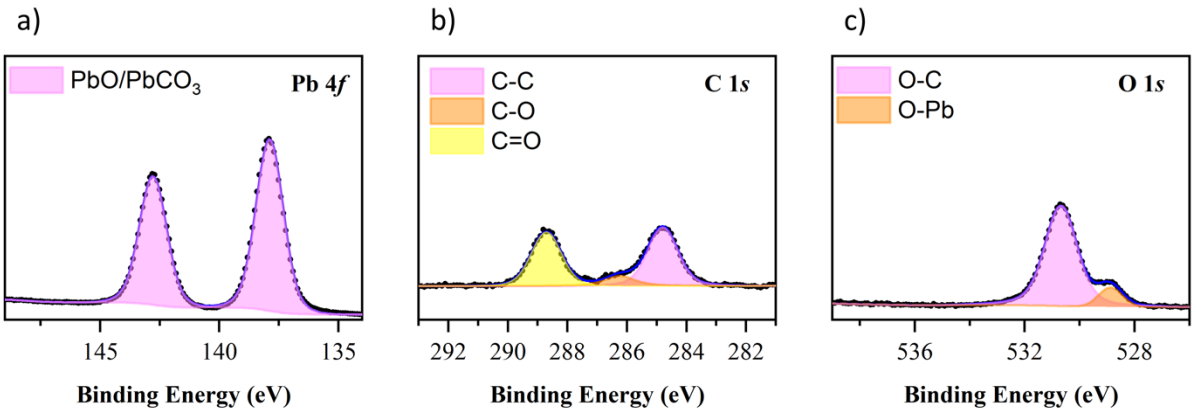

Figure 8.8 XPS core levels a) Pb 4*f*, b) C 1*s* and c) O 1*s* of calcined product.

8.4 Conclusions

A dissolution followed by precipitation method using NADES was proposed to recycle industrial lead paste. The study in previous chapters have shown the possibility of using MABA5 and LABet5 to recycle pure desulfurized lead paste. In this chapter, industrial desulfurized lead paste provided by Envirowales Ltd was successfully dissolved using MABA5 and the leached out as lead oxalate using the precipitation agent oxalic acid dihydrate. The precipitate was identified without the presence of plastics and SiO_2 fibres. The precipitate can be then calcined to PbO. A mixture of α-PbO and β-PbO have been obtained after the precipitate is calcined at 550 ^{o}C for 2 hours. Strict temperature control is required to obtain pure α-PbO or β-PbO.

Chapter 9 Conclusions

A precipitation followed by calcination method using NADESs was used to recycle desulfurized lead paste components. Lead compounds were initially dissolved in NADESs and then leached out as precipitates after reaction with the constituent carboxylic acid of NADESs. Two different NADESs were used to recycle lead compounds. One is malic acid/β-alanine/water (MABA) based NADES and the other one is lactic acid/betaine/water (LABet) based NADES. The precipitate obtained from MABA is confirmed to be lead malate dihydrate, which has only been limited studied. The precipitates obtained from LABet is confirmed to be a mixture of lead dilactate, D- and L- lead lactate. The crystal structure of D- and L- lead lactate and lead dilactate have not been reported so far. The work in this thesis have depicted the crystal structure of D- and L- lead lactate. Due to the poor crystal structure of lead dilactate, the crystal structure cannot be fully depicted.

Both precipitates, lead malate dihydrate and a mixture of lead lactate, have been calcined within the range between 100 ^{o}C and 550 ^{o}C to analyse the decomposition steps of the precipitate. Both precipitates have been identified to follow the similar decomposition pattern. The precipitates have been initially decomposed to a mixture of β-PbO, α-PbO and $2PbO{\cdot}PbCO_3$. Then $2PbO{\cdot}PbCO_3$ is further decomposed to $PbO{\cdot}PbCO_3$. Finally, $PbO{\cdot}PbCO_3$ and α-PbO are converted to β-PbO. Pure β-PbO were obtained after calcination at 550 ^{o}C for both precipitates. These results have shown the success of using NADESs to recycle lead compounds using the precipitation followed by calcination method. However, the drawback of using the constituent carboxylic acid of NADESs as leaching agent is that NADESs cannot be reused. To improve this method, the concept of using a precipitation agent has been proposed. Before the concept is put in practise, the dissolution behaviour and maximum lead concentration of lead compounds in NADESs have been analysed.

The 4-day concentration versus loading studies analysed the maximum lead concentration in solution. The dissolution studies of lead compounds in MABA5 have shown that MABA5 can achieve a maximum lead concentration of 104.0 g/L Pb for $2PbCO_3{\cdot}Pb(OH)_2$, 194.3 g/L Pb for $PbCO_3$, 224.0 g/L Pb for PbO and 170.0 g/L Pb for PbO_2 at 50 ^{o}C. The studies in LABet have

shown that the maximum lead concentration can achieve 675 g/L Pb for PbO (800 g/L loading, RT, 4 days) and 599 g/L Pb for PbO_2 (900 g/L loading, 50 ^oC, 4 days). During the concentration versus stirring time study, it was found that the concentration value might be higher between 6-96 hours due to over-saturation. The study in LABet has analysed the effect of water content on the maximum concentration and dissolution rate. It has shown that the viscosity of the solvent decreases with the increase of water content. As a result, the lead compounds dissolve quicker in LABet with higher water content. The maximum lead concentration drops with the increase of water content. For both MABA5 and LABet NADESs, the solution is an oversaturated solution when the maximum lead concentration is achieved. The solution can withstand the lead in the solution due to slow precipitation. For MABA5, lead compounds can stay in the solution for at least 24 hours until precipitation is occurred. For LABet, precipitation decreases gradually within 24 hours. The slow precipitation offers the chance of adding a precipitation agent to the solution before precipitation between lead species and the constituent carboxylic acid occurs.

To put this in practise, industrial desulfurized lead paste provided by Envirowales Ltd. was recycled with the precipitation followed by calcination method using MABA5 with the addition of a precipitation agent. The main components of industrial desulfurized lead paste were identified to be $NaOH{\cdot}(PbCO_3)_2$, $PbCO_3$, PbO_2 and β-PbO. Non-cyrstalline plastics and SiO_2 fibres have also been identified. The removal of SiO_2 fibres might be a potential issue.

Lead paste was firstly dissolved in MABA5 with 3 different stirring conditions. Only 80 % lead compounds can be dissolved when reacted at RT for 5 hours. Almost all lead compounds can be dissolved in MABA5 when reacted at RT for 2 days, while 94 % of lead lead compounds can be dissolved when reacted at 50 ^oC for 5 hours. 3 cycles were analysed in total. The dissolution efficiency remains similarly for each cycle when reacted at room temperature. The solubility decreases 1 g/L for each cyle when reacted at 50 ^oC. Considering energy saving, 50 ^oC for 5 hours may be ideal for industrial condition but at a cost of a slight decrease in dissolution efficiency of each cycle.

A precipitation agent oxalic acid dihydrate was added after each cycle. The precipitate was confirmed to be lead oxalate. From the SEM image of the precipitate, SiO_2 has not been

identified. This means that the SiO_2 has been removed along with the undissolved lead paste before precipitation agent is added. Pure lead oxalate precipitate is achieved. Then lead oxalate is calcined at 550 ^oC for 2 hours. A mixture of β-PbO and α-PbO is obtained. To obtain either pure β-PbO or α-PbO, a stricter temperature control is required.

The work in this thesis mainly focuses on the desulfurized lead paste or the components of desulfurized lead paste. It might be ideal if a NADES can dissolve the main component $PbSO_4$ as this can reduce the energy and cost during desulfurization step. Future work can be focused on the solvent exploration on the dissolution of $PbSO_4$ or sulfurized lead paste.

Additionally, the real source of the NADESs components comes from petrochemicals. Recycling of NADESs after each cycle is essential to reduce the environmental impact and the cost for the whole process. In this thesis, the energy required for the whole process including heating of NADESs, stirring with lead compounds and calcination of precipitates was not calculated. This can be done in future work to compare the energy consumption with current recycling process (pyrometallurgy and hydrometallurgy).

Appendix A.

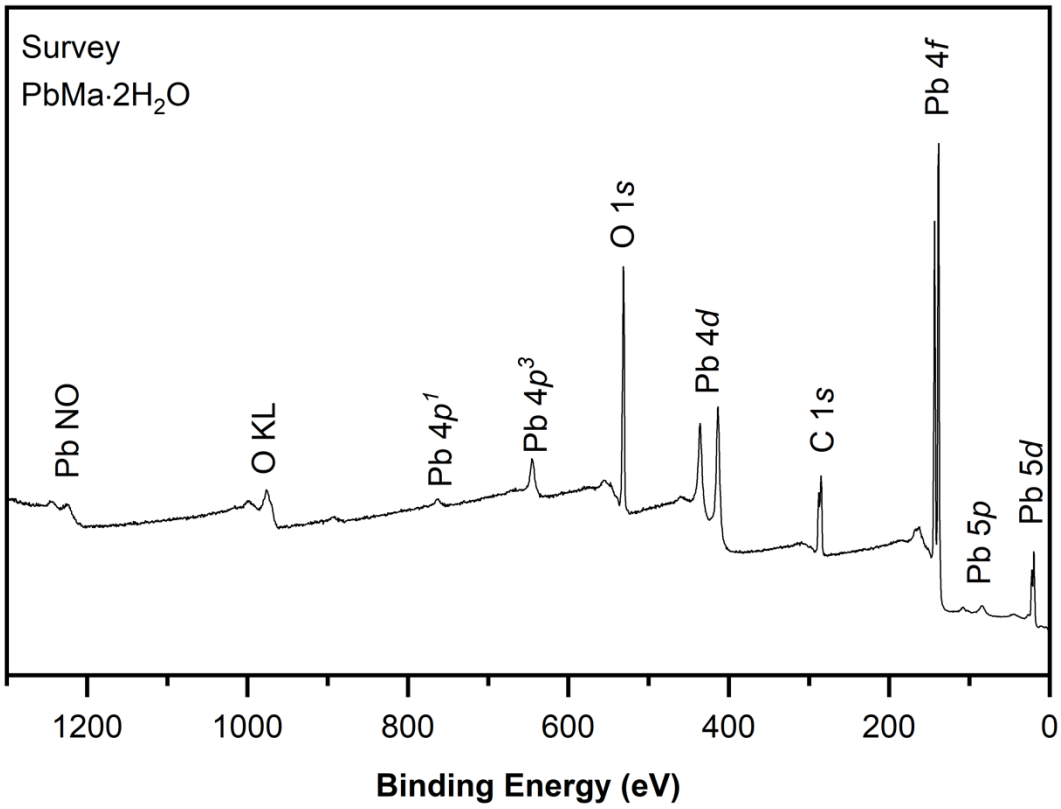

Figure A. 1 XPS survey of lead malate dihydrate precipitate.

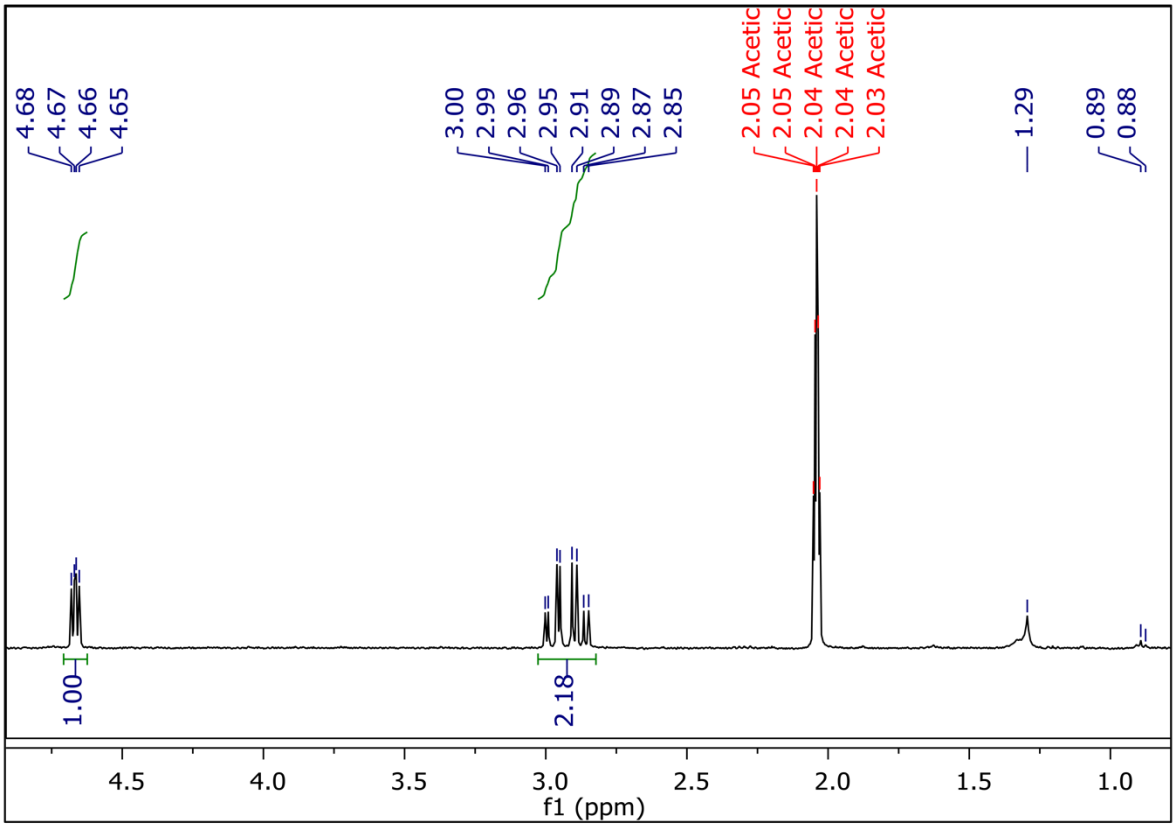

Figure A. 2 ^{1}H NMR (CD_3COOD) of lead malate dihydrate calcined at 116 ^{o}C for 2 hours.

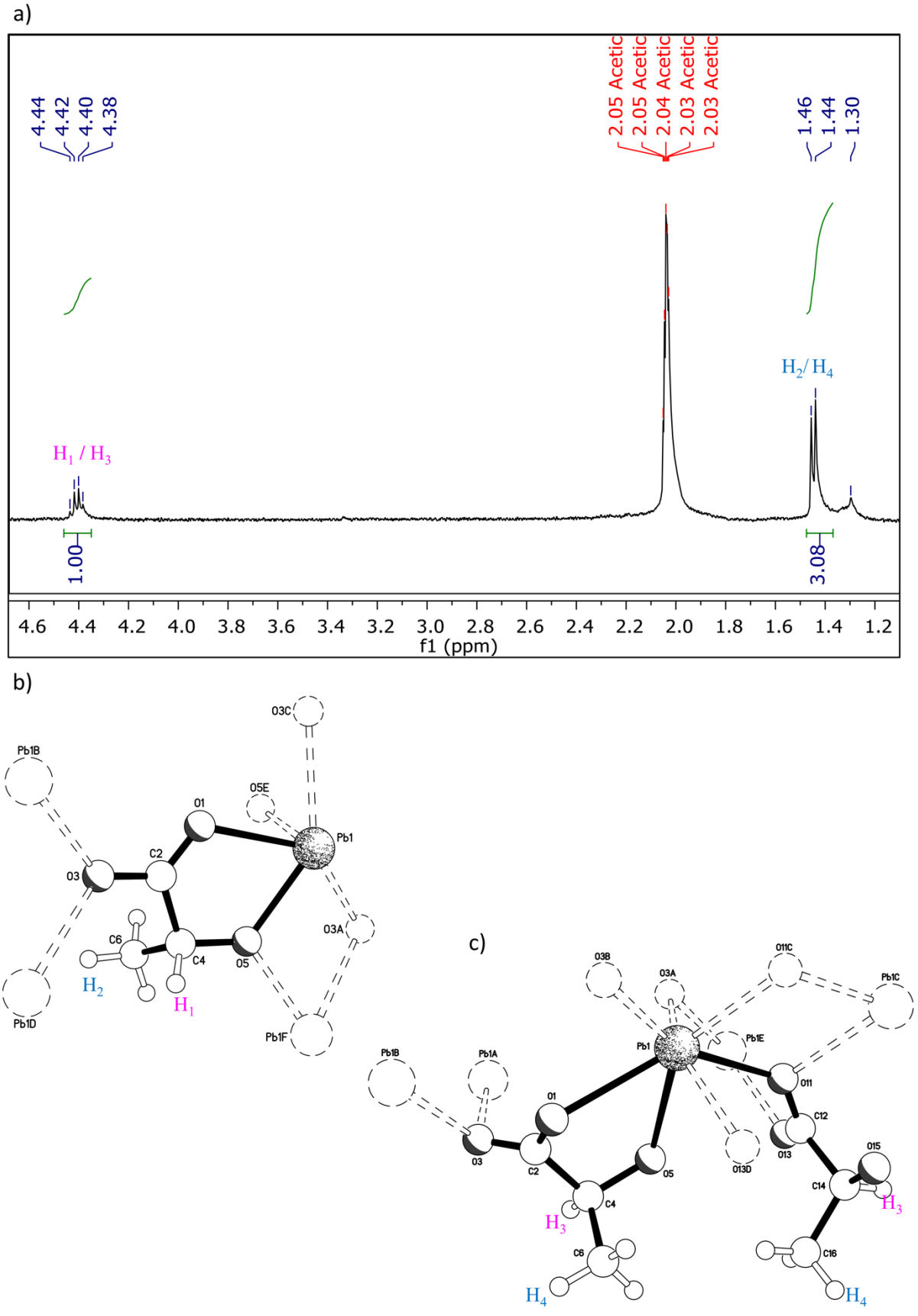

Figure A. 3 a) ^{1}H NMR (CD_3COOD) spectrum of lead lactate $Pb(LA)_x$ and the corresponding protons of ^{1}H NMR peaks of b) PbLA and c) $Pb(LA)_2$.

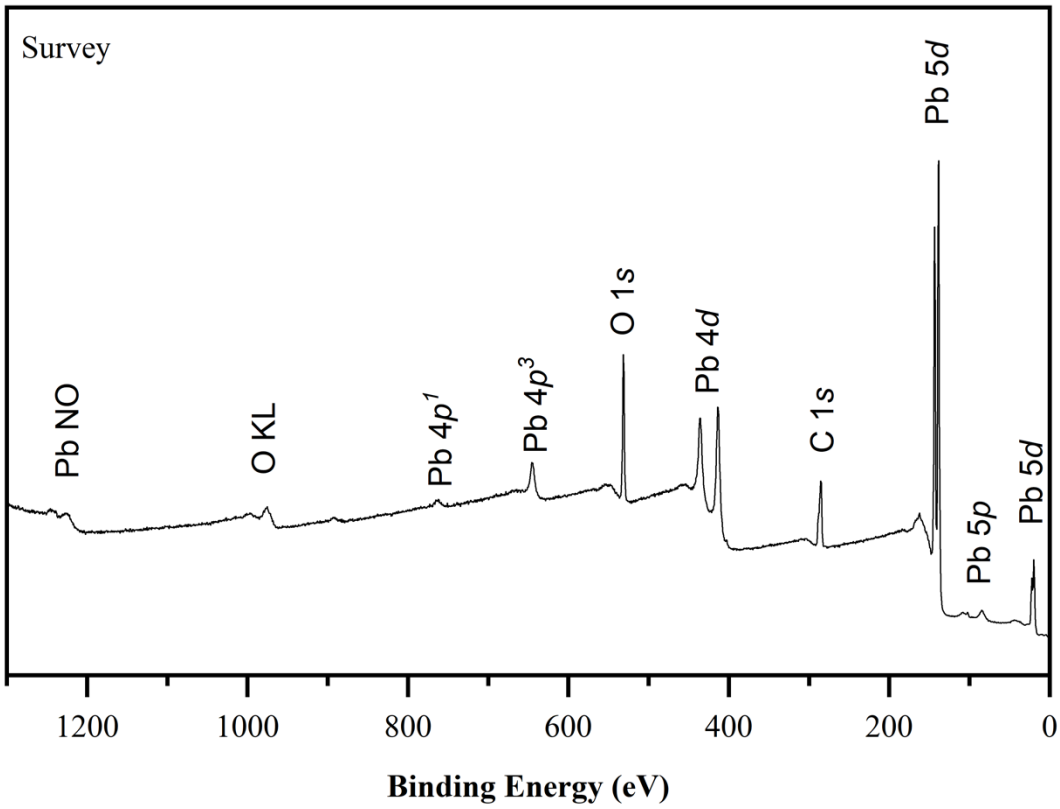

Figure A. 4 XPS survey of precipitated lead lactate.

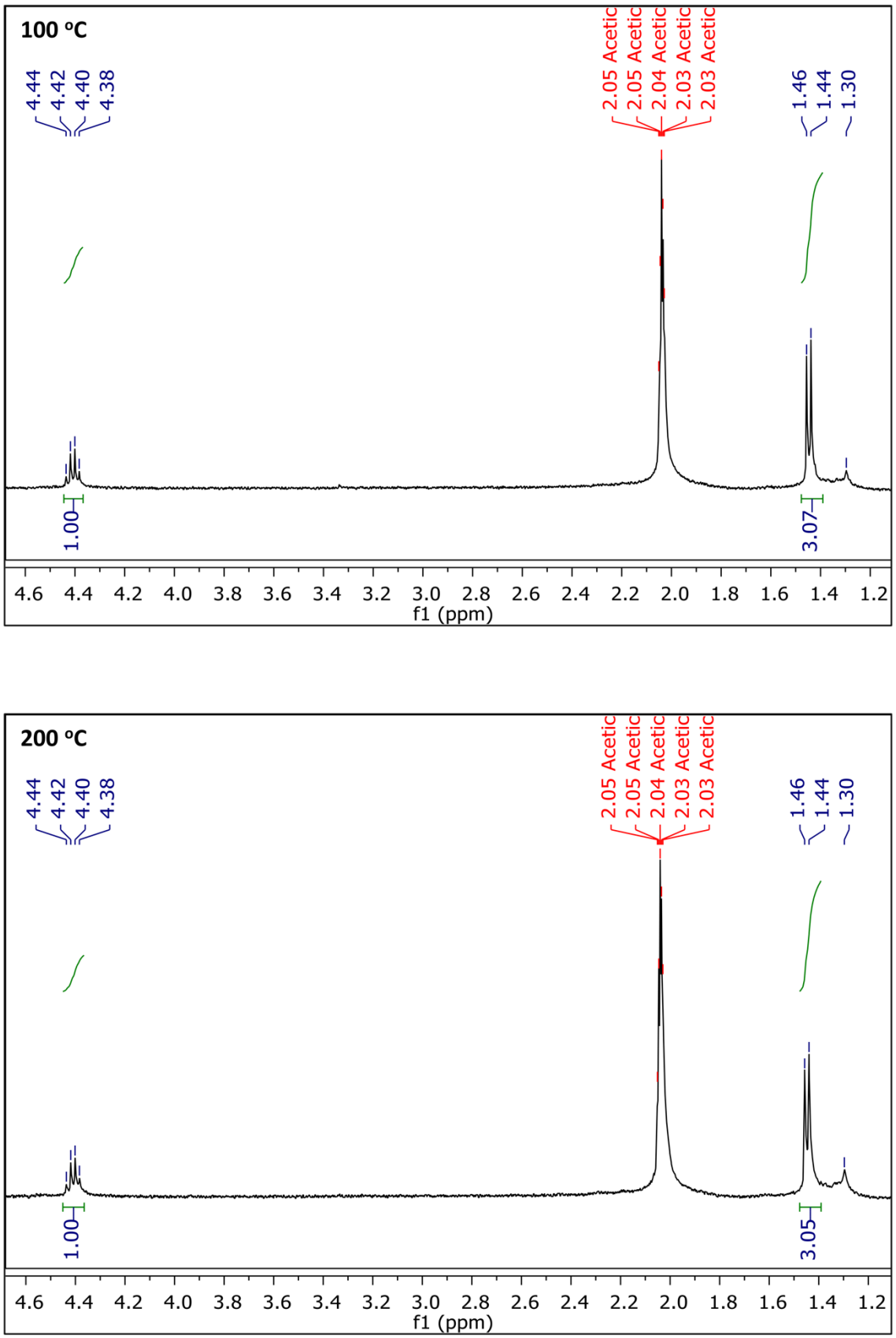

Figure A. 5 ^{1}H NMR (CD_3COOD) of lead lactate calcined products at 100 °C and 200 °C for 2 hours.

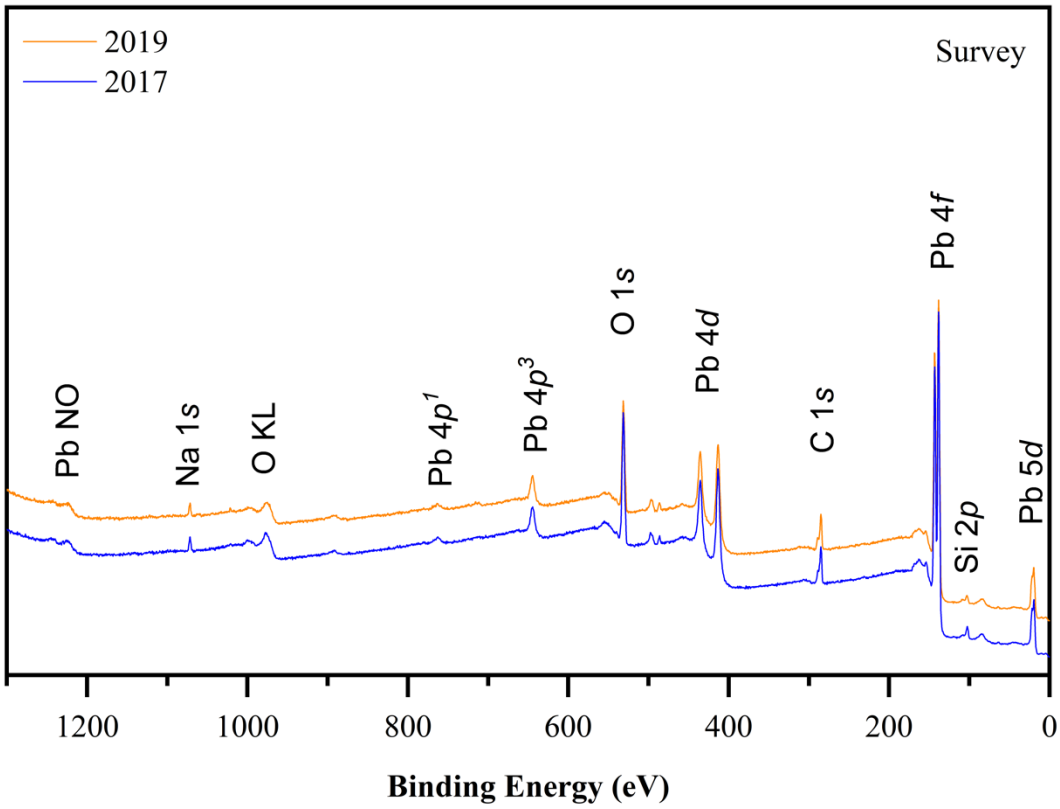

Figure A. 6 XPS survey of lead paste from Year 2017 and 2019.

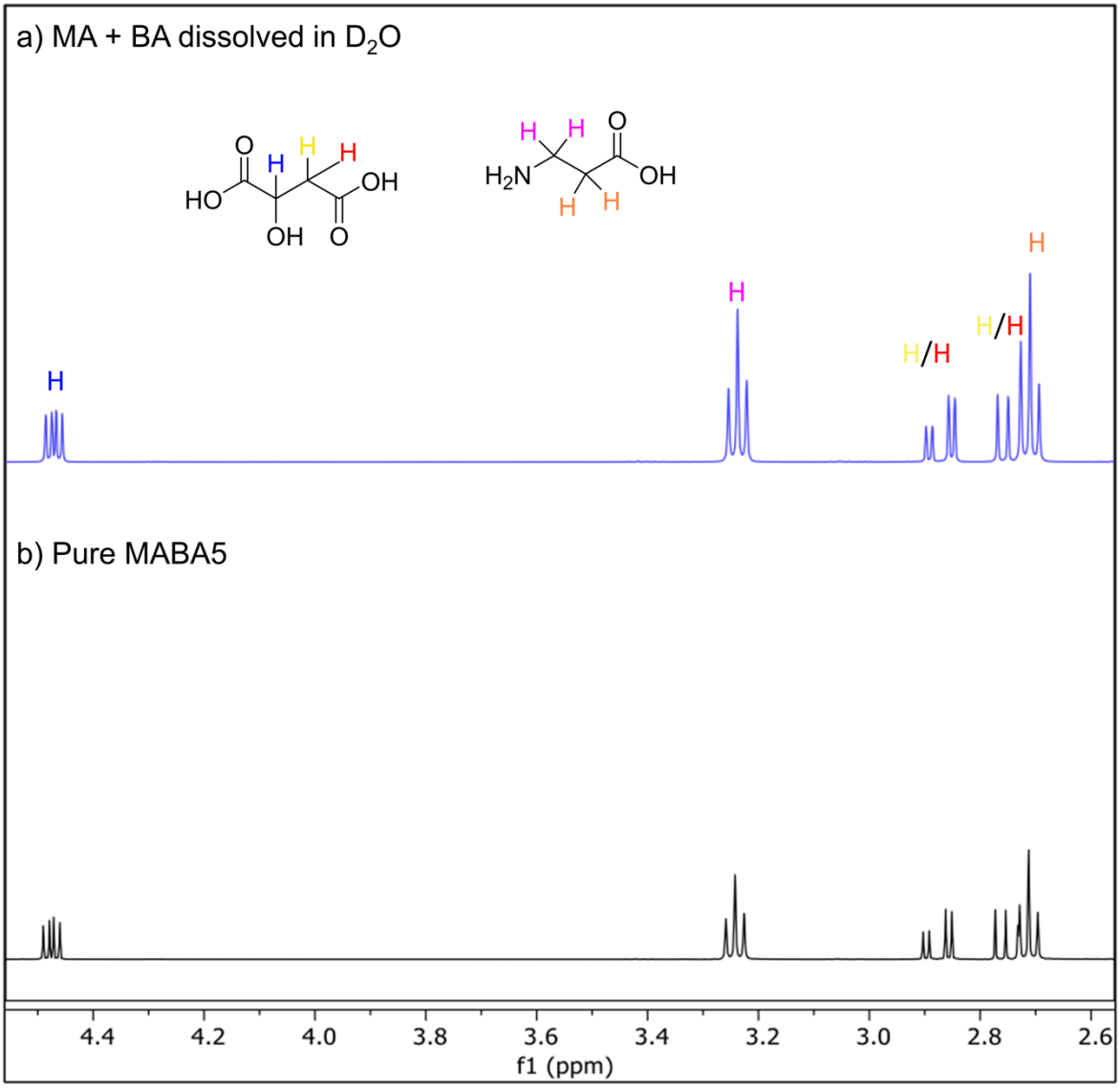

Figure A. 7 ^{1}H NMR (D_2O) of a) MA and BA dissolved in D_2O in a molar ratio of 1 : 1 and b) pure NADES.

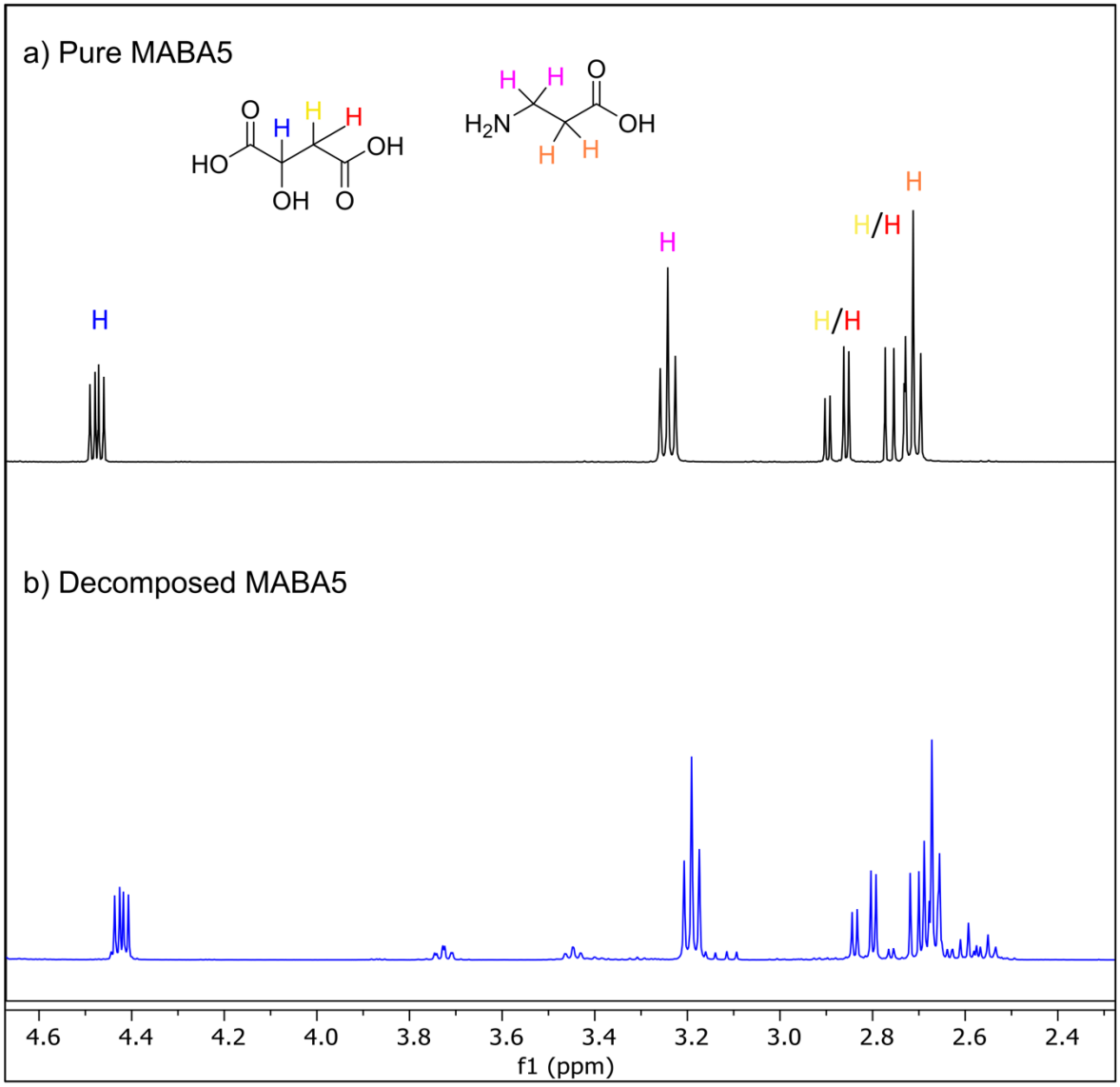

Figure A. 8 ^{1}H NMR (D_2O) comparison of pure MABA5 and decomposed MABA5.

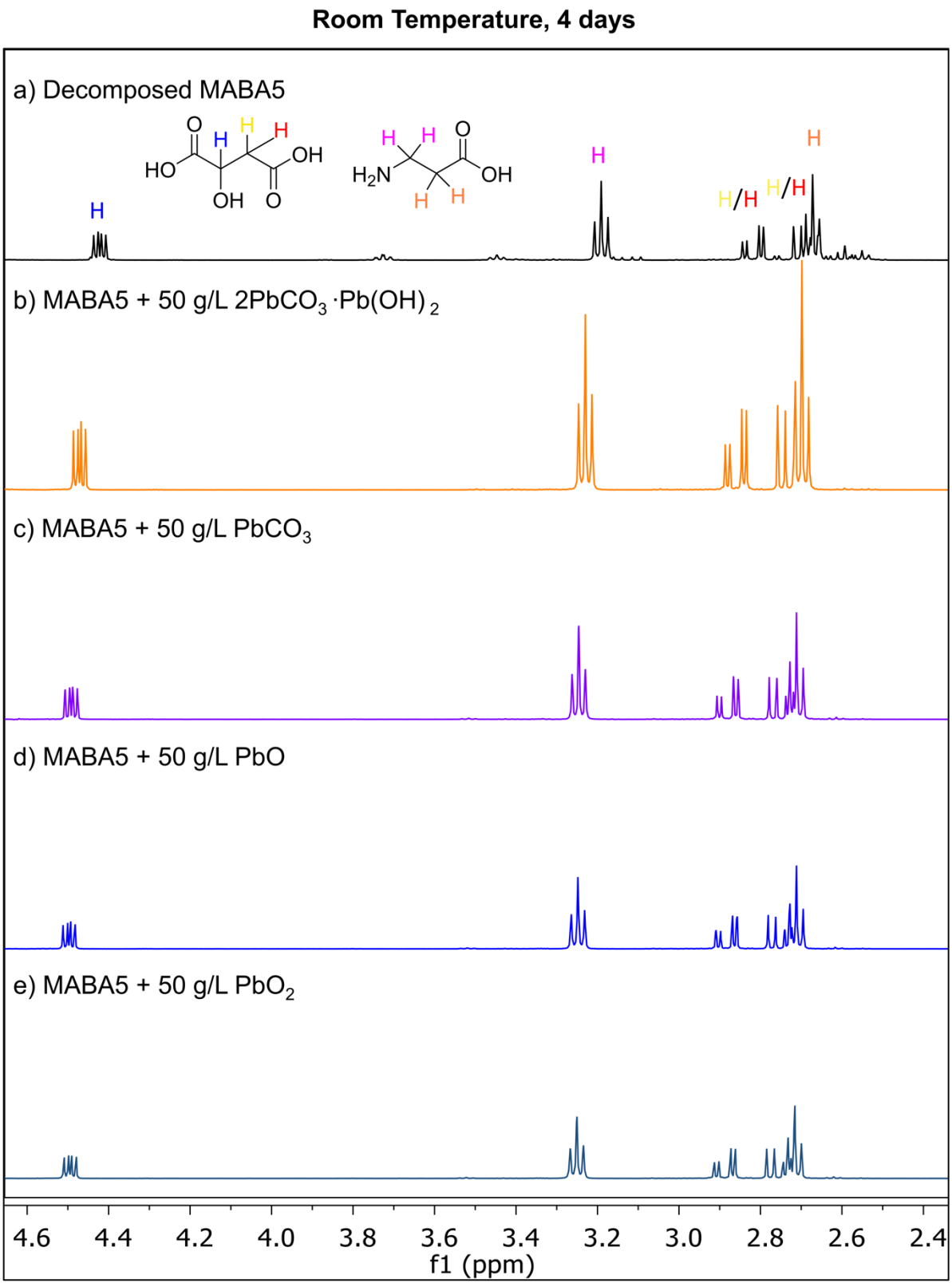

Figure A. 9 ^{1}H NMR (D_2O) of a) decomposed MABA5, b) MABA5 + 50 g/L $2PbCO_3 \cdot Pb(OH)_2$, c) MABA5 + 50 g/L $PbCO_3$, d) MABA5 + 50 g/L PbO and e) MABA5 + 50 g/L PbO_2 reacting at room temperature for 4 days.

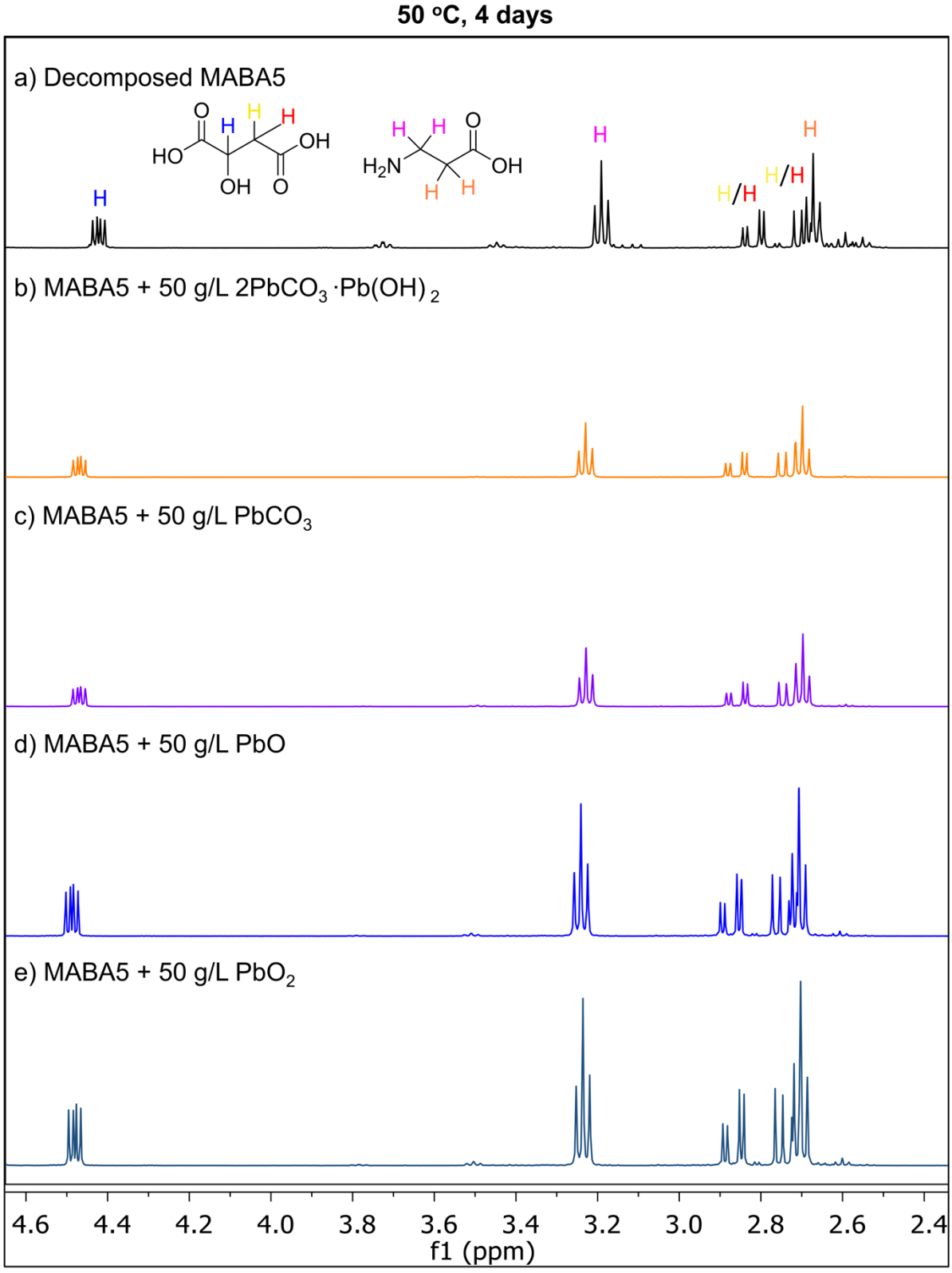

Figure A. 10 ^{1}H NMR (D_2O) of a) decomposed MABA5, b) MABA5 + 50 g/L $2PbCO_3 \cdot Pb(OH)_2$, c) MABA5 + 50 g/L $PbCO_3$, d) MABA5 + 50 g/L PbO and e) MABA5 + 50 g/L PbO_2 reacting at 50 °C for 4 days.

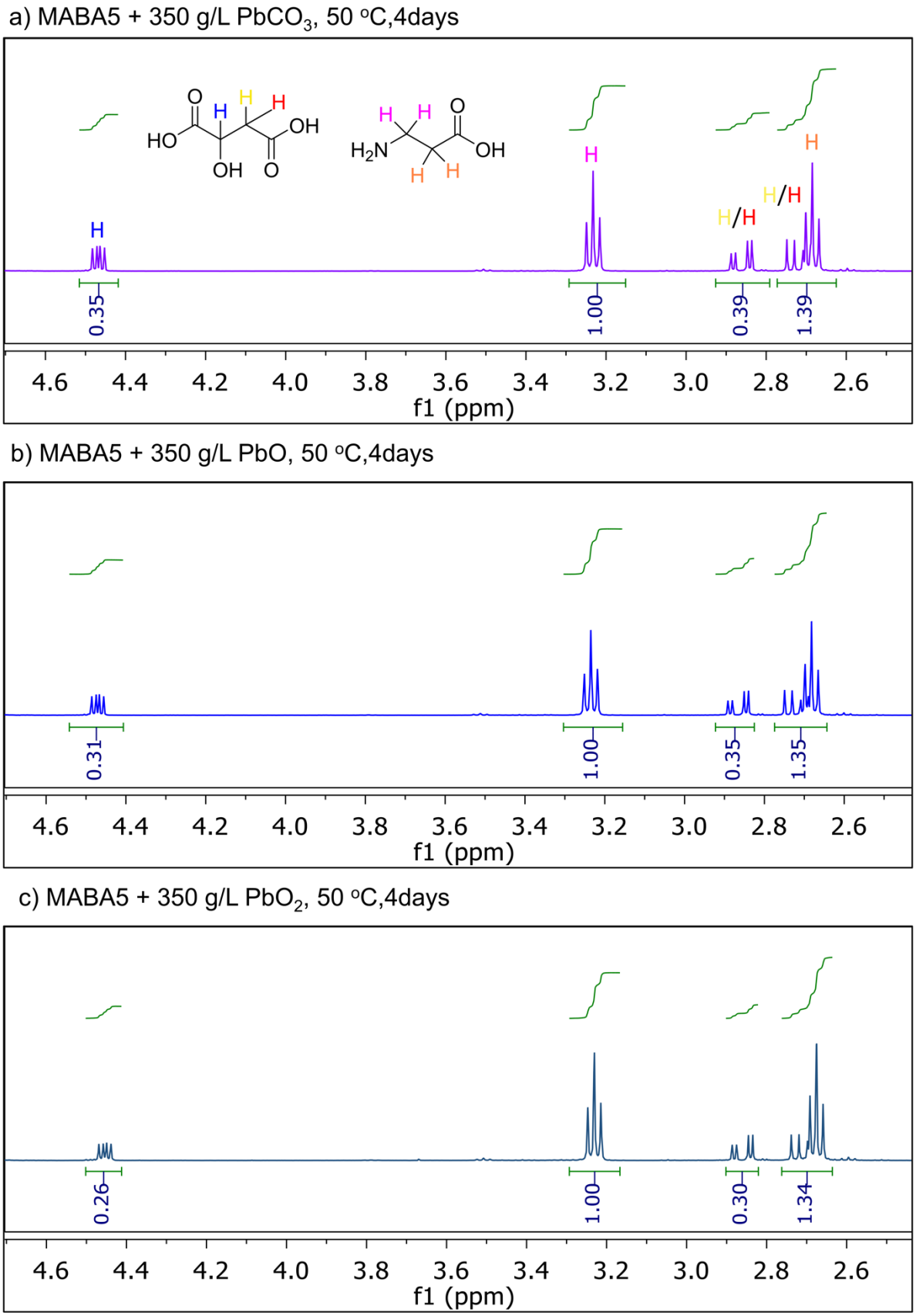

Figure A. 11 ^{1}H NMR (D_2O) of a) MABA5 350 g/L $PbCO_3$, b) MABA5 + 350 g/L PbO and c) MABA5 + 350 g/L PbO_2 reacting at 50 °C for 4 days.

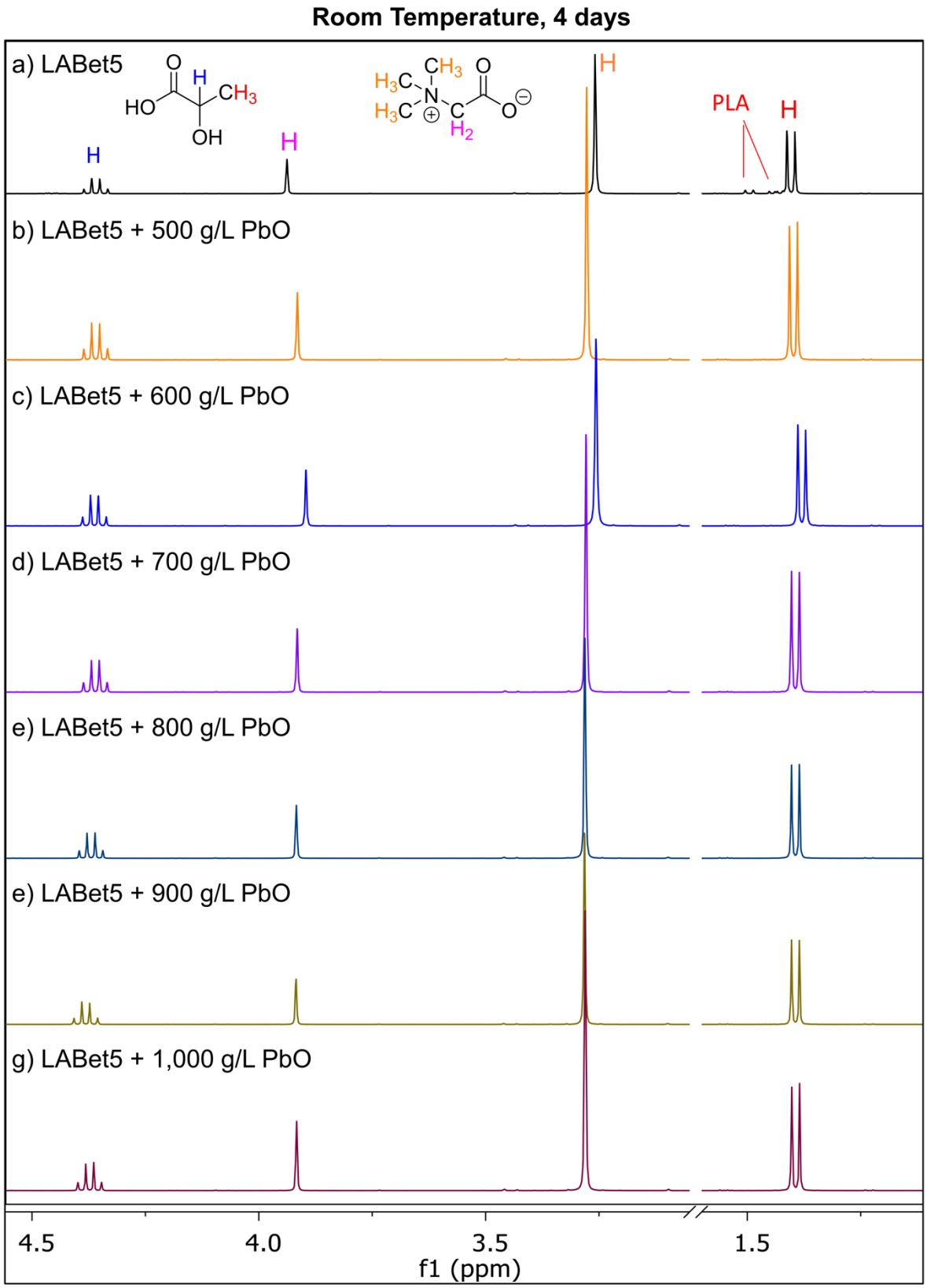

Figure A. 12 ^{1}H NMR (D_2O) of a) LABet5, b) – g) LABet5 + 600-1000 g/L PbO at an interval of 100 g/L reacting at RT for 4 days.

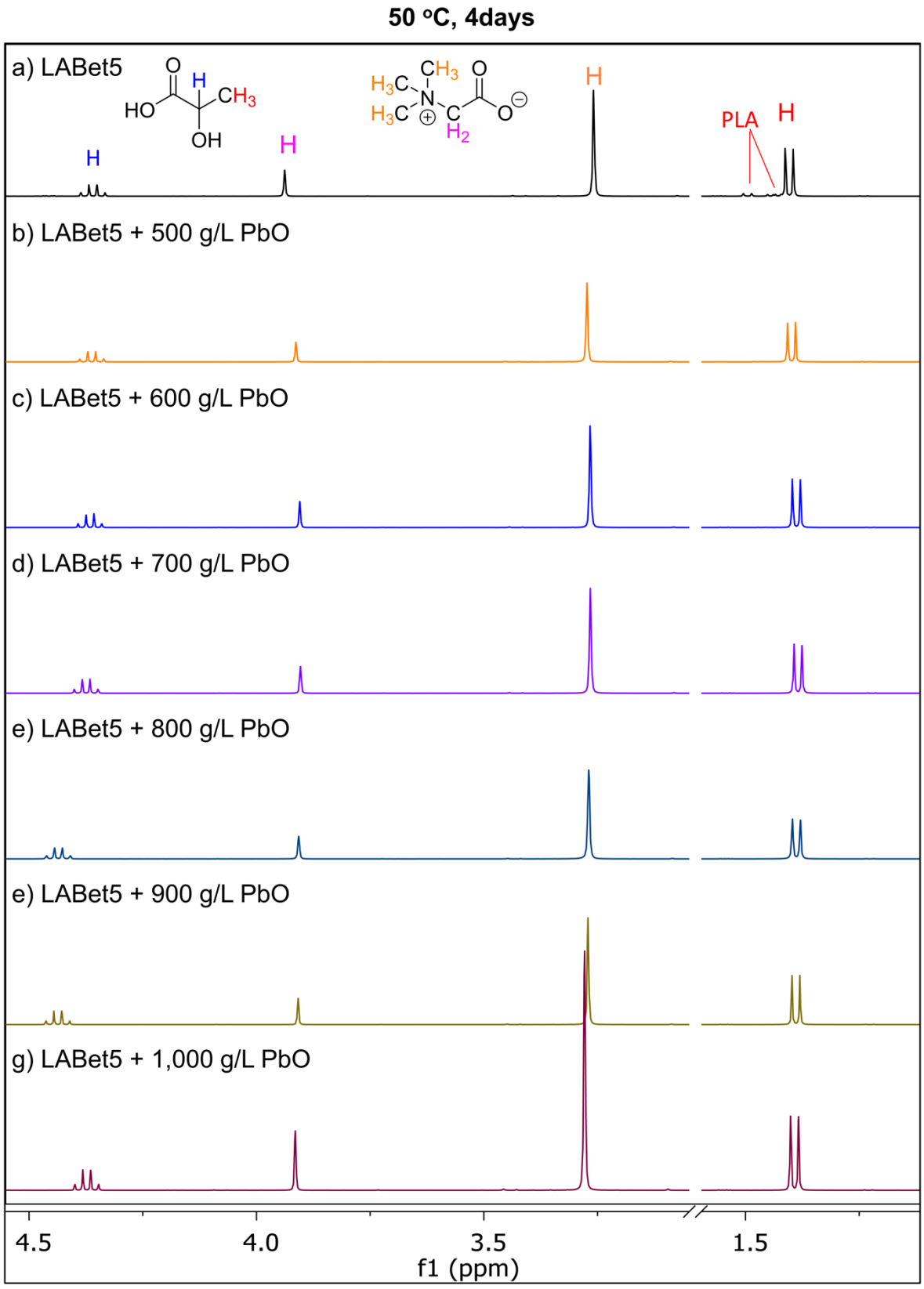

Figure A. 13 ^{1}H NMR (D_2O) of a) LABet5, b) – g) LABet5 + 600-1000 g/L PbO at an interval of 100 g/L reacting at 50 °C for 4 days.

a) LABet5

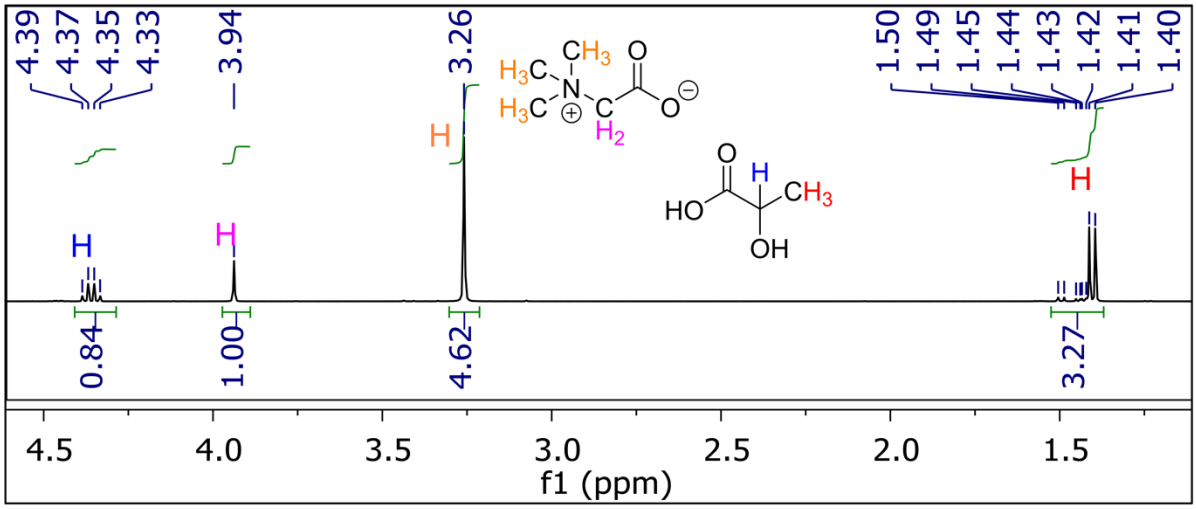

b) LABet5 + 200 g/L PbO_2, RT, 4days

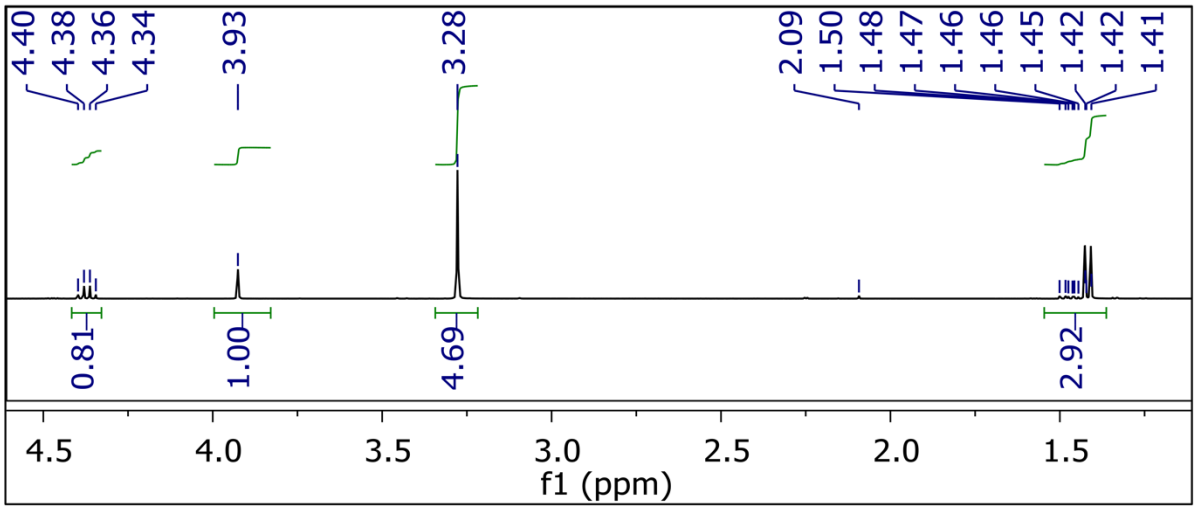

c) LABet5 + 500 g/L PbO_2, RT, 4days

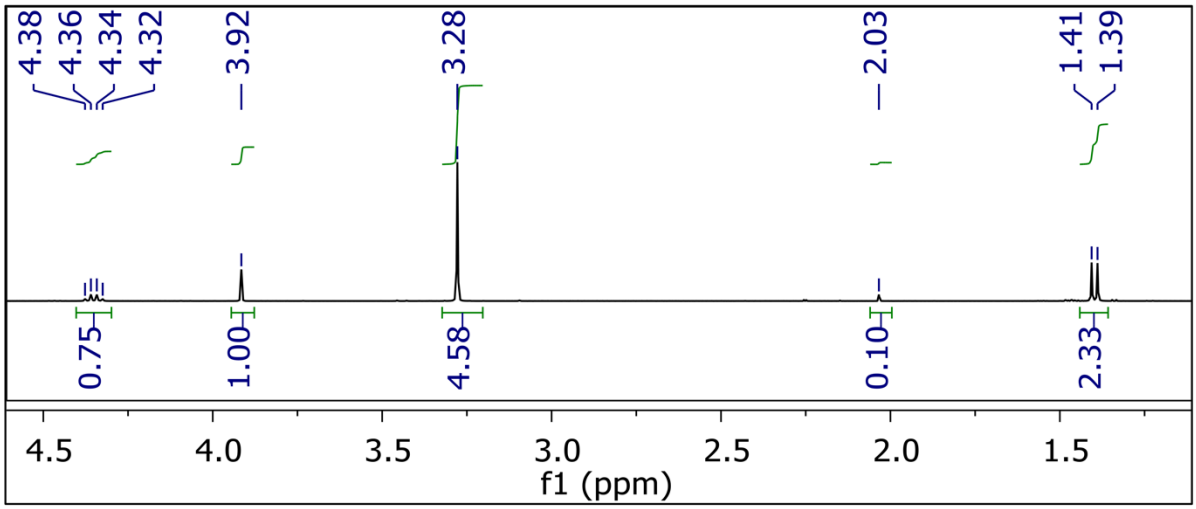

Graph continued on next page

d) LABet5 + 600 g/L PbO_2, RT, 4days

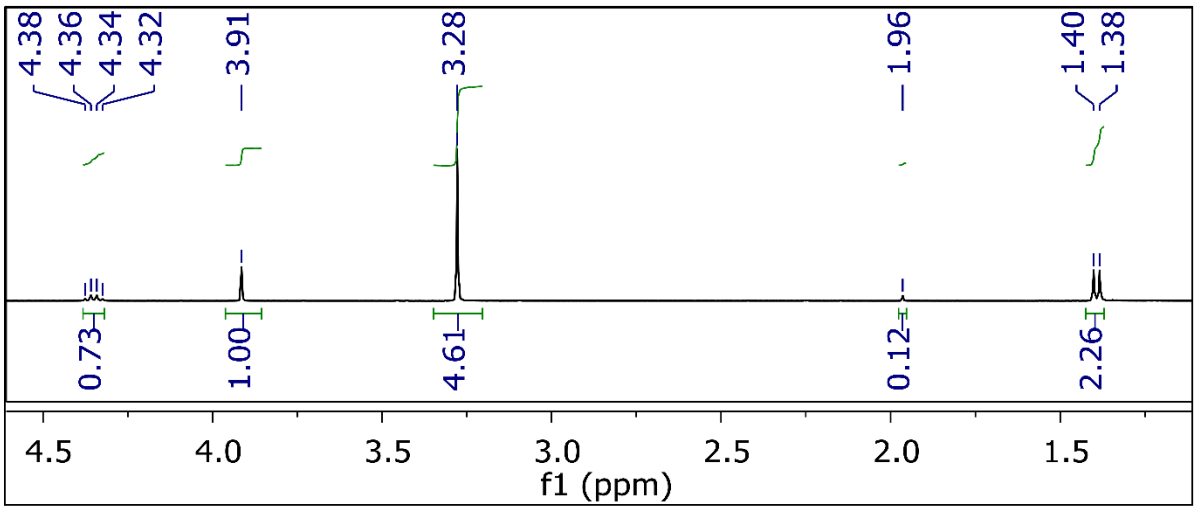

e) LABet5 + 700 g/L PbO_2, RT, 4days

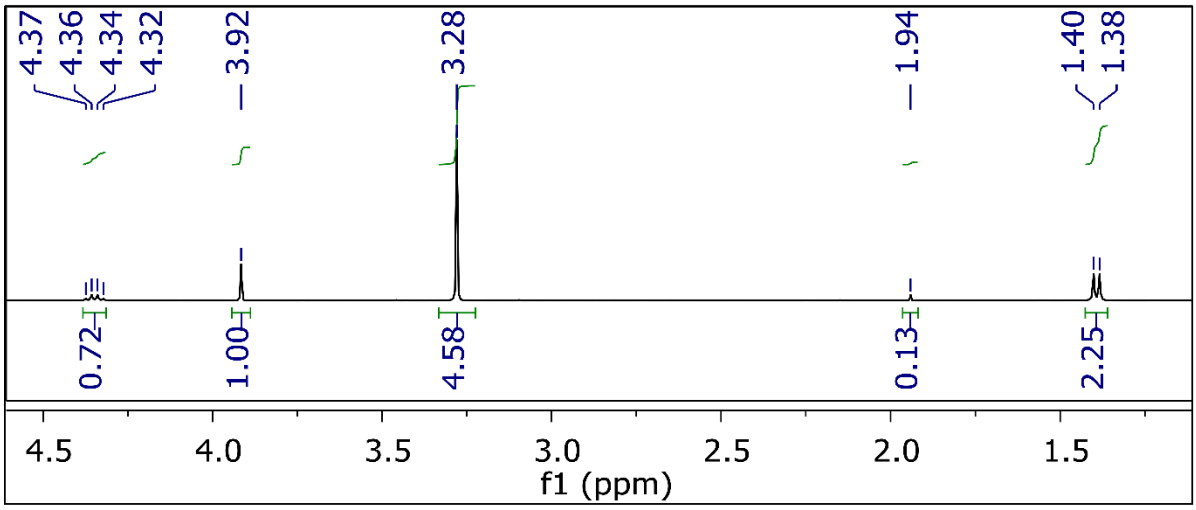

f) LABet5 + 800 g/L PbO_2, RT, 4days

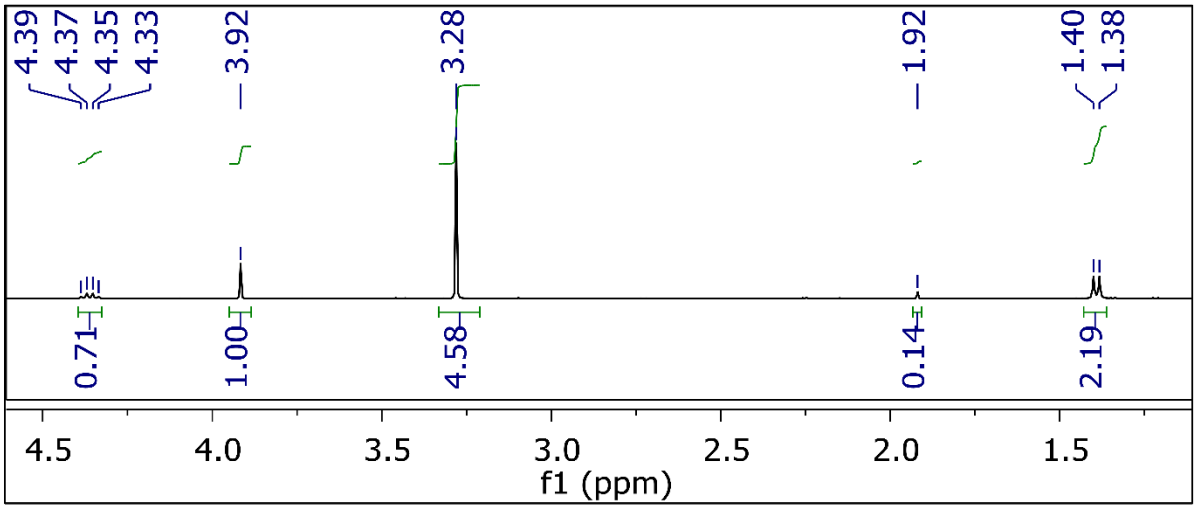

Graph continued on next page

g) LABet5 + 900 g/L PbO_2, RT, 4days

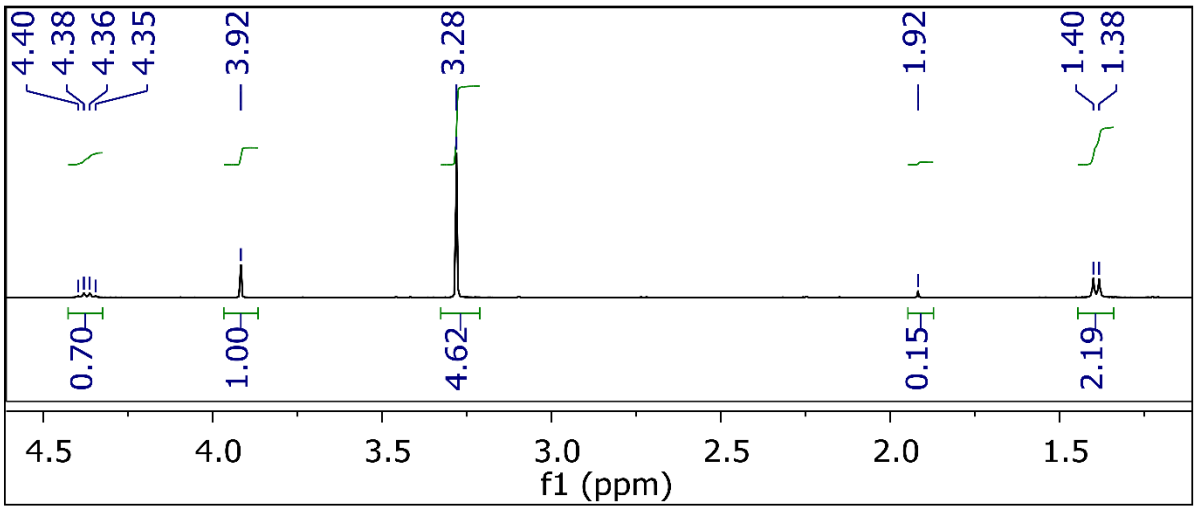

h) LABet5 + 1,000 g/L PbO_2, RT, 4days

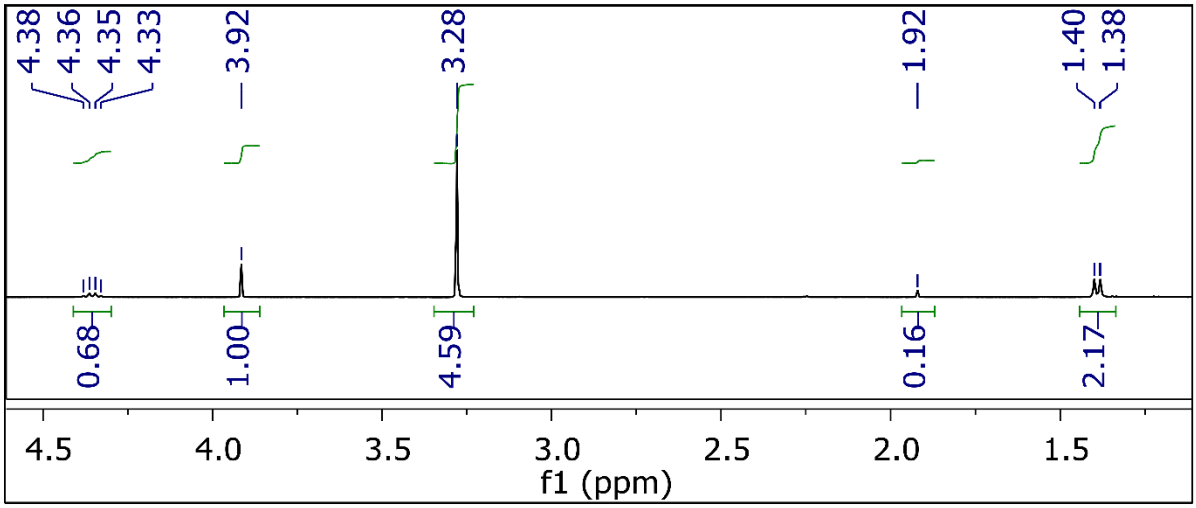

Figure A. 14 ^{1}H NMR (D_2O) of a) LABet5, b) LABet5 + 200 g/L PbO_2, c) – h) LABet5 + 500-1000 g/L PbO_2 at an interval of 100 g/L reacting at RT for 4 days.

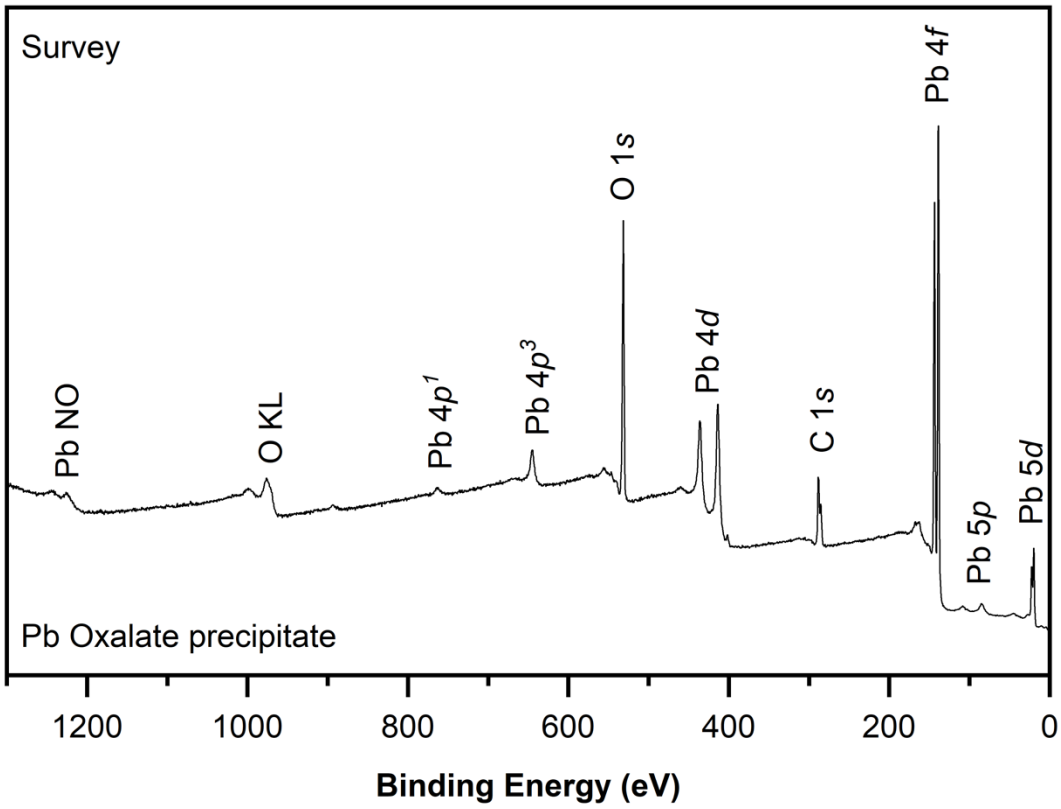

Figure A. 15 XPS survey of lead oxalate precipitates.

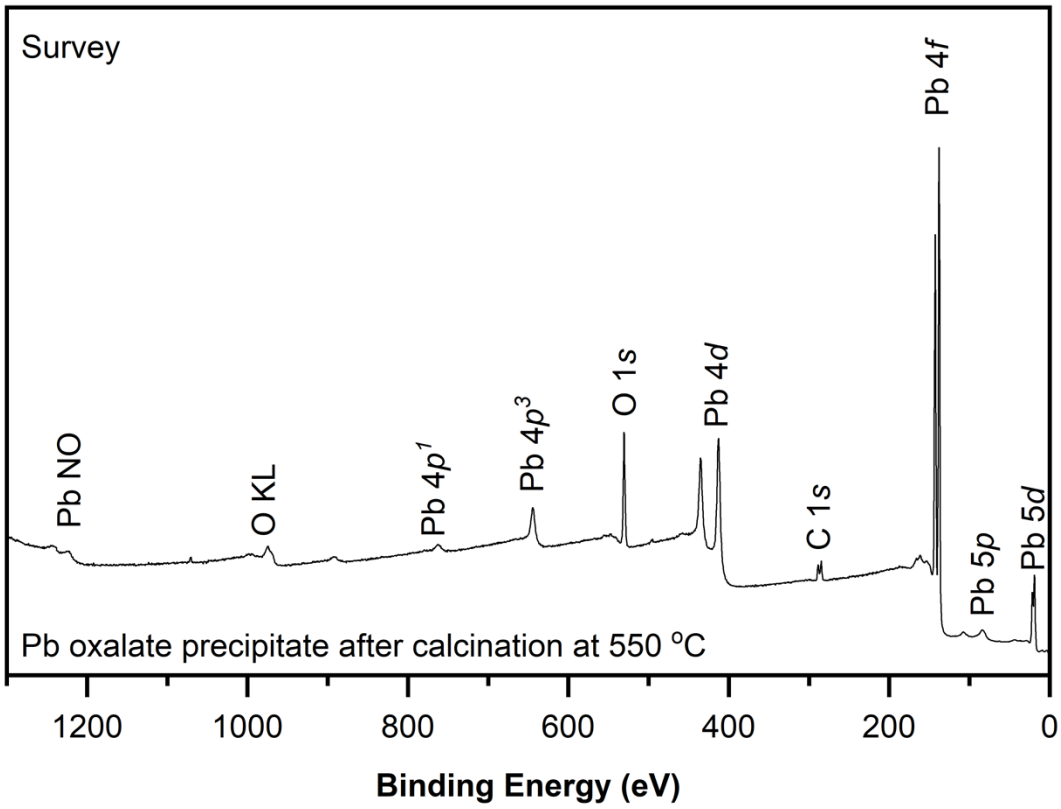

Figure A. 16 XPS survey of lead oxalate precipitate after calcination at 550 °C.

References

1. What Is An SLI Battery? https://batteryspecialists.com.au/blogs/news/what-is-an-sli-battery.
2. Lead Acid Battery Market Size, Share & Emerging Trends Analysis -2026. https://www.alliedmarketresearch.com/lead-acid-battery-market-A05962.
3. Ibrahim, H., Ilinca, A. & Perron, J. Energy storage systems-Characteristics and comparisons. *Renewable and Sustainable Energy Reviews* **12**, 1221–1250 (2008).
4. May, G. J., Davidson, A. & Monahov, B. Lead batteries for utility energy storage: A review. *J Energy Storage* **15**, 145–157 (2018).
5. Kala, S. & Mishra, A. Battery recycling opportunity and challenges in India. in *Materials Today: Proceedings* vol. 46 1543–1556 (Elsevier Ltd, 2021).
6. Brochin, R. *et al.* The Cellular Effect of Lead Poisoning and Its Clinical Picture. *The Georgetown Undergraduate Journal of Health Sciences* **5**, 1–8 (2008).
7. Wani, A. L., Ara, A. & Usmani, J. A. Lead toxicity: A review. *Interdiscip Toxicol* **8**, 55–64 (2015).
8. Needleman, H. Lead poisoning. *Annu Rev Med* **55**, 209–222 (2004).
9. Yamazaki, T., Sakurai, K. & Muramoto, K. I. Estimation of the residual capacity of sealed lead-acid batteries by neural network. in *INTELEC, International Telecommunications Energy Conference (Proceedings)* 210–214 (IEEE, 1998). doi:10.1109/intlec.1998.793500.
10. Posada, J. O. G. *et al.* Aqueous batteries as grid scale energy storage solutions. *Renewable and Sustainable Energy Reviews* **68**, 1174–1182 (2017).
11. Yang, J. *et al.* Review on the research of failure modes and mechanism for lead–acid batteries. *Int J Energy Res* **41**, 336–352 (2017).
12. Ruetschi, P. Aging mechanisms and service life of lead-acid batteries. *J Power Sources* **127**, 33–44 (2004).
13. Hao, H. *et al.* A Review of the Positive Electrode Additives in Lead-Acid Batteries. *Int J Electrochem Sci* **13**, 2329–2340 (2018).
14. Yang, J. *et al.* Review on the research of failure modes and mechanism for lead–acid batteries. *Int J Energy Res* **41**, 336–352 (2017).

15. Berndt, D. *Maintenance-free batteries: lead-acid, nickel/cadmium, nickel/hydride*. (Research Studies Press, 1993).
16. Pavlov, D. The Lead-Acid Battery Lead Dioxide Active Mass: A Gel-Crystal System with Proton and Electron Conductivity. *J Electrochem Soc* **139**, 3075–3080 (1992).
17. Fitas, R., Zerroual, L., Chelali, N. & Djellouli, B. Role of hydration water in the reduction process of PbO2 in lead / acid cells. *J Power Sources* **64**, 57–60 (1997).
18. Pavlov, D. Suppression of premature capacity loss by methods based on the gel-crystal concept of the PbO2 electrode. *J Power Sources* **46**, 171–190 (1993).
19. Pavlov, D., Rogachev, T., Nikolov, P. & Petkova, G. Mechanism of action of electrochemically active carbons on the processes that take place at the negative plates of lead-acid batteries. *J Power Sources* **191**, 58–75 (2009).
20. Pavlov, D. & Pashmakova, I. Influence of the size of PbSO4 crystals on their solubility and the significance of this process in the lead-acid battery. *J Appl Electrochem* **17**, 1075–1082 (1987).
21. Pavlov, D. & Nikolov, P. Lead–Carbon Electrode with Inhibitor of Sulfation for Lead-Acid Batteries Operating in the HRPSoC Duty. *J Electrochem Soc* **159**, A1215–A1225 (2012).
22. May, G. J., Davidson, A. & Monahov, B. Lead batteries for utility energy storage: A review. *J Energy Storage* **15**, 145–157 (2018).
23. Li, W. F., Jiang, L. H., Zhan, J. & Zhang, C. F. Technical Status and Progress of Lead Recycling of Battery. in *REWAS 2013: Enabling Materials Resource Sustainability* 279–285 (Springer, Cham, 2013). doi:10.1007/978-3-319-48763-2_29.
24. Ma, C., Shu, Y. & Chen, H. Preparation of high-purity lead oxide from spent lead paste by low temperature burning and hydrometallurgical processing with ammonium acetate solution. *RSC Adv* **6**, 21148–21155 (2016).
25. Chen, T. T. & Dutrizac, J. E. The mineralogical characterization of lead-acid battery paste. *Hydrometallurgy* **40**, 223–245 (1996).
26. Ellis, T. W. & Mirza, A. H. The refining of secondary lead for use in advanced lead-acid batteries. *J Power Sources* **195**, 4525–4529 (2010).
27. Sun, Z. *et al.* Spent lead-acid battery recycling in China – A review and sustainable analyses on mass flow of lead. *Waste Management* **64**, 190–201 (2017).
28. Zhang, W. *et al.* A critical review on secondary lead recycling technology and its prospect. *Renewable and Sustainable Energy Reviews* **61**, 108–122 (2016).

29. Lyakov, N. K., Atanasova, D. A., Vassilev, V. S. & Haralampiev, G. A. Desulphurization of damped battery paste by sodium carbonate and sodium hydroxide. *J Power Sources* **171**, 960–965 (2007).
30. Arai, K. & Toguri, J. M. Leaching of lead sulphate in sodium carbonate solution. *Hydrometallurgy* **12**, 49–59 (1984).
31. Gong, Y., Dutrizac, J. E. & Chen, T. T. The reaction of anglesite (PbSO4) crystals with sodium carbonate solutions. *Hydrometallurgy* **31**, 175–199 (1992).
32. U.S. Environmental Protection Agency. *Locating And Estimating Air Emissions From Sources Of Lead And Lead Compounds*. (1998).
33. Bleiwas, D. I. *Estimates of Electricity Requirements for the Recovery of Mineral Commodities, with Examples Applied to Sub-Saharan Africa*. (2011).
34. Trinkel, V. *et al.* Behavior of Chromium, Nickel, Lead, Zinc, Cadmium, and Mercury in the Blast Furnace - A Critical Review of Literature Data and Plant Investigations. *Ind Eng Chem Res* **54**, 11759–11771 (2015).
35. Pitt, C. H. & Wadsworth, M. E. *Assessment of energy requirements in proven and new copper processes. Final report*. http://www.osti.gov/servlets/purl/6878932-ffJrQ8/ (1980) doi:10.2172/6878932.
36. Vereecken, J. *EMC '91: Non-Ferrous Metallurgy—Present and Future*. (Springer, 1991).
37. Perez-Tello, M., Prieto-Sanchez, M. R., Rodriguez-Hoyos, O. & Sanchez-Corrales, V. M. A kinetic model for the oxidation of selenium and tellurium in an industrial Kaldo furnace. *JOM* **56**, 52–54 (2004).
38. Errington, W. J., Edwards, J. S. & Hawkins, P. Isamelt technology - current status and future development. *J South Afr Inst Min Metall* **97**, 161–167 (1997).
39. Nicol, S., Corrie, D., Barter, B., Nikolic, S. & Hogg, B. Adaptability of the ISASMELT^{TM} Technology for the Sustainable Treatment of Wastes. in *REWAS 2022: Developing Tomorrow's Technical Cycles (Volume I). The Minerals, Metals & Materials Series.* (eds. Lazou, A. et al.) 59–69 (Cham: Springer International Publishing, 2022). doi:10.1007/978-3-030-92563-5_8.
40. Hogg, B., Nikolic, S., Voigt, P. & Telford, P. ISASMELT^{TM} Technology for Sulfide Smelting. in *Extraction 2018. The Minerals, Metals & Materials Series.* (eds. Davis, B. R. et al.) 149–158 (Springer, Cham, 2018). doi:10.1007/978-3-319-95022-8_11.

41. Ahrned, F. The battery recycling loop: a European perspective. *J Power Sources* **59**, 107–108 (1996).
42. Fischer, P. & Maczek, H. The Present Status of Development of the QSL-Lead Process. *JOM 1982 34:6* **34**, 60–64 (2013).
43. Queneau, P. E. & Siegmund, A. Industrial-scale lead making with the QSL continuous oxygen converter. *JOM 1996 48:4* **48**, 38–44 (1996).
44. Queneau, P. E. The QSL reactor for lead and its prospects for Ni, Cu and Fe. *JOM* **41**, 30–35 (1989).
45. Siegmund, A. Primary lead production–a survey of existing smelters. *Lead-Zinc* 53–116 (2000).
46. The KIVCET Smelting Process. *Total Materia* https://www.totalmateria.com/page.aspx?ID=CheckArticle&site=ktn&NM=366.
47. Siegmund, A. Modern applied technologies for primary lead smelting at the beginning of the 21st century. *Proc. Yazawa International Symposium "Metallurgical and Materials Processing: Principles and Technologies", High-Temperature Metal Production* **2**, 43–62 (2003).
48. Sohn, H. Y. & Olivas-Martinez, M. Lead and Zinc Production. in *Treatise on Process Metallurgy* vol. 3 671–700 (Elsevier, 2014).
49. Blanpain, B., Arnout, S., Chintinne, M. & Swinbourne, D. R. Lead Recycling. in *Handbook of Recycling* 95–111 (Elsevier, 2014). doi:10.1016/B978-0-12-396459-5.00008-8.
50. Miguel, P., Robert, S. & Jerry D., S. Process for refining lead bullion. (2013).
51. lead processing - Refining | Britannica. https://www.britannica.com/technology/lead-processing/Refining.
52. Chuang, H. Y. *et al.* A follow-up comparison of blood lead levels between foreign and native workers of battery manufacturing in Taiwan. *Science of The Total Environment* **394**, 52–56 (2008).
53. Haefliger, P. *et al.* Mass lead intoxication from informal used lead-acid battery recycling in Dakar, Senegal. *Environ Health Perspect* **117**, 1535–1540 (2009).
54. Varshney, K., Varshney, P. K., Gautam, K., Tanwar, M. & Chaudhary, M. Current trends and future perspectives in the recycling of spent lead acid batteries in India. in *Materials Today: Proceedings* vol. 26 592–602 (Elsevier Ltd, 2019).
55. Prengaman, D. R. Recovering lead from batteries. *JOM* **47**, 31–33 (1995).

56. Prengaman, D. Raymond. & McDonald, H. B. Method of recovering lead values from battery sludge. U.S. Patent 4,229,271. (1980).
57. Ernest R., C. Jr., Agnes Y., L. & Danton L., P. Electrowinning of lead from H2SiF6 solution. U.S Patent 4,272,340. (1981).
58. Cole, E. R., Lee, A. Y. & Paulson, D. L. Update on Recovering Lead From Scrap Batteries. *JOM* **37**, 79–83 (1985).
59. Cole, E. R., Lee, A. Y. & Paulson, D. L. Recovery of Lead from Battery Sludge by Electrowinning. *JOM* **35**, 42–46 (1983).
60. Krauss, C. J. Cathode deposit control in lead electrorefining. *JOM* **28**, 4–9 (1976).
61. Olper, M. & Fracchia, P. Hydrometallurgical process for an overall recovery of the components of exhausted lead-acid batteries. U.S Patent 4,769,116. (1988).
62. Olper, M. & Pierluigi, M. Hydrometallurgical process for recovering in pure metal form all the lead contained in the active mass of exhausted batteries. U.S Patent 4,927,510. (1990).
63. Ferracin, L. C. *et al.* Lead recovery from a typical Brazilian sludge of exhausted lead-acid batteries using an electrohydrometallurgical process. *Hydrometallurgy* **65**, 137–144 (2002).
64. Ginatta, M. V. Method for the electrolytic production of lead. U.S Patent 4,451,340. (1984).
65. Koenig, A. E., MacEwan, J. U. & Larsen, E. C. Investigation of Lead Anodes in the Electrolysis of Zinc Sulfate Solutions. *Transactions of The Electrochemical Society* **79**, 345 (1941).
66. Nikoloski, A. N. & Nicol, M. J. Effect of cobalt ions on the performance of lead anodes used for the electrowinning of copper - A literature review. *Mineral Processing and Extractive Metallurgy Review* **29**, 143–172 (2007).
67. Maja, M., Penazzi, N., Baudino, M. & Ginatta, M. V. Recycling of lead/acid batteries: the Ginatta process. *J Power Sources* **31**, 287–294 (1990).
68. Moure Jr., W. B. & Etsell, T. H. Method for recovering lead from batteries. U.S Patent 5,211,818. (1993).
69. Bratt, G. C. & Pickering, R. W. Production of lead via ammoniacal ammonium sulfate leaching. *Metallurgical Transactions 1970 1:8* **1**, 2141–2149 (1970).

70. Díaz, G. & Andrews, D. Placid—A clean process for recycling lead from batteries. *JOM* **48**, 29–31 (1996).
71. Fassbender, S., Dreisinger, D. & Wu, Z. Recovering lead from a mixed oxidised material. U.S Patent 9,322,104. (2016).
72. Clarke, S. R., Clarke, R. L., Hurwitz, M. D., King, M. J. & Mould, S. Method for smelterless recycling of lead acid batteries. U.S Patent 9,837,689. (2017).
73. Clarke, S. R., Clarke, R. L., Hurwitz, M. D., King, M. J. & Mould, S. Devices and method for smelterless recycling of lead acid batteries. U.S Patent 10,665,907. (2020).
74. Fassbender, S., Dreisinger, D. & Wu, Z. Recovering lead from a lead material including lead sulphide. U.S Patent 9,322,105. (2016).
75. Pan, J., Sun, Y., Li, W., Knight, J. & Manthiram, A. A green lead hydrometallurgical process based on a hydrogen-lead oxide fuel cell. *Nat Commun* **4**, 1–6 (2013).
76. Dahlke, T., Ruffiner, O. & Cant, R. Production of HF from H2SiF6. *Procedia Eng* **138**, 231–239 (2016).
77. Sonmez, M. S. & Kumar, R. v. Leaching of waste battery paste components. Part 2: Leaching and desulphurisation of PbSO4 by citric acid and sodium citrate solution. *Hydrometallurgy* **95**, 82–86 (2009).
78. Sonmez, M. S. & Kumar, R. v. Leaching of waste battery paste components. Part 1: Lead citrate synthesis from PbO and PbO2. *Hydrometallurgy* **95**, 53–60 (2009).
79. Li, L. *et al.* Preparation and characterization of nano-structured lead oxide from spent lead acid battery paste. *J Hazard Mater* **203–204**, 274–282 (2012).
80. Yang, J., Kumar, R. V. & Singh, D. P. Combustion synthesis of PbO from lead carboxylate precursors relevant to developing a new method for recovering components from spent lead–acid batteries. *Journal of Chemical Technology & Biotechnology* **87**, 1480–1488 (2012).
81. Kumar, R. V. & Vasant Kumar, R. A low-cost green technology for recovering lead paste and lead-alloy grid materials for spent lead acid batteries. *Mineral Processing and Extractive Metallurgy* **126**, 89–93 (2017).
82. Zhu, X. *et al.* Leaching of spent lead acid battery paste components by sodium citrate and acetic acid. *J Hazard Mater* **250–251**, 387–396 (2013).
83. Marsh, K. N., Boxall, J. A. & Lichtenthaler, R. Room temperature ionic liquids and their mixtures—a review. *Fluid Phase Equilib* **219**, 93–98 (2004).

84. Kestin, J., Sokolov, M. & Wakeham, W. A. Viscosity of liquid water in the range −8 °C to 150 °C. *J Phys Chem Ref Data* **7**, 948 (2009).

85. Jarosik, A., Krajewski, S. R., Lewandowski, A. & Radzimski, P. Conductivity of ionic liquids in mixtures. *J Mol Liq* **123**, 43–50 (2006).

86. Chernikova, E. A. *et al.* Ionic liquids as heat transfer fluids: comparison with known systems, possible applications, advantages and disadvantages. *Russian Chemical Reviews* **84**, 875–890 (2015).

87. Abbott, A. P., Boothby, D., Capper, G., Davies, D. L. & Rasheed, R. K. Deep Eutectic Solvents formed between choline chloride and carboxylic acids: Versatile alternatives to ionic liquids. *J Am Chem Soc* **126**, 9142–9147 (2004).

88. Smith, E. L., Abbott, A. P. & Ryder, K. S. Deep Eutectic Solvents (DESs) and Their Applications. *Chem Rev* **114**, 11060–11082 (2014).

89. Abbott, A. P., Capper, G., Davies, D. L., Rasheed, R. K. & Tambyrajah, V. Novel solvent properties of choline chloride/urea mixtures. *Chemical Communications* 70–71 (2003) doi:10.1039/B210714G.

90. Kohli, R. Applications of Ionic Liquids in Removal of Surface Contaminants. *Developments in Surface Contamination and Cleaning: Applications of Cleaning Techniques Volume 11* 619–680 (2019) doi:10.1016/B978-0-12-815577-6.00016-5.

91. el Achkar, T., Greige-Gerges, H. & Fourmentin, S. Basics and properties of deep eutectic solvents: a review. *Environ Chem Lett* **19**, 3397–3408 (2021).

92. Hansen, B. B. *et al.* Deep Eutectic Solvents: A Review of Fundamentals and Applications. *Chem Rev* **121**, 1232–1285 (2021).

93. Abbott, A. P. *et al.* Preparation of novel, moisture-stable, Lewis-acidic ionic liquids containing quaternary ammonium salts with functional side chains. *Chemical Communications* 2010–2011 (2001) doi:10.1039/B106357J.

94. Abbott, A. P., Capper, G., Davies, D. L. & Rasheed, R. K. Ionic Liquid Analogues Formed from Hydrated Metal Salts. *Chemistry – A European Journal* **10**, 3769–3774 (2004).

95. Abbott, A. P., Barron, J. C., Ryder, K. S. & Wilson, D. Eutectic-based ionic liquids with metal-containing anions and cations. *Chemistry* **13**, 6495–6501 (2007).

96. Abbott, A. P., Capper, G., Davies, D. L. & Rasheed, R. Ionic liquids based upon metal halide/substituted quaternary ammonium salt mixtures. *Inorg Chem* **43**, 3447–3452 (2004).

97. Abbott, A. P. *et al.* Double layer effects on metal nucleation in deep eutectic solvents. *Physical Chemistry Chemical Physics* **13**, 10224–10231 (2011).

98. Abbott, A. P., el Ttaib, K., Ryder, K. S. & Smith, E. L. Electrodeposition of nickel using eutectic based ionic liquids. *Transactions of the IMF* **86**, 234–240 (2013).

99. Lloyd, D., Vainikka, T., Murtomäki, L., Kontturi, K. & Ahlberg, E. The kinetics of the Cu2+/Cu+ redox couple in deep eutectic solvents. *Electrochim Acta* **56**, 4942–4948 (2011).

100. Abood, H. M. A., Abbott, A. P., Ballantyne, A. D. & Ryder, K. S. Do all ionic liquids need organic cations? Characterisation of [AlCl2·nAmide]+AlCl4− and comparison with imidazolium based systems. *Chemical Communications* **47**, 3523–3525 (2011).

101. Abbott, A. P., Capper, G., McKenzie, K. J., Glidle, A. & Ryder, K. S. Electropolishing of stainless steels in a choline chloride based ionic liquid: an electrochemical study with surface characterisation using SEM and atomic force microscopy. *Physical Chemistry Chemical Physics* **8**, 4214–4221 (2006).

102. Karim, W. O. Electropolishing of pure metallic titanium in a deep eutectic solvent. *Arabian Journal of Chemistry* **14**, 102906 (2021).

103. Karim, W. O., Abbott, A. P., Cihangir, S. & Ryder, K. S. Electropolishing of nickel and cobalt in deep eutectic solvents. *Transactions of the IMF* **96**, 200–205 (2018).

104. Kityk, A. A., Protsenko, V. S., Danilov, F. I., Kun, O. v. & Korniy, S. A. Electropolishing of aluminium in a deep eutectic solvent. *Surf Coat Technol* **375**, 143–149 (2019).

105. Abbott, A. P., Dsouza, N., Withey, P. & Ryder, K. S. Electrolytic processing of superalloy aerospace castings using choline chloride-based ionic liquids. *Transactions of the IMF* **90**, 9–14 (2013).

106. Abbott, A. P., Capper, G., Davies, D. L., McKenzie, K. J. & Obi, S. U. Solubility of Metal Oxides in Deep Eutectic Solvents Based on Choline Chloride. *J Chem Eng Data* **51**, 1280–1282 (2006).

107. Söldner, A., Zach, J. & König, B. Deep eutectic solvents as extraction media for metal salts and oxides exemplarily shown for phosphates from incinerated sewage sludge ash. *Green Chemistry* **21**, 321–328 (2019).

108. Abbott, A. P. *et al.* Processing of Electric Arc Furnace Dust using Deep Eutectic Solvents. *Aust J Chem* **62**, 341–347 (2009).

109. Ru, J. *et al.* Effects of existence form and concentration of PbO on the conductivity of choline chloride–urea deep eutectic solvent. *J Mol Liq* **199**, 208–214 (2014).
110. Yang, H. & Reddy, R. G. Fundamental Studies on Electrochemical Deposition of Lead from Lead Oxide in 2:1 Urea/Choline Chloride Ionic Liquids. *J Electrochem Soc* **161**, D586–D592 (2014).
111. Liao, Y. S., Chen, P. Y. & Sun, I. W. Electrochemical study and recovery of Pb using 1:2 choline chloride/urea deep eutectic solvent: A variety of Pb species PbSO4, PbO2, and PbO exhibits the analogous thermodynamic behavior. *Electrochim Acta* **214**, 265–275 (2016).
112. Ru, J. *et al.* Preparation of porous lead from shape-controlled PbO bulk by in situ electrochemical reduction in ChCl–EG deep eutectic solvent. *Appl Surf Sci* **357**, 2094–2102 (2015).
113. Ru, J. *et al.* Mechanistic insight of in situ electrochemical reduction of solid PbO to lead in ChCl-EG deep eutectic solvent. *Electrochim Acta* **186**, 455–464 (2015).
114. Poll, C. G. *et al.* Electrochemical recycling of lead from hybrid organic–inorganic perovskites using deep eutectic solvents. *Green Chemistry* **18**, 2946–2955 (2016).
115. Coleman, F. *et al.* Lead(ii) chloride ionic liquids and organic/inorganic hybrid materials – a study of chloroplumbate(ii) speciation. *Dalton Transactions* **42**, 5025–5035 (2013).
116. Ballantyne, A. D., Hallett, J. P., Riley, D. J., Shah, N. & Payne, D. J. Lead acid battery recycling for the twenty-first century. *R Soc Open Sci* **5**, (2018).
117. Paiva, A. *et al.* Natural deep eutectic solvents - Solvents for the 21st century. *ACS Sustain Chem Eng* **2**, 1063–1071 (2014).
118. Dai, Y., van Spronsen, J., Witkamp, G. J., Verpoorte, R. & Choi, Y. H. Ionic liquids and deep eutectic solvents in natural products research: Mixtures of solids as extraction solvents. *J Nat Prod* **76**, 2162–2173 (2013).
119. Liu, Y. *et al.* Natural Deep Eutectic Solvents: Properties, Applications, and Perspectives. *J Nat Prod* **81**, 679–690 (2018).
120. Francisco, M., van den Bruinhorst, A. & Kroon, M. C. Low-Transition-Temperature Mixtures (LTTMs): A New Generation of Designer Solvents. *Angewandte Chemie International Edition* **52**, 3074–3085 (2013).

121. Dai, Y., Witkamp, G. J., Verpoorte, R. & Choi, Y. H. Tailoring properties of natural deep eutectic solvents with water to facilitate their applications. *Food Chem* **187**, 14–19 (2015).
122. Zhao, B. Y. *et al.* Biocompatible Deep Eutectic Solvents Based on Choline Chloride: Characterization and Application to the Extraction of Rutin from Sophora japonica. *ACS Sustain Chem Eng* **3**, 2746–2755 (2015).
123. Dai, Y., Witkamp, G. J., Verpoorte, R. & Choi, Y. H. Natural deep eutectic solvents as a new extraction media for phenolic metabolites in carthamus tinctorius L. *Anal Chem* **85**, 6272–6278 (2013).
124. Osowska, N. & Ruzik, L. New potentials in the extraction of trace metal using natural deep eutectic solvents (NADES). *Food Anal Methods* **12**, 926–935 (2019).
125. Osowska, N., Paduszyński, K., Matczuk, M. & Ruzik, L. New solvents for metal extraction – NADES. Prediction and optimization of efficient extraction of selected metals by ICP-MS/MS. *J Anal At Spectrom* **36**, 946–953 (2021).
126. Shikov, A. N. *et al.* The Impact of Natural Deep Eutectic Solvents and Extraction Method on the Co-Extraction of Trace Metals from Fucus vesiculosus. *Marine Drugs 2022, Vol. 20, Page 324* **20**, 324 (2022).
127. Huang, Y., Feng, F., Chen, Z.-G., Wu, T. & Wang, Z.-H. Green and efficient removal of cadmium from rice flour using natural deep eutectic solvents. *Food Chem* **244**, 260–265 (2017).
128. Yang, X., Zang, Y. Y., Yang, S. & Chen, Z. G. Green and efficient removal of heavy metals from Porphyra haitanensis using natural deep eutectic solvents. *J Sci Food Agric* **101**, 2930–2939 (2021).
129. Wlo, J. OVERVIEW OF AN INDUCTIVELY COUPLED PLASMA (ICP) SYSTEM. *International Journal of Chemical Research* **3**, 41–48 (2011).
130. Olesik, J. W. Elemental Analysis Using ICP-OES and ICP/MS. *Anal Chem* **63**, (1991).
131. Charles B, B. & Kenneth J, F. Concepts, Instrumentation and Techniques in Inductively Coupled Plasma Optical Emission Spectrometry. https://resources.perkinelmer.com/lab-solutions/resources/docs/gde_concepts-of-icp-oes-booklet.pdf (2004).

132. Pandey, A., Dalal, S., Dutta, S. & Dixit, A. Structural characterization of polycrystalline thin films by X-ray diffraction techniques. *Journal of Materials Science: Materials in Electronics* **32**, 1341–1368 (2021).
133. Fewster, P. F. Foundations and Advances A new theory for X-ray diffraction. *Acta Cryst* **70**, 257–282 (2014).
134. Mccusker, L. B., von Dreele, R. B., Cox, D. E., Loue, D. & Scardi, P. Rietveld refinement guidelines. *International Union of Crystallography Journal of Applied Crystallography J. Appl. Cryst* **32**, 36–50 (1999).
135. Toby, B. H. R factors in Rietveld analysis: How good is good enough? *Powder Diffr* **21**, 67–70 (2006).
136. Ma, H., Shieh, K.-J. & Qiao, T. X. Study of Transmission Electron Microscopy (TEM) and Scanning Electron Microscopy (SEM). *Nat Sci (East Lansing)* **4**, 14–22 (2006).
137. Smith, K. C. A. & Oatley, C. W. The scanning electron microscope and its fields of application. *British Journal of Applied Physics* **6**, 391 (1955).
138. Kanaya, K. & Kawakatsu, H. Secondary electron emission due to primary and backscattered electrons. *J Phys D Appl Phys* **5**, 1727 (1972).
139. Stevie, F. A. & Donley, C. L. Introduction to x-ray photoelectron spectroscopy. *Journal of Vacuum Science & Technology A* **38**, 063204 (2020).
140. Powell, C. J. Practical guide for inelastic mean free paths, effective attenuation lengths, mean escape depths, and information depths in x-ray photoelectron spectroscopy. *Journal of Vacuum Science & Technology A* **38**, 023209 (2020).
141. Shinotsuka, H., Tanuma, S., Powell, C. J. & Penn, D. R. Calculations of electron inelastic mean free paths. X. Data for 41 elemental solids over the 50eV to 200keV range with the relativistic full Penn algorithm. *Surface and Interface Analysis* **47**, 871–888 (2015).
142. Saadatkhah, N. *et al.* Experimental methods in chemical engineering: Thermogravimetric analysis—TGA. *Canadian Journal of Chemical Engineering* **98**, 34–43 (2020).
143. Schick, C. Differential scanning calorimetry (DSC) of semicrystalline polymers. *Analytical and Bioanalytical Chemistry* vol. 395 1589–1611 Preprint at https://doi.org/10.1007/s00216-009-3169-y (2009).

144. Gaffney, J. S., Marley, N. A. & Jones, D. E. Fourier Transform Infrared (FTIR) Spectroscopy. in *Characterization of Materials* 1104–1135 (John Wiley & Sons, Inc., 2012). doi:10.1002/0471266965.COM107.PUB2.

145. Hore, P. J. *Nuclear Magnetic Resonance*. (Oxford University Press, 2015).

146. Dai, Y., van Spronsen, J., Witkamp, G. J., Verpoorte, R. & Choi, Y. H. Natural deep eutectic solvents as new potential media for green technology. *Anal Chim Acta* **766**, 61–68 (2013).

147. Ghosh, A. & Rao, C. N. R. Chiral and Achiral Malate Frameworks with Different Dimensionalities. *Z Anorg Allg Chem* **634**, 1115–1122 (2008).

148. Arulmozhi, K. T. & Mythili, N. Studies on the chemical synthesis and characterization of lead oxide nanoparticles with different organic capping agents. *AIP Adv* **3**, 122122 (2013).

149. Ogundele, D. T., Azeez, S. O. & Jimoh, A. A. Chemical synthesis kinetics and dimensional characterization of nano-lead oxide powder. *Journal of the Turkish Chemical Society Section A: Chemistry* **9**, 227–236 (2022).

150. Ward, T. Capillary-pressure driven adhesion of rigid-planar surfaces. *J Colloid Interface Sci* **354**, 816–824 (2011).

151. Payne, D. J. *et al.* Experimental and theoretical study of the electronic structures of α-PbO and β-PbO2. *J Mater Chem* **17**, 267–277 (2007).

152. Pederson, L. R. Two-dimensional chemical-state plot for lead using XPS. *J Electron Spectros Relat Phenomena* **28**, 203–209 (1982).

153. Taylor, J. A. & Perry, D. L. An x-ray photoelectron and electron energy loss study of the oxidation of lead. *Journal of Vacuum Science & Technology A: Vacuum, Surfaces, and Films* **2**, 771–774 (1984).

154. Castro, V. I. B., Mano, F., Reis, R. L., Paiva, A. & Duarte, A. R. C. Synthesis and Physical and Thermodynamic Properties of Lactic Acid and Malic Acid-Based Natural Deep Eutectic Solvents. *J Chem Eng Data* **63**, 2548–2556 (2018).

155. Polat, S. Thermal degradation of calcium lactate pentahydrate using TGA/FTIR/MS: thermal kinetic and thermodynamics studies. *Indian Chemical Engineer* **64**, 1–14 (2021).

156. Yoon, I. S. *et al.* Characterization of calcium lactate prepared from butter clam Saxidomus purpuratus shell powder. *Korean Journal of Fisheries and Aquatic Sciences* **49**, 301–309 (2016).

157. Ahmad, A., Bedard, P., Wheat, T. A., Kuriakose, A. K. & McDonald, A. G. Surface area, XRD, and FTIR spectral characterization of chemically derived PbTiO3 ceramics. *J Solid State Chem* **93**, 220–227 (1991).

158. Ma, Y. & Qiu, K. Recovery of lead from lead paste in spent lead acid battery by hydrometallurgical desulfurization and vacuum thermal reduction. *Waste Management* **40**, 151–156 (2015).

159. Ballantyne, A. D. *et al.* Lead acid battery recycling for the twenty-first century. *R. Soc. Open Sci.* **5**, 171368 (2018).

160. Volpe, M. *et al.* Metallic lead recovery from lead-acid battery paste by urea acetate dissolution and cementation on iron. *Hydrometallurgy* **96**, 123–131 (2008).

161. Ramanjooloo, A., Bhaw-Luximon, A., Jhurry, D. & Cadet, F. 1H NMR Quantitative Assessment of Lactic Acid Produced by Biofermentation of Cane Sugar Juice. *Spectroscopy Letters* **42**, 296–304 (2009).

162. Viertorinne, M., Valkonen, J., Pitkänen, I., Mathlouthi, M. & Nurmi, J. Crystal and molecular structure of anhydrous betaine, (CH3)3NCH2CO2. *J Mol Struct* **477**, 23–29 (1999).

163. Poloju, S. *et al.* Oxidation of Lactic Acid by Manganese(III) in Sulfuric Acid Medium: Kinetics and Mechanism. *American Journal of Organic Chemistry* **2**, 58–62 (2012).

164. Fulmer, G. R. *et al.* NMR chemical shifts of trace impurities: Common laboratory solvents, organics, and gases in deuterated solvents relevant to the organometallic chemist. *Organometallics* **29**, 2176–2179 (2010).

165. Ma, C., Shu, Y. & Chen, H. Recycling lead from spent lead pastes using oxalate and sodium oxalate and preparation of novel lead oxide for lead-acid batteries. *RSC Adv* **5**, 94895–94902 (2015).

166. Laajalehto, K., Smart, R. S. C., Ralston, J. & Suoninen, E. STM and XPS investigation of reaction of galena in air. *Appl Surf Sci* **64**, 29–39 (1993).